UNIVERSITY OF SOUTHAMPTON

Partial Singular Integro-Differential Equations Models for Dryout in Boilers

Mphaka Joane Sankoela Mphaka

Doctor of Philosophy

Faculty of Mathematical Studies

October, 2000.

Dedicated to my parents 'Masenyai and Mofella Mphaka and in memory of all family members who, for one reason or another, had to "leave" us.

UNIVERSITY OF SOUTHAMPTON

ABSTRACT

FACULTY OF MATHEMATICAL STUDIES

MATHEMATICS

Doctor of Philosophy

PARTIAL SINGULAR INTEGRO-DIFFERENTIAL EQUATIONS MODELS FOR DRYOUT IN BOILERS

by Mphaka Joane Sankoela Mphaka

A two-dimensional model for the annular two-phase flow of water and steam, along with the dryout, in steam generating pipes of a liquid metal fast breeder reactor is proposed. The model is based on thin-layer lubrication theory and thin aerofoil theory. The exchange of mass between the vapour core and the liquid film due to evaporation of the liquid film is accounted for in the model. The mass exchange rate depends on the details of the flow conditions and it is calculated using some simple thermodynamic models. The change of phase at the free surface between the liquid layer and the vapour core is modelled by proposing a suitable Stefan problem. Appropriate boundary conditions for the model, at the onset of the annular flow region and at the dryout point, are stated and discussed. The resulting unsteady nonlinear singular integro-differential equation for the liquid film free surface is solved asymptotically and numerically (using some regularisation techniques) in the steady state case, for a number of industrially relevant cases. Predictions for the length to the dryout point from the entry of the annular regime are made. The influence of the constant parameter values in the model (e.g. the traction τ provided by the fast flowing vapour core on the liquid layer and the mass transfer parameter η) on the length to the dryout point is investigated.

The linear stability of the problem where the temperature of the pipe wall is assumed to be a constant is investigated numerically. It is found that steady state solutions to this problem are always unstable to small perturbations. From the linear stability results, the influence on the instability of the problem by each of the constant parameter values in the model is investigated. In order to provide a benchmark against which the results for this problem may be compared, the linear stability of some related but simpler problems is analysed. The results reinforce our conclusions for the full problem.

Contents

Acknowledgements

I would like to first of all acknowledge my supervisor Prof. Alistair Fitt for his advice, encouragement and time especially for those first three months of my research. I would also like to thank all other members of the Industrial Applied Mathematics group with whom I have had useful discussions in one way or the other. These include my advisor Prof. Colin Please, Dr. Giampaolo D'Alessandro and Dr. Jeff Dewynne (now at Oxford) for over-lending me his books for almost two years! I wish to extend my appreciation to all the members of the faculty office, in particular Mrs Yvonne Oliver, for their help from time to time with the administrative stuff.

I am very grateful to the Association of Commonwealth Universities in UK (and all those who handle all the administrative stuff, including Mrs. Sefika at LNMD!) for supporting me financially throughout this study. I cannot resist to mention that an opportunity to study (or live), for a considerable length of time, away from own country (for everybody) goes way beyond the academics; it provides a chance to celebrate (instead of being cynical or dubious about) people's differences in temperament, culture and all sorts of other things really.

I also wish to thank wholeheartedly all those who helped me and encouraged me throughout all the levels of my education; those who saw in me then what I could not possibly see in myself! These include all those at Thaba-Phats'oa Primary, Zenon High, Lesotho High and MACS, NUL! I would definitely not forget all the friends I have made throughout these times and whom, for some reason, we have kept in touch in one way or another; I wish you all the beauties and challenges of the uncertain but certainly bright future!

My greatest appreciations to Dr. Robert Craine (Bob!), Margery and their wonderful family for an unmeasurable support throughout my time here in Southampton - it is indeed those little positive debts that one cannot pay!

I have met and known an "uncountable" number of friends from all over the world here in Southampton. These include Martin Pope, Vladislav Putyatin, Michael Sharpe, Gabriela Gonzalez Castro, Eva Vincente Alonso, Sharon Kirkham, Marcus Tindall, ... - the list is truly inexhaustible but you know who you are guys - and all the very best to you all!

Most of all, to all the members of my family, my parents and a very special friend of mine Monehela Molapo: thank you so much for all the constant support, love, encouragement, tolerance and beyond, throughout my time here and all along! I know "Thank you" is not enough but it is the only one I can find at the moment.

Chapter 1

General Introduction

The study of multiphase flow dynamics is frequently undertaken in the areas of natural sciences and engineering. A multiphase flow is simply described by Wallis (1969) [90] as the simultaneous flow of several phases, where a phase is a state of matter, e.g. solid, liquid or gas. There are numerous publications on this subject which cover fields such as blood flow, dust storms, air pollution, fluidised beds, sedimentation and pneumatic conveyors. These publications include those of Soo (1967) [76], Wallis (1969) [90], Bergles & Ishigai (1981) [11], Azbel (1981) [6], Chisholm (1983) [18] and Whalley (1987) [92] to name but a few. Owing to the vast and broad scope of the subject of multiphase flows, we do not attempt to describe the study of all aspects of the subject here since this would distract the reader from the main theme of this thesis. This thesis is devoted to mathematical modelling and analysis of an "annular" two-phase flow of an evaporating thin viscous liquid film of water (adhering to a heated wall) and its fast flowing "vapour/gas core" (the technical terminology will become clearer as we describe the physical problem in section (1.1)).

It is important at this stage to mention that the modelling and the analysis of the annular two-phase flows (for the current conditions of interest) will involve the study of thin liquid flows. Owing to their frequent occurrence (both in nature and in engineering sciences), the subject of thin film flows (isothermal and otherwise) has always been, and still is, of paramount interest to both theorists and industrialists including experimentalists. As a result, the literature in this area is very large in its extent. It seems that much of the recent work performed on isothermal thin liquid films has been mostly motivated by painting processes in industry. This is not entirely surprising since many industrial processes involve a form of coating solid substrates with thin layers of paint, e.g. the electronics industry, the food industry and the paint industry to name but a few. Examples are presented in a review by Ruschak (1985) [70]. Among most recent publications in the literature (and many interesting mathematical modelling problems which arise in this area), we can mention, as examples, the

investigations of the closing and opening of holes in thin liquid films by Moriarty & Schwartz (1993) [53]; the study of drying paint layers by Howison *et al* (1997) [40]; the investigations on the spreading of thin liquid drops on planar substrates when subjected to a jet of air blowing normally to the substrate by McKinley *et al* (1999) [52]; the study of thin film curtain flows on rotating cylinders by Duffy & Wilson (1999) [27]; and the investigations into the blade coating phenomena by Ross *et al* (1999) [68]. A significant amount of the recent research involving the flow of non-isothermal thin liquid films (including the current problem of interest), on the other hand, has been largely motivated by the flows which are commonly observed in aerospace, power and process engineering industries. Examples include the study of ice and water film growth from incoming supercooled droplets by Myers & Hammond (1998) [55]; the study of the cooling of turbine blade tips, rocket engines, hot fuel element surfaces in hypothetical nuclear reactor accidents (see for example, a review by Bankoff (1994) [9]); and investigations on the growth of a vapour bubble in nucleate boiling by Wilson *et al* (1999) [95].

In the problem studied here (whose motivation is explained in section (1.1)), a mathematical model for the two-phase annular flow of water and vapour in steam generating pipes of a Liquid Metal Fast Breeder Reactor (LMFBR) is proposed and analysed. The main aim of the model is to allow predictions to be made for the position of "dryout point". The model is based on thin aerofoil theory and thin-layer lubrication theory and it takes into account the mass exchange between the liquid film and the gas core due to evaporation from the liquid film. The resulting governing equation is a partial nonlinear singular integro-differential equation for the liquid film free surface. It contains Hilbert transforms which are characterised by a Cauchy kernel of the form $(\xi - x)^{-1}$. The solutions of the equation are achieved by employing both appropriate asymptotic and numerical techniques. The linear stability of some solutions is investigated as well. Therefore, this thesis concerns mathematical modelling, asymptotic techniques and numerical methods.

1.1 The Physical Problem

Within a nuclear plant, the basis of nuclear energy development is natural uranium. This is mainly because its two isotopes U^{235} and U^{238} possess nuclear characteristics which are most favourable to the production of atomic energy in a reactor, see for example, Wyatt (1956) [96] and Wilke (1963) [93]. A nuclear reactor is an essential invention in which the radioactive substance concerned is converted into useful energy. In a very brief and over-simplified summary, the nuclear reactor consists mainly of two components, namely a reactor/core component (or a fuel element) and a boiling/heat exchange component. Fission and conversion take place in the reactor component in which heat is generated and transferred to a coolant.

Heat is then transferred from the coolant to water in the boiling component where steam is produced to drive turbines in order to create electricity. There are different kinds of nuclear reactors depending on many factors one of which is the type of coolant that is used. Some examples of these are explained in detail by Etherington (1958) [28]. In the Liquid Metal Fast Breeder Reactor, for example, a liquid metal is used as the coolant, a common choice being sodium since it has a high boiling point at atmospheric pressure and therefore the nuclear reactor may operate virtually unpressurised. Thus, in the event of Loss of Coolant Accident (LOCA) in which there is a break in the boundary of the nuclear system (Prosperetti & Plesset, 1984) [67], the damage and spread of contaminated material is minimised.

1.1.1 Flow Patterns

The boiling component of the nuclear reactor is composed of bundles of steam generating pipes. Water is pumped through the pipes, and heat is supplied from the liquid metal which flows in a counter-current direction in outer casings surrounding the pipes. As the water temperature increases, the water begins to vapourise resulting in a two-phase flow of water and steam. In a typical heat generating pipe, the water and the steam generated take up a variety of configurations known as flow patterns or flow regimes, see for example figure 1.1. Which particular flow pattern pertains depends upon the amount of each phase present, some external effects such as orientation of the pipe, and the flow conditions like pressure and heat flux. Detailed descriptions of the various flow regimes are given, for example, by Wallis (1969) [90], Collier & Thome (1994) [20]. In a brief summary, the flow essentially consists of a single-phase subcooled region near to the water inlet. The water in the subcooled region is heated to the saturation temperature. At some point beyond this region, along the pipe, the water gets superheated and the bubbles start to form at some suitable sites on the pipe. As the bubbles grow, they detach from the pipe wall and start to form a bubbly region. In this region, the vapour phase is distributed as discrete bubbles in a continuous liquid phase. The bubbles (whose sizes are negligible compared to the diameter of the pipe) are almost spherical in shape. The bubbles which are nearer to the subcooled region are typically smaller than those at the farther end of the bubbly region along the pipe. As more and more bubbles are produced and continue to grow larger, they amalgamate to form a plug flow region which gives way to annular flow region. Thus, plug flow is identified by large vapour bubbles which almost cover the whole diameter of the pipe. The bubbles are separated from the pipe wall and one another by a thin layer of liquid. At this stage, both the vapour and liquid flow rates are higher than of those in the bubbly region. As a result of the breakup of the large vapour bubbles in the plug region, a churn flow regime may be observed prior to the annular flow region. Churn flow is characterised by irregular and disturbed bubbles through liquid which is mainly found adjacent to the pipe wall.

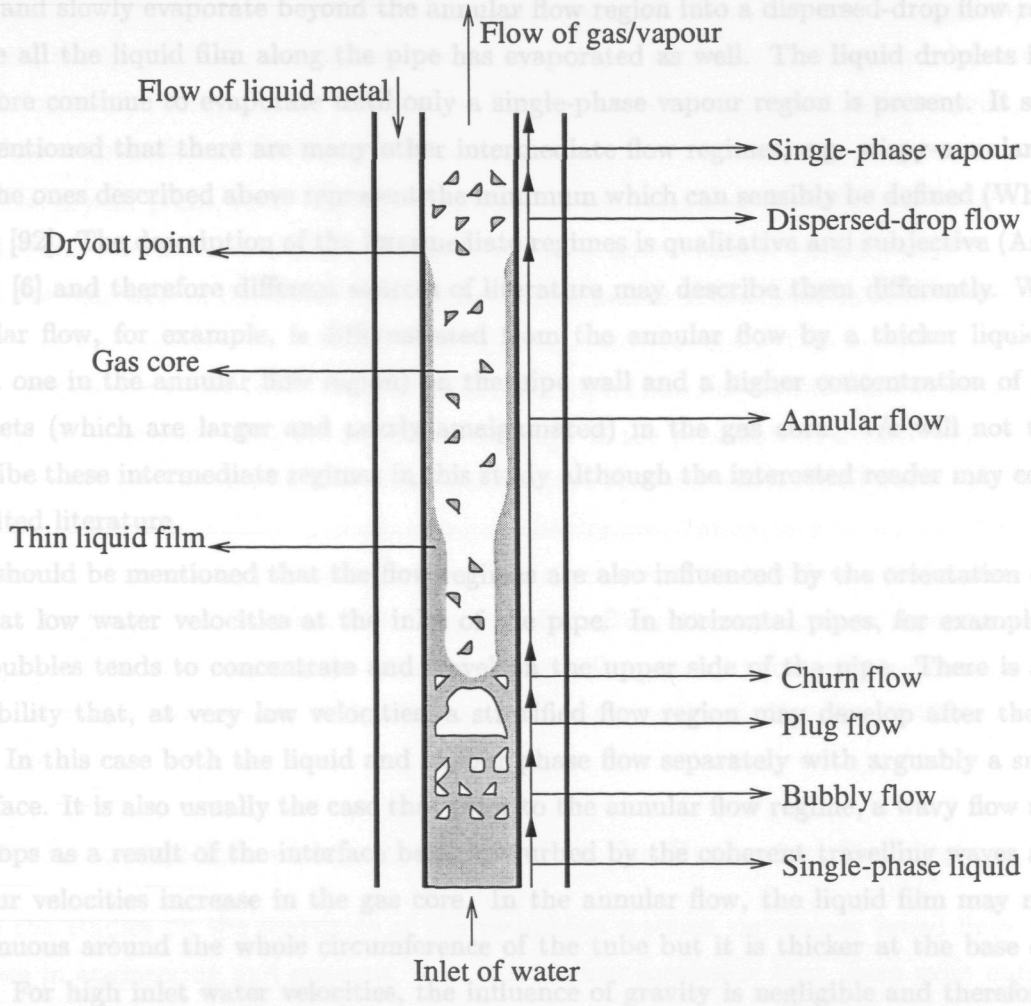

Figure 1.1: A schematic representation of a vertical boiler tube

In the annular region, a flow of continuous liquid film along the pipe wall surrounds a core of fast flowing gas. Typically, the gas contains some liquid droplets which are believed to be a result of break up of waves which are usually present at the liquid film free surface, and undercuttings of the liquid film free surface by the increasing velocities in the gas core. In this region, the liquid film is superheated. Thus, formation of the vapour bubbles at the pipe wall has significantly decreased to a point that it is negligible and the gas production is due to evaporation of the thin liquid film free surface. The liquid droplets in the gas core continue to exist and slowly evaporate beyond the annular flow region into a dispersed-drop flow region, where all the liquid film along the pipe has evaporated as well. The liquid droplets in the gas core continue to evaporate until only a single-phase vapour region is present. It should be mentioned that there are many other intermediate flow regimes, e.g. wispy-annular flow, but the ones described above represent the minimum which can sensibly be defined (Whalley, 1987) [92]. The description of the intermediate regimes is qualitative and subjective (Azabel, 1981) [6] and therefore different sources of literature may describe them differently. Wispy-annular flow, for example, is differentiated from the annular flow by a thicker liquid film (than one in the annular flow region) on the pipe wall and a higher concentration of liquid droplets (which are larger and nearly amalgamated) in the gas core. We will not try to describe these intermediate regimes in this study although the interested reader may consult the cited literature.

It should be mentioned that the flow regimes are also influenced by the orientation of the pipe at low water velocities at the inlet of the pipe. In horizontal pipes, for example, the gas bubbles tends to concentrate and travel on the upper side of the pipe. There is also a possibility that, at very low velocities, a stratified flow region may develop after the plug flow. In this case both the liquid and vapour phase flow separately with arguably a smooth interface. It is also usually the case that prior to the annular flow regime, a wavy flow region develops as a result of the interface being disturbed by the coherent travelling waves as the vapour velocities increase in the gas core. In the annular flow, the liquid film may not be continuous around the whole circumference of the tube but it is thicker at the base of the pipe. For high inlet water velocities, the influence of gravity is negligible and therefore the difference between the flow regimes in the vertical pipe and the horizontal one is virtually not existent.

1.1.2 The Annular Region and the Dryout Point

Within this study, we focus on the two-phase annular region for several reasons. Annular flow is the predominant flow regime present in evaporators, condensation operations, natural gas pipelines and steam generating systems (Wallis, 1969) [90]. This is well-supported by several published flow pattern diagrams where the different two-phase flow regimes are identified

as functions of mixture quality and mass velocity. Moreover, at the operating conditions of the liquid metal nuclear reactor, (which are approximately pressures of 200 bar and hence a water saturation temperature of $T_s = 365°C$) the flow pattern maps of Bennett *et al* (1965) [10] suggest that annular flow comprises at least $80 - 90\%$ of the two-phase flow region. Furthermore, the annular flow regime in steam generating pipes has a fundamental feature of an exchange of mass between the liquid film and the gas core. This phenomenon consists of evaporation of the liquid film, typically at the free boundary; droplet entrainment (from the liquid film into the gas core) which is believed to be a result of the break up of large amplitude coherent waves which are usually present at the surface of the liquid film; and deposition of liquid drops from the gas core. The annular flow regime also contains the dryout point, where complete evaporation of the liquid film occurs.

At the dryout point, there is a sharp increase in the temperature of the pipe wall because the thermal conductivity of the gas phase, which is now in direct contact with the wall, is much less than that of the liquid phase. The determination of the position of the dryout point is not a trivial problem (see also Fisher & Pearce, 1993)[29] since, for example, in the event that deposition of liquid drops occurs rapidly, the liquid film may reform hence rewetting and causing the temperature of the pipe wall to drop. If the processes of dryout and rewetting occur periodically, thermal stresses may be set up in the wall which could lead to cracking of the pipe. Therefore, a good understanding of the dryout phenomenon is essential to predict the lifetime of the steam generating pipes, as this process directly affects the integrity of the pipes. Moreover, the position of the dryout point affects the amount of evaporation which can occur in the pipes for a given value of the heat flux, and it is of great importance in the design of evaporators, steam boilers and nuclear reactors (Bankoff, 1994; Collier & Thome, 1994) [9], [20].

1.1.3 Some Models which are Related to the Presented Problem

Since the studies on the dynamics of the two-phase systems encompass broad lines of disciplines in engineering and sciences, then it is almost inevitable that there exist numerous related models to the current problem of interest. We do not make any attempt here to review all of these models. It is, however, important to mention at this stage that the analysis of the available publications (e.g. Soo, 1967; Wallis, 1969; Chisholm, 1983) [76], [90], [18] indicates that there is no standard type of equations generally agreed to describe the two-phase (and of course multiphase) flows. Usually, most two-phase flows are characterised by changes in many physical properties (e.g. density, viscosity, thermal conductivity) which are, in general, functions of space, time and other variables. Frequently, the dynamics of two-phase systems in pipes (as well as the current problem of interest) include heat and mass transfer thermodynamics. Thus, it is extremely difficult to develop mathematical models of

these systems. The general attitude adopted in the literature is that two-phase flows obey all the basic laws of fluid mechanics with equations more complicated and/or more numerous than those describing the single-phase flows. Thus the models are based on the conservation laws of mass, momentum and energy.

Practically all of the early literature indicates that the modelling of two-phase flows considered the mixture mass, momentum and energy conservation laws (see for example, a review by Yadigaroglu & Lahey, 1976) [97]. This is a simple, but also not accurate, method of analysing two-phase flows. The properties of the mixture, e.g. velocity, temperature, density and viscosity, are calculated average properties of the two phases. The challenge in the mixture modelling is then of developing techniques to determine these weighted average properties and rearranging the resulting equations until they resemble equivalent equations of a single-phase flow. There are numerous approaches in the literature adopted by researchers and we are not going to make a review of them here. However, it is worth mentioning that a frequently employed approach is to express the properties of each phase, in the conservation of mass, momentum and energy equations, in terms of a mixture quality. A mixture quality is defined as mass flux of one phase divided by total mass flux of the two phases. Later models, on the other hand, consider separately the conservation laws for each phase in order to improve accuracy of the mathematical representation. These equations can then be combined to describe the total flow. The equations are many with numerous unknowns. Thus, in general the problem is intractable. Therefore, it requires some simplifications and closure conditions which can only be supplied by prescribing appropriate interaction laws of mass, momentum and energy between the phases. This is non-trivial and researchers frequently resort to a great number of hypotheses.

Some examples of models which are related to the current problem of interest include those of Fisher & Pearce (1993) [29] and Whalley (1977) [91]. Fisher & Pearce (1993) [29] present a model for annular flow of water and steam at high pressures ($\sim$ 149 bars) in electrically heated (heat flux ranging from 60 to 65 KW/m^2) horizontal serpentine evaporators with typical radii and lengths of order 22.1 mm and 3.17 m, respectively. Fisher and Pearce's model takes into account evaporation of the liquid film and droplet entrainment from the gas core into the liquid layer. Whalley (1977) [91] proposes a two-phase annular flow model to calculate the dryout in a vertical rod bundle of a nuclear reactor at pressures between 10 and 68 bars. The heated length of the tubes is of order 3.66 m. The processes of droplet entrainment and deposition are both assumed to be major phenomena affecting the dryout process in this model. To analyse their models, Whalley (1977) [91], Fisher & Pearce (1993) [29] use numerous empirical engineering correlations. In fact these type of models, as put by (Kirillov *et al*, 1985) [46], are not developed to investigate directly the parameters which characterise the annular two-phase flow in pipes, but to describe analytically the conditions

of burnout or dryout heat transfer. The basic equations are that of the film flow rate, and the flow characteristics are described very schematically and empirically.

1.1.4 An Overview of Work Performed in this Thesis

We now summarise the work of this thesis. In chapter 2, an unsteady two-dimensional mathematical model for the two-phase flow of a thin liquid film (adjacent to a heated pipe wall) and its fast flowing gas core, along with the dryout point, is proposed. A number of assumptions, relevant to the current conditions of interest, are made and discussed in detail. The thin liquid film is modelled by employing thin-layer lubrication theory. The flow in the gas core is modelled as an incompressible, inviscid and irrotational flow. The liquid film adjacent to the wall is treated as a small perturbation to the gas flow. This allows the application of the thin aerofoil theory. A constitutive equation for the transfer of mass, by evaporation, from the liquid film into the gas core is proposed by specifying an appropriate Stefan problem.

Chapters 3 and 4 deal with numerical solutions of the steady state cases of the model when a constant wall temperature is specified and when a specific non-constant wall temperature is prescribed, respectively. Chapter 5 is mainly concerned with linear stability analysis (with respect to small temporal perturbations) of the steady state numerical solutions obtained for the constant wall temperature problem. The results are compared with those analysed for some simple paradigm problems. Finally, chapter 6 summarises some conclusions and discusses possible further work.

All of the numerical results presented in this thesis have been computed using programs which the author has written in FORTRAN-77. In many cases, some specified NAG library routines have been employed and a specific reference is given in the thesis whenever and wherever one is used.

Chapter 2

The Full Unsteady Model

In this chapter, we systematically develop an unsteady mathematical model for the dry-out front position. The resulting model amounts to a nonlinear singular integro-differential equation for the unknown liquid film free surface. Plausible boundary conditions are stated. Before we proceed with the mathematical modelling, however it is instructive to review some previous relevant work.

2.1 Literature Review

2.1.1 Mathematical Modelling

Owing to some previous modelling of various physical phenomena, nonlinear singular integro-differential equations already exist in the literature. Fitt *et al* (1985) [32] propose a simple model which gives a steady nonlinear integro-differential equation to investigate the aerodynamics of slot film cooling by injection of an inviscid fluid from a slot into a uniform cross flow. The model assumes both the injected and the free-stream to be potential flows. In order to ensure that the injection is weak, it is further assumed in the model that the slot pressure exceeds the cross flow pressure by only a small amount. Some theoretical results are obtained and are found to be in good agreement with experimental observations at low injection rates. Some variations of the Fitt *et al* (1985) [32] model are investigated by several other authors. The effects of altering the geometry of the upstream end of the slot on the mass flow are studied by Fitt & Wilmott (1994) [34]. In this paper the original model is augmented with a term obtained from a known upstream end geometry. Fitt & Stefanidis (1998) [33] include the energy equation in the original problem to enable predictions of the film cooling effectiveness produced by the slot injection into the cross flow to be made. Fitt & Lattimer (1996) [31] extend the Fitt *et al* (1985) [32] problem to include the effects of introducing a downstream suction slot. In the absence of the upstream injection slot, Lat-

timer & Fitt (1998) [47] investigate transient effects by assuming that the unsteadiness in the resulting problem is driven by a time dependent suction slot pressure. Pope (1999) [65] studies the problem of de-icing (removal of a thin ice layer) by the injection of heated fluid from a slot. Just like the other models mentioned earlier, this problem is also a development of the original model by Fitt *et al* (1985) [32]. A complementary problem of slot suction from an inviscid channel flow, when the suction and free stream total pressure heads are equal, is investigated by Dewynne *et al* (1989) [25]. Other authors use hodograph techniques (by using Christofel transformations, for example) to model fluid flows in some complicated physical geometries, and the resulting equations of motion are nonlinear singular integro-differential equations. Forbes & Schwartz (1982) [35] tackle a two-dimensional problem of steady flow of a fluid with a free surface over a semicircular obstacle on the bottom of a stream. A hodograph variable is specified and the problem is transformed from an otherwise difficult physical space into a simpler hodograph space. Similar techniques are employed to study other problems in various difficult geometries by a number of authors. These include King & Bloor (1987) [44] in their study of a steady free surface flow of an ideal fluid over a semi-infinite step; Asavanant & Vanden-Broeck (1994) [4] who investigate two-dimensional flows past a parabolic obstacle lying on the free surface in a fluid of infinite depth; and Tuck & Vanden-Broeck (1998) [87] who study "ploughing flows", i.e. flows over shallowly-submerged bodies which may be thought of as a model for an agricultural plough.

All of the above models concentrate exclusively on inviscid incompressible and irrotational flows. There are a few models in the literature, however, which incorporate some viscous effects. Spence & Sharp (1985) [78] study a pressure-driven fluid fracture problem whereas Spence *et al* (1987) [79] consider the case of buoyancy-driven fluid fracture. These authors formulate their problems in terms of singular integro-differential equations governing the elastic deformations of the crack wall boundaries. The equations are then coupled with the differential equations of lubrication theory for viscous incompressible flows in the cracks. The resulting governing equations for the models are nonlinear singular integro-differential equations. Another interesting physical problem which is closely related in structure to the one which we model in this chapter, is the study of thin isothermal viscous liquid layers supported by steady air flow surface traction (King & Tuck, 1993) [45]. The air not only exerts the shear traction on the liquid layer, but also leads to a non-uniform pressure whose size is determined by the shape of the layer. Upon employing thin aerofoil theory and lubrication theory approximations, the problem is reduced to a nonlinear singular integro-differential equation for the unknown shape of the liquid layer. This problem (like all the other models which include viscous effects in this literature review) differs fundamentally from the one that we model in this chapter because we account for both the transfer of mass from the superheated (i.e. heated above saturation temperature) liquid layer into the gas

core flow and the change of phase at the unknown boundary of the liquid layer. Therefore, the associated boundary conditions also differ considerably.

2.1.2 Numerical Methods

It is worth mentioning at this point that, due to their frequent appearance in modelling physical phenomena, a vast amount of literature is available on the numerical solution of linear (or linearised) singular integral equations. The interested reader is referred to a wide range of numerical techniques presented by various authors in the literature, see for example, Tuck (1991) [86], Chakrabarti & Tsahoo (1996) [16], Cuminato (1996) [21], Kim (1998) [43], De Klerk *et al* (1995) [23], Frankel (1995) [37] and Fitt *et al* (1995) [30]. Other authors compute the singular behaviour of the linear Cauchy singular integral equations with both constant and variable coefficients (Srivastav, 1992; Li & Srivastav, 1997) [84], [49]. Although numerical methods for linear equations are interesting, they are not really applicable to our problem. Here, we will therefore focus briefly on some of the references which employ numerical techniques to solve nonlinear singular integro-differential equations and these are much rarer. An obvious reason for undertaking this part of literature review is to learn of what may be already available for application when we will be tackling the current problem numerically later in this thesis.

In an analysis of a nonlinear singular integro-differential equation governing the local temperature during transient radioactive heat transfer in a plane layer, Prasad & Hering (1970) [66] present a purely numerical method for solving the problem. Their technique uses a least squares approximation for the function within the integral operator to reduce the equation to a system of ordinary differential equations. Predictor-corrector methods are then employed to solve the resulting system of differential equations. Owing to the complex nature of their problem and approximations involved, the problem of analysing the convergence, stability and error bounds for the numerical scheme is not even attempted. Spence & Sharp (1985) [78], in their study of pressure-drive fluid fracture, and Spence *et al* (1987) [79], in their study of buoyancy-driven fluid fracture, rearrange the original nonlinear singular integro-differential equation into an alternative form in which the unknown function may be approximated using an expansion technique. The basis functions chosen for the expansion are based on Chebyshev polynomials with unknown coefficients. The Chebyshev expansion is augmented by a term possessing the correct singular behaviour at an appropriate point. The unknown coefficients are determined by a constrained nonlinear optimisation technique. On the other hand, Spence *et al* (1988) [77] employ similarity techniques (self-similar) to analyse their unsteady model. Fitt et al (1985) [32], O'Malley *et al* (1991) [58], Fitt & Wilmott (1994) [34], Fitt & Stefanidis (1998) [33], Fitt & Lattimer (1996) [31] and Pope (1999) [65] all invert their singular integro-differential equations and then integrate the resulting equations appropriately

to remove any derivatives of the unknown function. After applying the relevant boundary conditions to evaluate the constants of integration and inversion, the problem is then solved numerically by employing a direct iterative relaxation scheme. The success of this numerical technique is primarily made possible by the fact that the resulting equation contains no principal-value integrals. It is not clear, however, whether the fact that the behaviour of the unknown function at one (or more) end point contains a logarithmic singularity also plays an important role. King & Tuck (1993) [45], instead, employ regularisation techniques to deal with the singular behaviour of the derivative of the unknown function near an end point prior to any numerical manipulations. Their resulting equation is then discretised using finite differences and a collocation method is employed to evaluate the Cauchy principal-value integral. The final challenge of King & Tuck (1993) [45] is to solve a set of nonlinear algebraic equations for the unknown function at discrete points, and this is done using a Powell's method as implemented in the NAG library routine C05NBF.

As a result of using a conformal mapping technique to map a region of complicated geometry, which is occupied by an irrotational inviscid fluid, to a region with a simpler geometry, Bloor (1978) [12], Schwartz & Vanden-Broeck (1979) [73], Forbes & Schwartz (1982) [35] and King & Bloor (1987) [44] also solve various nonlinear singular integral equations using different, but closely related, computational techniques. In general, the methods are based upon finite difference approximations. The domain of the independent variable is subdivided into subintervals. The derivatives are approximated by appropriate finite difference formulae. Evaluation of the Cauchy principal-value integrals includes use of Taylor expansions of the integrand about a point, singularity removal by some elementary transformations and singularity subtraction leaving a singular integral plus a natural-logarithm term. Ordinary integrals are calculated using Simpson's rule. Finally, iterative methods are employed to solve the resulting set of nonlinear algebraic equations.

An analysis of Newton iteration numerical methods is carried out by Junghanns (1994) [42] for some classes of nonlinear singular integral equations. It might be useful to mention at this stage that Varley & Walker (1989) [89] obtain analytical solutions (not numerical) to certain classes of linear singular integro-differential equations over an infinite range. However, the closed-form solution of nonlinear singular integro-differential equations over a finite range still remains an open question.

2.2 A Model for Dryout Front Position

We now proceed to develop a mathematical model in order to allow predictions to be made for the length to the dryout point. As mentioned in chapter 1 section (1.1.2), the annular flow region is characterised by the transfer of mass at the interface between the liquid film

and the gas core. Suggested mechanisms by which this phenomenon occurs are entrainment of liquid drops from the liquid film to the gas core due to undercutting of crests on the film free surface, deposition of liquid drops from the gas core and evaporation in the liquid film. Typically, the liquid in the thin film is superheated (see for example Kirillov *et al*, 1985; Higuera, 1987; Prosperetti & Plesset, 1984) [46], [39], [67] and therefore evaporates at the interface between the liquid film and the gas core. This superheating is possibly due to suppression of a complex phenomenon of heterogeneous nucleation and ordinary boiling by, for example, either heating or depressurising the liquid very rapidly (Higuera, 1987) [39]. The rate of evaporation depends on the external heat flux supplied to the boiling pipes. At the operating conditions of interest the results of Collier (1972) [19] suggest that neither entrainment nor deposition occurs rapidly. Therefore, we assume the dryout phenomenon is mainly driven by evaporation of the liquid film. Deposition, as one might expect, seems to be directly proportional to the concentration of liquid droplets in the gas core (Whalley, 1977, 1987; Fisher & Pearce, 1993) [91], [92], [29] while on the other hand, the process of droplet entrainment appears to be a subtle matter. We adopt a simple approach in modelling this problem, since in any mathematical modelling of a problem it is always good practice to build a model from the simplest foundations (Alpabhai *et al*, 1997) [1]. It is rarely successful to try and combine all realistic features into a model from the start. It should be noted, however, that adjustments can be made in our models to account for these other factors. In this study we concentrate exclusively on the problem when the dryout phenomenon is driven by the evaporation process from the liquid film free surface.

2.3 Liquid Film Flow

We proceed by first considering the thin liquid layer adjacent to the heated pipe wall. The flow in the gas core will be considered later. In order to suggest the qualitative details of the flow in the liquid film, some typical parameter values are required. (It should be pointed out that in this study, all of the thermal and physical values have been taken from Schmidt (1969) [72], Irvine & Harnett (1976) [41] as at the pressures of interest, the literature is not unanimous and different sources may give different values.) Typical operating conditions of interest are given by parameter values in the nomenclature table in appendix A. We note, in particular, that typical pipes have an internal radius of order $a \sim 7$ mm. Moreover, liquid layer thicknesses and velocities of order $h_0 \sim 0.1$ - 1 mm and $U \sim 1$ cm/sec, respectively, are considered typical. The pressure throughout the whole system is close to 200 bar so that the saturation temperature of water is given by $T_s = 365°\text{C}$. On entry to the pipe, the water has a temperature of 240°C and thus has a density of 491 kg/m^3. For a typical mass flux of 2000 kg/m^2/sec the water velocity at the pipe entry is thus about 4.07 m/sec. At the top of the

pipe where all the water has been converted to steam, the vapour has density 171 kg/m^3 and by mass conservation the gas velocity here is thus approximately 11.70 m/sec.

We assume that the film consists of an incompressible Newtonian fluid (since water has a low molecular weight, approximately 18.015 (Lide & Frederiskse, 1996 - 1997) [50], and is thus a Newtonian fluid (Skelland, 1967) [74]). The layer is evaporating so that at the vapour-liquid interface there is mass loss, momentum transfer and energy consumption. The liquid in the thin film is superheated and therefore non-boiling except at the free boundary where it is assumed to be at the saturation temperature. We also assume that initially the free surface is not disturbed, i.e. there is no rippling. Since $h_0/a \ll 1$, we analyse a two-dimensional problem and neglect the effects of axisymmetry. Without loss of generality, we study the flow in horizontally orientated pipes. We employ Cartesian coordinates to describe the system; the schematic configuration is shown in figure (2.1). We assume that $x = 0$ corresponds to an initial measurement of the film thickness $y = h(x,t)$, while $x = L(t)$ corresponds to the dimensional length to the dryout point and is to be determined. The coordinates x and y are the lateral and vertical coordinates respectively, and t denotes time. Under

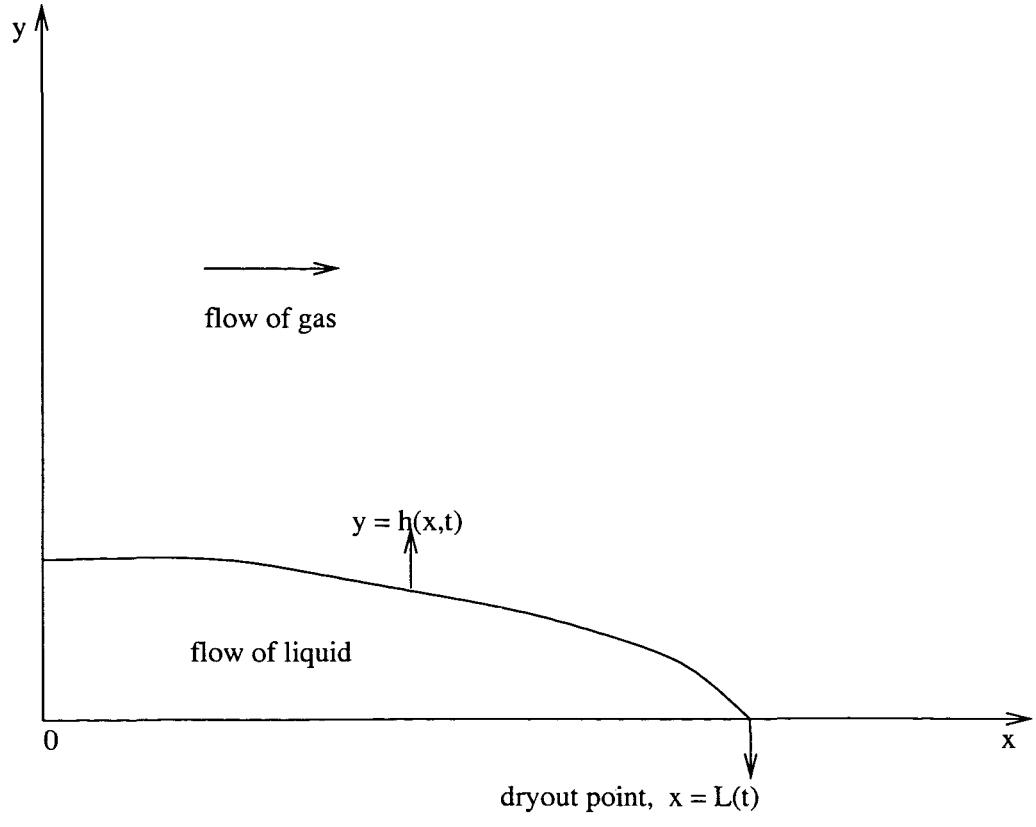

Figure 2.1: A schematic representation of the liquid-gas interface relative to the liquid film.

these circumstances, the flow in the liquid film is governed by the standard two-dimensional

Navier-Stokes equations

$$\begin{aligned} u_x + v_y &= 0, \\ \rho\left(u_t + uu_x + vu_y\right) &= -p_x + \mu\left(u_{xx} + u_{yy}\right), \\ \rho\left(v_t + uv_x + vv_y\right) &= -\rho g - p_y + \mu\left(v_{xx} + v_{yy}\right), \end{aligned} \tag{2.1}$$

where u and v are the x and y components of velocity $\mathbf{q}$ of the liquid respectively and p is pressure in the liquid film. The constants ρ and μ are the density and dynamic viscosity of the liquid respectively, and g is the acceleration due to gravity in the system. Typical values for μ and ρ at the operating conditions of interest are approximately given by 6.44×10^{-5} N sec/m^2 and 491 kg/m^3, respectively.

2.3.1 Interfacial Mass and Momentum Balances

The equations are now closed by prescribing appropriate conditions at the boundaries. At the vapour-liquid interface $y = h(x,t)$, there is a transfer of mass from the liquid layer into the gas core by a phase change at a yet unknown rate. On denoting the mass per unit area per unit time transferred from the liquid to the gas by $\dot{M}$, and assuming that any mass escaping at the free surface does so in the direction of the outward-pointing normal of the free surface (since the mass in the tangential direction is not escaping, it is still part of the film free surface), we have (Delhaye, 1974) [24]

$$\dot{M} = \rho\left(\mathbf{q} - \mathbf{q}_i\right) \cdot \hat{\mathbf{n}}, \tag{2.2}$$

where $\mathbf{q}_i$ is the velocity of the interface whose components are obtained from the kinematic condition of the free surface,

$$v_i = h_t + u_i h_x, \tag{2.3}$$

and $\hat{\mathbf{n}}$ is the outward-pointing unit normal to the interface. In two dimensions, $\hat{\mathbf{n}}$ is given by

$$\hat{\mathbf{n}} = \left(h_x^2 + 1\right)^{-\frac{1}{2}} \begin{pmatrix} -h_x \\ 1 \end{pmatrix}.$$

Thus, in two dimensions $\dot{M}$ is given by

$$\dot{M} = \rho\left\{-\left(u - u_i\right) h_x + v - v_i\right\} \left(h_x^2 + 1\right)^{-\frac{1}{2}}.$$

Hence the application of (2.3) yields

$$\dot{M} = \rho\left(-h_x u - h_t + v\right) \left(h_x^2 + 1\right)^{-\frac{1}{2}}. \tag{2.4}$$

We now assume that surface tension s is a constant s_0. This is a valid approximation since we assume, in the analysis, that all of the interface is at the saturation temperature T_s and

therefore, if the surface tension is represented by an equation of state $s = s_0 - \gamma(T - T_s)^r$ (where $r = 1, 2$ e.g. $r = 1$, Pearson (1958) [60], Davis (1987) [22] and Burelbach *et al* (1988) [14]; $r = 2$, Oron & Rosenau (1994) [59]) for the surface tension gradient γ, for example, then $s = s_0$ the surface tension at the saturation temperature of the liquid. It should be mentioned however, that surface tension may also depend on other scalar fields like the electrical field and the concentration of foreign materials on the interface (Levich & Krylov, 1968) [48]; for simplicity we consider a clean interface here. With this assumption of constant surface tension, it implies that all the surface tension gradient terms are equal to zero. Thus, the shear stress at the interface effectively vanishes so that conservation of momentum tangential to the interface (Levich & Krylov, 1968) [48] yields

$$\dot{M}\left(\mathbf{q} - \mathbf{q}_g\right) \cdot \hat{\mathbf{t}} - \left(\boldsymbol{\Upsilon} - \boldsymbol{\Upsilon}_g\right) \cdot \hat{\mathbf{n}} \cdot \hat{\mathbf{t}} = 0, \tag{2.5}$$

where $\hat{\mathbf{t}}$ is the tangential unit vector to the interface, $\mathbf{q}_g = (u_g, v_g)$ denotes the velocity in the gas core and it is not yet known, $\boldsymbol{\Upsilon}$ and $\boldsymbol{\Upsilon}_g$ are appropriate stress tensors of the liquid and the vapour respectively. The term $\dot{M}\left(\mathbf{q} - \mathbf{q}_g\right) \cdot \hat{\mathbf{n}}$ is a reactive pressure at the interface known as vapour recoil (Burelbach *et al*, 1988; Bankoff, 1971) [14], [8] exerted by the vapour leaving normal to the interface. Both $\boldsymbol{\Upsilon}$ and $\boldsymbol{\Upsilon}_g$ are assumed to take an explicit form given by

$$\boldsymbol{\Upsilon} = \begin{pmatrix} 2\mu u_x & \mu\left(u_y + v_x\right) \\ \mu\left(u_y + v_x\right) & 2\mu v_y \end{pmatrix}, \tag{2.6}$$

$$\boldsymbol{\Upsilon}_g = \begin{pmatrix} 2\mu_g u_{gx} & \mu_g\left(u_{gy} + v_{gx}\right) \\ \mu_g\left(u_{gy} + v_{gx}\right) & 2\mu_g v_{gy} \end{pmatrix}. \tag{2.7}$$

That is, for simplicity, we have assumed that the flow in the gas core is also incompressible. The validity of the latter assumption will be justified later in section (2.4). We then define the tangential traction $\tau(x,t)$ exerted on the free surface of the liquid film by the fast moving in the core by

$$\boldsymbol{\Upsilon}_g \cdot \hat{\mathbf{n}} \cdot \hat{\mathbf{t}} = -\tau \hat{\mathbf{t}} \cdot \hat{\mathbf{t}}.$$

Thus, in two dimensions, τ is given by

$$\tau = \left\{\mu_g\left(u_{gy} + v_{gx}\right)\left(1 - h_x^2\right) + 2\mu_g h_x\left(v_{gy} - u_{gx}\right)\right\}\left(1 + h_x^2\right)^{-1}, \tag{2.8}$$

where μ_g is the dynamic viscosity of the vapour. However, for simplicity, we will assume that τ is a known parameter even though this is not a necessary requirement. Therefore, the shear stress boundary condition at the interface gives

$$\mu\left[\left(u_y + v_x\right)\left(1 - h_x^2\right) + 2h_x\left(v_y - u_x\right)\right]\left(1 + h_x^2\right)^{-1} = \tau. \tag{2.9}$$

It should be noted that in deriving equations (2.8) and (2.9), we have employed a no-tangential slip condition at the interface $y = h(x,t)$ in equation (2.5), i.e.

$$(\mathbf{q} - \mathbf{q}_g) \cdot \hat{\mathbf{t}} = 0. \tag{2.10}$$

It should be noticed that the validity of (2.10) holds since neither of the two fluids has been assumed to be inviscid at this stage.

The normal stress boundary condition at the interface balances the normal stress with the product of surface tension times twice the mean Gaussian curvature of the interface (Atherton & Homsy, 1976) [5] so that

$$\dot{M}\,(\mathbf{q} - \mathbf{q}_g) \cdot \hat{\mathbf{n}} - (p - p_g)\,\hat{\mathbf{n}} \cdot \hat{\mathbf{n}} - (\boldsymbol{\Upsilon} - \boldsymbol{\Upsilon}_g) \cdot \hat{\mathbf{n}} \cdot \hat{\mathbf{n}} = s_0 h_{xx} \left(1 + h_x^2\right)^{-\frac{3}{2}}, \tag{2.11}$$

where $p_g(x,t)$ is pressure in the gas core and is yet to be determined. In two dimensions equation (2.11) leads to

$$\left\{\rho\left(-uh_x - h_t + v\right)\left[-h_x\left(u_g - u\right) + v_g - v\right] - 2\mu\left[v_y + u_x h_x^2 - h_x\left(u_y + v_x\right)\right]\right\} \times \left(1 + h_x^2\right)^{-1} + N - (p - p_g) = s_0 h_{xx}\left(1 + h_x^2\right)^{-\frac{3}{2}}, \tag{2.12}$$

where N is given by

$$N = 2\mu_g\left\{v_{gy} + u_{gx}h_x^2 - h_x\left(u_{gy} + v_{gx}\right)\right\}\left(1 + h_x^2\right)^{-1}.$$

Finally, on the solid surface $y = 0$, the no-slip condition implies

$$u = v = 0. \tag{2.13}$$

(It might be important to recall at this stage that $\dot{M}$ is still not yet known. A constitutive equation for $\dot{M}$ is derived in terms of h in section (2.6).)

2.3.2 Nondimensionalisation

In order to compare terms we need to nondimensionalise the variables. Depending on the choice of a timescale, this will lead to various nondimensional models. In the liquid film we set $x = L_0\bar{x}$, $y = \epsilon L_0\bar{y}$, $h = \epsilon L_0\bar{h}$, $u = U\bar{u}$, $v = \epsilon U\bar{v}$, and $p = (\rho U^2/\epsilon^2 Re)\,\bar{p}$, where L_0 is the length to the dryout point in the steady state case and it is unknown, $\epsilon = h_0/L_0$, $Re = UL_0/\nu$ is the Reynolds number and $\nu = \mu/\rho$ is the dimensional kinematic viscosity of the liquid. The scaling with the unknown length L_0 merits some comment. It implies that we have an idea about the order of magnitude for L_0 and that we anticipate (as it is a case in practice) the difference between the unsteady length $L(t)$ and L_0 to be of small order of magnitude.

With these scalings, only two timescales, each determined by the boundary condition (driving the unsteadiness of the problem) at the onset of the annular flow ($x = 0$), are enough. This point will be reiterated again later in this chapter in section (2.6). We first develop our models in detail under the fast timescale $t = (L_0/U)\bar{t}$, and at the end we state and discuss the models under the long timescale $t = (L_0/\epsilon U)\bar{t}$. With the fast timescale $t = (L_0/U)\bar{t}$, equation (2.4) becomes

$$\dot{M} = \rho\epsilon U \left(-\bar{h}_{\bar{x}}\bar{u} - \bar{h}_{\bar{t}} + \bar{v}\right)\left(\epsilon^2\bar{h}_{\bar{x}}^2 + 1\right)^{-\frac{1}{2}}, \tag{2.14}$$

and therefore to lowest order in ϵ we have

$$\dot{M} = \rho U\epsilon \left(-\bar{h}_{\bar{x}}\bar{u} - \bar{h}_{\bar{t}} + \bar{v}\right). \tag{2.15}$$

This effectively fixes the order of magnitude of the mass exchange required to produce dryout in an order $L(t)$ distance. On defining the nondimensional rate of mass flow $\dot{m}$ by $\dot{M} = \rho U\epsilon\dot{m}$, (2.15) becomes

$$\dot{m} = \left(-\bar{h}_{\bar{x}}\bar{u} - \bar{h}_{\bar{t}} + \bar{v}\right). \tag{2.16}$$

In general, equation (2.16) is not valid at the tip where the assumptions of the thin-layer lubrication theory break. There, the velocities in the x and y directions are comparable. Therefore, the problem would need some new scalings near this point. However, for simplicity, we will assume that (2.16) is valid up to the dryout point.

In order to proceed with the analysis of equation (2.16) we need expressions for $\bar{u}$ and $\bar{v}$ in terms of $\bar{h}$. These may be obtained by solving (2.1) subject to (2.9), (2.12) and (2.13). With the above scalings, the nondimensional problem to solve is

$$\begin{aligned}
\bar{u}_{\bar{x}} + \bar{v}_{\bar{y}} &= 0, \\
\epsilon^2 Re\left(\bar{u}_{\bar{t}} + \bar{u}\bar{u}_{\bar{x}} + \bar{v}\bar{u}_{\bar{y}}\right) &= -\bar{p}_{\bar{x}} + \epsilon^2\bar{u}_{\bar{x}\bar{x}} + \bar{u}_{\bar{y}\bar{y}}, \\
\epsilon^2 Re\left(\bar{v}_{\bar{t}} + \bar{u}\bar{v}_{\bar{x}} + \bar{v}\bar{v}_{\bar{y}}\right) &= -\bar{g} - \frac{\bar{p}_{\bar{y}}}{\epsilon^2} + \epsilon^2\bar{v}_{\bar{x}\bar{x}} + \bar{v}_{\bar{y}\bar{y}},
\end{aligned} \tag{2.17}$$

subject to the boundary conditions

$$\left[\left(\bar{u}_{\bar{y}} + \epsilon^2\bar{v}_{\bar{x}}\right)\left(1 - \epsilon^2\bar{h}_{\bar{x}}^2\right) + 2\epsilon^2\bar{h}_{\bar{x}}\left(\bar{v}_{\bar{y}} - \bar{u}_{\bar{x}}\right)\right]\left(1 + \epsilon^2\bar{h}_{\bar{x}}^2\right)^{-1} = \bar{\tau}, \tag{2.18}$$

$$\begin{aligned}
&\left\{\rho U^2\left(-\bar{u}\bar{h}_{\bar{x}} - \bar{h}_{\bar{t}} + \bar{v}\right)\left[-\bar{h}_{\bar{x}}\left(\epsilon\bar{u}_g - \epsilon^2\bar{u}\right) + \left(\bar{v}_g - \epsilon^2\bar{v}\right)\right]\right. \\
&\left. -\frac{2\mu U}{\epsilon L_0}\left[\epsilon\bar{v}_{\bar{y}} + \epsilon^3\bar{u}_{\bar{x}}\bar{h}_{\bar{x}}^2 - \epsilon\bar{h}_{\bar{x}}\left(\bar{u}_{\bar{y}} + \epsilon^2\bar{v}_{\bar{x}}\right)\right]\right\}\left(1 + \epsilon^2\bar{h}_{\bar{x}}^2\right)^{-1} \\
&\qquad + \bar{N} - \frac{\rho U^2}{\epsilon^2 Re}\bar{p} + \epsilon\rho_\infty U_\infty^2\bar{p}_g = S\epsilon\bar{h}_{\bar{x}\bar{x}}\left(1 + \epsilon^2\bar{h}_{\bar{x}}^2\right)^{-\frac{3}{2}}
\end{aligned} \tag{2.19}$$

on $\bar{y} = \bar{h}(\bar{x}, \bar{t})$; and

$$\bar{u} = \bar{v} = 0, \tag{2.20}$$

on $\bar{y} = 0$. The nondimensional quantities $\bar{g}$, $\bar{N}$ and $\bar{\tau}$ are defined by $\bar{g} = (\epsilon^2 Re L_0/U^2)\, g$, $N = (2\mu_g U_\infty/L_0)\,\bar{N}$ and $\tau = (\mu U/\epsilon L_0)\bar{\tau}$, respectively. The dimensional variable N is given by

$$N = \frac{2\mu_g U_\infty}{L_0}\left\{\bar{v}_{g\bar{y}} + \epsilon^2 \bar{h}_{\bar{x}}^2 \bar{u}_{g\bar{x}} - \epsilon \bar{h}_{\bar{x}}\left(\bar{u}_{g\bar{y}} + \bar{v}_{g\bar{x}}\right)\right\}\left(1 + \epsilon^2 \bar{h}_{\bar{x}}^2\right)^{-1},$$

where, in the gas core (cf. section (2.4)), the variables x, y, p_g and $\mathbf{q}_g$ are respectively scaled with $x = L_0\bar{x}$, $y = L_0\bar{y}$, $\mathbf{q}_g = U_\infty \bar{\mathbf{q}}_g \sim \epsilon^{-1} U \bar{\mathbf{q}}_g$ and $p_g = \epsilon \rho_\infty U_\infty^2 \bar{p}_g$. The dimensional parameters U_∞, ρ_∞ and μ_∞ are respectively the typical speed, density and dynamic viscosity of gas far upstream of the dryout point. It should be emphasised though, that the scalings for τ are correct only when $\mu(U/\epsilon\mu_g U_\infty) \sim O(1)$, which can be confirmed, by considering the typical parameter values given in the nomenclature table, that $\mu(U/\epsilon\mu_g U_\infty) \sim 9.58$. The surface tension s_0 has been scaled with $s_0 = (3\mu U/\epsilon L_0)\bar{s}_0$ following several studies of capillary phenomena (see for example Williams & Davis, 1982) [94] where the surface tension is usually scaled with the thickness of the liquid film. We will comment further about the scaling of the surface tension in section (2.6). The nondimensional parameter $S = (\epsilon L_0/\mu U)s_0$ is an inverse capillary number and is therefore a measure of the importance of surface tension effects.

2.3.3 Thin-Layer Lubrication Analysis

Examining the orders of magnitude of the dimensionless constants involved, we find that (approximating L_0 using $L_t \sim 6.1$ m - the length of the tube that is heated) $\epsilon \sim 1.64\times10^{-4}$ and $\epsilon^2 Re \sim 0.012$, so that a thin layer analysis is appropriate, $\rho U^2 \sim 0.049$, $\mu U/\epsilon L_0 \sim 6.54\times10^{-4}$, $\mu_g U_\infty/L_0 \sim 6.85 \times 10^{-5}$ which are small too, $\rho U^2/\epsilon^2 Re \sim 4.08$ and $\epsilon\rho_g U_\infty^2 \sim 4.04$ which are both $O(1)$ and thus suggesting that to the leading order pressure is continuous across the interface. The gravitational term $\bar{g} \sim 1.18$ (which is of $O(1)$) and thus $\epsilon^2\bar{g} \sim 3.17 \times 10^{-8}$ is small. (It should be mentioned that even though we develop our models solely for the case of horizontal pipes, it will be shown later however that even for vertical pipes the models, with appropriate definition of variables, still hold.)

To leading order we therefore have to solve the familiar nondimensional lubrication equations

$$\bar{u}_{\bar{x}} + \bar{v}_{\bar{y}} = 0, \tag{2.21}$$

$$\bar{p}_{\bar{x}} = \bar{u}_{\bar{y}\bar{y}}, \tag{2.22}$$

$$\bar{p}_{\bar{y}} = 0, \tag{2.23}$$

subject to the boundary conditions

$$\bar{u}_{\bar{y}} = \bar{\tau}, \qquad \text{on } \bar{y} = \bar{h}(\bar{x}, \bar{t}), \tag{2.24}$$

and

$$\bar{u} = \bar{v} = 0 \qquad \text{on } \bar{y} = 0. \tag{2.25}$$

In addition, $\bar{p} = \bar{p}(\bar{x}, \bar{t})$ is continuous across the interface and hence will be determined by the dynamics in the gas core.

On solving (2.21), (2.22) and (2.23) for $\bar{u}$ and $\bar{v}$ subject to conditions (2.24) and (2.25) we obtain

$$\begin{aligned} \bar{u} &= \frac{1}{2}\bar{p}_{\bar{x}}\bar{y}\left(\bar{y} - 2\bar{h}\right) + \bar{\tau}\bar{y}, \\ \bar{v} &= \frac{1}{6}\bar{p}_{\bar{x}\bar{x}}\bar{y}^2\left(3\bar{h} - \bar{y}\right) + \frac{1}{2}\bar{p}_{\bar{x}}\bar{y}^2\bar{h}_{\bar{x}} - \frac{1}{2}\bar{\tau}_{\bar{x}}\bar{y}^2. \end{aligned} \tag{2.26}$$

Substituting (2.26) into (2.16) we get a nondimensional equation for $\bar{h}$ in terms of $\dot{m}$

$$\dot{m} = \left(\frac{1}{3}\bar{p}_{\bar{x}}\bar{h}^3 - \frac{1}{2}\bar{\tau}\bar{h}^2\right)_{\bar{x}} - \bar{h}_{\bar{t}}, \tag{2.27}$$

where $\bar{p}_{\bar{x}}$ is to be derived in section (2.4).

2.4 Gas Core Flow

In order to find an expression for $\bar{p}_{\bar{x}}$ in terms of $\bar{h}$ and therefore close equation (2.27), we have to take into account the flow in the gas core. We assume that in the gas core, far away from the interface, the gas is inviscid (this assumption is discussed further later on in this section). In addition, velocities are much higher in the vapour core than in the liquid film (Prosperetti & Plesset, 1984) [67]. Hence the changes in the vapour density originating at the liquid-vapour interface are quickly convected away from the interface. As a result, we take the vapour density as a constant in this study so that we have an incompressible flow of gas in the core. Essentially, in the gas core, we assume an inviscid and irrotational incompressible flow of gas in which the Bernoulli equation

$$\phi_t + \frac{1}{2}\left(u_g^2 + v_g^2\right) + gy + \frac{p_g}{\rho_g} = C(t), \tag{2.28}$$

holds, for some function $C(t)$. We treat the flow in the liquid film adjacent to the pipe wall as a perturbation to the main flow in the gas core (see Figure (2.2)). The function $\phi(x, y, t)$ is the velocity potential of the gas and therefore, the velocity components u_g and v_g respectively satisfy $u_g = \phi_x$ and $v_g = \phi_y$. All other variables are as defined earlier, but are written with a subscript g to signify their reference to the gas. Since the flow in the gas core is inviscid and irrotational, it satisfies the Laplace equation

$$\phi_{xx} + \phi_{yy} = 0. \tag{2.29}$$

The assumption that the flow of gas in the core is inviscid warrants some discussion. If the gas flow is inviscid it implies that the stress exerted is normal to the liquid-vapour interface, i.e. there is no shear stress. In the previous section (2.3) however, we have assumed that

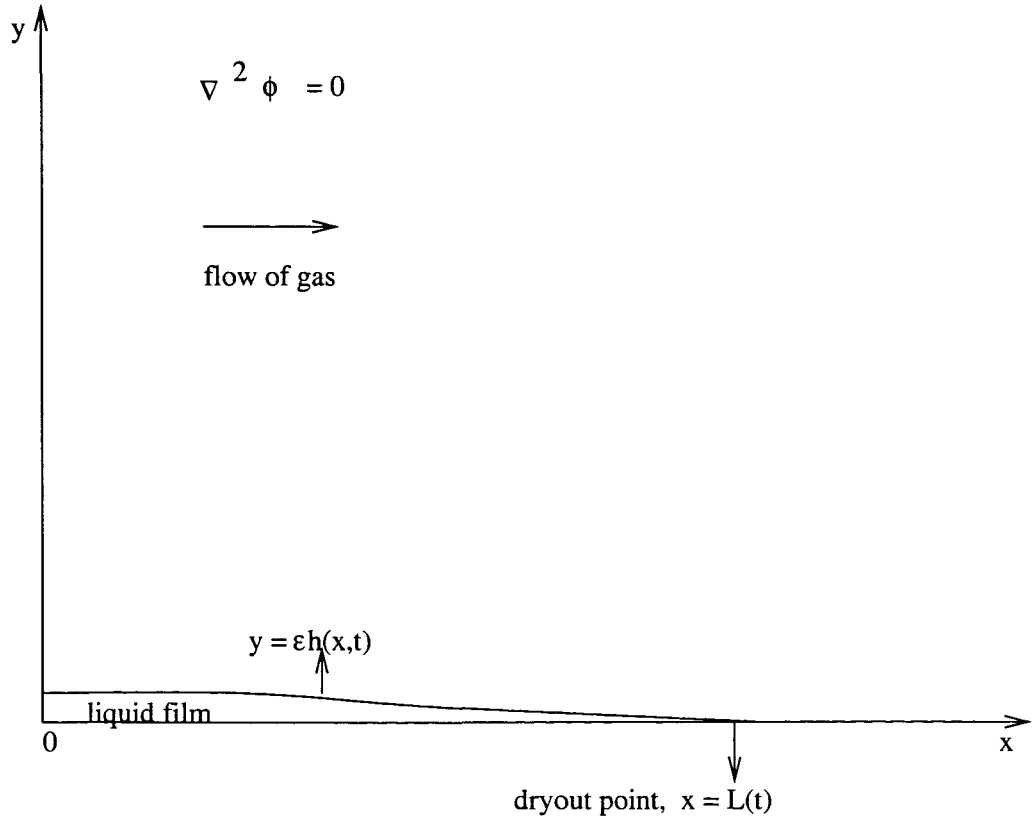

Figure 2.2: A schematic representation of the liquid-gas interface relative to the gas core.

the fast flowing gas in the core provides a tangential traction on the liquid film free surface; therefore the gas cannot be totally inviscid. We can expect, due to viscous effects, that adjacent to the liquid film free surface there is a thin gas-flow viscous boundary layer. The traction (in general a function of x and t) that is supposed to be produced by this boundary layer on the liquid film is alternatively provided by the traction parameter τ as explained earlier in section (2.3). Furthermore, on assuming that the liquid film is sufficiently thin and streamlined in such a way that separation cannot occur then we can treat the rest of the gas in the core as inviscid (Newman, 1977; King & Tuck, 1993) [56], [45]. It should be pointed out that in reality the flow in the gas is turbulent, see for example Kirillov *et al* (1985) [46]. However, as a first approximation which captures the modelling and analytical study of this problem we adopt, for simplicity, a laminar flow.

2.4.1 Nondimensionalisation

We now proceed by nondimensionalising the variables in the gas core. It is appropriate to set $p_g = \epsilon\rho_\infty U_\infty^2 \bar{p}_g$, $x = L_0\bar{x}$, $y = L_0\bar{y}$, $u_g = U_\infty \bar{u}_g$, $v_g = U_\infty \bar{v}_g$, $h = L_0\bar{h}$, $t = (L_0/U)\bar{t} \sim (L_0/\epsilon U_\infty)\bar{t}$ and $\phi = L_0 U_\infty \bar{\phi}$, where, as mentioned earlier, the dimensional parameters U_∞ and ρ_∞ are respectively typical speed and density of the gas upstream of dryout, far away from the perturbation. This gives

$$\bar{p}_{g\bar{x}} = -\left(\bar{\phi}_{\bar{x}\bar{t}} + \epsilon^{-1}\left[\bar{u}_g\bar{u}_{g\bar{x}} + \bar{v}_g\bar{v}_{g\bar{x}}\right]\right), \tag{2.30}$$

from Bernoulli's equation (2.28), and

$$\bar{\phi}_{\bar{x}\bar{x}} + \bar{\phi}_{\bar{y}\bar{y}} = 0, \tag{2.31}$$

from the Laplace equation (2.29).

We now have to specify appropriate boundary conditions. Far away from the perturbation, the disturbance must vanish hence we must have

$$\bar{\phi}_{\bar{x}} \to 1, \ \bar{\phi}_{\bar{y}} \to 0, \qquad \text{as } \bar{x}^2 + \bar{y}^2 \to \infty. \tag{2.32}$$

On $y = \epsilon h(x,t)$, mass conservation dictates that

$$\dot{M} = -\rho_g\left(\mathbf{q}_g - \mathbf{q}_i\right)\cdot\hat{\mathbf{n}}. \tag{2.33}$$

In two dimensions, to leading order, equation (2.33) leads to

$$\dot{M} = -\rho_g U_g\left(-\epsilon\bar{h}_{\bar{x}}\bar{u}_g - \epsilon^2\bar{h}_{\bar{t}} + \bar{v}_g\right). \tag{2.34}$$

We know, from section (2.3), that $\dot{M} = \rho U\epsilon\dot{m}$. We use this fact and a consistent approximation $U_g \sim U/\epsilon$ (as seen earlier in section (2.3)) to write (2.34) as

$$-\epsilon^2\bar{h}_{\bar{t}} - \epsilon\bar{h}_{\bar{x}}\bar{\phi}_{\bar{x}} + \bar{\phi}_{\bar{y}} + \frac{\rho}{\rho_g}\epsilon^2\dot{m} = 0, \tag{2.35}$$

where we recall that $\bar{u}_g = \bar{\phi}_{\bar{x}}$, $\bar{v}_g = \bar{\phi}_{\bar{y}}$ and (see the nomenclature table) $\rho/\rho_g \sim 2.87$ which is $O(1)$.

2.4.2 Thin Aerofoil Theory Approximation

We now seek an asymptotic expansion of the solution to (2.31) as the thickness parameter $\epsilon \to 0$. In the limit, the liquid film thickness reduces to a line $y = 0$ which causes no disturbance of the flow in the gas core. Thus, the basic solution is the uniform parallel flow with speed U_g. We therefore expect $\bar{\phi}$ to be of the form

$$\bar{\phi}(\bar{x}, \bar{y}, \bar{t}; \epsilon) = \bar{x} + \epsilon\bar{\phi}_1(\bar{x}, \bar{y}, \bar{t}) + \epsilon^2\bar{\phi}_2(\bar{x}, \bar{y}, \bar{t}) + \cdots. \tag{2.36}$$

We adopt standard thin aerofoil theory assumptions (see for example Van Dyke, 1975; Newman, 1977) [88], [56]. We calculate (2.36) at the free boundary $\bar{y} = \epsilon\bar{h}(\bar{x}, \bar{t})$. On assuming that all the $\bar{\phi}_i(\bar{x}, \bar{y}, \bar{t})$ $(i = 1, 2, \cdots)$ are analytic at $\bar{y} = 0$, we then expand the right hand side of (2.36) in Taylor series to obtain

$$\bar{\phi}(\bar{x}, \epsilon\bar{h}, \bar{t}; \epsilon) = \bar{x} + \epsilon\bar{\phi}_1(\bar{x}, 0, \bar{t}) + \epsilon^2\left[\bar{h}\bar{\phi}_{1\bar{y}}(\bar{x}, 0, \bar{t}) + \bar{\phi}_2(\bar{x}, 0, \bar{t})\right] + \cdots.$$

It then follows that

$$\begin{aligned}
\bar{\phi}_{\bar{x}} &= 1 + \epsilon\bar{\phi}_{1\bar{x}}(\bar{x}, 0, \bar{t}) + \epsilon^2\left[\bar{h}_{\bar{x}}\bar{\phi}_{1\bar{y}}(\bar{x}, 0, \bar{t}) + \bar{h}\bar{\phi}_{1\bar{y}\bar{x}}(\bar{x}, 0, \bar{t}) + \bar{\phi}_{2\bar{x}}(\bar{x}, 0, \bar{t})\right] + \cdots, \\
\bar{\phi}_{\bar{y}} &= \epsilon\bar{\phi}_{1\bar{y}}(\bar{x}, 0, \bar{t}) + \epsilon^2\left[\bar{h}_{\bar{y}}\bar{\phi}_{1\bar{y}}(\bar{x}, 0, \bar{t}) + \bar{h}\bar{\phi}_{1\bar{y}\bar{y}}(\bar{x}, 0, \bar{t}) + \bar{\phi}_{2\bar{y}}(\bar{y}, 0, \bar{t})\right] + \cdots.
\end{aligned}$$

Hence equation (2.35) gives

$$\begin{aligned}
-\epsilon^2\bar{h}_{\bar{t}} - \epsilon\bar{h}_{\bar{x}}\left[1 + \epsilon\bar{\phi}_{1\bar{x}}(\bar{x}, \bar{y}, \bar{t}) + \cdots\right] + \epsilon\bar{\phi}_{1\bar{y}}(\bar{x}, \bar{y}, \bar{t}) + \epsilon^2\left[\bar{h}_{\bar{y}}\bar{\phi}_{1\bar{y}}(\bar{x}, \bar{y}, \bar{t}) + \right. \\
\left.\bar{h}\bar{\phi}_{1\bar{y}\bar{y}}(\bar{x}, \bar{y}, \bar{t}) + \bar{\phi}_2(\bar{x}, \bar{y}, \bar{t})\right] + \cdots + \epsilon^2\frac{\rho}{\rho_g}\dot{m} = 0,
\end{aligned} \tag{2.37}$$

at $\bar{y} = 0$. The velocity potential $\bar{\phi}(\bar{x}, \bar{y}, \bar{t}; \epsilon)$ in (2.31) thus satisfies, to order ϵ,

$$\bar{\phi}_{1\bar{x}\bar{x}} + \bar{\phi}_{1\bar{y}\bar{y}} = 0,$$

subject to the boundary conditions (from (2.32) and (2.37) respectively)

$$\begin{aligned}
\bar{\phi}_{1\bar{x}} = 0,\ \bar{\phi}_{1\bar{y}} = 0, \qquad &\text{as} \quad \bar{x}^2 + \bar{y}^2 \to \infty, \\
\bar{\phi}_{1\bar{y}} = \bar{h}_{\bar{x}}, \qquad &\text{on} \quad \bar{y} = 0.
\end{aligned}$$

By representing the interface $\bar{y} = \epsilon\bar{h}(\bar{x}, \bar{t})$ as a distribution of sinks and sources along the x-axis, an appropriate velocity potential for the gas flow is given by

$$\bar{\phi}_1 = \frac{1}{2\pi}\int_{-\infty}^{1+l(\bar{t})} f(\xi, \bar{t}) \ln\left((\bar{x} - \xi)^2 + \bar{y}^2\right) d\xi, \tag{2.38}$$

where $f(\xi,\bar{t})$ is unknown and has to be determined. It has been assumed, for simplicity, that $L(\bar{t})$ can be written as $L(\bar{t}) = L_0 + G(\bar{t})$ for some function $G(\bar{t})$. Therefore $l(\bar{t})$ is defined by $l(\bar{t}) = G(\bar{t})/L_0$ and it is also not known at this stage. It should be mentioned that $L(\bar{t})$ may be written in other forms; however the current form is convenient for the linear stability analysis of this problem that takes place later in this thesis.

The mass conservation at $y = \epsilon h(x,t)$, equation (2.33), warrants some comment. In the light of the above systematic analysis, (2.33) suggests that, since $\dot{M}$ is $O(\epsilon)$ and the flow velocity is much higher in the gas core than in the liquid film then as far as the gas core flow is concerned, the interface $y = \epsilon h(x,t)$ is a streamline. Thus the boundary condition that must be imposed is

$$-\epsilon^2 \bar{h}_{\bar{t}} - \epsilon \bar{h}_{\bar{x}} \bar{\phi}_{\bar{x}} + \bar{\phi}_{\bar{y}} = 0, \qquad \text{at } \bar{y} = \epsilon \bar{h}.$$

On differentiating $\bar{\phi}_1$ in (2.38) with respect to $\bar{y}$ we obtain

$$\bar{\phi}_{1\bar{y}} = \frac{1}{\pi} \int_{-\infty}^{1+l(\bar{t})} f(\xi,\bar{t}) \frac{\bar{y}}{(\bar{x}-\xi)^2 + \bar{y}^2} d\xi. \tag{2.39}$$

Taking the limit of $\bar{\phi}_{1\bar{y}}$ as $\bar{y} \to 0$ and applying the boundary condition at $\bar{y} = 0$ we get

$$\lim_{\bar{y}\to 0} \bar{\phi}_{1\bar{y}} = \frac{f(\bar{x},\bar{t})}{\pi} = \frac{\bar{h}_{\bar{x}}}{\pi}, \tag{2.40}$$

where (2.40) is obtained from (2.39) by observing that as $\bar{y} \to 0$ the integrand tends to zero except for the point $\xi = \bar{x}$. At this point, the integrand tends to infinity. Thus, $\bar{y}\{(\bar{x}-\xi)^2 + \bar{y}^2\}^{-1}$ behaves like a delta Dirac function and hence we obtain (2.40). It then follows that $\bar{u}_g$ and $\bar{v}_g$ respectively satisfy

$$\bar{u}_g = \bar{\phi}_{\bar{x}} = 1 + \epsilon \lim_{\bar{y}\to 0} \bar{\phi}_{1\bar{x}} = 1 + \frac{\epsilon}{\pi} \fint_{-\infty}^{1+l(\bar{t})} \frac{\bar{h}_\xi(\xi,\bar{t})}{\bar{x}-\xi} d\xi, \tag{2.41}$$

$$\bar{v}_g = \frac{\epsilon}{\pi} \lim_{\bar{y}\to 0} \bar{\phi}_{1\bar{y}} = \epsilon \bar{h}_{\bar{x}}(\bar{x},\bar{t}), \tag{2.42}$$

where $\fint$ denotes a Cauchy Principal Value integral. Therefore, from equations (2.30), (2.41) and (2.42), on assuming that $\bar{h}_{\bar{x}}(\bar{x},\bar{t}) = 0$ for $\bar{x} \le 0$, an expression for $\bar{p}_{g\bar{x}}$ is given by

$$\bar{p}_{g\bar{x}} = -\frac{\epsilon}{\pi} \left(\fint_0^{1+l(\bar{t})} \frac{\bar{h}_\xi(\xi,\bar{t})}{\bar{x}-\xi} d\xi \right)_{\bar{x}\bar{t}} - \frac{1}{\pi} \left(\fint_0^{1+l(\bar{t})} \frac{\bar{h}_\xi(\xi,\bar{t})}{\bar{x}-\xi} d\xi \right)_{\bar{x}} - \epsilon \left\{ \frac{1}{\pi^2} \fint_0^{1+l(\bar{t})} \frac{\bar{h}_\xi(\xi,\bar{t})}{\bar{x}-\xi} d\xi \times \left(\fint_0^{1+l(\bar{t})} \frac{\bar{h}_\xi(\xi,\bar{t})}{\bar{x}-\xi} d\xi \right)_{\bar{x}} + \frac{1}{\pi} \bar{h}_{\bar{x}} \bar{h}_{\bar{x}\bar{x}} \right\}.$$

Therefore, to lowest order, the equation for the dimensional pressure gradient in the gas core is

$$p_{gx} = \frac{\rho_\infty U_\infty^2 \epsilon}{L_0} \left\{ \frac{1}{\pi} \left(\fint_0^{r(\bar{t})} \frac{\bar{h}_\xi(\xi,\bar{t})}{\xi-\bar{x}} d\xi \right)_{\bar{x}} \right\}, \tag{2.43}$$

where $r(\bar{t}) = 1 + l(\bar{t})$.

The assumption that $\bar{h}_{\bar{x}}(\bar{x},\bar{t}) = 0$ for all $\bar{x} \leq 0$ warrants some discussion. This assumption implies that at all times the film layer is flat for all $\bar{x} \leq 0$. This is obviously untrue as it has already been discussed earlier that prior to the annular region, there are some several complicated flow regimes. We however argue that, since the annular flow regime occupies most of the boiler tube, there should be a point along the pipe where the annular flow regime is of constant thickness (even if it was not flat, but the shape was known, then this could easily be included). Therefore, for practical simplifications, we measure the length to the dryout from this point. This assumption will be revisited again later in the analysis.

2.5 Shear Stress Constitutive Law

Concerning a constitutive equation for the tangential stress τ, we will assume here (in order to keep the amount of algebra manageable when computing the solutions to this problem later in this study) that τ (and hence $\bar{\tau}$) is a known prescribed constant. A constitutive equation that has been adopted in the literature is a simple law $\tau = f_{gw}\rho_\infty U_\infty^2/2$ (Thwaites, 1960; Sadatomi *et al*, 1993; King & Tuck, 1993) [85], [71], [45]. With the current scalings then the nondimensional shear stress would be $\bar{\tau} = f_{gw}\epsilon L_0\rho_\infty U_\infty^2/2\mu U$. The parameter $f_{gw} \geq 0$, in the thin layer approximation, is the coefficient of friction of steam on the wet pipe wall. Since $\bar{\tau}$ is expected to be of order 1, it then implies that f_{gw} should be small. In general, f_{gw} is not known. It may however be determined empirically and experimentally for different materials in various conditions of interest (see for example Whalley, 1987) [92]. In a general case under the current conditions, the constitutive equation for the dimensional τ should be given by equation (2.8)

$$\tau = \frac{\mu_g U_\infty}{L_0}\left[(\bar{u}_{g\bar{y}} + \bar{v}_{g\bar{x}})\left(1 - \epsilon^2\bar{h}_{\bar{x}}^2\right) + 2\epsilon\bar{h}_{\bar{x}}\left(\bar{v}_{g\bar{y}} - \bar{u}_{g\bar{x}}\right)\right]\left(1 + \epsilon^2\bar{h}_{\bar{x}}^2\right)^{-1}.$$

Expressions for $\bar{u}_g$ and $\bar{v}_g$ at the unknown liquid free surface are obtained from the thin aerofoil theory, equations (2.41) and (2.42) respectively, so that to leading order

$$\tau = \frac{\epsilon\mu_g U_\infty}{L_0}\bar{h}_{\bar{x}\bar{x}}.$$

Thus the nondimensional $\bar{\tau}$, under the current scalings, should be given by

$$\bar{\tau} = \frac{\epsilon\mu_g U_\infty}{\mu U}\bar{h}_{\bar{x}\bar{x}} \sim \frac{\mu_g}{\mu}\bar{h}_{\bar{x}\bar{x}}.$$

It can be confirmed from the parameter values given in the nomenclature that $\mu_g/\mu \approx 0.54$ which is of $O(1)$. However, as stated earlier, we will assume here for convenience and simplicity that $\bar{\tau}$ is a known constant.

2.6 Mass Transfer Constitutive Law

We proceed to complete the development of the equation (2.27) for a general mass exchange rate $\dot{m}$. In general, $\dot{m}$ depends on the details of the flow conditions and we will calculate these using simple thermodynamics models.

We assume, for reasons explained earlier, that the transfer of mass from the liquid film to the gas core is mainly affected by the evaporation process, i.e. deposition and entrainment are ignored. We further recall that the liquid in the thin film is superheated, hence the mass transfer is due to convective boiling (Whalley, 1987) [92] in which heat is transferred by conduction and convection through the film and evaporation takes place at the liquid-vapour interface. Thus, the interface is regarded as being at the saturation temperature.

On ignoring the viscous dissipation term, the flow of heat in the liquid film is governed by the equation

$$\rho c_p \left(T_t + uT_x + vT_y\right) = k\left(T_{xx} + T_{yy}\right), \tag{2.44}$$

where the parameters c_p and k are respectively the specific heat and thermal conductivity of the liquid (typical values are given in the nomenclature table) and T denotes temperature. In reality, c_p and k will be functions of T but are assumed to be constants here for convenience and simplicity.

2.6.1 Robin Condition

We now have to prescribe appropriate boundary conditions for (2.44). The mass transfer is by phase change at the liquid-vapour interface $y = h(x,t)$, hence, as mentioned earlier, we regard the interface to be at the saturation temperature $T = T_s$. At the pipe wall $y = 0$, we prescribe a general Robin boundary condition

$$kT_y = -\zeta(x,t)\left(T(x,t)|_{y=0} - T_m\right), \tag{2.45}$$

where T_m is the typical temperature of the liquid metal, $\zeta(x,t)$ is the heat transfer coefficient which we regard as "known" and, for thermodynamic reasons (see for example, Babits, 1968; Sprackling, 1991) [7], [83], is required to be a positive quantity.

2.6.1.1 Nondimensionalisation

In order to compare terms in (2.44), we proceed by scaling variables using the thin-layer scalings $x = L_0\bar{x}$, $y = \epsilon L_0\bar{y}$, $u = U\bar{u}$, $v = \epsilon U\bar{v}$, $t = (L_0/U)\bar{t}$ and $T = T_s + \bar{T}\left(T_w - T_s\right)$, to yield

$$\bar{T}_{\bar{t}} + \bar{u}\bar{T}_{\bar{x}} + \bar{v}\bar{T}_{\bar{y}} = \frac{k}{L_0\rho U c_p}\left(\bar{T}_{\bar{x}\bar{x}} + \frac{1}{\epsilon^2}\bar{T}_{\bar{y}\bar{y}}\right), \tag{2.46}$$

where T_w is a typical wall temperature. On using the typical parameter values given in the nomenclature table, it may be confirmed that

$$\begin{aligned} \frac{k}{L_0 \rho U c_p \epsilon^2} &\sim 32.76, \\ \frac{k}{L_0 \rho U c_p} &\sim 8.81 \times 10^{-7}. \end{aligned}$$

Thus to the lowest order, equation (2.46) reduces to

$$\bar{T}_{\bar{y}\bar{y}} = 0. \tag{2.47}$$

In nondimensional variables (2.45) is

$$\bar{T}_{\bar{y}} = -\bar{V}(\bar{x}, \bar{t}), \tag{2.48}$$

where $\bar{V}(\bar{x}, \bar{t})$ is defined by

$$\bar{V}(\bar{x}, \bar{t}) = \frac{\epsilon L_0}{k} \zeta(x, t) \frac{T|_{y=0} - T_s}{T_w - T_m}.$$

On solving (2.47) subject to (2.45) and $T = T_s$ at $y = h(x, t)$ we obtain

$$\bar{T} = \bar{V}(\bar{x}, \bar{t})(\bar{h}(\bar{x}, \bar{t}) - \bar{y}).$$

2.6.2 Stefan Condition

The change of phase as the liquid boils at the interface must now be considered. On assuming that the temperature in the gas core remains constant and neglecting the surface entropy term, the standard Stefan condition (see for example Rubinstein, 1971) [69] asserts that

$$[kT_y]^{gas}_{liquid} = -\rho \frac{D}{Dt}(y - h(x,t)) \left\{ \lambda + \frac{1}{2} \left(\{(\mathbf{q}_g - \mathbf{q}_i) \cdot \hat{\mathbf{n}}\}^2 - \{(\mathbf{q} - \mathbf{q}_i) \cdot \hat{\mathbf{n}}\}^2 \right) \right\}, \tag{2.49}$$

where the square brackets indicate the jump in a quantity from the liquid to the gas side, λ is the latent heat of vapourisation of the liquid (typical value is given in the nomenclature table), $D/Dt = \partial_t + \mathbf{q} \cdot \nabla$ is the usual material derivative and, we recall, $\mathbf{q}_i$ is the velocity of the interface. Physically, this condition says that the thermal energy, which is conducted to the interface from the liquid side, is partly conducted away into the vapour and in part used to cause the phase change.

2.6.2.1 Nondimensionalisation

On invoking the thin-layer scalings $x = L_0 \bar{x}$, $y = \epsilon L_0 \bar{y}$, $h = \epsilon L_0 \bar{h}$, $u = U\bar{u}$, $v = \epsilon U \bar{v}$, $t = (L_0/U)\bar{t}$ and $T = T_s + \bar{T}(T_w - T_s)$ to nondimensionalise variables, equation (2.49) becomes

$$\bar{T}_{\bar{y}} = -(\bar{v} - \bar{u}\bar{h}_{\bar{x}} - \bar{h}_{\bar{t}}) \left\{ \eta + \frac{\epsilon^3 \rho L_0 U}{2} \left[U_\infty^2 (-\bar{u}_g \bar{h}_{\bar{x}} + \bar{v}_g - \bar{h}_{\bar{t}})^2 - U^2 (-\bar{u}\bar{h}_{\bar{x}} + \bar{v} - \bar{h}_{\bar{t}})^2 \right] \right\}, \tag{2.50}$$

where $\eta = (U\rho L_0 \lambda \epsilon^2/k\,(T_w - T_s))$ is a nondimensional parameter which, as the analysis will show, characterises the transfer of mass from the liquid film into the gas core. From the typical values given in the nomenclature table, we observe that

$$\frac{\epsilon^3 \rho L_0 U U_\infty^2}{2} \sim \frac{\epsilon \rho L_0 U^3}{2} \sim 2.46 \times 10^{-7},$$
$$\frac{\epsilon^3 \rho L_0 U^3}{2} \sim 6.59 \times 10^{-15}.$$

Hence, to the leading order, $\bar{T}_{\bar{y}}$ is given by

$$\bar{T}_{\bar{y}} = -\eta\,(\bar{v} - \bar{u}\bar{h}_{\bar{x}} - \bar{h}_{\bar{t}})\,. \tag{2.51}$$

We recall, from equation (2.16), that $\dot{m} = \bar{v} - \bar{u}\bar{h}_{\bar{x}} - \bar{h}_{\bar{t}}$, therefore we conclude from (2.51) that

$$\dot{m} = -\frac{\bar{T}_{\bar{y}}}{\eta}. \tag{2.52}$$

Finally equations (2.48) and (2.52) give

$$\dot{m} = \frac{\bar{V}(\bar{x}, \bar{t})}{\eta}. \tag{2.53}$$

Equation (2.53) is a mass transfer constitutive law. It relates the interfacial mass flux $\dot{m}$ to the heat transfer coefficient at the boundary pipe wall. It thus confirms that the parameter η indeed characterises the mass transfer from the liquid. For $\eta \gg 1$, i.e. a liquid with large latent heat, the mass transfer is small and dryout may not occur. For liquids with small latent heat, the mass transfer is so great that a liquid film may not be established and dryout occurs immediately. For the operating conditions of interest, the typical parameter values given in the nomenclature table imply

$$\eta \sim \frac{1.18}{T_w - T_s},$$

indicating that with a few degrees of superheat in the liquid, dryout will occur at an $O(1)$ distance from the inset of the annular flow.

2.7 The Full Model

Since both the mass transfer and the shear stress constitutive laws are now known, then the final full nondimensional problem that must be solved, from equations (2.27), (2.43) and (2.53), is

$$\frac{\bar{V}}{\eta} = \left\{ \frac{\bar{h}^3}{3\pi} \left(\int_0^{r(\bar{t})} \frac{\bar{h}_\xi(\xi, \bar{t})}{\xi - \bar{x}} d\xi \right)_{\bar{x}} - \frac{\bar{h}^2}{2} \bar{\tau} \right\}_{\bar{x}} - \bar{h}_{\bar{t}}. \tag{2.54}$$

On the long timescale $t \geq (L_0/\epsilon U)\bar{t}$, things change at a rate which is so slow that the problem is equivalent to solving a steady problem at different times, a quasi-steady problem (this can

easily be verified by following similar analysis as above). In this case, equation (2.54) reduces to

$$\frac{\bar{V}}{\eta} = \left\{ \frac{\bar{h}^3}{3\pi} \left(\int_0^{r(\bar{t})} \frac{\bar{h}_\xi(\xi,\bar{t})}{\xi - \bar{x}} d\xi \right)_{\bar{x}} - \frac{\bar{h}^2}{2} \bar{\tau} \right\}_{\bar{x}} . \tag{2.55}$$

It may also easily be verified that timescales greater than $t = (L_0/U)\bar{t}$ are not allowable in the current model. In such cases $\dot{M} \gg O(1)$, relative to the liquid film. Physically, this means that the layer does not form at all.

For vertical pipes, it can be shown (by going through similar analysis as above) that under the current conditions of interest and appropriate redefining of variables, we obtain models very similar to (2.54) and (2.55). That is to say, in the fast timescale $t = (L_0/U)\bar{t}$ for example, the final equation that must be solved is

$$\frac{\bar{V}}{\eta} = \left\{ \frac{\bar{h}^3}{3\pi} \left(\int_0^{r(\bar{t})} \frac{\bar{h}_\xi(\xi,\bar{t})}{\xi - \bar{x}} d\xi \right)_{\bar{x}} - \frac{\bar{h}^2}{2} (\bar{\tau} + \bar{g}) \right\}_{\bar{x}} - \bar{h}_{\bar{t}}, \tag{2.56}$$

where in this case x refers to a vertical Cartesian coordinate and y denotes the lateral ones. It is evident from (2.56) that in this case the gravitational term $\bar{g}$ is important. It should be mentioned however, that solving (2.56) cannot be mathematically different from solving (2.54) as the constant $\bar{g}$ can be absorbed into the traction parameter $\bar{\tau}$. Henceforth we assume that $\bar{\tau}$ includes the effects of gravity.

As a final comment on (2.54), we consider what would happen if surface tension was to be included. In section (2.3), in order to keep the surface tension in the problem, we could scale the surface tension s_0 with $s_0 = (3\mu U/\epsilon^2 L_0)\,\bar{s}_0$ instead of $s_0 = (3\mu U/\epsilon L_0)\,\bar{s}_0$. Thus, in the fast timescale $t = (L_0/U)\,\bar{t}$, to leading order the normal stress boundary condition (2.19) at the interface $\bar{y} = \bar{h}(\bar{x},\bar{t})$ would become

$$-\bar{p} + \bar{C}\bar{p}_g = \bar{S}\bar{h}_{\bar{x}\bar{x}},$$

where $\bar{C}$ and $\bar{S}$ are respectively given by $\bar{C} = \epsilon^3 Re \rho_\infty U_\infty^2/\rho U^2$ and $\bar{S} = S\epsilon^2 Re/\rho U^2$. From the typical parameter values given in the nomenclature table in the appendix, it can be confirmed that $\bar{C} \sim 1.01$ which is of $O(1)$ and $\bar{S} \sim 4.01 \times 10^{-5} S$ (which suggests that the inverse capillary number S has to be very large in order that surface tension effects are important in this problem). The thin aerofoil analysis in section (2.4) together with equations (2.53) and (2.27) lead to a nondimensional equation for $\bar{h}$

$$\frac{\bar{V}}{\eta} = \left\{ \frac{\bar{C}}{3\pi} \bar{h}^3 \left(\int_0^{r(\bar{t})} \frac{\bar{h}_\xi(\xi,\bar{t})}{\xi - \bar{x}} d\xi \right)_{\bar{x}} - \frac{\bar{h}^2}{2} \bar{\tau} \right\}_{\bar{x}} - \bar{h}_{\bar{t}} - \frac{\bar{S}}{3\pi} \left(\bar{h}^3 \bar{h}_{\bar{x}\bar{x}\bar{x}} \right)_{\bar{x}}, \tag{2.57}$$

instead of equation (2.54). In this thesis, we will not generally use equation (2.57) though.

2.7.1 Heat Transfer Coefficient Constitutive Laws

For practical purposes, a constitutive equation for the heat transfer coefficient $\bar{V}(\bar{x},\bar{t})$ in equation (2.53) must be proposed in order to make any progress with calculations on the full model (2.54) (or with (2.55), (2.56) or (2.57)). This may be tackled in a number of ways. Here we will consider a case where the temperature at the pipe wall is assumed to be a known function of x and t, i.e. $T|_{y=0} = T_W(x,t)$. Other ways would include the case when $\bar{V}(\bar{x},\bar{t})$ is assumed to be constant (we will comment again about this case later in this section).

We proceed here by solving equation (2.47) for $\bar{T}$. As mentioned earlier, we assume the temperature at the wall $y = 0$ is a known function of x and t, $T|_{y=0} = T_W(x,t)$. Solution of (2.47) subject to $T = T_s$ on $y = h(x,t)$ and $T = T_W(x,t)$ at $y = 0$ yields

$$\bar{T} = \left(\frac{T_W(x,t) - T_s}{T_w - T_s}\right)\left(1 - \frac{\bar{y}}{\bar{h}}\right). \tag{2.58}$$

In this case, (2.52) gives

$$\dot{m} = \left(\frac{T_W(x,t) - T_s}{T_w - T_s}\right)\frac{1}{\eta\bar{h}}, \tag{2.59}$$

where (2.59) is the constitutive law for the mass transfer. Thus, the constitutive equation for the heat transfer coefficient $\bar{V}(\bar{x},\bar{t})$ in this case, from (2.53), is given by

$$\bar{V}(\bar{x},\bar{t}) = \left(\frac{T_W(x,t) - T_s}{T_w - T_s}\right)\frac{1}{\bar{h}}. \tag{2.60}$$

2.7.2 Constant Wall Temperature Problem

We suppose that in practice boilers, evaporators etc., are arranged in such a way that the wall temperature is as close to constant as possible (in circumstances where this might not be the case, another problem in the liquid metal should be solved). We therefore assume for simplicity that $T_W(x,t) = T_w$, so that (2.59) implies

$$\dot{m} = \frac{1}{\eta\bar{h}}, \tag{2.61}$$

which is singular at the dryout point $\bar{h} = 0$. The final full nondimensional problem that must be solved, from equation (2.54), with $\bar{V}(\bar{x},\bar{t})$ given by $\bar{V}(\bar{x},\bar{t}) = 1/\bar{h}$ from equation (2.61), is then

$$\frac{1}{\eta\bar{h}} = \left\{\frac{\bar{h}^3}{3\pi}\left(\int_0^{r(\bar{t})}\frac{\bar{h}_\xi(\xi,\bar{t})}{\xi - \bar{x}}d\xi\right)_{\bar{x}} - \frac{\bar{h}^2}{2}\bar{\tau}\right\}_{\bar{x}} - \bar{h}_{\bar{t}}. \tag{2.62}$$

Similarly, equations (2.55), (2.56) and (2.57) will respectively become

$$\frac{1}{\eta\bar{h}} = \left\{\frac{\bar{h}^3}{3\pi}\left(\int_0^{r(\bar{t})}\frac{\bar{h}_\xi(\xi,\bar{t})}{\xi - \bar{x}}d\xi\right)_{\bar{x}} - \frac{\bar{h}^2}{2}\bar{\tau}\right\}_{\bar{x}}, \tag{2.63}$$

$$\frac{1}{\eta\bar{h}} = \left\{\frac{\bar{h}^3}{3\pi}\left(\int_0^{r(\bar{t})}\frac{\bar{h}_\xi(\xi,\bar{t})}{\xi - \bar{x}}d\xi\right)_{\bar{x}} - \frac{\bar{h}^2}{2}(\bar{\tau} + \bar{g})\right\}_{\bar{x}} - \bar{h}_{\bar{t}}, \tag{2.64}$$

$$\frac{1}{\eta\bar{h}} = \left\{\frac{\bar{C}}{3\pi}\bar{h}^3\left(\int_0^{r(\bar{t})}\frac{\bar{h}_{\xi}(\xi,\bar{t})}{\xi-\bar{x}}d\xi\right)_{\bar{x}} - \frac{\bar{h}^2}{2}\bar{\tau}\right\}_{\bar{x}} - \bar{h}_{\bar{t}} - \frac{\bar{S}}{3\pi}\left(\bar{h}^3\bar{h}_{\bar{x}\bar{x}\bar{x}}\right)_{\bar{x}}. \tag{2.65}$$

Evidently, the nonlinear singular nature of the above equations renders it extremely unlikely that it will be possible to find closed-form solutions. In the steady state analysis in chapter 3, we solve (2.62) using both asymptotic and numerical techniques. We will begin by considering some special limiting cases which will motivate a numerical method for the full problem. It will also be argued later, in the same chapter, that solving (2.65) numerically should not be fundamentally different from solving (2.62).

2.7.3 A Varying Wall Temperature Problem

As mentioned in section (2.7.2), in the case when the wall temperature is not constant then a problem in the liquid metal should be solved for temperature profiles. However, this is a non-trivial task. It requires careful modelling of the flow problem and the knowledge of pressure (which is in general a function of x and t) in the liquid metal. Further, in some cases (see for example, Ockendon & Ockendon, 1977; Pearson, 177) [57], [61] it may be appropriate to propose a constitutive equation for the liquid metal viscosity (which is in general a function of temperature). It is extremely unlikely that the resulting model could be solved in closed-form. Hence, it is unhelpful for the current purpose. An outline for this problem, in the current conditions of interest, will be briefly presented in section (2.8). Here, we observe that if the temperature at the pipe wall is given by

$$T_W(x,t) = T_s + (T_w - T_s)\bar{h}^2,$$

(in which case $\bar{V}(\bar{x},\bar{t})$ is given by $\bar{V}(\bar{x},\bar{t}) = \bar{h}(\bar{x},\bar{t})$) then from (2.54) we obtain

$$\frac{\bar{h}}{\eta} = \left\{\frac{h^3}{3\pi}\left(\int_0^{r(\bar{t})}\frac{\bar{h}_{\xi}(\xi,\bar{t})}{\xi-\bar{x}}d\xi\right)_{\bar{x}} - \frac{\bar{\tau}}{2}\bar{h}^2\right\}_{\bar{x}} - \bar{h}_{\bar{t}}. \tag{2.66}$$

This problem may not have any obvious physical relevance whatsoever (though it will be seen that the results for this case are realistic). However equation (2.66) is relatively simpler to solve (as it will be seen later in this study) than both equations (2.62) and (2.67). Hence solving (2.66) encourages different numerical techniques (which are tackled in chapter 4) for these types of problems. Further, the steady state solutions to (2.66) help us to explain some of unexpected behaviour in the numerical results (in particular, the pressure profile curves) of equations (2.62) and (2.67).

2.7.4 Constant Wall Heat Flux Problem

In industrial settings, it is customary to assume a constant heat flux at the pipe wall supplied by the liquid metal. In most cases the value of the flux quoted is simply a figure derived from

the known properties of the total heat input provided by the reactor. It is questionable how such a pointwise heat flux may be either measured or maintained, or whether it is reasonable to assume that it does not change along the tube. However, if such is the case, then the equation that must be solved, from (2.66) or (2.54), is

$$\frac{1}{\eta} = \left\{ \frac{\bar{h}^3}{3\pi} \left(\fint_0^{r(\bar{t})} \frac{\bar{h}_{\xi}(\xi, \bar{t})}{\xi - \bar{x}} d\xi \right)_{\bar{x}} - \frac{\bar{\tau}}{2} \bar{h}^2 \right\}_{\bar{x}} - \bar{h}_{\bar{t}}, \tag{2.67}$$

where the nondimensional heat transfer coefficient $\bar{V}(\bar{x}, \bar{t})$ is simply a constant and has been absorbed into the heat mass transfer parameter η in equation (2.67).

2.7.5 Initial and Boundary Conditions of the Full Model

The modelling formulation must be completed by the specification of appropriate initial and boundary conditions. The boundary conditions for this problem are far from trivial. To begin with, it should be observed that (2.62) [or (2.66) or (2.67)] requires the prescription of at least four boundary conditions (the reasons for this will become clearer as we discuss these conditions further in the particular case in chapter 3). At the dryout point, where the liquid film vanishes at all times, the obvious boundary condition to impose is that $\bar{h}(r(\bar{t})) = 0$. The function $r(\bar{t})$ is not known a priori. We require that $\bar{h}(\bar{x}, \bar{t}) \sim (r(\bar{t}) - \bar{x})^p$ as $\bar{x} \to r(\bar{t})$, for the appropriate real value p to be determined as part of solution. We assume that at the onset of the annular flow $\bar{x} = 0$, $\bar{h}(0, \bar{t})$ is known at all times $\bar{t}$. It is convenient to assume that $\bar{h}(0, \bar{t})$ is a constant equal to $\bar{h}_0$ (say) for all $\bar{t}$. Another boundary condition may be obtained by assuming that in practice the pressure at $\bar{x} = 0$ can be measured and therefore it is known. Equally, we may require that $\bar{h}_0$ satisfy the pressure gradient condition (which is obtained by insisting that the mass flux should always vanish at the dryout point) at $\bar{x} = 0$. The final boundary condition comes from the fact that we do not allow infinite values of pressure at $\bar{x} = 0$ so that $\bar{h}_{\bar{x}}(0, \bar{t}) = 0$ (again this condition will become clearer as it is discussed further in chapter 3). As far as the initial conditions are concerned, it is sensible to assume that $\bar{h}(\bar{x}, 0) = \bar{h}(\bar{x})$, for some steady state solution $\bar{h}(\bar{x})$, and $r(\bar{t}) = 1$ at $\bar{t} = 0$.

2.8 Problem in the Liquid Metal

In this section we set up a plausible problem in the liquid metal. This problem should be important for obtaining the boundary temperature to be prescribed at the wall $y = 0$ when solving the problem in the liquid layer. We should mention, however, that it is not our main aim to solve this problem here (since it is highly unlikely that the problem may be solved in closed-form, hence rendering it unhelpful for the purposes of solving any of the problems in the liquid layer). It should be emphasised that we will not return to this problem, but we

just set it up to show that it could be done. Figure (2.3) shows a schematic representation of the whole problem. For convenience, the dryout point is at $x = 0$ measured from the entry to

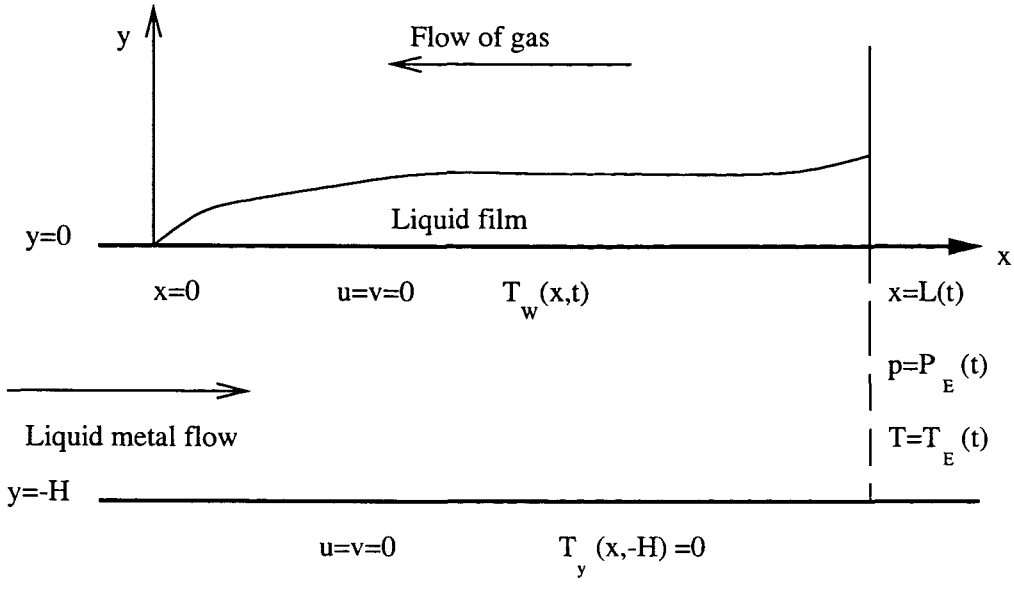

Figure 2.3: A schematic representation of the problem in the liquid metal.

the annular regime at $x = L(t)$. We assume, for simplicity, that the flow in the liquid metal has the characteristic velocity U_m, constant density ρ_m, constant specific heat c_{pm}, constant thermal conductivity k_m, typical temperature T_m and dynamic viscosity $\mu(x,T)$ to account for some essential coupling between the energy and momentum equations.

Considering the pipes (in which the liquid metal flows) whose typical length is approximately equal to the typical length of the steam generating pipes (6.1 m) and possess a characteristic diameter $H \sim 0.012$ m, we consider here a two-dimensional problem. For simplicity and to avoid unnecessary complications, we consider a quasi-steady state and incompressible flow in the liquid metal. It is convenient to write $L(t)$ as $L(t) = L_0 + \delta G(t)$, for some function $G(t)$, L_0 is the length to the dryout point in the steady state case and $\delta(> 0)$ is small and is defined by $\delta = H/L_0$. On approximating L_0 by the characteristic length of the pipe then $\delta \sim 1.97 \times 10^{-3}$.

We now nondimensionalise variables by setting (thin-layer scalings but in a different layer) $x = L_0\bar{x}$, $y = \delta L_0\bar{y} = H\bar{y}$, $u = U_m\bar{u}$, $v = \delta U_m\bar{v}$, $p = (\rho_m U_m^2/\delta^2 Re_m)\,\bar{p}$, $T = T_m + \bar{T}\,(T_w - T_m)$, $t = (L_0/\delta U_m)\,\bar{t}$ and $\mu = \mu_m\bar{\mu}(\bar{x},\bar{T})$ where $Re_m = U_m L_0\rho_m/\mu_m$ and μ_m are respectively the Reynolds number and the typical dynamic viscosity of the flow in the liquid metal. All the other variables retain their usual meanings but they should be understood to refer to the flow in the liquid metal in this section. Under these circumstances, the two-

dimensional Navier-Stokes equations for the flow in the liquid metal become

$$\begin{aligned}
\bar{u}_{\bar{x}} + \bar{v}_{\bar{y}} &= 0, \\
\delta^2 Re_m \left(\delta \bar{u}_{\bar{t}} + \bar{u}\bar{u}_{\bar{x}} + \bar{v}\bar{u}_{\bar{y}}\right) &= -\bar{p}_{\bar{x}} + \delta^2 \left(\bar{\mu}(\bar{x},\bar{T})\bar{u}_{\bar{x}}\right)_{\bar{x}} + \left(\bar{\mu}(\bar{x},\bar{T})\bar{u}_{\bar{y}}\right)_{\bar{y}}, \\
\delta^2 Re_m \left(\delta \bar{v}_{\bar{t}} + \bar{u}\bar{v}_{\bar{x}} + \bar{v}\bar{v}_{\bar{y}}\right) &= -\bar{g} - \frac{\bar{p}_{\bar{y}}}{\delta^2} + \delta^2 \left(\bar{\mu}(\bar{x},\bar{T})\bar{v}_{\bar{x}}\right)_{\bar{x}} + \left(\bar{\mu}(\bar{x},\bar{T})\bar{v}_{\bar{y}}\right)_{\bar{y}}, \\
\delta \bar{T}_{\bar{t}} + \bar{u}\bar{T}_{\bar{x}} + \bar{v}\bar{T}_{\bar{y}} &= A\left(\bar{T}_{\bar{x}\bar{x}} + \frac{1}{\delta^2}\bar{T}_{\bar{y}\bar{y}}\right) + B\bar{\mu}(\bar{x},\bar{T})\left(\frac{\bar{u}_{\bar{y}}}{\delta}\right)^2,
\end{aligned}$$

where the nondimensional parameters $\bar{g}$, A and B are respectively given by

$$\bar{g} = \frac{\delta^2 Re_m L_0}{U_m^2} g,$$

$$A = \frac{k_m}{L_0 \rho_m U_m c_{pm}},$$

and

$$B = \frac{\mu_m U_m}{\rho_m c_{pm} \left(T_w - T_m\right) L_0},$$

where g is, as usual, the acceleration due to gravity and T_w is the typical temperature of the heated pipe wall at $y = 0$. In the energy equation, only the dominant term $(\bar{u}_{\bar{y}}/\delta)^2$ from the viscous dissipation term has been included.

In order to suggest the qualitative details of the flow in the liquid metal, typical orders of magnitude for $\delta^2 Re_m$, A and B are required. However, getting typical parameter values is not easy for this problem. In this section, all the typical physical parameter values for the liquid metal have been taken from Bolz & Tuve (1973) [13] (different sources in the literature may give different values). At typical operating temperatures of 673 K, the physical parameter values for liquid sodium are typically given by $c_{pm} \sim 1280.30$ J/kg/K, $\rho_m \sim 858.56$ kg/m^3, $k_m \sim 71.09$ W/m/K, $\mu_m \sim 2.85 \times 10^{-4}$ Ns/m^2 and $T_m \sim 673$ K while $T_w \sim 640$ K. Therefore, for a typical velocity of $U_m \sim 0.1$ m/s in the liquid metal, $A \sim 1.06 \times 10^{-4}$, $B \sim -7.86 \times 10^{-13}$ and thus $B/\delta^2 \sim 2.01 \times 10^{-7}$ (which is small) while $A/\delta^2 = \bar{A} \sim 27.31$ (and it is of $O(1)$). The parameters $\delta^2 Re_m$ and $\bar{g}$ are typically (and respectively) given by $\delta^2 Re_m \sim 7.13$ (which is of $O(1)$) and $\bar{g} \sim 713g$, where the magnitude of g is $g \sim 9.8$ (hence $\delta^2 \bar{g} \sim 2.77 \times 10^{-3} g$ and it is small).

Therefore, to leading order, the Navier-Stokes equations reduce to

$$\bar{u}_{\bar{x}} + \bar{v}_{\bar{y}} = 0, \tag{2.68}$$

$$\bar{u}\bar{u}_{\bar{x}} + \bar{v}\bar{u}_{\bar{y}} = -\bar{p}_{\bar{x}} + \left(\bar{\mu}(\bar{x},\bar{T})\bar{u}_{\bar{y}}\right)_{\bar{y}}, \tag{2.69}$$

$$\bar{p}_{\bar{y}} = 0, \tag{2.70}$$

$$\bar{u}\bar{T}_{\bar{x}} + \bar{v}\bar{T}_{\bar{y}} = \bar{A}\bar{T}_{\bar{y}\bar{y}}. \tag{2.71}$$

The sensible boundary conditions to impose on the equations (2.68) - (2.71) are $\bar{u} = \bar{v} = 0$, (the no-slip condition) at the pipe boundary walls $\bar{y} = 0$ and $\bar{y} = -1$ and $\bar{T}_{\bar{y}} = 0$ at $\bar{y} = -1$

(i.e. the outer casing wall is assumed to be totally insulated). Finally, we assume that both the dimensional pressure and temperature, $P_E(t)$ and $T_E(t)$ respectively, can be measured and therefore are known at the entry to the annular regime $x = L(t)$. The dimensional temperature $T = T_W(x,t)$ at the pipe wall $y = 0$ is unknown and it has to be found. Since $\bar{\mu}(\bar{x},\bar{T})$ in equation (2.69) does not appear in the energy equation (2.71), then it is reasonable and convenient to treat it as a constant and ignore the dependence on $\bar{x}$.

The system of equations (2.68) - (2.71) is very challenging to solve numerically (due to nonlinearity and coupling of some dependent variables). However, we observe that when the flow in the liquid metal is a fully developed Poiseuille flow at all times, we can then write

$$\bar{u}(\bar{x},\bar{y},\bar{t}) = F(\bar{t})\bar{y}(\bar{y}+1),$$

for some function $F(\bar{t})$. Then we obtain that $\bar{v}(\bar{x},\bar{y},\bar{t}) = 0$ so that the no-slip condition holds at the boundary walls. As a result, equation (2.70) tells us that the pressure $\bar{p}$ is a function of $\bar{x}$ and $\bar{t}$ only. From equation (2.69), in nondimensional form, we have

$$p_x = (\mu u_y)_y,$$

so that on integrating with respect to x we obtain

$$p = \frac{2\mu U_m}{\delta^2 L_0^2} F(t)x + \text{a constant}.$$

We apply the boundary contain $p = P_E(t)$ at $x = L(t)$ to yield

$$p = \frac{2\mu U_m}{\delta^2 L_0^2} F(t)x + P_E(t).$$

Thus, in nondimensional variables, p is given by

$$\bar{p} = 2\bar{\mu}F(\bar{t})(\bar{x}-1) + \bar{P}_E(\bar{t}),$$

to leading order. The nondimensional function $\bar{P}_E(\bar{t})$ is given by

$$\bar{P}_E(\bar{t}) = \frac{\delta^2 Re_m}{\rho_m U_m^2} P_E(t).$$

The dimensional temperature T has to be obtained by solving (2.71)

$$F(t)y\left(\frac{y}{H}+1\right)T_x = AL_0HT_{yy}, \tag{2.72}$$

subject to the boundary conditions $T_y = 0$ at $y = -H$, $T = T_E(t)$ at $x = L(t)$ and $T = T_W(x,t)$ at $y = 0$ is to be calculated. For any given nonzero $F(t)$, (2.72) can only be solved numerically and (for reasons given earlier in this section) we do not pursue this problem any further in this study.

Chapter 3

Steady States for the Constant Wall Temperature Problem

Prior to any attempts to solve the unsteady problem subject to appropriate initial and boundary conditions, it is instructive to analyse and try to understand steady state situations. Owing to the nonlinear singular nature of the governing equation, it is extremely unlikely that the problem can ever be solved in closed-form except for particular special cases. Therefore, it is inevitable that we have to resort to asymptotic and numerical techniques in order to obtain any information from the model. We start by analysing some paradigm problems, mainly to motivate an appropriate numerical method for the full nonlinear problem (steady state version of (2.62)) which will be tackled in section (3.2).

3.1 Limiting Cases and Paradigm Problems

We define $\dot{M}$ by $\dot{M} = Q_x$, where Q is the dimensional rate of mass transfer per unit length at the free surface. In this case the dimensional version of equation (2.27) may be integrated, where we recall that in the liquid film $\dot{M} = \rho U \epsilon \dot{m}$, $x = L_0 \bar{x}$, $h = \epsilon L_0 \bar{h}$, $\tau = (\mu U / \epsilon L_0)\,\bar{\tau}$, $p = (\rho U^2 / \epsilon^2 Re)\,\bar{p}$ and $Re = U L_0 \rho / \mu$. On assuming that p_x is finite at the dryout point $h = 0$ (or if it is not, then at least it does not blow up faster than h^3 tends to zero at this point), we impose, for simplicity, the boundary condition $Q = 0$ there. Under these circumstances we have

$$Q = \frac{\rho}{\mu}\left(\frac{h^3}{3}p_x - \frac{h^2}{2}\tau\right) = \rho L_0 U \epsilon \left(\frac{\bar{h}^3}{3}\bar{p}_{\bar{x}} - \frac{\bar{h}^2}{2}\bar{\tau}\right), \tag{3.1}$$

from which we get

$$p_x = \frac{3\mu U}{\epsilon^2 L_0^2}\left(\frac{\bar{Q}}{\bar{h}^3} + \frac{\bar{\tau}}{2\bar{h}}\right), \tag{3.2}$$

where Q has been appropriately scaled, from (3.1), by $Q = \rho U L_0 \epsilon \bar{Q}$ and $\bar{Q}$ is nondimensional. Comparing equation (3.2) and a steady case of (2.43), i.e. closing the equation by matching the dimensional pressure gradients p_x and p_{gx} across the interface $y = \epsilon h$, leads to

$$\frac{\bar{Q}}{\bar{h}^3} + \frac{\bar{\tau}}{2\bar{h}} = \frac{\theta}{\pi} \left(\fint_0^1 \frac{\bar{h}_\xi(\xi)}{\xi - \bar{x}} d\xi \right)_{\bar{x}}, \tag{3.3}$$

where $\theta = \rho_\infty U_\infty^2 \epsilon^3 L_0 / 3U\mu$ is a nondimensional parameter and measures the relative orders of magnitude of the pressures in the two regions of flow. Using the typical parameter values given in the nomenclature table, it may be confirmed that $\theta \sim 0.32$ and hence is of order 1.

3.1.1 Boundary Conditions

We now need to prescribe appropriate boundary conditions for this problem. We note that due to the nonlinearity and singular nature of these equations, no theory exists to determine sufficient conditions for existence and uniqueness of solutions. However, since equation (3.3) has two derivatives and one Hilbert transform we might expect to specify three conditions to uniquely determine the solution. To emphasise this point we look at an example of a very simple singular integral equation of the finite type

$$\fint_0^1 \frac{\bar{h}_\xi(\xi)}{\xi - \bar{x}} d\xi = 1. \tag{3.4}$$

Equation (3.4) possesses one Hilbert transform and a derivative. However, a general solution of (3.4) is

$$\bar{h}(\bar{x}) = C_2 + C_1 \sin^{-1}(\sqrt{\bar{x}}) - \sqrt{\bar{x}(1 - \bar{x})}. \tag{3.5}$$

Equation (3.5) has two constants, C_1 from the inversion of (3.4) and C_2 from the integration of $\bar{h}_{\bar{x}}(\bar{x})$ with respect to $\bar{x}$. Thus, we would have to specify two boundary conditions in order to obtain a unique solution $\bar{h}(\bar{x})$ from (3.5). Therefore, it is sensible to anticipate prescription of three boundary conditions in order to determine a unique solution to (3.3) if it exists.

The annular flow regime occupies most of the boiler tube, therefore we assume that at some point along the tube, the annular flow regime is of known constant thickness and the gas core pressure is known at this point. Moreover, from the steady state of the Bernoulli equation (2.28), we observe that the dimensional pressure in the gas core, to lowest order, is

$$p_g = p_\infty + \frac{\rho_\infty U_\infty^2 \epsilon}{\pi} \fint_0^1 \frac{\bar{h}_\xi(\xi)}{\xi - \bar{x}} d\xi. \tag{3.6}$$

The dimensional parameter p_∞ is the typical pressure in the gas core far upstream of dryout. At $\bar{x} = 0$ equation (3.6) yields

$$\fint_0^1 \frac{\bar{h}_\xi(\xi)}{\xi} d\xi = \frac{\pi}{\epsilon} \left(\frac{p_{g0} - p_\infty}{\rho_\infty U_\infty^2} \right). \tag{3.7}$$

Thus, (3.7) indeed suggests that $\bar{h}_{\bar{x}}(0) = 0$ for the integral to exist. In other words, $\bar{h}_{\bar{x}}(0) = 0$ is a boundary condition which is consistent with the thin aerofoil theory which has been used to model the pressure in the gas core in order to have finite pressure at the onset of annular flow, $\bar{x} = 0$. We also know that the dryout point is at $\bar{x} = 1$. Therefore we have to solve (3.3) subject to

$$\bar{h}_{\bar{x}}(0) = 0, \ \bar{h}(1) = 0, \ p_g = p_{g0}, \tag{3.8}$$

where p_{g0} is dimensional gas core pressure at $x = 0$. If the dimensional thickness $h(0)$ is known from measurements, we can then calculate the dimensional length to dryout from

$$L_0 = \frac{h(0)}{\epsilon \bar{h}(0)}. \tag{3.9}$$

In other words, we need to solve the dimensional equation with a known $h(0)$, $h_x(0) = 0$, $p_g = p_{g0}$ and $h(L_0) = 0$. This determines L_0. It is like an eigenvalue problem.

It would be ideal if the dryout length could be calculated from the conditions prescribed at the entry to the boiler tube. However, it is evident that to determine the length of the annular flow and hence the dryout point, requires some initial data concerning the annular regime itself. Since the flow regimes prior to annular are very complicated, it might be very difficult to take measurements there. Therefore the conditions described in (3.8), approximate as they are, seem to be practically reasonable.

3.1.2 Analysis of the Integral Equation

As mentioned earlier equation (3.3) is nonlinear, therefore any attempts to determine closed-form solutions for general mass exchange rates are likely to prove fruitless. These difficulties imply that we are mostly restricted to using asymptotic and numerical methods. However, the well-posedness of the problem may be checked for a few special cases. We analytically solve one such simple case below.

A relatively easy special case of (3.3) is obtained when $\bar{Q} = k_1 \bar{h}^3$ and $\bar{\tau} = 2k_2 \bar{h}$, for some constants k_1 and k_2,

$$\frac{1}{\pi} \fint_0^1 \frac{\bar{h}_\xi(\xi)}{\xi - \bar{x}} d\xi = K\bar{x} - C_1, \tag{3.10}$$

where $K\theta = k_1 + k_2$ and C_1 is an arbitrary constant of integration. Physically, this implies that we assume the rate of liquid mass escaping at free surface per unit area is directly proportional to the product of the square of the film free surface, h^2, and its slope, h_x. While the traction on the free surface (provided by the flow of vapour in the gas core) is directly proportional to the thickness of the liquid layer, h. It should be mentioned that these assumptions may not be realistic at all; however, using them we can obtain a closed-form solution. Equation (3.10) may then be inverted by standard methods (for example see

Muskhelishvili, 1953) [54] to yield

$$\bar{h}_{\bar{x}}(\bar{x}) = \frac{1}{\pi}\sqrt{\frac{1-\bar{x}}{\bar{x}}}\int_0^1 \sqrt{\frac{\xi}{1-\xi}}\frac{C_1 - K\xi}{\xi - \bar{x}}d\xi + \frac{C_2}{\sqrt{\bar{x}(1-\bar{x})}}, \tag{3.11}$$

where C_2 is an arbitrary constant arising from inversion of the singular integral in (3.10). Simplification of (3.11) leads to

$$\bar{h}_{\bar{x}}(\bar{x}) = \sqrt{\frac{1-\bar{x}}{\bar{x}}}\left(C_1 - \frac{K}{2}(1+2\bar{x})\right) + \frac{C_2}{\sqrt{\bar{x}\,(1-\bar{x})}}, \tag{3.12}$$

and upon imposing the boundary condition (3.8), $\bar{h}_{\bar{x}}(\bar{x}) = 0$ at $\bar{x} = 0$, gives

$$C_1 + C_2 = \frac{K}{2}. \tag{3.13}$$

From the pressure condition (3.7) and equation (3.12), at $\bar{x} = 0$, we get

$$\int_0^1 \frac{\bar{h}_\xi(\xi)}{\xi}d\xi = \int_0^1 \frac{1}{\xi}\left\{\sqrt{\frac{1-\xi}{\xi}}\left(C_1 - \frac{K}{2}(1+2\xi)\right) + \frac{C_2}{\sqrt{\xi\,(1-\xi)}}\right\}d\xi,$$

which simplifies to give

$$C_2 - \frac{K}{2} = \frac{(p_{g0} - p_\infty)\,\pi}{\epsilon\rho_\infty U_\infty^2}. \tag{3.14}$$

Integration of equation (3.12) with respect to $\bar{x}$ leads to

$$\bar{h}(\bar{x}) = \left(C_1 - \frac{3}{4}K + 2C_2\right)\sin^{-1}\left(\sqrt{\bar{x}}\right) + \left(C_1 - \frac{K}{4} - \frac{K}{2}\bar{x}\right)\sqrt{\bar{x}\,(1-\bar{x})} + A.$$

On imposing the boundary condition $\bar{h}(1) = 0$ at the dryout point implies

$$A = -\frac{\pi}{2}\left(C_1 - \frac{3}{4}K + 2C_2\right),$$

so that, on using (3.13) and (3.14), we have

$$\bar{h}(\bar{x}) = \left(P + \frac{K}{4}\right)\sin^{-1}(\sqrt{\bar{x}}) - \left(P + \frac{K}{4} + \frac{K}{2}\bar{x}\right)\sqrt{\bar{x}(1-\bar{x})} - \frac{\pi}{2}\left(P + \frac{K}{4}\right),$$

where $P(< 0)$ is given by $P = (p_{g0} - p_\infty)/\epsilon\rho_\infty U_\infty^2$. In this case the dryout length is given, from (3.9), by

$$L_0 = \frac{8h(0)}{\pi(K - 4P)}.$$

It is then evident that, for any finite fixed $h(0)$, the length to the dryout L_0 is inversely proportional to $K - 4P$. Since $P < 0$ then for any any $K > 0$, the liquid film cannot be formed for values of $K - 4P \to \infty$. On the other hand, if we can allow $K \leq 0$ then there will be some cases when the dryout point cannot be established at all. Such cases are possible when $K - 4P = 0$, e.g. when $K = 0$ and the pressure through the pipe is a constant equal to p_∞. This example may be unrealistic in its physical conception but it however suggests that the problem may be well-posed. Other choices of $\bar{Q}$ and $\bar{\tau}$ which make the integral equation linear in $\bar{h}$ may be possible but we now wish to move on to solving the nonlinear problem (3.3) in the cases where the mass exchange rates are considered known.

3.1.3 An Inversion Technique Using Properties of Abel's Equation

Before we proceed to solve (3.3) numerically, it should first be mentioned however, for completeness, that (3.10) can also be inverted alternatively using properties of Abel's equation. We briefly outline here a method due to Peters (1963, 1968) [62], [63]. For convenience and ease of notation we drop bars and write $h_x(x) = \phi(x)$ and $(Kx - C_1)\pi = f(x)$. The left hand side of (3.10) is then rewritten as

$$\begin{aligned} \int_0^1 \frac{\phi(\xi)}{\xi - x} d\xi &= \int_0^1 \frac{1 + \xi - x - \xi + x}{\xi - x} \phi(\xi) d\xi \\ &= \int_0^1 \phi(\xi) d\xi + x \int_0^1 \frac{\phi(\xi)}{\xi - x} d\xi - \int_0^1 \frac{\xi \phi(\xi)}{\xi - x} d\xi + \int_0^1 \frac{\phi(\xi)}{\xi - x} d\xi \\ &= \int_0^1 \phi(\xi) d\xi + x f(x) - \int_0^1 \frac{\xi \phi(\xi)}{\xi - x} d\xi + f(x), \end{aligned} \tag{3.15}$$

where use of (3.10) has been employed. Substitution of (3.15) into (3.10) then gives

$$\int_0^1 \frac{\xi \phi(\xi)}{\xi - x} d\xi = x f(x) + \int_0^1 \phi(\xi) d\xi,$$

which can be rewritten as

$$\int_0^1 \frac{\xi \phi(\xi) d\xi}{\left(\sqrt{\xi^2} - \sqrt{x^2}\right)\sqrt{x}} = \sqrt{x} f(x) + \frac{\int_0^1 \phi(\xi) d\xi}{\sqrt{x}}. \tag{3.16}$$

Equation (3.16) may be integrated with respect to x to yield

$$-\int_0^1 \ln \left| \frac{\sqrt{\xi} - \sqrt{x}}{\sqrt{\xi} + \sqrt{x}} \right| \sqrt{\xi} \phi(\xi) d\xi = \int_0^x \sqrt{\xi} f(\xi) d\xi + 2\sqrt{x} \int_0^1 \phi(\xi) d\xi. \tag{3.17}$$

It is observed that the integral

$$\int \frac{d\beta}{\sqrt{(\xi - \beta)(x - \beta)}} = -2 \ln \left| \frac{\sqrt{\xi - \beta} + \sqrt{x - \beta}}{\sqrt{\xi - x}} \right| + \text{ a constant},$$

so that the definite integral

$$\int_0^x \frac{d\beta}{\sqrt{(\xi - \beta)(x - \beta)}} = \ln \left| \frac{(\sqrt{\xi} + \sqrt{x})^2}{\xi - x} \right| = \ln \left| \frac{\sqrt{\xi} + \sqrt{x}}{\sqrt{\xi} - \sqrt{x}} \right| = -\ln \left| \frac{\sqrt{\xi} - \sqrt{x}}{\sqrt{\xi} + \sqrt{x}} \right|.$$

Therefore (3.17) can be rewritten as

$$\int_0^x \left\{ \sqrt{\xi} \phi(\xi) \int_0^\xi \frac{d\beta}{\sqrt{(\xi - \beta)(x - \beta)}} \right\} d\xi + \int_x^1 \left\{ \sqrt{\xi} \phi(\xi) \int_0^x \frac{d\beta}{\sqrt{(\xi - \beta)(x - \beta)}} \right\} d\xi = \int_0^x \sqrt{\xi} f(\xi) d\xi + 2\sqrt{x} \int_0^1 \phi(\xi) d\xi. \tag{3.18}$$

An appropriate change of order of integration on the left hand side terms of equation (3.18) yields

$$\int_0^x \left\{ \frac{1}{\sqrt{x - \beta}} \int_\beta^x \frac{\sqrt{\xi} \phi(\xi) d\xi}{\sqrt{\xi - \beta}} \right\} d\beta + \int_0^x \left\{ \frac{1}{\sqrt{x - \beta}} \int_x^1 \frac{\sqrt{\xi} \phi(\xi) d\xi}{\sqrt{\xi - \beta}} \right\} d\beta = \int_0^x \sqrt{\xi} f(\xi) d\xi + 2\sqrt{x} \int_0^1 \phi(\xi) d\xi,$$

which simplifies to

$$\int_0^x \left\{ \frac{1}{\sqrt{x-\beta}} \int_\beta^1 \frac{\sqrt{\xi}\phi(\xi)d\xi}{\sqrt{\xi-\beta}} \right\} d\beta = \int_0^x \sqrt{\xi} f(\xi)d\xi + 2\sqrt{x}\int_0^1 \phi(\xi)d\xi. \tag{3.19}$$

It is then noted that the solution to Abel's equation

$$\int_0^x \frac{\phi(\beta)}{\sqrt{x-\beta}} d\beta = g(x)$$

is given by (see for example Arfken, 1985) [3]

$$\phi(x) = \frac{1}{\pi}\left(\int_0^x \frac{g(\beta)}{\sqrt{x-\beta}} d\beta \right)_x = \frac{1}{\pi}\left(\frac{g(0)}{\sqrt{x}} + \int_0^x \frac{g_\beta(\beta)}{\sqrt{x-\beta}} d\beta \right),$$

where integration by parts has been used. Thus, an application of this result on equation (3.19) yields

$$\int_\beta^1 \frac{\sqrt{\xi}\phi(\xi)}{\sqrt{\xi-\beta}} d\xi = \frac{1}{\pi}\int_0^\beta \frac{\sqrt{x} f(x)}{\sqrt{\beta-x}} dx + \int_0^1 \phi(\xi)d\xi, \tag{3.20}$$

where use of the result

$$\int_0^\beta \frac{dx}{\sqrt{x(\beta-x)}} = \pi.$$

has been employed. It is noted that the solution to the integral equation

$$\int_\beta^1 \frac{\phi(\xi)}{\sqrt{\xi-\beta}} d\xi = G(\beta)$$

can be deduced from the Abel's equation as

$$\phi(\xi) = -\frac{1}{\pi}\left(\int_\xi^1 \frac{G(\beta)}{\sqrt{\beta-\xi}} d\beta \right)_\xi.$$

Therefore, equation (3.20) leads to

$$\sqrt{\xi}\phi(\xi) = \frac{1}{\pi}\frac{\int_0^1 \phi(\xi)d\xi}{\sqrt{1-\xi}} - \frac{1}{\pi^2}\left(\int_\xi^1 \left\{ \frac{1}{\sqrt{\beta-\xi}} \int_0^\beta \frac{\sqrt{x} f(x)dx}{\sqrt{\beta-x}} \right\} d\beta \right)_\xi, \tag{3.21}$$

where use of the integral

$$I = \int_\xi^1 \frac{\left(\int_0^1 \phi(\xi)d\xi\right)}{\sqrt{\beta-\xi}} d\beta = 2\sqrt{1-\xi}\int_0^1 \phi(\xi)d\xi$$

and hence

$$\frac{dI}{d\xi} = -\frac{\int_0^1 \phi(\xi)d\xi}{\sqrt{1-\xi}},$$

have been employed. Upon changing the order of integration in the second term on the right hand side of (3.21), the equation can then further be manipulated (the details are given in Peters (1963) [62]) to give a standard inversion formula

$$\phi(\xi) = -\frac{1}{\pi^2\sqrt{\xi(1-\xi)}}\int_0^1 \frac{\sqrt{x(1-x)} f(x)}{x-\xi} dx - \frac{C}{\sqrt{\xi(1-\xi)}}, \tag{3.22}$$

where C is a constant given by

$$\frac{1}{\pi}\int_0^1 \phi(x)dx.$$

It should be recalled that, in relation to the paradigm problem in section (3.1.2), $\phi(x)$ and $f(x)$ are given by $\phi(x) = h_x(x)$ and $f(x) = Kx - C_1$ respectively (where bars are omitted for convenience). Thus, we could invert (3.10) using (3.22) instead of (3.11) to get

$$h_x(x) = \frac{1}{\pi\sqrt{x(1-x)}}\int_0^1 \frac{\sqrt{\xi(1-\xi)}}{\xi - x}\left(C_1 - K\xi\right)d\xi + \frac{C}{\sqrt{x(1-x)}}. \tag{3.23}$$

However, it would be very difficult to proceed analytically. It can be shown, using standard techniques, that

$$\int_0^1 \frac{\sqrt{\xi(1-\xi)}}{\xi - x}d\xi = \pi + \frac{\pi}{2}(2x+3),$$

$$\int_0^1 \frac{\sqrt{\xi(1-\xi)}}{\xi - x}\xi d\xi = -\frac{\pi}{2}(2x+3) + \pi \times$$

$$\left\{\frac{x^7}{6x^4(1-x)^4 + 4x^2(1-x)^6 + 4x^6(1-x)^2 + x^8 + (1-x)^8}\right.$$

$$-\frac{x^2\left[(1-x)^4 + 3x^2(1-x)^2 + 3x^4\right]}{2\left[3x^4(1-x)^2 + (1-x)^2 + (1-x)^6 + x^6 + 3x^2(1-x)^4\right]}$$

$$\left.+\frac{3x^2\left[4(1-x)^2 + 3x^2\right]}{16\left[(1-x)^4 + 2x^2(1-x)^2 + x^4\right]} - \frac{5x^2}{16\left[(1-x)^2 + x^2\right]}\right\}.$$

Therefore, in this case, it would be very difficult to proceed (as in section (3.1.2)) to solve (3.10) in closed-form using the inversion formula (3.23).

3.1.4 Numerical Solution

3.1.4.1 A Conventional Method

As an initial step to solving (3.3) numerically, we start by first solving a very special case

$$\frac{1}{\pi}\left(\int_0^1 \frac{\bar{h}_\xi(\xi)}{\xi - \bar{x}}d\xi\right)_{\bar{x}} = 1, \tag{3.24}$$

subject to the boundary conditions (3.8). We do this as (3.24) can be solved analytically and therefore we can compare our numerical solution to the analytical one, thus checking the accuracy of our numerical method.

As far as numerical methods are concerned, we pretend that (3.24) cannot be integrated explicitly with respect to $\bar{x}$ and thus treat it as if it were nonlinear in $\bar{h}(\bar{x})$. We discretise the interval $[0,1]$ by dividing it into n equal subintervals $[\xi_j, \xi_{j+1}]$, where $\xi_j = j/n$ are mesh points, n denotes the number of mesh points and $0 \leq j \leq n-1$. We use finite differences

(see for example Smith, 1994) [75] to approximate $\bar{p}_{\bar{x}}$, where

$$\bar{p}_{\bar{x}} = \left\{ \fint_0^1 \frac{\bar{h}_\xi(\xi)}{\xi - \bar{x}} d\xi \right\}_{\bar{x}},$$

at mesh points and we collocate $\bar{p}$ at mid-mesh points where it can be evaluated. We assume that the Cauchy integral

$$\fint_0^1 \frac{\bar{h}_\xi(\xi)}{\xi - \bar{x}} d\xi$$

may be approximated by the sum of the integrals in each subinterval $[\xi_j, \xi_{j+1}]$. Essentially, we are approximating the integral using a trapezoidal rule. We further suppose that $\bar{h}_{\bar{x}}(\bar{x})$ is a constant in each subinterval, i.e. we approximate the solution $\bar{h}$ by linear functions in each subinterval. It is then clear from the boundary condition $\bar{h}_{\bar{x}}(0) = 0$ that $\bar{h}(\bar{x}_0) = \bar{h}(\bar{x}_1)$. Then assuming that we know $\bar{h}(\xi_0)$, a parameter that has to be chosen in order that the solution satisfies the pressure condition, equation (3.24) becomes

$$\frac{1}{\pi} \frac{\bar{p}_{i+\frac{1}{2}} - \bar{p}_{i-\frac{1}{2}}}{\xi_{i+\frac{1}{2}} - \xi_{i-\frac{1}{2}}} = 1, \qquad 2 \le i \le n-1, \tag{3.25}$$

where $\bar{p}_{i\pm 1/2}$ and $\xi_{i\pm 1/2}$ are respectively given by

$$\begin{aligned} \bar{p}_{i\pm\frac{1}{2}} &= \fint_0^1 \frac{\bar{h}_\xi(\xi)}{\xi - \xi_{i\pm\frac{1}{2}}} d\xi, \\ \xi_{i\pm\frac{1}{2}} &= \frac{i \pm \frac{1}{2}}{n}, \end{aligned}$$

and are the mid-mesh points.

Equation (3.25) can also be written as

$$\sum_{j=1}^{n} \frac{\bar{h}_j - \bar{h}_{j-1}}{(\xi_j - \xi_{j-1})(\xi_{i+\frac{1}{2}} - \xi_{i-\frac{1}{2}})} \left(\int_{\xi_{j-1}}^{\xi_j} \frac{1}{\xi - \xi_{i+\frac{1}{2}}} d\xi - \int_{\xi_{j-1}}^{\xi_j} \frac{1}{\xi - \xi_{i-\frac{1}{2}}} d\xi \right) = \pi,$$

where $\bar{h}_j = \bar{h}(\xi_j)$. After integrating and imposing the boundary conditions $\bar{h}_0 = \bar{h}_1$ and $\bar{h}_n = 0$ we get an $(n-2) \times (n-2)$ system of linear equations

$$\sum_{j=2}^{n-1} (\bar{h}_j - \bar{h}_{j-1}) \ln \left| \frac{(2j - 2i + 1)^2}{(2j - 2i + 3)(2j - 2i - 1)} \right| = \frac{\pi}{n^2} + \bar{h}_1 \ln \left| \frac{(3 - 2i)^2}{(1 - 2i)(5 - 2i)} \right|.$$

We solve this system for values of $\bar{h}_j$ using the NAG library routine F04ATF and $\bar{h}_1 = \bar{h}_0$ is a prescribed parameter. The method uses an LU factorisation with partial pivoting and iterative refinement. Results are plotted against the mesh points for different values of n. In each case the numerical results, see for example figures (3.1), (3.2) and (3.3), are compared with the analytical solution of (3.24) which, for example when $\bar{h}(0) = 3\pi/8$, is

$$\bar{h}(\bar{x}) = -\frac{3}{4} \sin^{-1}(\sqrt{\bar{x}}) + \left(\frac{3}{4} - \frac{\bar{x}}{2}\right) \sqrt{\bar{x}(1 - \bar{x})} + \frac{3}{8}\pi. \tag{3.26}$$

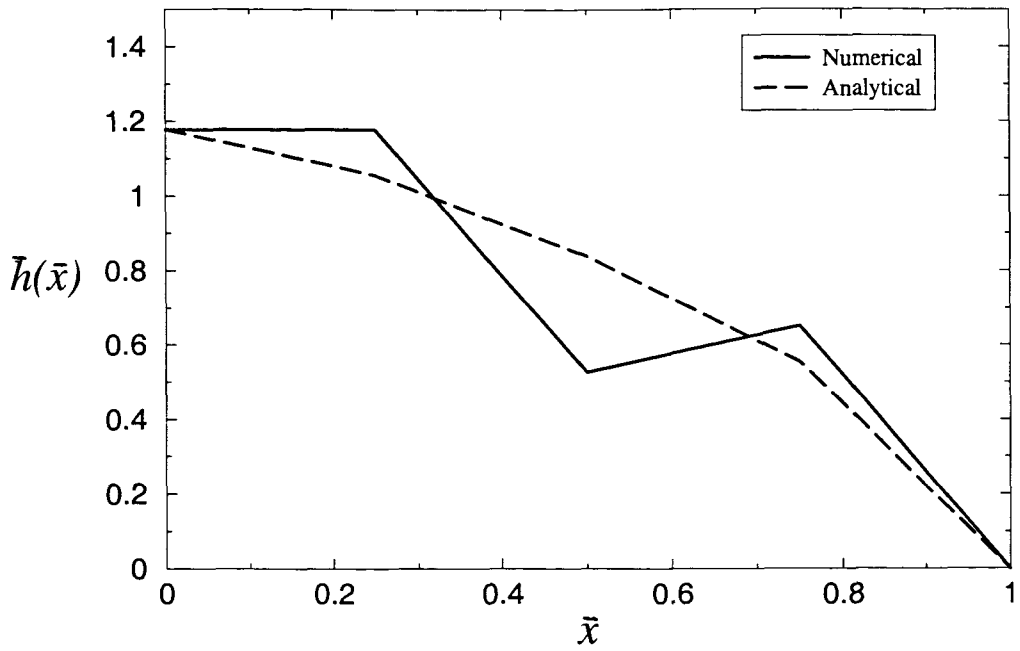

Figure 3.1: Graph of $\bar{h}(\bar{x})$ $(n = 5)$.

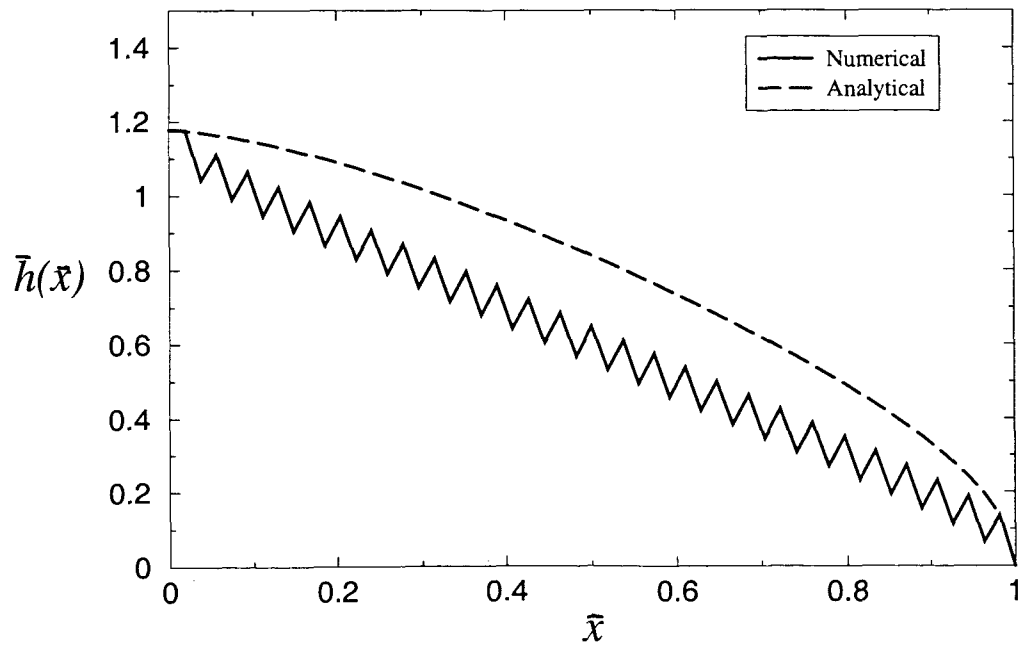

Figure 3.2: Graph of $\bar{h}(\bar{x})$ $(n = 55)$.

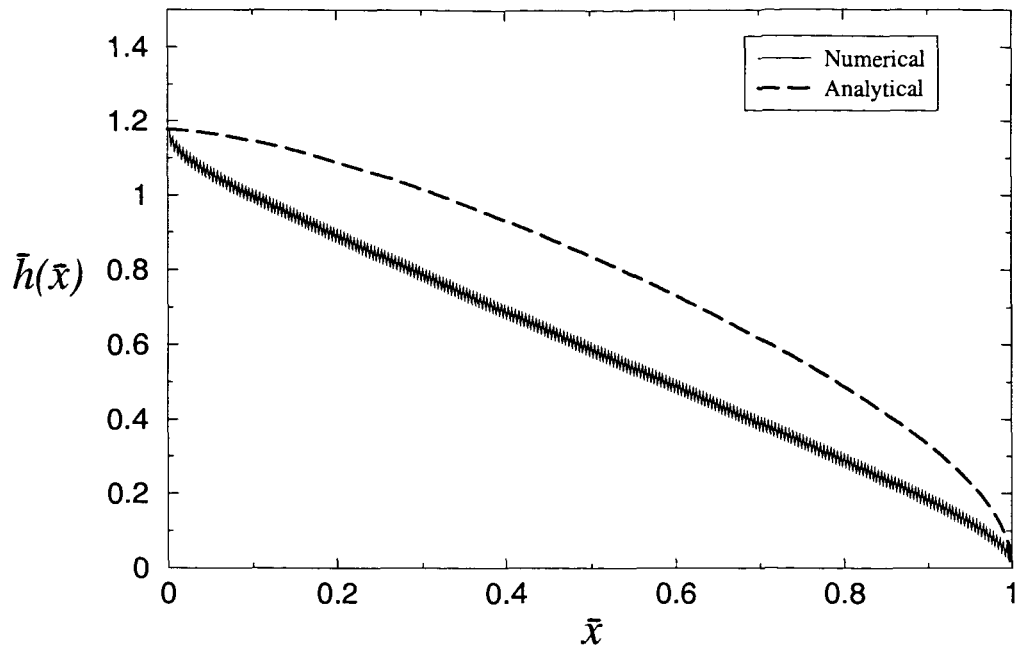

Figure 3.3: Graph of $\bar{h}(\bar{x})$ ($n = 495$).

It is observed that the results of this conventional method are not satisfactory in comparison to the analytic solution. For $n = 5$, a curve for the analytic solution appears to be an average of the numerical solution. However, as the number of mesh points is increased, the numerical results do not approximate the analytic solution satisfactorily at all (see figures (3.1) to (3.3)). Therefore, it is necessary to devise other computational methods in order to obtain a satisfactory numerical solution to this problem.

3.1.4.2 A Different Approach

It is obvious from the analytical solution (3.26) that near $\bar{x} = 1$, $\bar{h}(\bar{x}) \to 0$ like $\sqrt{1-\bar{x}}$. Therefore, there is a singularity in the slope of $\bar{h}(\bar{x})$ as $\bar{h}_{\bar{x}}(\bar{x}) \to \infty$ near $\bar{x} = 1$. It is this singularity in $\bar{h}(\bar{x})$ at $\bar{x} = 1$ which disrupts the conventional numerical scheme. As a remedy, we instead solve a regularised problem by considering a stretched coordinate where $\bar{h}(\bar{x}) \to 0$ linearly near $\bar{x} = 1$. We put

$$\bar{h}(\bar{x}) = H(y), \qquad \text{where } y^2 = 1 - \bar{x}.$$

Under these circumstances equation (3.24) becomes

$$\frac{1}{\pi}\left(\int_0^1 \frac{H_u(u)}{y^2 - u^2} du\right)_y = 2y, \tag{3.27}$$

subject to the boundary conditions $H(y) = 0$ at $y = 0$, $H_y(y) = 0$ at $y = 1$ with $H(1)$ a known parameter.

Equation (3.27) is then discretised in the conventional way, as described in section (3.1.4.1), to give an $(n-2) \times (n-2)$ system of linear equations

$$\sum_{j=0}^{n-3} (\bar{h}_{n-j} - \bar{h}_{n-j-1}) \times$$

$$\left(\frac{1}{2i+1} \ln \left| \frac{(2i+2j+3)(2i-2j+1)(2i-2(j+1)-1)(2i+2(j+1)+1)}{(2i-2j-1)(2i+2j+1)(2i+2(j+1)+3)(2i-2(j+1)+1)} \right| - \right.$$

$$\left. \frac{1}{2i-1} \ln \left| \frac{(2i+2j+1)(2i-2j-1)(2i-2(j+1)-3)(2i+2(j+1)-1)}{(2i-2j-3)(2i+2j-1)(2i+2(j+1)+1)(2i-2(j+1)-1)} \right| \right) =$$

$$\frac{2i}{n^4}\pi - \bar{h}_1 \left(\frac{1}{2i+1} \ln \left| \frac{(2i+2(n-2)+3)(2i-2(n-2)+1)}{(2i-2(n-2)-1)(2i+2(n-2)+1)} \right| - \right.$$

$$\left. \frac{1}{2i-1} \ln \left| \frac{(2i+2(n-2)+1)(2i-2(n-2)-1)}{(2i-2(n-2)-3)(2i+2(n-2)-1)} \right| \right), \qquad 1 \leq i \leq n-2.$$

The system is then solved for values of $\bar{h}_j$, as explained earlier, using the NAG library routine F04ATF. Results of this method compare well with the analytical results (see figures (3.4), (3.5), and (3.6)). The transformation removes the singularity in $\bar{h}_{\bar{x}}(\bar{x})$ at $\bar{x} = 1$ so that the

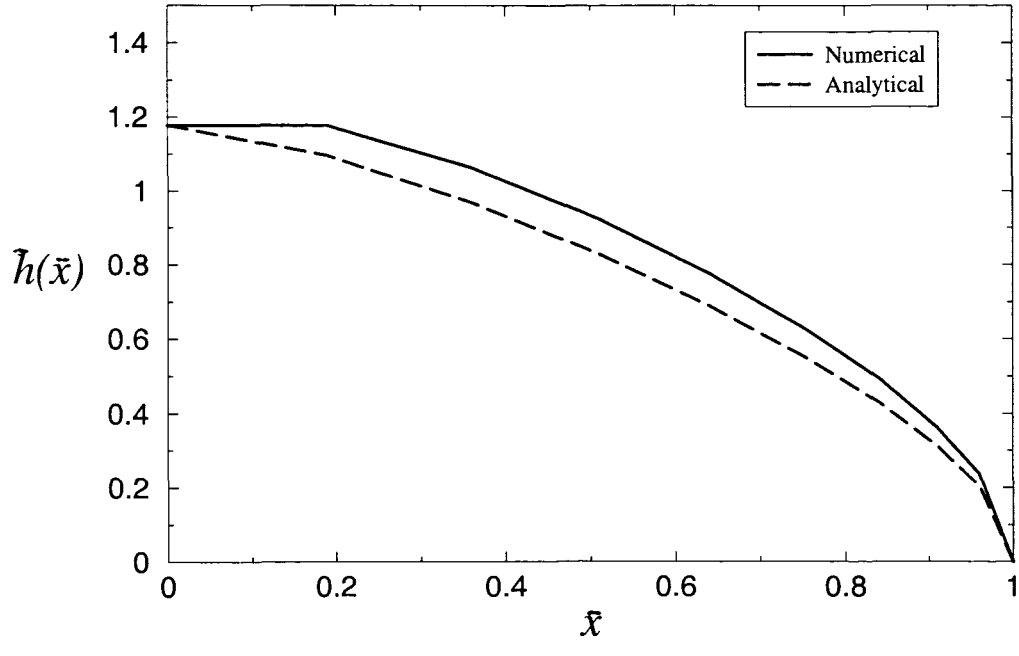

Figure 3.4: Graph of $\bar{h}(\bar{x})$ $(n = 11)$.

numerical method works better. However, there is evidently a price to be paid because the transformation enormously increases the amount of algebra involved in the problem.

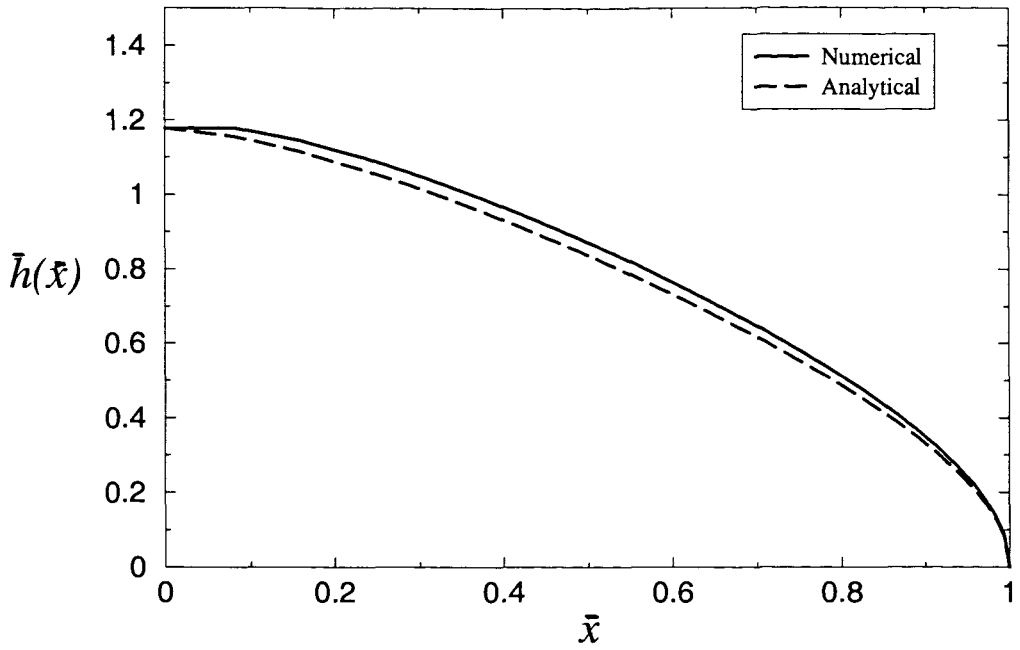

Figure 3.5: Graph of $\bar{h}(\bar{x})$ $(n = 25)$.

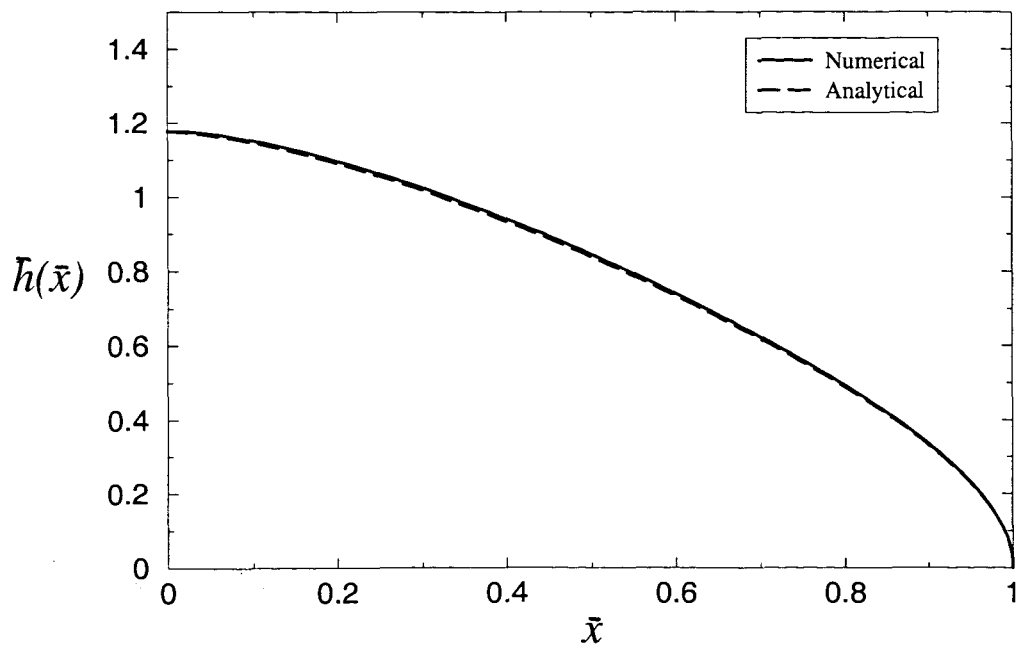

Figure 3.6: Graph of $\bar{h}(\bar{x})$ $(n = 100)$.

3.1.5 A Nonlinear Problem

The previous paradigm problem in section (3.1.2) could be solved in closed-form. Hence the asymptotic behaviour of the solution could be deduced from the analytical solution itself. The numerical solution could also be compared with the closed-form solution in order to check the validity and the accuracy of the computational method. On the other hand, the full problem we intend finally to solve is highly nonlinear and the chances are extremely remote that closed-form solutions could be obtained. Therefore, we need to develop some asymptotic techniques in order to get an insight into the behaviour of the unknown solution near the end point $x = 1$ (where non-uniformities may be anticipated to arise). We will further require some techniques for testing the accuracy of our numerical method in this case. In order to proceed, we first consider a nonlinear special case of the finite range nonlinear singular integro-differential equation (3.3) where the dynamics of $\dot{m}$ and $\bar{\tau}$ are ignored. In other words, (3.3) is solved for $\bar{h}$ given that $\dot{m}$ and $\bar{\tau}$ are prescribed parameters. In general $\dot{m} = \dot{m}(h(x))$, details of which have been given previously by simple thermodynamic models and we must solve the steady case of problems (2.62) and (2.63). However, we hope this special case, physically unrealistic as it may be in its conception, will give us an insight as to how and whether we can solve the full nonlinear problem numerically. In equation (3.3), it is not known whether in general the quantity $\bar{Q}$ has to be negative or positive.

We recall that $\dot{m} = \bar{Q}_{\bar{x}}$ with the boundary condition $\bar{Q} = 0$ imposed at the dryout point, $\bar{x} = 1$. Therefore, with this fictitious approximation of a constant $\dot{m}$, $\bar{Q} = \dot{m}\,(\bar{x} - 1)$. It is obvious that if $\dot{m} > 0$ then $\bar{Q} < 0$ for all $\bar{x}$ in [0,1]. We now have to solve (3.3), written explicitly in this case as,

$$\frac{\dot{m}}{\bar{h}^3(\bar{x})}(\bar{x} - 1) + \frac{\bar{\tau}}{2\bar{h}(\bar{x})} = \frac{\theta}{\pi}\left(\int_0^1 \frac{\bar{h}_\xi(\xi)}{\xi - \bar{x}} d\xi\right)_{\bar{x}}. \tag{3.28}$$

In effect it can be observed that (3.28) is identical to the constant heat flux problem from equation (2.67)

$$\left\{\frac{\bar{h}^3}{3\pi}\left(\int_0^1 \frac{\bar{h}_\xi(\xi)}{\xi - \bar{x}} d\xi\right)_{\bar{x}} - \frac{\tilde{\tau}}{2}\bar{h}^2\right\}_{\bar{x}} = \frac{1}{\eta}, \tag{3.29}$$

in the special case when $\dot{m} = 3/\eta$, $\bar{\tau} = 3\tilde{\tau}$ and $\theta = 1$. To show this, we assume that the mass flux

$$\frac{\bar{h}^3}{3\pi}\left(\int_0^1 \frac{\bar{h}_\xi(\xi)}{\xi - \bar{x}} d\xi\right)_{\bar{x}},$$

vanishes at the dryout point $\bar{x} = 1$ where $\bar{h}(\bar{x}) = 0$. Effectively, this fixes the regularity condition for this problem. Integration of (3.29) with respect to $\bar{x}$ then gives

$$\frac{\bar{h}^3}{3\pi}\left(\int_0^1 \frac{\bar{h}_\xi(\xi)}{\xi - \bar{x}} d\xi\right)_{\bar{x}} - \frac{\tilde{\tau}}{2}\bar{h}^2 = -\frac{1}{\eta}(1 - \bar{x}). \tag{3.30}$$

Now, equation (3.30) can obviously be rewritten as

$$\frac{3}{\eta\bar{h}^3(\bar{x})}(\bar{x}-1)+\frac{3\tilde{\tau}}{2\bar{h}(\bar{x})}=\frac{1}{\pi}\left(\int_0^1\frac{\bar{h}_\xi(\xi)}{\xi-\bar{x}}d\xi\right)_{\bar{x}},$$

and hence the result follows.

For simplicity and for demonstration purposes, in the subsequent section (3.1.5.1) we will solve a far much simpler case than equation (3.28). (Equation (3.28) may be solved in exactly the same way but the amount of algebra will be more involved.) We will therefore assume that in equation (3.3) the quantity $\bar{Q}$ is taken to be a negative constant $-\dot{Q}$. Physically, this corresponds to the case where the mass transfer from the film is constant and does not depend on the film thickness (so that $\dot{m}=0$). This problem will serve to demonstrate both the asymptotic analysis and the numerical technique.

3.1.5.1 Asymptotics and Regularisation

At the upstream end $\bar{x}=1$ (dryout point) the thickness $\bar{h}(\bar{x})$ must vanish. Therefore, the nonlinear term $-\dot{Q}/\bar{h}^3$, which dominates the left hand side of (3.28), must be balanced by at least one other large term in the equation.

In the earlier special case considered, we recall that the singular integral equation was linear and it could be solved all in closed-form. Then from the analytical solution, one could observe how the problem should be regularised so that the numerical method could be employed to satisfactorily solve the problem. In the current case we do not know $\bar{h}(\bar{x})$ analytically, therefore in order to proceed we resort to asymptotic approximations. We assume that the main contribution from the Cauchy integral comes from a small region near $\bar{x}=1$ where we suppose $\bar{h}(\bar{x})\sim A\,(1-\bar{x})^p$, for some positive constants A and $p(<1)$ to be determined by performing an asymptotic balance in the equation. Intuitively, in this particular case the nonlinear term $-\dot{Q}/\bar{h}^3$ must be balanced by the large negative gas flow pressure gradient on the right hand side of (3.28). This implies that as $\bar{x}\to 1$, $\bar{h}(\bar{x})$ must tend to zero as

$$\bar{h}(\bar{x})\sim\left(\frac{\dot{Q}4\pi}{\theta}\right)^{\frac{1}{4}}(1-\bar{x})^{\frac{1}{2}}.$$

Encouraged by our experience of solving the paradigm problem (3.24), and the work by King & Tuck (1993) [45] (who solved a steady nonlinear singular integro-differential equation to determine the unknown shape of a thin liquid layer supported by steady air-flow surface traction) we set

$$\bar{h}(\bar{x})=\left(\frac{\dot{Q}4\pi}{\theta}\right)^{\frac{1}{4}}H(y),\qquad\text{where } y^2=1-\bar{x},$$

to regularise (3.28). We then have to solve

$$\left(\frac{-\dot{Q}}{H^3(y)}\sqrt{\frac{\theta}{4\pi\dot{Q}}}+\frac{\bar{\tau}}{2H(y)}\right)\sqrt{\frac{\pi}{\theta\dot{Q}}}y=\left(\fint_0^1\frac{H_u(u)}{y^2-u^2}du\right)_y, \tag{3.31}$$

with $H(y)\to 0$ as $y\to 0$, $H_y(1)=0$ and $H(1)$ is prescribed. The regularisation of the thickness $\bar{h}(\bar{x})$ is important since, as seen earlier, the singular behaviour of $\bar{h}_{\bar{x}}(\bar{x})$ as $\bar{x}\to 1$ seriously degrades conventional discretisations of the integro-differential equation.

Equation (3.31) may now be conventionally discretised and solved numerically for H where three parameters, H_n, $\dot{Q}$ and $\bar{\tau}$ would have to be specified and varied at will. However, it is numerically convenient to set $\bar{h}(\bar{x})=\bar{h}_0 g(\bar{x})$ in (3.3) so that we have to solve

$$\frac{M}{g^3}+\frac{\Gamma}{g}=\frac{\theta}{\pi}\left(\fint_0^1\frac{g_\xi(\xi)}{\xi-\bar{x}}d\xi\right)_{\bar{x}}, \tag{3.32}$$

where M and Γ are respectively $M=\dot{Q}/\bar{h}_0^4$, $\Gamma=\bar{\tau}/2\bar{h}_0^2$, subject to boundary conditions $g(0)=1$, $g_{\bar{x}}(0)=0$ and $g(1)=0$, for any $\bar{h}_0>0$.

On performing asymptotic approximations of (3.32), as detailed above, we obtain that as $\bar{x}\to 1$, $g(\bar{x})$ must tend to zero as

$$g(\bar{x})\sim\left(\frac{4M\pi}{\theta}\right)^{\frac{1}{4}}(1-\bar{x})^{\frac{1}{2}}.$$

The problem is then regularised by setting

$$g(\bar{x})=\left(\frac{4M\pi}{\theta}\right)^{\frac{1}{4}}G(y)\qquad\text{with } y^2=1-\bar{x}.$$

We now have to solve a regularised problem

$$\left(\frac{\pi}{M\theta}\right)^{\frac{1}{2}}\left\{-\frac{M}{G^3}\left(\frac{\theta}{4M\pi}\right)^{\frac{1}{2}}+\frac{\Gamma}{G}\right\}y=\left(\fint_0^1\frac{G_u(u)}{y^2-u^2}du\right)_y, \tag{3.33}$$

subject to boundary conditions $G(1)=(\theta/4M\pi)^{1/4}$, $G_y(1)=0$ and $G(0)=0$.

3.1.5.2 Numerical Scheme and Results

Equation (3.33) is then discretised in the conventional way, i.e. a mesh $u_j=j/n$ is defined on the interval $[0,1]$ with $G_u(u)$ assumed constant in each subinterval $[u_j,u_{j+1}]$. In other words, the function G is approximated by linear functions in each subinterval. The pressure gradient

$$p_y=\left\{\fint_0^1\frac{G_u(u)}{y^2-u^2}du\right\}_y,$$

is evaluated by finite differences. We collocate (3.33) at the mid-mesh points and the resulting $(n-2) \times (n-2)$ set of nonlinear algebraic equations is given by

$$\sum_{j=0}^{n-1} (G_{j+1} - G_j) \left(\frac{1}{2i+1} \ln \left| \frac{(2i+2j+3)(2i-2j+1)}{(2i-2j-1)(2i+2j+1)} \right| - \frac{1}{2i-1} \ln \left| \frac{(2i+2j+1)}{(2i-2j-3)} \times \frac{(2i-2j-1)}{(2i+2j-1)} \right| \right) - \frac{i}{n^4} \left(\frac{\pi}{M\theta} \right)^{\frac{1}{2}} \left(-\frac{M}{G_i^3} \left(\frac{\theta}{4M\pi} \right)^{\frac{1}{2}} - \frac{2i+1}{n^2} \frac{\Gamma}{G_i} \right) = 0, \tag{3.34}$$

for $1 \leq i \leq n-2$, where $G_0 = 0$, $G_n = G_{n-1} = (\theta/(4M\pi))^{1/4}$ and M and Γ are specified.

The system is then solved iteratively for values of G_j by Powell's method using the NAG library routine C05NBF. This method uses a combination of Newton and steepest-descent iterations. An initial guess for the solution is taken to be linear functions in each subinterval $[u_j, u_{j+1}]$. The g_j values are recovered from those of G_j using a relationship

$$g_j = \left(\frac{4M\pi}{\theta} \right)^{\frac{1}{4}} G_{n-j}, \ 0 \leq j \leq n.$$

The values of g_j are then plotted against $\bar{x}_j$, $\bar{x}_j = 1 - u_j^2$, for $0 \leq j \leq n$ (see for example figure (3.7)).

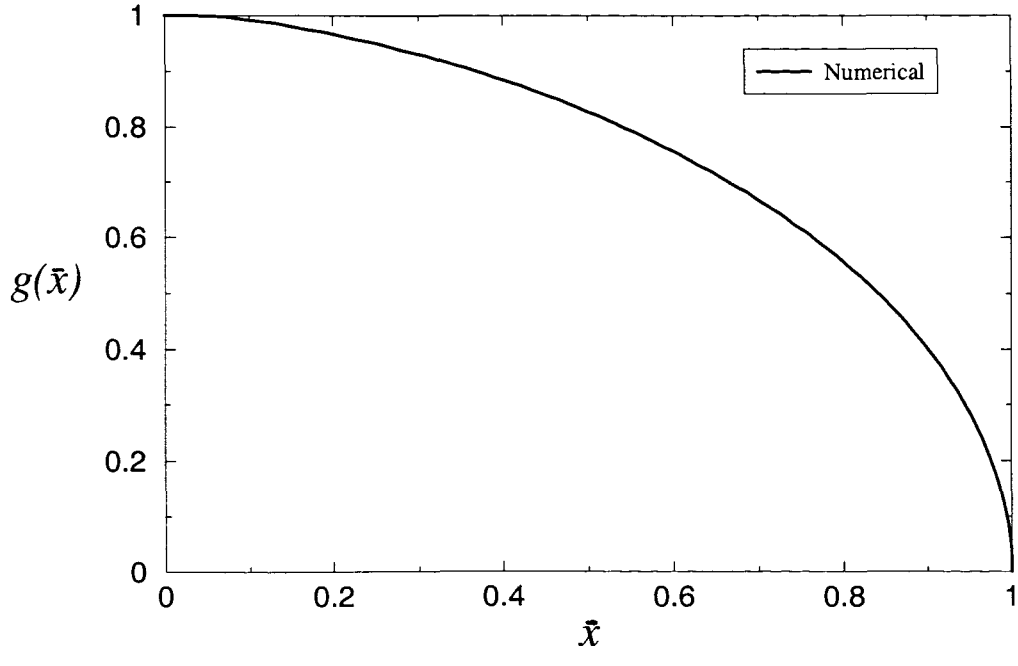

Figure 3.7: Graph of $g(\bar{x})$, $M = 1.0$, $\Gamma = 1.0$ ($n = 60$).

The residual error in the numerical method is checked by evaluating each side of (3.33) using the computed numerical results for G, and with just 60 points, the error is of order

between 10^{-8} and 10^{-10}. The sensitivity of the numerical method's accuracy to the choice of grid is examined by increasing the number of mesh points and there is no change at all. Respective illustrative results are shown in tables (3.1) and (3.2).

Table 3.1: The computed left and right hand sides of equation (3.33), $n = 60$.

(left-hand side of equation (3.33))/n^3	(right-hand side of equation (3.33))/n^3
-3.4319983209766$\times 10^{-08}$	-3.4319983364776$\times 10^{-08}$
-5.7219241008031$\times 10^{-08}$	-5.7219241027164$\times 10^{-08}$
-8.0151785494553$\times 10^{-08}$	-8.0151785544487$\times 10^{-08}$
-1.0313309239400$\times 10^{-07}$	-1.0313309230887$\times 10^{-07}$
-1.2617864099689$\times 10^{-07}$	-1.2617864096696$\times 10^{-07}$
-1.4930415355307$\times 10^{-07}$	-1.4930415364852$\times 10^{-07}$
-1.7252544690301$\times 10^{-07}$	-1.7252544683381$\times 10^{-07}$
-1.9585866046224$\times 10^{-07}$	-1.9585866048016$\times 10^{-07}$
$\vdots$	$\vdots$
-6.8519016656996$\times 10^{-07}$	-6.8519016652359$\times 10^{-07}$
-7.1495301153696$\times 10^{-07}$	-7.1495301176883$\times 10^{-07}$
-7.4531852115604$\times 10^{-07}$	-7.4531852093556$\times 10^{-07}$
-7.7632459123378$\times 10^{-07}$	-7.7632459101436$\times 10^{-07}$
-8.0801138340682$\times 10^{-07}$	-8.0801138357576$\times 10^{-07}$
-8.4042176207048$\times 10^{-07}$	-8.4042176215384$\times 10^{-07}$
-8.7360133805391$\times 10^{-07}$	-8.7360133805839$\times 10^{-07}$
-9.0759896848271$\times 10^{-07}$	-9.0759896858032$\times 10^{-07}$
$\vdots$	$\vdots$
-1.6833040542487$\times 10^{-06}$	-1.6833040543052$\times 10^{-06}$
-1.7474296200718$\times 10^{-06}$	-1.7474296200179$\times 10^{-06}$
-1.8149122203705$\times 10^{-06}$	-1.8149122204215$\times 10^{-06}$
-1.8861343835772$\times 10^{-06}$	-1.8861343835772$\times 10^{-06}$
-1.9615636688746$\times 10^{-06}$	-1.9615636688746$\times 10^{-06}$
-2.0417926323933$\times 10^{-06}$	-2.0417926323933$\times 10^{-06}$
-2.1276141594599$\times 10^{-06}$	-2.1276141594599$\times 10^{-06}$
-2.2201965660681$\times 10^{-06}$	-2.2201965660681$\times 10^{-06}$

Table 3.2: The computed left and right hand sides of equation (3.33), $n = 70$.

(left hand side of equation (3.33))/n^3	(right hand side of equation (3.33))/n^3
-1.6117973461395$\times 10^{-08}$	-1.6117973114169$\times 10^{-08}$
-2.6869707487590$\times 10^{-08}$	-2.6869707358407$\times 10^{-08}$
-3.7632536402413$\times 10^{-08}$	-3.7632536670543$\times 10^{-08}$
-4.8411608283313$\times 10^{-08}$	-4.8411608328744$\times 10^{-08}$
-5.9212069825471$\times 10^{-08}$	-5.9212069696528$\times 10^{-08}$
-7.0039127925471$\times 10^{-08}$	-7.0039127913953$\times 10^{-08}$
-8.0898010164976$\times 10^{-08}$	-8.0898010267356$\times 10^{-08}$
-9.1794023212022$\times 10^{-08}$	-9.1794023212022$\times 10^{-08}$
$\vdots$	$\vdots$
-3.8030660960309$\times 10^{-07}$	-3.8030660964884$\times 10^{-07}$
-3.9426232171084$\times 10^{-07}$	-3.9426232154198$\times 10^{-07}$
-4.0845574463214$\times 10^{-07}$	-4.0845574480995$\times 10^{-07}$
-4.2289956801862$\times 10^{-07}$	-4.2289956800995$\times 10^{-07}$
-4.3760718913259$\times 10^{-07}$	-4.3760718905604$\times 10^{-07}$
-4.5259271530648$\times 10^{-07}$	-4.5259271533573$\times 10^{-07}$
-4.6787108051342$\times 10^{-07}$	-4.6787108052335$\times 10^{-07}$
-4.8345805856406$\times 10^{-07}$	-4.8345805863114$\times 10^{-07}$
$\vdots$	$\vdots$
-9.5563633056128$\times 10^{-07}$	-9.5563633051395$\times 10^{-07}$
-9.8692301430570$\times 10^{-07}$	-9.8692301425888$\times 10^{-07}$
-1.0196929169265$\times 10^{-06}$	-1.0196929168999$\times 10^{-06}$
-1.0541068106002$\times 10^{-06}$	-1.0541068106390$\times 10^{-06}$
-1.0903614932174$\times 10^{-06}$	-1.0903614933002$\times 10^{-06}$
-1.1287069918118$\times 10^{-06}$	-1.1287069917665$\times 10^{-06}$
-1.1694793502372$\times 10^{-06}$	-1.1694793501831$\times 10^{-06}$
-1.2131770497869$\times 10^{-06}$	-1.2131770498170$\times 10^{-06}$

3.2 The Full Nonlinear Problem

We are now in a position to solve the full steady nonlinear problem where the dynamics of $\dot{m}$ are taken into account. We recall that the equation is

$$\left\{\frac{\bar{h}^3}{3}\left(\frac{1}{\pi}\fint_0^1 \frac{\bar{h}_\xi(\xi)}{\xi-\bar{x}}d\xi\right)_{\bar{x}} - \frac{\bar{h}^2}{2}\bar{\tau}\right\}_{\bar{x}} = \frac{1}{\eta\bar{h}}. \tag{3.35}$$

It should be recalled that equation (3.35) has to be solved subject to the boundary conditions $\bar{h}_{\bar{x}}(0) = 0$, $\bar{h}(\bar{x}) = 0$ at the dryout point $\bar{x} = 1$, $\bar{h}(0) = \bar{h}_0$ is known and the pressure gradient condition or the related pressure condition, from equation (3.6),

$$\fint_0^1 \frac{\bar{h}_\xi(\xi)}{\xi-\bar{x}}d\xi = \pi\frac{p_g - p_\infty}{\epsilon\rho_\infty U_\infty^2},$$

has to be satisfied at $\bar{x} = 0$.

3.2.1 Analytical Treatment

We continue here by first deriving the integral equation that has to satisfied by $\bar{h}(\bar{x})$. This integral equation does not contain any derivatives of the unknown function $\bar{h}(\bar{x})$ or principal-value integrals. Therefore, it may be possible to compute $\bar{h}(\bar{x})$ from this equation by direct iterative methods, see for example Pope (1999) [65], Fitt & Wilmott (1994) [34]. It is not obvious nonetheless, whether this numerical technique can be successful in solving the current problem. In the previous problems where this technique has been used successfully, the behaviour of the unknown function at one (or more) end point contains a logarithmic singularity which, as it will be shown, is not the case here. Our main interest here of deriving the integral equation for $\bar{h}(\bar{x})$ however, is to explore, in the process, whether in general it may be possible to solve this problem numerically using some interpolation techniques as in Spence *et al* (1987) [79], for example, who solves a problem which contains a singularity stronger than logarithm near an end point. We proceed by assuming that in (3.35), we can write

$$\frac{1}{\pi}\left(\fint_0^1 \frac{\bar{h}_\xi(\xi)}{\xi-\bar{x}}d\xi\right)_{\bar{x}} = f_{\bar{x}}(\bar{x}), \tag{3.36}$$

for some function $f(\bar{x})$. Equation (3.36) then integrates to give

$$\frac{1}{\pi}\fint_0^1 \frac{\bar{h}_\xi(\xi)}{\xi-\bar{x}}d\xi = f(\bar{x}) - C_1, \tag{3.37}$$

where C_1 is a constant of integration. On inverting (3.37) by standard methods we obtain

$$\bar{h}_{\bar{x}}(\bar{x}) = \frac{1}{\pi}\sqrt{\frac{1-\bar{x}}{\bar{x}}}\fint_0^1 \sqrt{\frac{\xi}{1-\xi}}\frac{C_1 - f(\xi)}{\xi-\bar{x}}d\xi + \frac{C_2}{\sqrt{\bar{x}(1-\bar{x})}}, \tag{3.38}$$

where C_2 is an arbitrary constant arising from inversion of the singular integral. We apply the boundary condition $\bar{h}_{\bar{x}}(\bar{x}) = 0$ at $\bar{x} = 0$ to get

$$C_1 + C_2 = \frac{1}{\pi}\int_0^1 \frac{f(\xi)}{\sqrt{\xi(1-\xi)}}d\xi. \tag{3.39}$$

Upon imposing the pressure boundary condition at $\bar{x} = 0$, we obtain

$$\int_0^1 \left\{ \frac{1}{\pi}\sqrt{\frac{1-\beta}{\beta}}\frac{1}{\beta}\int_0^1 \sqrt{\frac{\xi}{1-\xi}}\frac{C_1 - f(\xi)}{\xi-\beta}d\xi + \frac{C_2}{\beta\sqrt{\beta(1-\beta)}} \right\} d\beta = \frac{\pi(p_{g0}-p_\infty)}{\epsilon\rho_\infty U_\infty^2}, \tag{3.40}$$

where we recall that $p_{g0} = p_g(0)$ is the dimensional gas core pressure at the onset of the annular flow $\bar{x} = 0$. It can easily be shown by using standard techniques that

$$\begin{aligned}
\int_0^1 \sqrt{\frac{\xi}{1-\xi}}\frac{C_1}{\xi-\beta}d\xi &= C_1\pi, \\
\int_0^1 \frac{C_2}{\beta\sqrt{\beta(1-\beta)}}d\beta &= 2C_2 \lim_{\beta\to 0}\sqrt{\frac{1-\beta}{\beta}}, \\
\int_0^1 \frac{1}{\beta}\sqrt{\frac{1-\beta}{\beta}}d\beta &= 2\lim_{\beta\to 0}\sqrt{\frac{1-\beta}{\beta}} - \pi.
\end{aligned}$$

Thus, (3.40) becomes

$$\begin{aligned}
2C_1 \lim_{\beta\to 0}\sqrt{\frac{1-\beta}{\beta}} + 2C_2 \lim_{\beta\to 0}\sqrt{\frac{1-\beta}{\beta}}C_1 = \int_0^1 \left\{ \frac{1}{\pi}\sqrt{\frac{1-\beta}{\beta}}\frac{1}{\beta}\int_0^1 \sqrt{\frac{\xi}{1-\xi}}\frac{f(\xi)}{\xi-\beta}d\xi \right\} d\beta \\
+C_1\pi\frac{\pi(p_{g0}-p_\infty)}{\epsilon\rho_\infty U_\infty^2}.
\end{aligned} \tag{3.41}$$

Using integration by parts, we can write

$$\begin{aligned}
\int_0^1 \sqrt{\frac{\xi}{1-\xi}}\frac{f(\xi)}{\xi-\beta}d\xi = f(0)\pi + \int_0^1 f_\xi(\xi)\left\{ \sqrt{\frac{\beta}{1-\beta}}\ln\left|\frac{\sqrt{(1-\beta)\xi}+\sqrt{\beta(1-\xi)}}{\sqrt{\xi-\beta}}\right| + \right. \\
\left. \tan^{-1}\sqrt{\frac{1-\xi}{\xi}} \right\} d\xi,
\end{aligned}$$

and

$$\int_0^1 \frac{f(\xi)}{\sqrt{\xi(1-\xi)}}d\xi = f(0)\pi + \int_0^1 f_\xi(\xi)\tan^{-1}\sqrt{\frac{1-\xi}{\xi}}d\xi.$$

Hence we get

$$\begin{aligned}
\int_0^1 \sqrt{\frac{\xi}{1-\xi}}\frac{f(\xi)}{\xi-\beta}d\xi = \sqrt{\frac{\beta}{1-\beta}}\int_0^1 f_\xi(\xi)\ln\left|\frac{\sqrt{(1-\beta)\xi}+\sqrt{\beta(1-\xi)}}{\sqrt{\xi-\beta}}\right| d\xi \\
+\int_0^1 \frac{f(\xi)}{\sqrt{\xi(1-\xi)}}d\xi.
\end{aligned} \tag{3.42}$$

Therefore, (3.41) and (3.42) imply

$$2C_1 \lim_{\beta\to 0}\sqrt{\frac{1-\beta}{\beta}} + 2C_2 \lim_{\beta\to 0}\sqrt{\frac{1-\beta}{\beta}} - C_1\pi = \left(2\lim_{\beta\to 0}\sqrt{\frac{1-\beta}{\beta}} - \pi\right)\frac{1}{\pi}\times$$
$$\int_0^1 \frac{f(\xi)}{\sqrt{\xi(1-\xi)}}d\xi + \frac{1}{\pi}\int_0^1 \left\{\frac{1}{\beta}\int_0^1 f_\xi(\xi)\ln\left|\frac{\sqrt{(1-\beta)\xi}+\sqrt{\beta(1-\xi)}}{\sqrt{\xi-\beta}}\right|d\xi\right\}d\beta$$
$$+\frac{\pi(p_{g0}-p_\infty)}{\epsilon\rho_\infty U_\infty^2}. \qquad (3.43)$$

However, by equation (3.39), we find

$$2C_1 \lim_{\beta\to 0}\sqrt{\frac{1-\beta}{\beta}} + 2C_2 \lim_{\beta\to 0}\sqrt{\frac{1-\beta}{\beta}} = 2\lim_{\beta\to 0}\sqrt{\frac{1-\beta}{\beta}}\frac{1}{\pi}\int_0^1 \frac{f(\xi)}{\sqrt{\xi(1-\xi)}}d\xi,$$

so that the constants C_1 and C_2 are respectively given by

$$C_1 = -\frac{\pi(p_{g0}-p_\infty)}{\epsilon\rho_\infty U_\infty^2} - \frac{1}{\pi^2}\int_0^1 \left\{\frac{1}{\beta}\int_0^1 f_\xi(\xi)\ln\left|\frac{\sqrt{(1-\beta)\xi}+\sqrt{\beta(1-\xi)}}{\sqrt{\xi-\beta}}\right|d\xi\right\}d\beta$$
$$+\frac{1}{\pi}\int_0^1 \frac{f(\xi)}{\sqrt{\xi(1-\xi)}}d\xi, \qquad (3.44)$$

$$C_2 = \frac{\pi(p_{g0}-p_\infty)}{\epsilon\rho_\infty U_\infty^2} + \frac{1}{\pi^2}\int_0^1 \left\{\frac{1}{\beta}\int_0^1 f_\xi(\xi)\ln\left|\frac{\sqrt{(1-\beta)\xi}+\sqrt{\beta(1-\xi)}}{\sqrt{\xi-\beta}}\right|d\xi\right\}d\beta. \qquad (3.45)$$

Integration of (3.38) with respect to $\bar{x}$ and application of the boundary condition $\bar{h}(1) = 0$ yield

$$\bar{h}(\bar{x}) = \left\{-\frac{\pi}{2} + \sin^{-1}\sqrt{\bar{x}} + \sqrt{\bar{x}(1-\bar{x})}\right\}\left\{C_1 - \frac{1}{\pi}\int_0^1 \frac{f(\xi)}{\sqrt{\xi(1-\xi)}}d\xi\right\} + C_2\times$$
$$\left(2\sin^{-1}\sqrt{\bar{x}} - \pi\right) + \frac{1}{\pi}\int_{\bar{x}}^1 \left\{\int_0^1 f_\xi(\xi)\ln\left|\frac{\sqrt{(1-\beta)\xi}+\sqrt{\beta(1-\xi)}}{\sqrt{\xi-\beta}}\right|d\xi\right\}d\beta. \qquad (3.46)$$

The constants C_1 and C_2 are respectively given by equations (3.44) and (3.45). Thus, (3.46) implies

$$\bar{h}(\bar{x}) = -\frac{\pi}{2}C_2 + \frac{1}{\pi}\int_{\bar{x}}^1 \left\{\int_0^1 f_\xi(\xi)\ln\left|\frac{\sqrt{(1-\beta)\xi}+\sqrt{\beta(1-\xi)}}{\sqrt{\xi-\beta}}\right|d\xi\right\}d\beta$$
$$+C_2\left\{\sqrt{\bar{x}(1-\bar{x})} + \sin^{-1}\sqrt{\bar{x}}\right\}. \qquad (3.47)$$

The system (3.35) and (3.47) may be solved numerically using interpolation techniques. We continue however, for completeness, to obtain the integral equation which has to be satisfied by $\bar{h}(\bar{x})$. The parameter $\bar{h}(0) = \bar{h}_0$ is not independent of the dimensional pressure drop $(p_{g0} - p_\infty)$ and it has to be specified in such a way that

$$\bar{h}_0 = -\frac{\pi(p_{g0}-p_\infty)}{2\epsilon\rho_\infty U_\infty^2} + \frac{1}{2\pi}\int_0^1 \left\{\frac{2\beta-1}{\beta}\int_0^1 f_\xi(\xi)\ln\left|\frac{\sqrt{(1-\beta)\xi}+\sqrt{\beta(1-\xi)}}{\sqrt{\xi-\beta}}\right|d\xi\right\}d\beta. \qquad (3.48)$$

From (3.45), C_2 should also satisfy

$$C_2 = -\bar{h}_0\frac{2}{\pi} + \frac{2}{\pi^2}\int_0^1 f_\xi(\xi)\ln\left|\frac{\sqrt{(1-\beta)\xi}+\sqrt{\beta(1-\xi)}}{\sqrt{\xi-\beta}}\right|d\xi. \qquad (3.49)$$

It will be become clearer in section (3.2.2) that from (3.35), $\bar{h}^3(\bar{x})\, f_{\bar{x}}(\bar{x})|_{\bar{x}=0} \sim 0$ near $\bar{x} = 1$, with the result that

$$f_{\bar{x}}(\bar{x}) = \frac{3}{2}\frac{\bar{\tau}}{\bar{h}(\bar{x})} - \frac{3}{\bar{h}^3(\bar{x})}\int_{\bar{x}}^{1} \frac{d\beta}{\eta \bar{h}(\beta)}.$$

Thus, $\bar{h}(\bar{x})$ satisfies the integral equation

$$\bar{h}(\bar{x}) = \left\{-\frac{\pi}{2} + \sin^{-1}\sqrt{\bar{x}} + \sqrt{\bar{x}(1-\bar{x})}\right\} C_2 + \frac{1}{\pi}\int_{\bar{x}}^{1} \left\{\int_0^1 \left(\frac{3}{2}\frac{\bar{\tau}}{\bar{h}(\xi)} - \frac{3}{\bar{h}^3(\xi)}\int_{\xi}^{1} \frac{d\lambda}{\eta \bar{h}(\lambda)}\right) \times \ln\left|\frac{\sqrt{(1-\beta)\xi} + \sqrt{\beta(1-\xi)}}{\sqrt{\xi - \beta}}\right| d\xi\right\} d\beta,$$

where C_2 and $\bar{h}_0$ are related by

$$C_2 = -\bar{h}_0 \frac{2}{\pi} + \frac{2}{\pi^2}\int_0^1 \left\{\left(\frac{3}{2}\frac{\bar{\tau}}{\bar{h}(\xi)} - \frac{3}{\bar{h}^3(\xi)}\int_{\xi}^{1} \frac{d\lambda}{\eta \bar{h}(\lambda)}\right) \ln\left|\frac{\sqrt{(1-\beta)\xi} + \sqrt{\beta(1-\xi)}}{\sqrt{\xi - \beta}}\right| d\xi\right\} d\beta.$$

3.2.2 Asymptotic Analysis

We have seen in our examination of the previous two paradigm problems that the knowledge of the asymptotic behaviour of the unknown solution is very important in the numerical computation of this type of problem. Therefore, it is sensible to perform the asymptotic analysis of the current problem under consideration. It can easily be observed from (3.47) in section (3.2.1), that if (3.45) is defined and finite near $\bar{x} = 1$, then $\bar{h}(\bar{x}) \sim (1-\bar{x})^{1/2}$ In which case, an inspection of (3.35) then reveals that $\bar{\tau}$ must be specifically equal to zero and $f_{\bar{x}}(\bar{x}) \sim -6(1-\bar{x})^{-1}/\eta$ near $\bar{x} = 1$. We observe that in order to treat equation (3.47) numerically using interpolation techniques (see for example Spence *et al*, 1987)[79], we may write

$$f_{\bar{x}}(\bar{x}) = [\bar{x}(1-\bar{x})]^{-1} \sum_{j=0}^{N} A_j T_j\left(X(\bar{x})\right),$$

for some positive integer N, so that $f_{\bar{x}}(\bar{x}) \sim \bar{x}^{-1}$ near $\bar{x} = 0$ and $f_{\bar{x}}(\bar{x}) \sim (1-\bar{x})^{-1}$ near $\bar{x} = 1$. The functions T_j are the Chebyschev series and the function $X(\bar{x})$ has to be ingeniously chosen so that, if at all possible, the integrals

$$\int_0^1 \frac{1}{\beta}\left\{\int_0^1 \frac{T_j(X(\xi))}{\xi(1-\xi)} \ln\left|\frac{\sqrt{(1-\beta)\xi} + \sqrt{\beta(1-\xi)}}{\sqrt{\xi-\beta}}\right| d\xi\right\} d\beta,$$

$$\int_{\bar{x}}^1 \left\{\int_0^1 \frac{T_j(X(\xi))}{\xi(1-\xi)} \ln\left|\frac{\sqrt{(1-\beta)\xi} + \sqrt{\beta(1-\xi)}}{\sqrt{\xi-\beta}}\right| d\xi\right\} d\beta,$$

$$\int_0^1 \frac{T_j(X(\xi))}{\xi(1-\xi)} \ln\left|\frac{\sqrt{(1-\bar{x})\xi} + \sqrt{\bar{x}(1-\xi)}}{\sqrt{\xi-\bar{x}}}\right| d\xi,$$

can be evaluated in closed-form. The coefficients A_j may then be obtained by demanding that equation (3.35) be satisfied within some specified tolerance. We do not pursue this approach

further here since it is restrictive to the special case $\bar{\tau} = 0$ and more importantly, it may not always be possible to find some suitable functions $X(\bar{x})$ in this problem. It is therefore instructive to consider other appropriate asymptotic expansions of (3.35) for general values of $\bar{\tau}$.

At the dryout point, $\bar{x} = 1$, where $\bar{h}(\bar{x})$ vanishes, there is only one possibility that the nonlinear term $1/\eta\bar{h}$ balances with the first term on the left hand side of equation (3.35). That is to say that near $\bar{x} = 1$, on assuming the power law $\bar{h}(\bar{x}) \sim \bar{A}(1-\bar{x})^p$ for some positive constants $\bar{A}$ and p (< 1), we have

$$\frac{1}{\eta\bar{A}(1-\bar{x})^p} \sim \left\{ -\frac{\bar{A}^4}{3\pi} p(1-\bar{x})^{3p} \left(\fint_0^1 \frac{(1-\xi)^{p-1}}{\xi - \bar{x}} d\xi \right)_{\bar{x}} \right\}_{\bar{x}}. \tag{3.50}$$

We now make a substitution $1 - \xi = (1 - \bar{x})u$ under the integral sign so that (3.50), in the asymptotic limit near $\bar{x} = 1$, leads to

$$\frac{1}{\eta\bar{A}(1-\bar{x})^p} \sim \left\{ -p(p-1)\frac{\bar{A}^4}{3\pi}(1-\bar{x})^{4p-2} \int_0^\infty \frac{u^{p-1}}{u-1} du \right\}_{\bar{x}}. \tag{3.51}$$

Equation (3.51) implies $p \sim 3/5$ so that $\bar{h}(\bar{x}) \sim \bar{A}(1-\bar{x})^{3/5}$ and hence $\bar{h}_{\bar{x}}(\bar{x}) \sim -3\bar{A}(1-\bar{x})^{-2/5}/5$ near $\bar{x} = 1$. The semi-infinite range integral on the right hand side of (3.51) exists in the Cauchy principal sense and we calculate it using standard complex variable techniques (see for example Spiegel, 1964; Carrier *et al*, 1966) [80], [15]. We consider

$$\oint_\Gamma \frac{z^{p-1}}{z-1} dz, \qquad z = u + iv.$$

We choose Γ to be a contour as shown in the schematic figure (3.8) where $z = 0$ is a branch and the positive real axis is the branch line. The integrand has a simple pole at $z = 1$. In reality, the lines BC and DA coincide with the real axis. The integral from A to B is equal to zero by Cauchy theorem and the integral from C to D is also zero in the limit radii $\epsilon \to 0$ and $R \to \infty$. Therefore, the only contributing integrals are

$$\int_\epsilon^R \frac{u^{p-1}}{u-1} du,$$

from D to A, and

$$\int_\epsilon^R \frac{ue^{2\pi i(p-1)}}{ue^{2\pi i} - 1} du,$$

from B to C where the argument of z has changed by 2π. The two integrals have residues 1 and $e^{2\pi i(p-1)}$ respectively. Thus, by residue theorem and on taking the limits $\epsilon \to 0$, $R \to \infty$ we have

$$\int_0^\infty \frac{u^{p-1}}{u-1} du \left(1 - e^{2\pi i(p-1)}\right) = \pi i \left(1 + e^{2\pi i(p-1)}\right),$$

which implies that

$$\begin{aligned} \int_0^\infty \frac{u^{p-1}}{u-1} du &= \pi i \frac{e^{-p\pi i} + e^{p\pi i} e^{2\pi i}}{e^{-p\pi i} - e^{p\pi i} e^{-2\pi i}} \\ &= -\pi \cot(p\pi). \end{aligned}$$

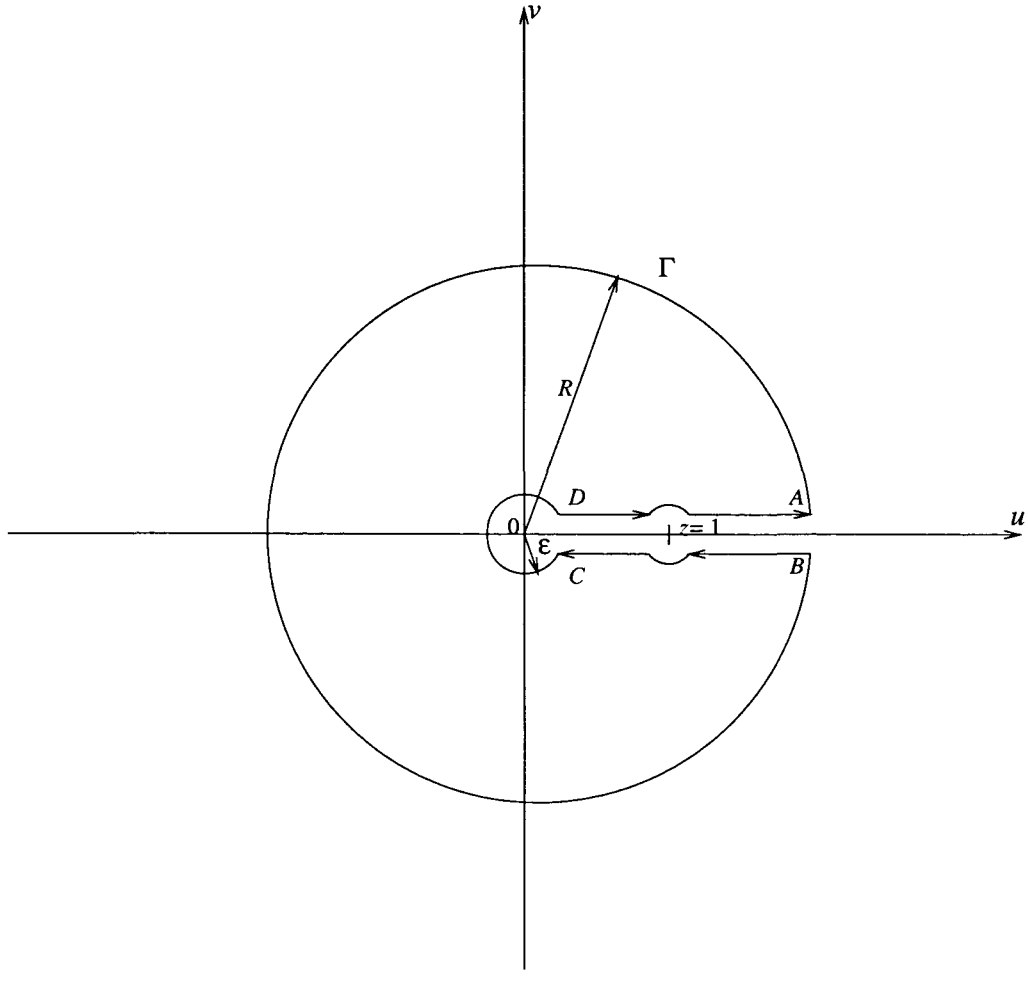

Figure 3.8: a schematic figure showing z in the complex plane (u, v)

As a result, $\bar{A}$ is given by $\bar{A} = (125\,|\tan(3\pi/5)|\,/4\eta)^{1/5}$.

Before we proceed, we observe that, after going through similar asymptotics as above on the problem with surface tension included (equation (2.65)), the only possibility is that near the dryout point $\bar{x} = 0$ the nonlinear term $1/\eta\bar{h}$ must be balanced by the surface tension term $\bar{S}\left(\bar{h}^3\bar{h}_{\bar{x}\bar{x}\bar{x}}\right)_{\bar{x}}/3\pi$. Hence, as one would expect, the singularity in $\bar{h}_{\bar{x}}(\bar{x})$ is reduced since now $\bar{h}(\bar{x}) \sim \bar{B}(1-\bar{x})^{4/5}$ and thus $\bar{h}_{\bar{x}}(\bar{x}) \sim -4\bar{B}(1-\bar{x})^{-1/5}/5$, for a positive constant $\bar{B}$, near $\bar{x} = 1$. However, since the surface tension term does not completely flatten the layer thickness $\bar{h}(\bar{x})$ near $\bar{x} = 1$ (unlike in other studies, e.g. King & Tuck (1993) [45]), then as far as the numerical method is concerned, the approach cannot be different from the one we employ to solve (3.35).

3.2.3 Regularisation and Pressure Gradient Condition

We now proceed to regularise the problem (3.35) by setting

$$\bar{h}(\bar{x}) = \left(\frac{125\left|\tan\left(\frac{3}{5}\pi\right)\right|}{4\eta}\right)^{\frac{1}{5}} H(y) \qquad \text{with } y^{\frac{5}{3}} = 1-\bar{x},$$

so that, after integration with respect to y (in order to avoid calculations of higher order derivatives numerically in the subsequent numerical solution), we then have to solve

$$-\frac{5}{3\eta}\left(\frac{4\eta}{125\chi}\right)^{\frac{1}{5}}\int_0^y \frac{u^{\frac{2}{3}}}{H(u)}du = \left(\frac{125\chi}{4\eta}\right)^{\frac{4}{5}}\frac{1}{5\pi}\frac{H^3}{y^{\frac{2}{3}}}\left(\fint_0^1 \frac{H_u(u)}{y^{\frac{5}{3}}-u^{\frac{5}{3}}}du\right)_y - \frac{1}{2}\left(\frac{4\eta}{125\chi}\right)^{\frac{2}{5}} H^2\bar{\tau} + C, \tag{3.52}$$

where C is a constant of integration and $\chi = |\tan(3\pi/5)|$.

We solve (3.52) subject to boundary conditions (3.8), i.e. $H(y) = 0$ at $y = 0$, $H_y(1) = 0$, $H(y) = (4\eta/125\chi)^{1/5}\bar{h}(0)$ at $y = 1$ and the pressure condition has to be satisfied here. From the pressure condition (3.6), in nondimensional form, we obtain the pressure gradient condition

$$\left(\fint_0^1 \frac{\bar{h}_\xi(\xi)}{\xi-\bar{x}}d\xi\right)_{\bar{x}}\Bigg|_{\bar{x}=0} = \pi\bar{p}_{g\bar{x}}|_{\bar{x}=0}\,.$$

We then obtain, in the regularised variables,

$$\left(\fint_0^1 \frac{H_u(u)}{y^{\frac{5}{3}}-u^{\frac{5}{3}}}du\right)_y\Bigg|_{y=1} = -\left(\frac{4\eta}{125\chi}\right)^{\frac{1}{5}}\pi\bar{p}_{gy}\Bigg|_{y=1},$$

where we recall that $\bar{p}_g$ is the nondimensional pressure in the gas core. The quantity $\bar{p}_{gy}|_{y=1}$ may be or may not be measurable in practice. If it is, then the constant C in equation (3.52) can be evaluated trivially. Nonetheless, whether this is the case or not, since pressure gradient

is an unknown function which depends on $H(y)$ in this problem, we are not physically allowed to dictate both $H(y)$ and $\bar{p}_{gy}$ at $y = 1$ independently. Therefore, it is mathematically sufficient to calculate C directly from (3.52), using known properties of the solution $H(y)$, and this will give us an appropriate physical pressure gradient condition which must be satisfied at $y = 1$.

We exploit the regularity condition, $H(y) \sim y$ near $y = 0$, in order to obtain the pressure gradient condition at the onset of the annular flow, $y = 1$, in terms of $H(1)$. We note from (3.52) that in actual fact C is given by

$$\begin{aligned} C &= -\frac{1}{5\pi}\left(\frac{125\chi}{4\eta}\right)^{\frac{4}{5}} \lim_{y\to 0}\left\{\frac{H^3}{y^{\frac{2}{3}}}\left(\int_0^1 \frac{H_u(u)}{y^{\frac{5}{3}}-u^{\frac{5}{3}}}du\right)_y\right\} \\ &\sim -\frac{1}{5\pi}\left(\frac{125\chi}{4\eta}\right)^{\frac{4}{5}} \lim_{y\to 0}\left\{y^{\frac{7}{3}}\left(\int_0^1 \frac{H_u(u)}{y^{\frac{5}{3}}-u^{\frac{5}{3}}}du\right)_y\right\}, \end{aligned} \tag{3.53}$$

as $H(y) \sim y$ near $y = 0$. We define a variable z by $y \ll z \ll 1$. We then write

$$I_l = \int_0^1 \frac{H_u(u)}{y^{\frac{5}{3}}-u^{\frac{5}{3}}}du = \int_0^z \frac{H_u(u)}{y^{\frac{5}{3}}-u^{\frac{5}{3}}}du - \int_z^1 \frac{H_u(u)}{u^{\frac{5}{3}}}\left(1+\left(\frac{y}{u}\right)^{\frac{5}{3}}+\left(\frac{y}{u}\right)^{\frac{10}{3}}\cdots\right)du. \tag{3.54}$$

We know that $H(y)$ is continuously differentiable at the points $y = 1$ and $y = 0$ since we recall that $H_y(y) = 0$ at $y = 1$, $H(y) \sim y$ and therefore $H_y(y) \sim 1$ near $y = 0$. In addition, we require that H is continuously differentiable at z. We then use integration by parts to expand the terms on the right hand side of equation (3.54) to give

$$\begin{aligned} I_l = {} & H_u(z)\left(\int \frac{du}{y^{\frac{5}{3}}-u^{\frac{5}{3}}}\right)\Big|_{u=z} - H_u(0)\left(\int \frac{du}{y^{\frac{5}{3}}-u^{\frac{5}{3}}}\right)\Big|_{u=0} - \int_0^z \left[H_{uu}(u)\int_0^z \frac{du}{y^{\frac{5}{3}}-u^{\frac{5}{3}}}\right]du \\ & - \left\{\left(H_u(u)\int \frac{du}{u^{\frac{5}{3}}}\right)\Big|_{u=1} - H_u(z)\left(\int \frac{du}{u^{\frac{5}{3}}}\right)\Big|_{u=z} - \int_z^1 \left[H_{uu}(u)\int \frac{du}{u^{\frac{5}{3}}}\right]du\right\} \\ & - y^{\frac{5}{3}}\int_z^1 \frac{H_u(u)}{u^{\frac{10}{3}}}du - \cdots, \end{aligned} \tag{3.55}$$

which implies that

$$\begin{aligned} I_l \sim {} & -\left(\int \frac{du}{y^{\frac{5}{3}}-u^{\frac{5}{3}}}\right)\Big|_{u=0} - \int_0^z \left[H_{uu}(u)\int_0^z \frac{du}{y^{\frac{5}{3}}-u^{\frac{5}{3}}}\right]du + \\ & \int_z^1 \left[H_{uu}(u)\int \frac{du}{u^{\frac{5}{3}}}\right]du - y^{\frac{5}{3}}\int_z^1 \frac{H_u(u)}{u^{\frac{10}{3}}}du - \cdots. \end{aligned} \tag{3.56}$$

On the right hand side terms of equation (3.55) (in order to arrive at (3.56)), $H_y(0) \sim 1$ has been used in the second term, $H_y(1) = 0$ has been employed so that the fourth term vanishes and finally, the fact that $y \ll z$ has been exploited so that in the asymptotic limit the first term on the right hand side of (3.55) is

$$H_u(z)\left(\int \frac{du}{y^{\frac{5}{3}}-u^{\frac{5}{3}}}\right)\Big|_{u=z} \sim -H_u(z)\left(\int \frac{du}{u^{\frac{5}{3}}}\right)\Big|_{u=z},$$

and it cancels with the fifth term in the equation. We further make an important observation that the third and the sixth terms on the right hand side of (3.55) perfectly cancel with each other. The reason is, in the third term, the contribution only comes from the integral evaluated at $u = z$ as H_{yy} and all other higher order derivatives of H are zero at $y = 0$. On the other hand, the contribution from the sixth term only comes from the integral evaluated at $u = z$ since $H(1)$ is a constant and therefore all its derivatives are equal to zero. Finally, it is important to observe that all other remaining terms on the right hand side of (3.55) are very small, in particular the leading order term is of $O(y/z^2)^{5/3}$. Thus, to leading order, equation (3.56) is simply

$$I_l = -\left(\int \frac{du}{y^{\frac{5}{3}} - u^{\frac{5}{3}}}\right)\Bigg|_{u=0}. \tag{3.57}$$

We use two consecutive substitutions $(u/y)^{5/6} = \sin(\theta)$ and $\sin(\theta) = t^5$ to transform the integral

$$\int \frac{du}{y^{5/3} - u^{5/3}}$$

into

$$\frac{6}{y^{2/3}} \int \frac{t^5}{1 - t^{10}} dt.$$

This term can now be evaluated by partial fractions to yield

$$\begin{aligned}
\int \frac{1}{y^{\frac{5}{3}} - u^{\frac{5}{3}}} du = \frac{6}{y^{\frac{2}{3}}} \Bigg\{ & -\frac{1}{10} \ln\left|-1 + s^2\right| + \frac{1}{40} \times \\
& \ln \left| \left(2s^2 + s - \sqrt{5}s + 2\right) \left(2s^2 + s + \sqrt{5}s + 2\right) \left(2s^2 - s - \sqrt{5}s + 2\right) \left(2s^2 - s + \sqrt{5}s + 2\right) \right| \\
& + \frac{\sqrt{5}}{40} \ln \left| \frac{\left(2s^2 + s + \sqrt{5}s + 2\right) \left(2s^2 - s - \sqrt{5}s + 2\right)}{\left(2s^2 + s - \sqrt{5}s + 2\right) \left(2s^2 - s + \sqrt{5}s + 2\right)} \right| \\
& + \frac{2\sqrt{5} + 1}{20\sqrt{10 + 2\sqrt{5}}} \left[\tan^{-1}\left(\frac{4s + 1 - \sqrt{5}}{\sqrt{10 + 2\sqrt{5}}} \right) - \tan^{-1}\left(\frac{4s - 1 + \sqrt{5}}{\sqrt{10 + 2\sqrt{5}}} \right) \right] \\
& + \frac{2\sqrt{5} - 1}{20\sqrt{10 - 2\sqrt{5}}} \left[\tan^{-1}\left(\frac{4s - 1 - \sqrt{5}}{\sqrt{10 - 2\sqrt{5}}} \right) - \tan^{-1}\left(\frac{4s + 1 + \sqrt{5}}{\sqrt{10 - 2\sqrt{5}}} \right) \right] \Bigg\},
\end{aligned}$$

where $s = (u/y)^{1/6}$. Thus, equations (3.53) and (3.57) imply that

$$C \sim \lim_{y \to 0} \left(y^{\frac{7}{3}} \left\{ \frac{1}{y^{\frac{2}{3}}} [\text{ a constant}] \right\}_y \right) = 0.$$

This is equivalent to a condition which dictates that at the onset of the annular flow $y = 1$, the pressure gradient is

$$\begin{aligned}
\frac{1}{5\pi} \left(\frac{125\chi}{4\eta}\right)^{\frac{4}{5}} H^3(1) \left(\fint_0^1 \frac{H_u(u)}{y^{\frac{5}{3}} - u^{\frac{5}{3}}} du \right)_y \Bigg|_{y=1} &= -\frac{5}{3\eta} \left(\frac{4\eta}{125\chi}\right)^{\frac{1}{5}} \int_0^1 \frac{u^{\frac{2}{3}}}{H(u)} du \\
&\quad + \frac{1}{2} \left(\frac{125\chi}{4\eta}\right)^{\frac{2}{5}} H^2(1)\bar{\tau}.
\end{aligned} \tag{3.58}$$

Rearranging and simplifying (3.52) implies that we have to solve

$$\left(\frac{4\eta}{125\chi}\right)^{\frac{2}{5}}\pi\frac{y^{\frac{2}{3}}}{H^3(y)}\left\{-\frac{25}{3\eta}\left(\frac{4\eta}{125\chi}\right)^{\frac{3}{5}}\int_0^y\frac{u^{\frac{2}{3}}}{H(u)}du+\frac{5H^2(y)}{2}\bar{\tau}\right\}=\left(\fint_0^1\frac{H_u(u)}{y^{\frac{5}{3}}-u^{\frac{5}{3}}}du\right)_y, \quad (3.59)$$

subject to $H(0)=0$, $H_y(1)=0$ and $H(1)$ is a specified constant which satisfy equation (3.58).

3.2.4 Numerical Scheme

The nonlinear regularised problem (3.59) may now be solved numerically. The problem is discretised in the conventional way as repeatedly described in the previous paradigm problems. We define a mesh $u_j=j/n$ for $0\leq j\leq n-1$ on the interval $[0,1]$, where n is as usual the number of mesh-points. We then assume, for simplicity, that H can be approximated by linear functions in each subinterval $[u_j,u_{j+1}]$. The pressure gradient on the right hand side of (3.59), $\bar{p}_{gy}$, is approximated by finite differences and (3.59) is collocated at the mid-mesh points by insisting that $\bar{p}_{gy}$ is satisfied exactly there. In order to keep a balance of accuracy, speed and complexity in the numerical computations, we further assume that the singular integral

$$\bar{p}_g=\fint_0^1\frac{H_u(u)}{y^{\frac{5}{3}}-u^{\frac{5}{3}}}du,$$

may be approximated using the trapezoidal rule so that it is equal to the sum of the integrals in each subinterval $[u_j,u_{j+1}]$. We therefore have to solve a set of nonlinear algebraic equations

$$\sum_{j=0}^{n-1}6n^2\Big(H_{j+1}-H_j\Big)\Big(I_{1+}-I_{1-}\Big)=\left(\frac{4\eta}{125\chi}\right)^{\frac{2}{5}}\pi\left(\frac{i}{n}\right)^{\frac{2}{3}}\left\{-\frac{25}{3\eta}\left(\frac{4\eta}{125\chi}\right)^{\frac{3}{5}}\frac{1}{H_i^3}\times\right.$$
$$\left.\left[\frac{3}{2}\left(\frac{1}{n}\right)^{\frac{2}{3}}+I_2\right]+\frac{5}{2}\frac{\bar{\tau}}{H_i}\right\},\quad 1\leq i\leq n-2. \quad (3.60)$$

The integrals $I_{1\pm}$ and I_2 are respectively given by

$$I_{1\pm}=\int_{u_j}^{u_{j+1}}\frac{1}{u_{i\pm\frac{1}{2}}^{\frac{5}{3}}\pm u^{\frac{5}{3}}}du, \quad (3.61)$$

$$I_2=\sum_{j=1}^{i}\int_{u_j}^{u_{j+1}}\frac{u^{\frac{2}{3}}}{H(u)}du. \quad (3.62)$$

The integral in equation (3.62) is approximated by

$$\int_{u_j}^{u_{j+1}}\frac{u^{\frac{2}{3}}}{m\left(u-\frac{mu_j-H_j}{m}\right)}du=\frac{1}{m}\left\{\frac{3}{2}\left(u_{j+1}^{\frac{2}{3}}-u_j^{\frac{2}{3}}\right)+Q_j^{\frac{2}{3}}\left[\ln\left|\frac{u_{j+1}^{\frac{1}{3}}-Q_j^{\frac{1}{3}}}{u_j^{\frac{1}{3}}-Q_j^{\frac{1}{3}}}\right|\right.\right.$$

$$-\frac{1}{2}\ln\left|\frac{u_{j+1}^{\frac{2}{3}}+u_{j+1}^{\frac{1}{3}}Q_j^{\frac{1}{3}}+Q_j^{\frac{2}{3}}}{u_j^{\frac{2}{3}}+u_j^{\frac{1}{3}}Q_j^{\frac{1}{3}}+Q_j^{\frac{2}{3}}}\right|\Bigg]$$

$$+Q_j^{\frac{2}{3}}\sqrt{3}\left[\tan^{-1}\left\{\frac{1}{\sqrt{3}}\left(\frac{2u_{j+1}^{\frac{2}{3}}}{Q_j^{\frac{1}{3}}}+1\right)\right\}-\tan^{-1}\left\{\frac{1}{\sqrt{3}}\left(\frac{2u_j^{\frac{2}{3}}}{Q_j^{\frac{1}{3}}}+1\right)\right\}\right]\Bigg\},$$

where $H(u)$ has been approximated by piece-wise linear functions

$$H(u)=mu-(mu_j-H_j)\,,$$

in each interval $[u_j,u_{j+1}]$. Clearly, m and Q_j are respectively given by

$$m=\frac{H_{j+1}-H_j}{u_{j+1}-u_j},$$
$$Q_j=\frac{mu_j-H_j}{m}.$$

As a result of calculating (3.57), we find that the integrals I_2 and $I_{1\pm}$, after putting in the limits and performing some straightforward algebraic simplifications, are respectively given by

$$I_2=\sum_{j=1}^{i}\frac{1}{n\left(H_{j+1}-H_j\right)}\Bigg\{\frac{3}{2}\frac{(j+1)^{\frac{2}{3}}-j^{\frac{2}{3}}}{n^{\frac{2}{3}}}+\left(\frac{n^2\left(H_{j+1}-H_j\right)j-H_j}{n\left(H_{j+1}-H_j\right)}\right)^{\frac{2}{3}}\times$$

$$\left[\ln\left|\frac{((j+1)n\left(H_{j+1}-H_j\right))^{\frac{1}{3}}-\left(n^2\left(H_{j+1}-H_j\right)j-H_j\right)^{\frac{1}{3}}}{(jn\left(H_{j+1}-H_j\right))^{\frac{1}{3}}-\left(n^2\left(H_{j+1}-H_j\right)j-H_j\right)^{\frac{1}{3}}}\right|-\right.$$

$$\frac{1}{2}\ln\left|\frac{((j+1)\left(H_{j+1}-H_j\right))^{\frac{2}{3}}+((j+1)\left(H_{j+1}-H_j\right)\left(n^2\left(H_{j+1}-H_j\right)j-H_j\right))^{\frac{1}{3}}+}{(j\left(H_{j+1}-H_j\right))^{\frac{2}{3}}+(j\left(H_{j+1}-H_j\right)\left(n^2\left(H_{j+1}-H_j\right)j-H_j\right))^{\frac{1}{3}}+}\right.$$

$$\left.\frac{\left(n^2\left(H_{j+1}-H_j\right)j-H_j\right)^{\frac{2}{3}}}{\left(n^2\left(H_{j+1}-H_j\right)j-H_j\right)^{\frac{2}{3}}}\right|+\sqrt{3}\left\{\tan^{-1}\left(\frac{1}{3}\left(2\left(\frac{(j+1)\left(n\left(H_{j+1}-H_j\right)\right)}{n^2\left(H_{j+1}-H_j\right)j-H_j}\right)^{\frac{1}{3}}+1\right)\right)-\right.$$

$$\left.\left.\tan^{-1}\left(\frac{1}{3}\left(2\left(\frac{j\left(n\left(H_{j+1}-H_j\right)\right)}{n^2\left(H_{j+1}-H_j\right)j-H_j}\right)^{\frac{1}{3}}+1\right)\right)\right\}\Bigg]\Bigg\},$$

and

$$
\begin{aligned}
I_{1\pm} = \left(\frac{2n}{2i\pm 1}\right)^{\frac{2}{3}} \Bigg\{ & -\frac{1}{10}\ln\left|\frac{-1+\left(\frac{2j\pm 2}{2i\pm 1}\right)^{\frac{1}{3}}}{-1+\left(\frac{2j}{2i\pm 1}\right)^{\frac{1}{3}}}\right| + \\
& \frac{1}{40}\ln\left|\frac{\left(2\left(\frac{2j\pm 2}{2i\pm 1}\right)^{\frac{1}{3}}+\left(\frac{2j\pm 2}{2i\pm 1}\right)^{\frac{1}{6}}\left(1-\sqrt{5}\right)+2\right)\left(2\left(\frac{2j\pm 2}{2i\pm 1}\right)^{\frac{1}{3}}+\left(\frac{2j\pm 2}{2i\pm 1}\right)^{\frac{1}{6}}\left(1+\sqrt{5}\right)+2\right)}{\left(2\left(\frac{2j}{2i\pm 1}\right)^{\frac{1}{3}}+\left(\frac{2j}{2i\pm 1}\right)^{\frac{1}{6}}\left(1-\sqrt{5}\right)+2\right)\left(2\left(\frac{2j}{2i\pm 1}\right)^{\frac{1}{3}}+\left(\frac{2j}{2i\pm 1}\right)^{\frac{1}{6}}\left(1+\sqrt{5}\right)+2\right)}\times \right. \\
& \left.\frac{\left(2\left(\frac{2j\pm 2}{2i\pm 1}\right)^{\frac{1}{3}}-\left(\frac{2j\pm 2}{2i\pm 1}\right)^{\frac{1}{6}}\left(1+\sqrt{5}\right)+2\right)\left(2\left(\frac{2j\pm 2}{2i\pm 1}\right)^{\frac{1}{3}}-\left(\frac{2j\pm 2}{2i\pm 1}\right)^{\frac{1}{6}}\left(1-\sqrt{5}\right)+2\right)}{\left(2\left(\frac{2j}{2i\pm 1}\right)^{\frac{1}{3}}-\left(\frac{2j}{2i\pm 1}\right)^{\frac{1}{6}}\left(1+\sqrt{5}\right)+2\right)\left(2\left(\frac{2j}{2i\pm 1}\right)^{\frac{1}{3}}-\left(\frac{2j}{2i\pm 1}\right)^{\frac{1}{6}}\left(1-\sqrt{5}\right)+2\right)}\right| + \\
& \frac{\sqrt{5}}{40}\ln\left|\frac{\left(2\left(\frac{2j\pm 2}{2i\pm 1}\right)^{\frac{1}{3}}+\left(\frac{2j\pm 2}{2i\pm 1}\right)^{\frac{1}{6}}\left(1+\sqrt{5}\right)+2\right)\left(2\left(\frac{2j\pm 2}{2i\pm 1}\right)^{\frac{1}{3}}-\left(\frac{2j\pm 2}{2i\pm 1}\right)^{\frac{1}{6}}\left(1+\sqrt{5}\right)+2\right)}{\left(2\left(\frac{2j\pm 2}{2i\pm 1}\right)^{\frac{1}{3}}+\left(\frac{2j\pm 2}{2i\pm 1}\right)^{\frac{1}{6}}\left(1-\sqrt{5}\right)+2\right)\left(2\left(\frac{2j\pm 2}{2i\pm 1}\right)^{\frac{1}{3}}-\left(\frac{2j\pm 2}{2i\pm 1}\right)^{\frac{1}{6}}\left(1-\sqrt{5}\right)+2\right)}\times \right. \\
& \left.\frac{\left(2\left(\frac{2j}{2i\pm 1}\right)^{\frac{1}{3}}+\left(\frac{2j}{2i\pm 1}\right)^{\frac{1}{6}}\left(1-\sqrt{5}\right)+2\right)\left(2\left(\frac{2j}{2i\pm 1}\right)^{\frac{1}{3}}-\left(\frac{2j}{2i\pm 1}\right)^{\frac{1}{6}}\left(1-\sqrt{5}\right)+2\right)}{\left(2\left(\frac{2j}{2i\pm 1}\right)^{\frac{1}{3}}+\left(\frac{2j}{2i\pm 1}\right)^{\frac{1}{6}}\left(1+\sqrt{5}\right)+2\right)\left(2\left(\frac{2j}{2i\pm 1}\right)^{\frac{1}{3}}-\left(\frac{2j}{2i\pm 1}\right)^{\frac{1}{6}}\left(1+\sqrt{5}\right)+2\right)}\right| + \\
& \frac{\sqrt{5}+5}{10\sqrt{10+2\sqrt{5}}}\left[\tan^{-1}\left(\frac{4\left(\frac{2j\pm 2}{2i\pm 1}\right)^{\frac{1}{6}}+1-\sqrt{5}}{\sqrt{10+2\sqrt{5}}}\right)-\tan^{-1}\left(\frac{4\left(\frac{2j}{2i\pm 1}\right)^{\frac{1}{6}}+1-\sqrt{5}}{\sqrt{10+2\sqrt{5}}}\right)+\right. \\
& \left.\tan^{-1}\left(\frac{4\left(\frac{2j}{2i\pm 1}\right)^{\frac{1}{6}}-1+\sqrt{5}}{\sqrt{10+2\sqrt{5}}}\right)-\tan^{-1}\left(\frac{4\left(\frac{2j\pm 2}{2i\pm 1}\right)^{\frac{1}{6}}-1+\sqrt{5}}{\sqrt{10+2\sqrt{5}}}\right)\right]+ \\
& \frac{\sqrt{5}-5}{10\sqrt{10-2\sqrt{5}}}\left[\tan^{-1}\left(\frac{4\left(\frac{2j\pm 2}{2i\pm 1}\right)^{\frac{1}{6}}-1-\sqrt{5}}{\sqrt{10-2\sqrt{5}}}\right)-\tan^{-1}\left(\frac{4\left(\frac{2j}{2i\pm 1}\right)^{\frac{1}{6}}-1-\sqrt{5}}{\sqrt{10-2\sqrt{5}}}\right)+\right. \\
& \left.\left.\tan^{-1}\left(\frac{4\left(\frac{2j}{2i\pm 1}\right)^{\frac{1}{6}}+1+\sqrt{5}}{\sqrt{10-2\sqrt{5}}}\right)-\tan^{-1}\left(\frac{4\left(\frac{2j\pm 2}{2i\pm 1}\right)^{\frac{1}{6}}+1+\sqrt{5}}{\sqrt{10-2\sqrt{5}}}\right)\right]\right\}.
\end{aligned}
$$

The system (3.60) is then solved iteratively for the values of H by Powell's method as implemented in the NAG library routine C05NBF. As explained earlier, this method uses a combination of Newton and steepest descent iterations. The initial guess to the solution is taken to be a function which is piecewise linear on $[0,1]$, i.e. linear in each subinterval $[u_j, u_{j+1}]$. The system (3.60) is solved subject to the boundary conditions $H_0 = 0$, $H_n = H_{n-1}$ and H_n has to be prescribed such that the numerical solution satisfies the pressure boundary condition (3.58). The parameters $\bar{\tau}$ and η are specified and may be varied at will. For fixed values of $\bar{\tau}$ and η, H_n is altered until the converged numerical solution satisfies the boundary condition (3.58) within some specified tolerance. Thus, H_n (and hence the nondimensional length to the dryout point) is obtained as an eigenvalue to this problem. Essentially, this

implies that it may not be always possible to obtain a numerical solution which satisfies all the prescribed boundary conditions for arbitrarily specified values of η and $\bar{\tau}$. Once H_n (together with the computed solution for $H(y)$) is obtained, it is then trivial to calculate the dimensional length to the dryout point from equation (3.9) if the dimensional $h(0)$ can be measured in practice. For clarity, it should be mentioned that due to the complexity of the computations in this problem, a tolerance (or absolute error) of magnitude less or equal to 1×10^{-5} has been employed for convenience in this study. It should also be noted that the discrete version of (3.58) is exactly (3.60) with $i = n$.

In general, a numerical solution may be easily obtained for $n \leq 17$. For $n > 17$, a continuation method (where a previous converged numerical solution is used as a starting value) has to be employed. It should be mentioned however, that even when $n \leq 17$, it is possible for the numerical scheme not to converge which may lead to wrong impressions that a solution does not exist for some combinations of certain values of the specified parameters η and $\bar{\tau}$. Therefore, it is crucial in this problem that the initial guess to the solution must be close enough to the required solution and this requires a lot of intuition. As a result, the method can take a long time before one satisfactory converged numerical solution is obtained. It is customary in numerical computations to quote the exact amount of time the numerical scheme takes for it to converge to the correct solution. It is almost impossible to do that here because the amount of time taken is controlled by many parameters, e.g. how far the initial guess to the solution is from the solution itself, after how many points can the continuation method be employed, how long does it take to find the appropriate h_0 so that the numerical solution satisfies all the appropriate boundary conditions for each combination of the prescribed parameters H_n, η and $\bar{\tau}$. This implies that it would not be abnormal in this problem for the numerical method to take completely different amounts of time to reach the same converged numerical solution if the choice of initial parameters is different. The accuracy of the numerical results, on the other hand, can be checked by evaluating each side of equation (3.59). Illustrative results are shown in table (3.3) for $\eta = \bar{\tau} = 1.0$ where the number of mesh points $n = 100$. The values of $\bar{h}_j$ are recovered from those of H_j using the relationship

$$\bar{h}_j = \left(\frac{125\chi}{4\eta}\right)^{\frac{1}{5}} H_{n-j},\ 0 \leq j \leq n,$$

and the results are shown and discussed in the next section below.

3.2.5 Numerical Results and Discussions

In this section we present and discuss numerical solutions of equation (3.60). We begin with figure (3.9) which shows plots of different numerical solutions to (3.60). None of the solutions shown by various dotted lines in this figure satisfy the boundary condition (3.58) and hence

Table 3.3: a table showing the computed left and right hand sides of equation (3.59) when $n = 100$ points.

(left hand side of equation (3.59))	(right hand side of equation (3.59))
-1348.6295919936	-1348.6295919946
-1853.5718199877	-1853.5718199890
-961.56742628979	-961.56742628957
-710.18724183416	-710.18724183411
-584.98065706458	-584.98065706462
-506.91613418576	-506.91613418565
-452.17521258971	-452.17521258918
-410.97677037539	-410.97677037547
⋮	⋮
-169.20973850158	-169.20973850169
-165.58172052767	-165.58172052758
-162.14296448477	-162.14296448483
-158.87808700445	-158.87808700443
-155.77337996565	-155.77337996573
-152.81658414089	-152.81658414092
-149.99669906233	-149.99669906234
-147.30382245842	-147.30382245842
⋮	⋮
-108.17057086541	-108.17057086546
-106.97304065314	-106.97304065312
-105.80816643502	-105.80816643501
-104.674546504705	-104.674546504705
-103.570860944285	-103.570860944285
-102.495865689865	-102.495865689865
-101.448387123678	-101.448387123678
-100.427317141391	-100.427317141391

$\bar{h}_{\bar{x}}(\bar{x}) = 0$ at $\bar{x} = 0$. Thus, the results depicted in this figure suggest that for each combination

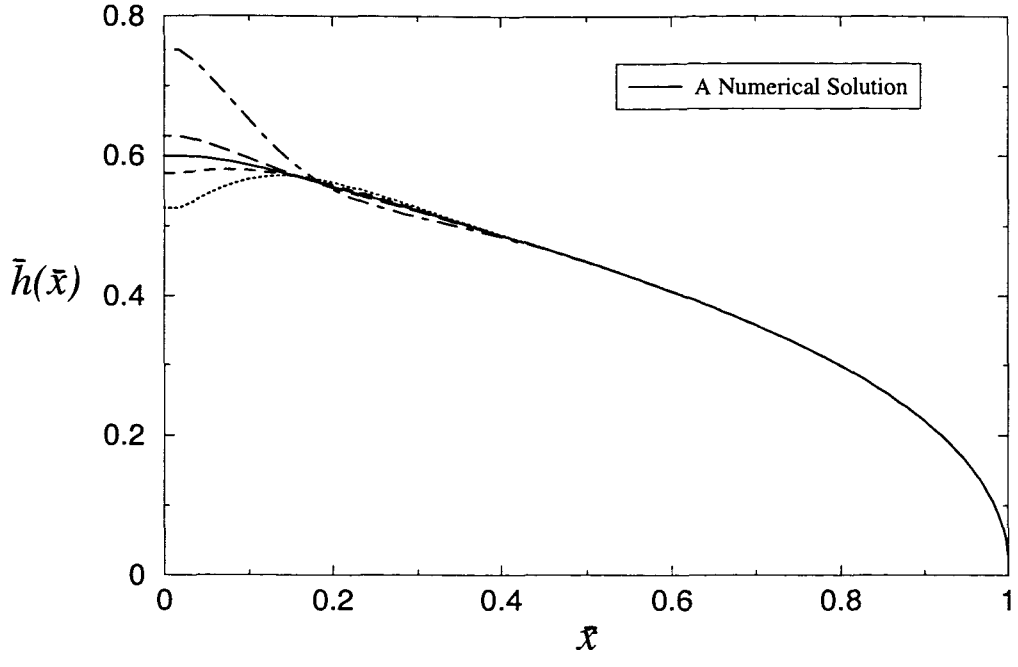

Figure 3.9: Plots of the liquid film free surface $\bar{h}(\bar{x})$ when $\bar{\tau} = 1.0$ and $\eta = 1.0$ for $n = 100$ points.

of the parameters $\bar{h}_0$, $\bar{\tau}$ and η, there is a unique solution which satisfies all the prescribed boundary conditions to the problem. It is further observed that only the acceptable solution is monotonic. In figure (3.10), it is moreover illustrated that these other solutions are not only unsatisfactory (with regard to the boundary conditions at the onset of the annular flow $\bar{x} = 0$) but they also give a false length to the dryout point. Figures (3.10) and (3.9) are essentially the same but in figure (3.10) the dryout point is allowed to move by scaling the problem differently (the details are given below) while in figure (3.9) the dryout point is fixed at $\bar{x} = 1$.

From the results shown in figure (3.11), it is obvious that an increase (decrease) in the mass transfer parameter η, results in a decrease (increase) in the thickness of the liquid film. It may not be obvious nevertheless as to what this result, in the present form, may imply about the physics of the problem. Equation (3.35), together with the appropriate boundary conditions have been proposed so that predictions for the dryout point can be made. However, for numerical convenience, the approach that has been adopted in solving the problem hides the fact that this is a moving boundary problem. Presumably η should determine the establishment of the dryout at an order L_0 length from the onset of the annular flow. It should then be of practical interest to know how the dryout point varies with the mass transfer parameter η. To accomplish this, we rescale the variables in equation (3.35).

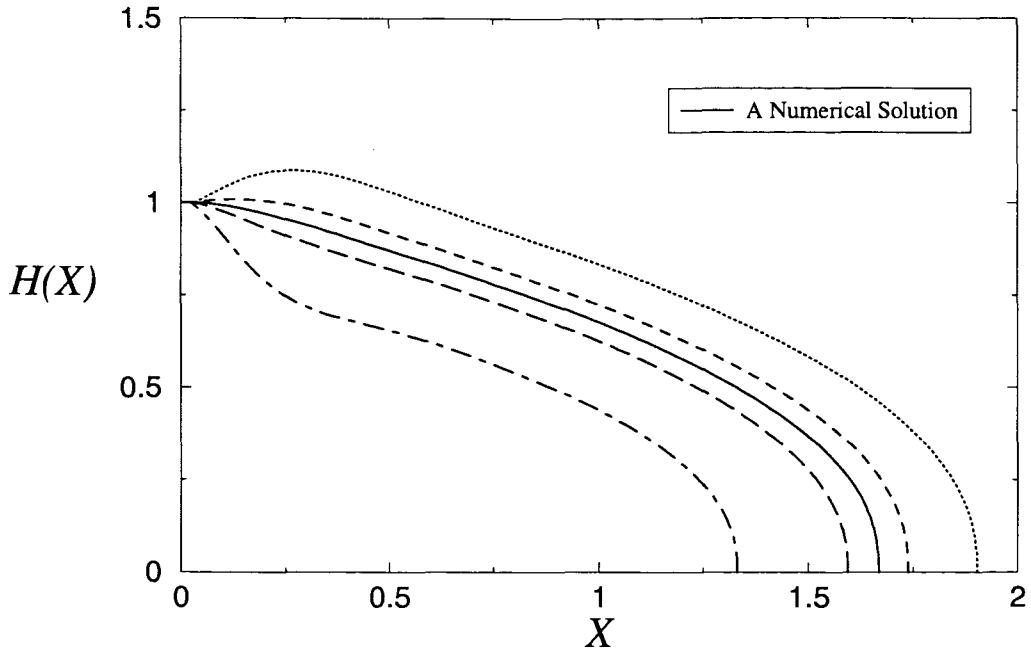

Figure 3.10: Plots of the liquid film free surface $\mathcal{H}(X)$ when $\bar{\tau} = 1.0$ and $\eta = 1.0$ ($n = 100$).

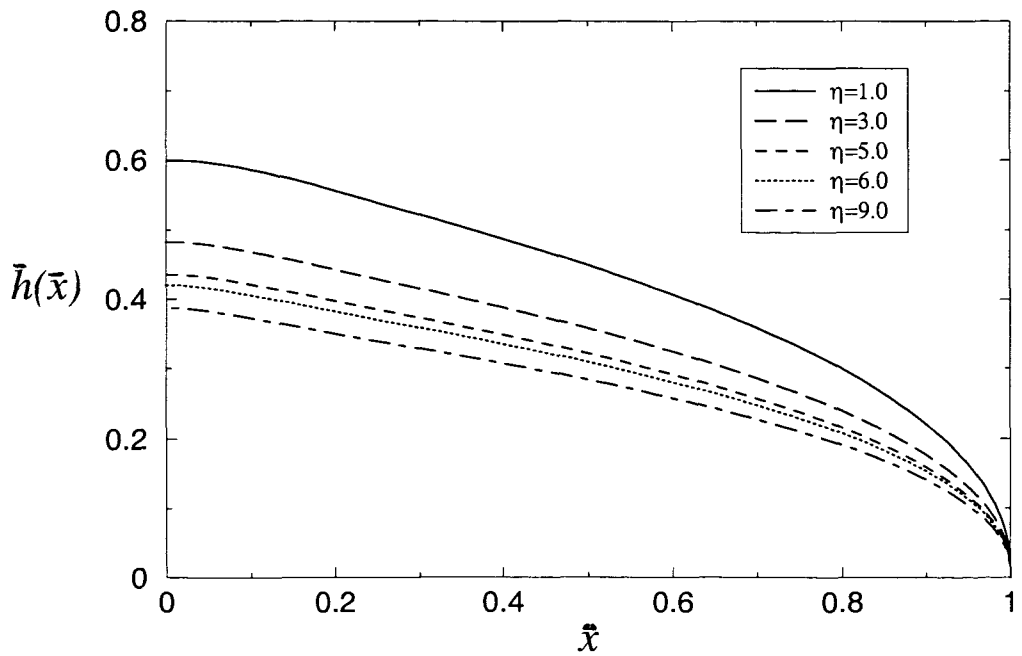

Figure 3.11: Plots of the effects of varying the mass transfer parameter η on liquid film free surface $\bar{h}(\bar{x})$ when $\bar{\tau} = 1.0$ ($n = 100$).

We set $\bar{h}(\bar{x}) = \bar{h}_0\mathcal{H}(X)$ where X is appropriately defined by $\bar{x} = \bar{h}_0 X$ and $\bar{h}_0 = \bar{h}(0)$. In this case (3.35) becomes

$$\left\{\frac{\mathcal{H}^3}{3\pi}\left(\int_0^{\frac{1}{\bar{h}_0}} \frac{\mathcal{H}_\Psi(\Psi)}{\Psi - X}d\Psi\right)_X - \frac{\bar{\tau}}{2}\mathcal{H}^2\right\}_X = \frac{1}{\kappa\mathcal{H}}, \tag{3.63}$$

where $\kappa = \eta\bar{h}_0^2$. It is then important to note that (3.35) can be solved in the form of equation (3.63) subject to boundary conditions $\mathcal{H}(0) = 1$, $\mathcal{H}_X(0) = 0$, $\mathcal{H}\left(1/\bar{h}_0\right) = 0$ and $\mathcal{H}(X) \sim \left(125\bar{h}_0^2\left|\tan\left(3\pi/5\right)/4\eta\right|\right)^{1/5}\left(1/h_0 - X\right)^{3/5}$ near the dryout point $X = 1/\bar{h}_0$. However, there is no need to solve the problem again at this point, for we have got all the information we need at hand. Since the solution to equation (3.63) does not exist for every arbitrarily prescribed parameters $\bar{\tau}$, η and $\bar{h}_0$, then the relationship between the length to the dryout point $L(0) = L_0$ and η can be achieved from the data we already have by plotting $\mathcal{H}(X)$ against X for various values of η and $\bar{h}_0$ (at a fixed value of $\bar{\tau}$) for which the solution to (3.35) (and hence (3.63)) exists and satisfies all the prescribed boundary conditions. Illustrative results are shown in figures (3.12) and (3.13). Both figures (3.12) and (3.13) indicate that,

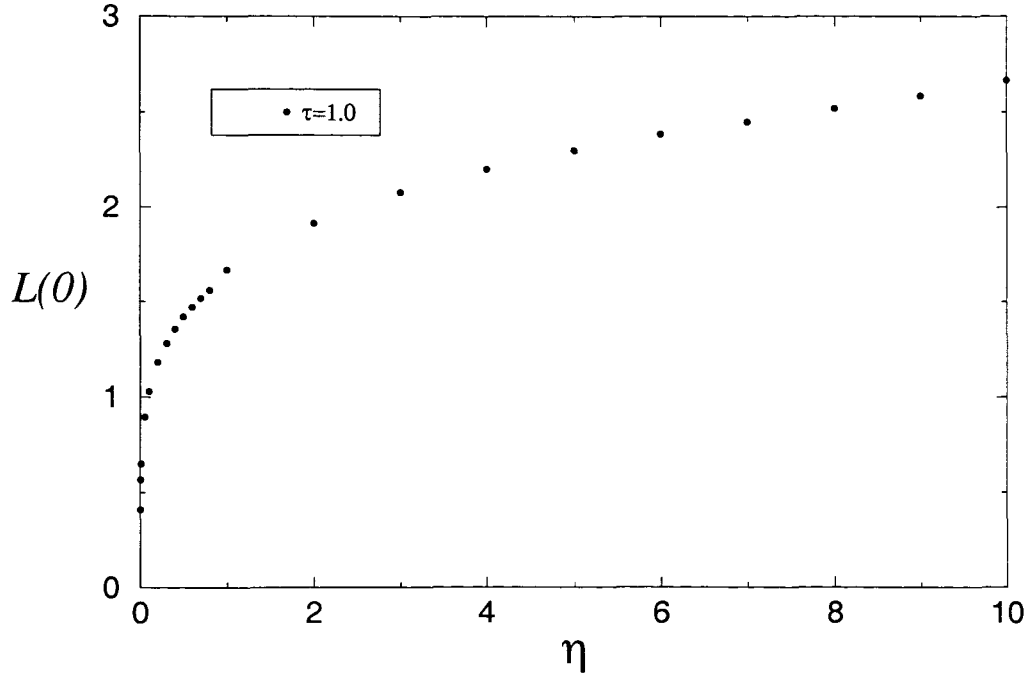

Figure 3.12: Plots of the length to dryout point, L_0, against the heat mass transfer parameter η.

as one would expect, an increase in η (or using a liquid with larger latent heat) the mass transfer is small and dryout is postponed further downstream. On the other hand, for $\eta \ll 1$ (or a liquid with small latent heat) the mass transfer is so high that the liquid film may not be established and dryout occurs immediately. In figure (3.12), each point on the curve is

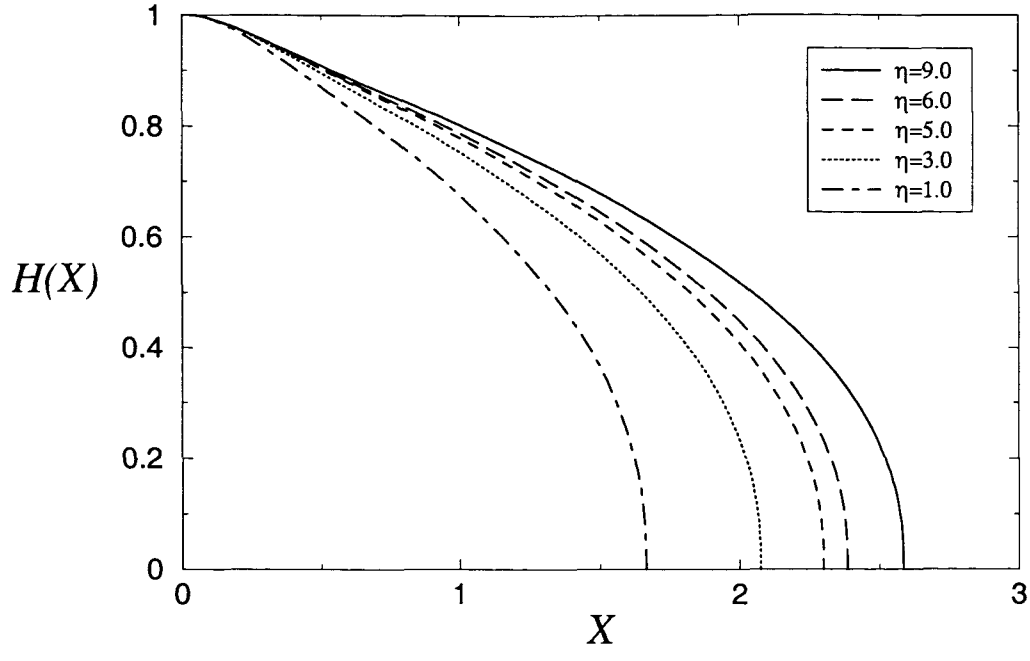

Figure 3.13: Plots of the liquid film free surface $\mathcal{H}(X)$ for various values of the mass transfer parameter η, for a fixed traction parameter $\bar{\tau} = 1.0$.

painstakingly obtained by numerically solving equation (3.35). It is observed from this curve that when η is roughly less or equal to 1, a small increase in η leads to a large increase in the length to the dryout point L_0. When $\eta > 1$, the increase in the length to the dryout due to an increase in η becomes less vigorous and seems to approach a steadily linear relationship between η and L_0. Since it is increasingly difficult to obtain the numerical solutions for $\bar{h}(\bar{x})$ as η gets very small, in this work computations have been performed down to $\eta = 0.001$.

It is evident from the results in figure (3.14) that an increase in $\bar{\tau}$ (the tangential traction provided by the fast flow of vapour in the gas core) results in a decrease in the thickness of the liquid film but it is difficult to make an analysis of the physical implications of these results in the present form. However, from the later scaled form of the problem, equation (3.63), it appears (see figure (3.15)) that the increase in the traction parameter $\bar{\tau}$ tends to slowly but gradually stretch the liquid layer and hence the position of the dryout point. Figure (3.16) shows the relationship between the length to the dryout point and the traction parameter $\bar{\tau}$. It is fascinating to observe from this graph that even for large values of $\bar{\tau}$, the length to the dryout point is still merely $O(1)$ and it seems it is likely to remain so even for values of $\bar{\tau} \to \infty$.

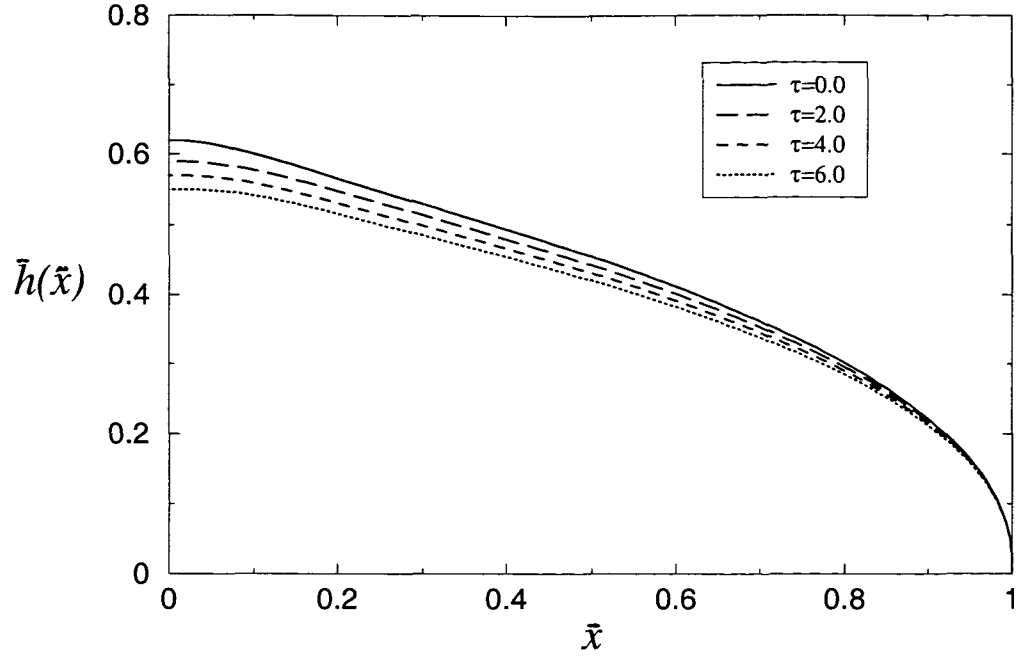

Figure 3.14: Plots of the liquid film free surface $\bar{h}(\bar{x})$ when $\eta = 1.0$ ($n = 100$).

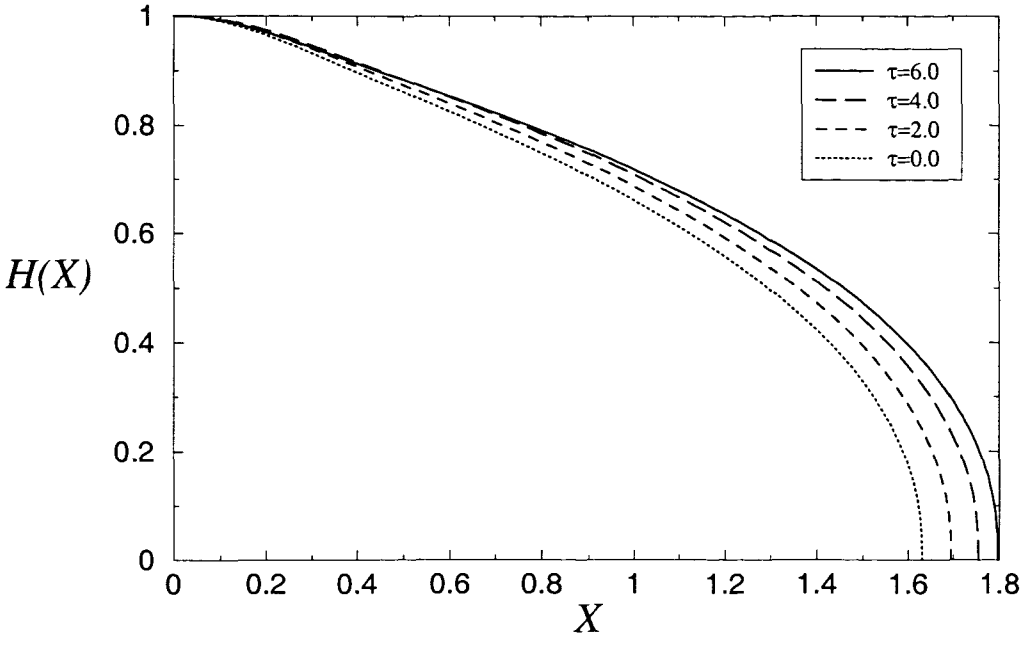

Figure 3.15: Plots of the liquid film free surface $\mathcal{H}(X)$ for various values of the tangential parameter $\bar{\tau}$, for a fixed mass transfer parameter $\eta = 1.0$.

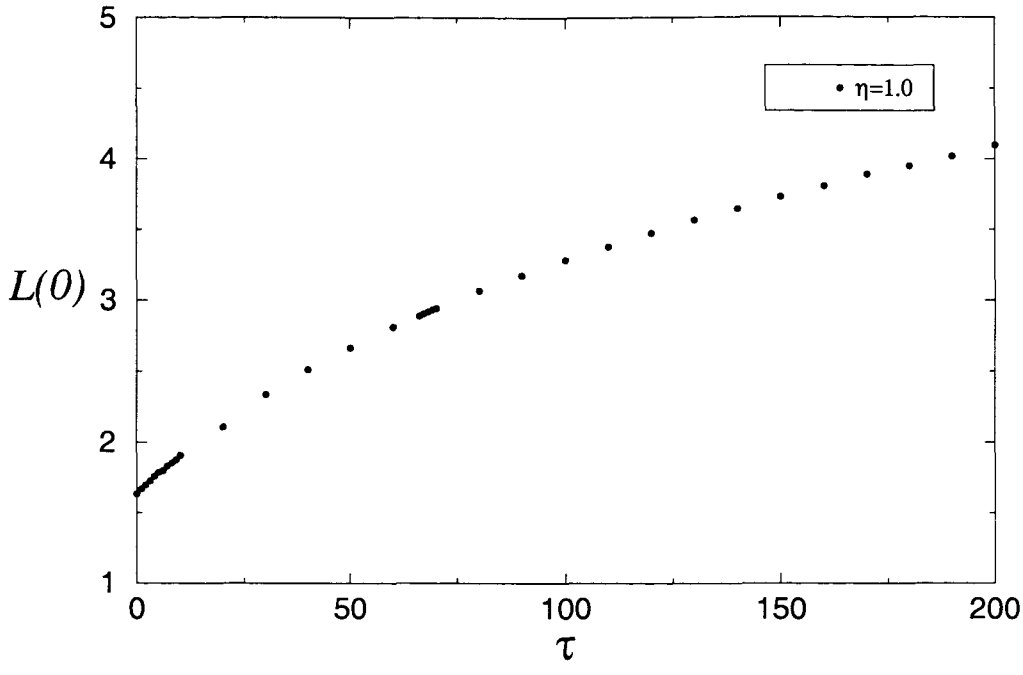

Figure 3.16: Plots of the length to dryout point, L_0, against the traction parameter $\bar{\tau}$.

3.2.5.1 Pressure and Pressure Gradient Effects

To reiterate, numerical solutions to (3.59) have been obtained through prescribing the pressure gradient (3.58), instead of pressure, at the onset of the annular flow regime. We recall that in this problem, the pressure is given by

$$\bar{p}_g = \frac{p_g - p_\infty}{\epsilon \rho_\infty U_\infty^2} = \frac{1}{\pi} \int_0^1 \frac{\bar{h}_\xi(\xi)}{\xi - \bar{x}} d\xi. \tag{3.64}$$

Thus, pressure can be calculated from the numerically computed $\bar{h}(\bar{x})$ at every point $\bar{x}$. It makes sense then to pose a question; can a solution $\bar{h}(\bar{x})$ to (3.59) always be obtained for any prescribed value of pressure gradient (and/or pressure) at $\bar{x} = 0$? This is investigated numerically by solving (3.59) numerous times prescribing (3.58) and holding $\bar{\tau}$ a constant while η is being varied. The process is then repeated with η kept constant while $\bar{\tau}$ is varied. Then the pressure at $\bar{x} = 0$ is calculated from (3.64) and a graph of pressure against pressure gradient at $\bar{x} = 0$ is plotted. The results are depicted in figure (3.17). What is fascinating is the observation that these results produce a single curve instead of a family of curves corresponding to either values of $\bar{\tau}$ or η. From this curve it is very compelling to argue that the relationship between the pressure gradient and pressure at the onset of annular flow regime, for those solutions which exist, is a one-to-one relationship irrespective of the parameter values of the problem. Physically, this result reinforces the view that indeed the solution $\bar{h}(\bar{x})$ is unique. Further, it appears from the graph that as the magnitude of the

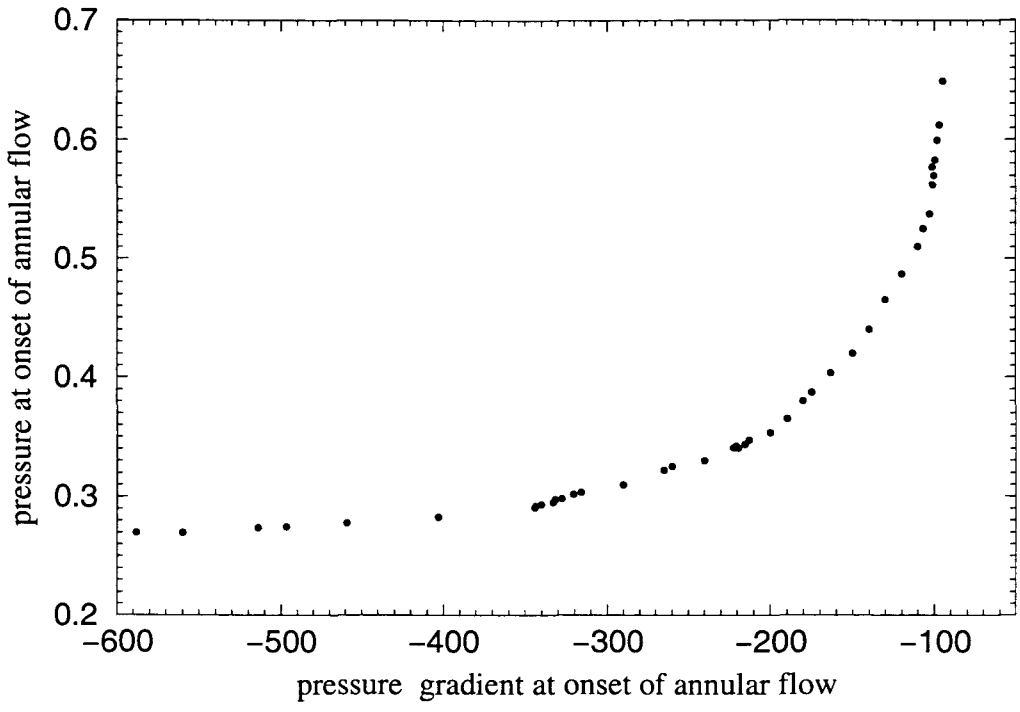

Figure 3.17: Plots of the pressure $\bar{p}_g$ against the pressure gradient $\bar{p}_{g\bar{x}}$ at the onset of the annular flow $\bar{x} = 0$, for various values of $\bar{\tau}$ and η.

pressure gradient values at the onset of the annular flow tend to infinity, the values of the pressure there approach a constant 0.27. Thus suggesting that there may not be any solutions, $\bar{h}(\bar{x})$, to equation (3.59) for prescribed values of the pressure approximately less or equal to 0.27. Similarly, it can be inferred from the graph that as values of the pressure at $\bar{x} = 0$ are increased indefinitely, then the corresponding values of the pressure gradient there tend to a negative constant nearly equal to -110,0. Hence suggesting that there may not exist solutions to equation (3.59) for the values of the pressure gradient greater than -110.0.

Having computed (3.64), we can now look at other interesting pressure related phenomena. Figures (3.18) and (3.19) show the pressure profiles in the annular flow regime and far downstream of dryout for an increase in both η ($\bar{\tau}$ held constant) and $\bar{\tau}$ (η kept constant). In general, the pressure is positive at $\bar{x} = 0$ before rising sharply to reach a positive maximum near the start of the annular flow. It then decreases, rapidly near $\bar{x} = 0$, and then gradually downstream to achieve an infinite negative minimum at the dryout point before increasing gradually to almost zero far downstream of dryout. The results in figures (3.18) and (3.19) can be presented in another form as shown in figures (3.20) and (3.21) respectively. In this case, it is easy to observe the effects of both η and $\bar{\tau}$ on the value of the pressure minimum point. We observe from figure (3.20) that, apart from translating the dryout point, changes in η do not have any effect on the value of the pressure minimum point. On the other hand,

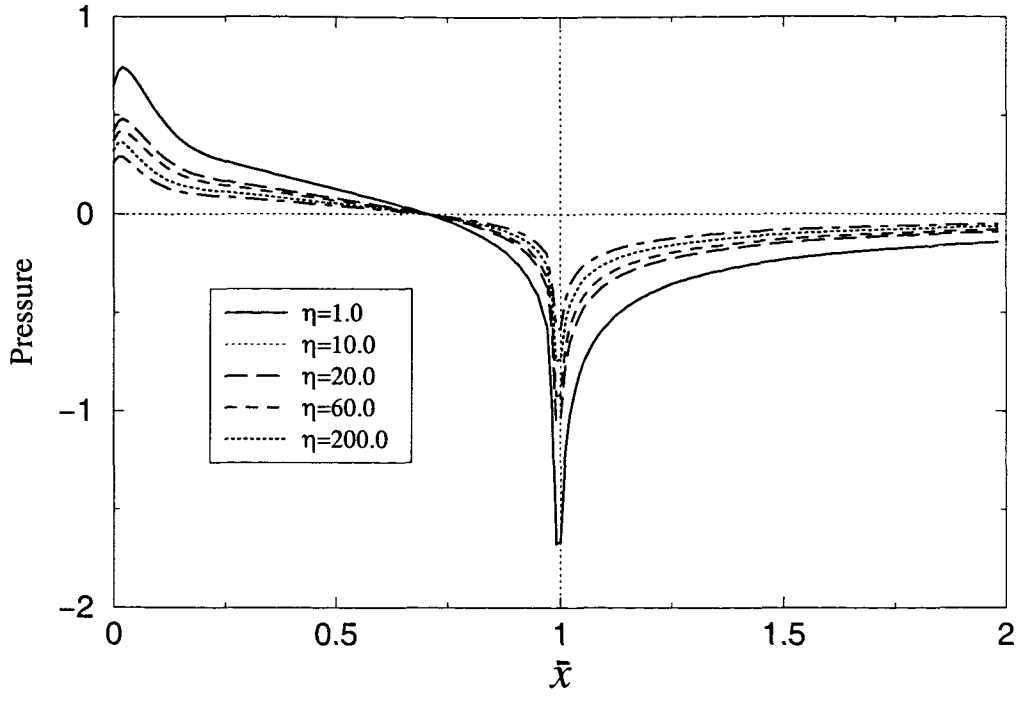

Figure 3.18: Plots of the pressure $\bar{p}_g(\bar{x})$ in the annular flow regime and far downstream of the dryout point, for various values of η when $\bar{\tau}$ is held constant at $\bar{\tau} = 0.0$.

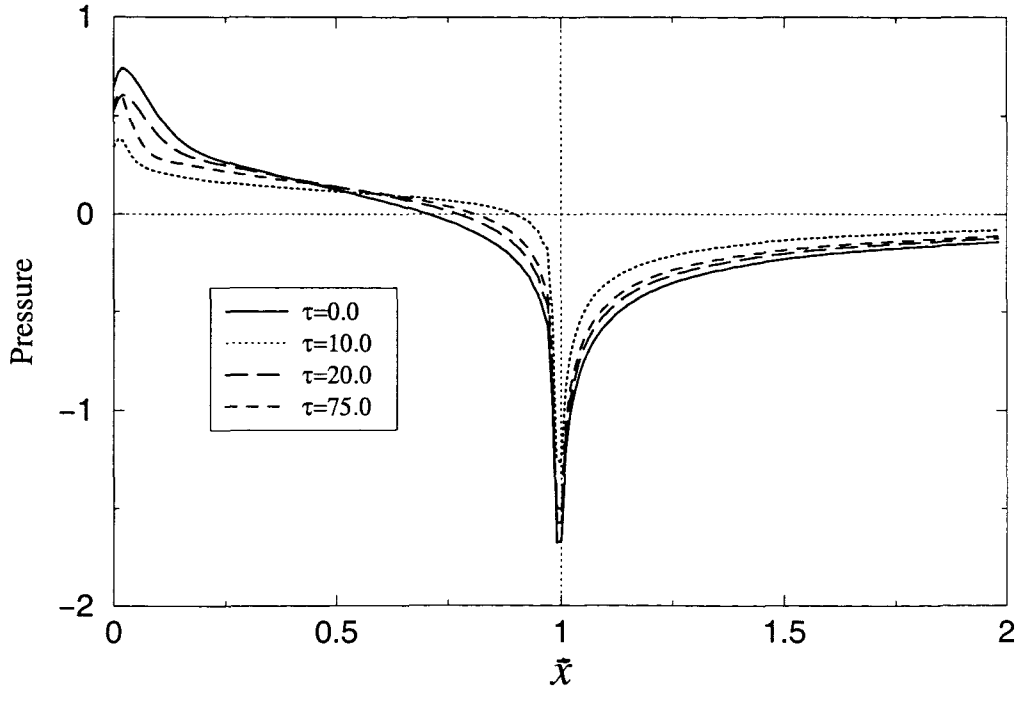

Figure 3.19: Plots of the pressure $\bar{p}_g(\bar{x})$ in the annular flow regime and far downstream of the dryout point, for various values of $\bar{\tau}$ when η is held constant at $\eta = 1.0$.

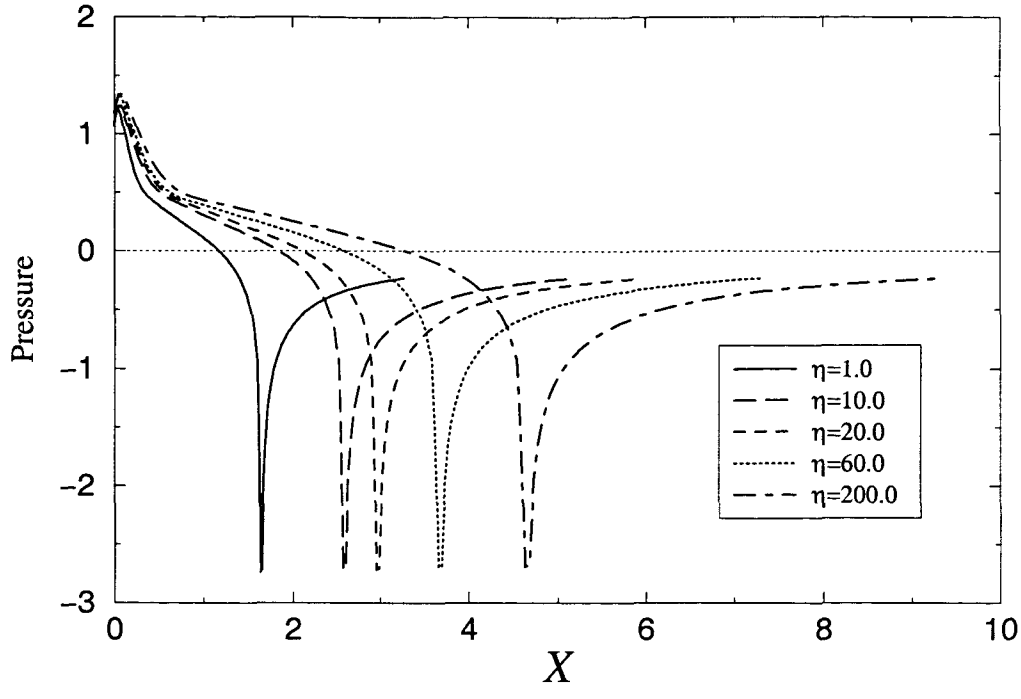

Figure 3.20: Plots of the pressure $\bar{p}_g(\bar{x})$ in the annular flow regime and far downstream, for various values of η where $\bar{\tau}$ is held constant at $\bar{\tau} = 0.0$.

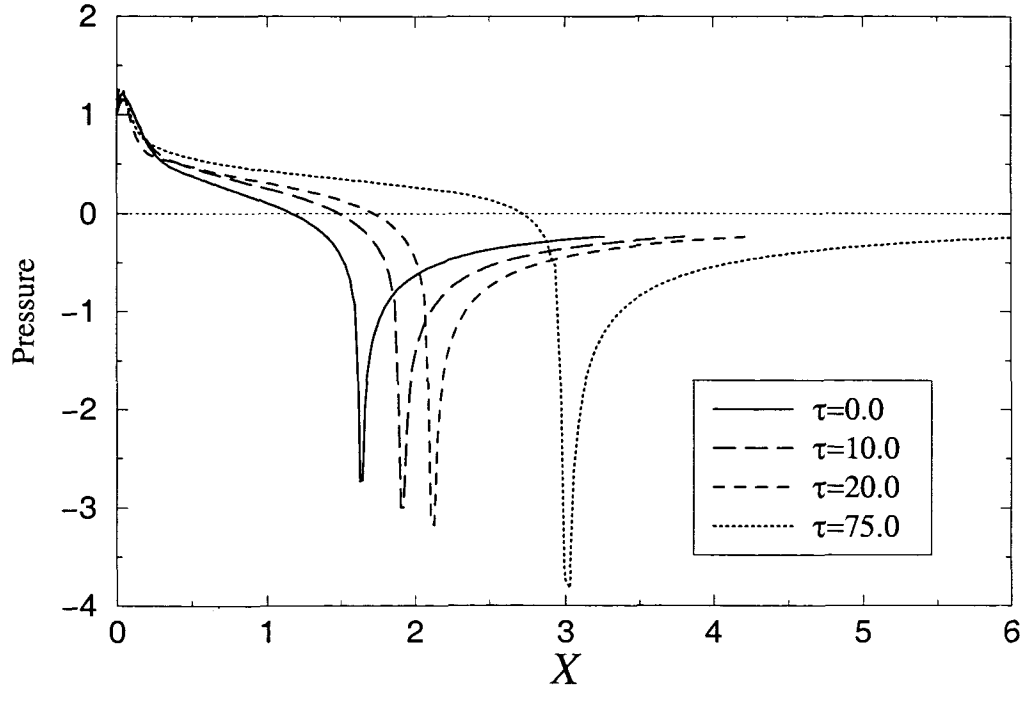

Figure 3.21: Plots of the pressure $\bar{p}_g(\bar{x})$ in the annular flow regime and far downstream, for various values of $\bar{\tau}$ where η is held constant at $\eta = 1.0$.

from figure (3.21) it is clear that, in addition to translating the position of the dryout point, the increase in $\bar{\tau}$ does gradually decrease the minimum value of the pressure. The infiniteness of the negative minimum in the pressure at the dryout point is attributed to the singularity of $\bar{h}_{\bar{x}}(\bar{x})$ there. It is not difficult to construct examples to illustrate analytically that if the liquid film free surface attaches tangentially at the dryout point, i.e. $\bar{h}_{\bar{x}}(1) = 0$, then this negative minimum should be smooth (and this is verified by the results of problem (4.1), figures (4.12) to (4.15) in chapter 4). We must mention that in reality, this singularity in $\bar{h}_{\bar{x}}(\bar{x})$ at the dryout might be smoothed out by other processes, for example the deposition of the droplets from the gas core onto the liquid film, which are not accounted for in the current model. The plots of pressure are usually very important (for example, in wind tunnel experiments) for comparison between theoretical and experimental results. It has proved, however, impossible to obtain any literature (if at all available) concerning experimental work with regard to this problem. It is nevertheless hoped that when such literature is available and obtainable, it will compare very well with our results for the current conditions of interest.

We proceed here to make further observations. In figures (3.22) and (3.23), we illustrate

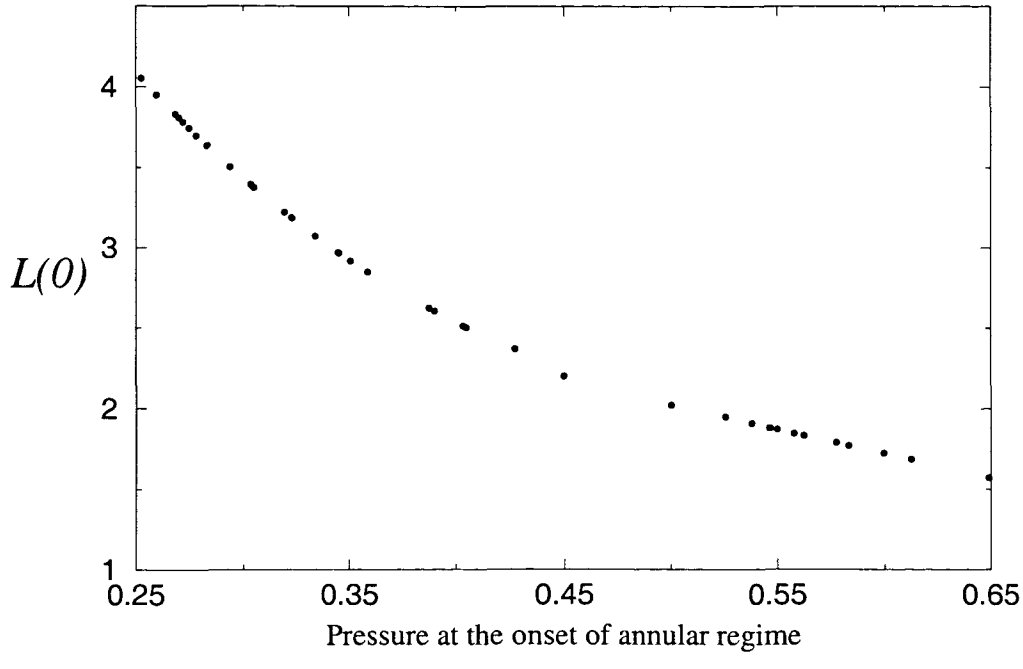

Figure 3.22: Plots of the length to the dryout $L(0)$ against the pressure $\bar{p}(\bar{x})$ at $\bar{x} = 0$ for various of the traction parameter $\bar{\tau}$ and mass transfer parameter η.

the influence of both pressure and pressure gradient at the onset of the annular flow $\bar{x} = 0$, respectively. Both graphs are obtained by solving (3.59) numerous times for various values of η (keeping $\bar{\tau}$ a constant) and vice versa. Then the length to the dryout $L(0)$, or equally L_0, is calculated, as explained earlier in this section, from each result. The fascinating physical

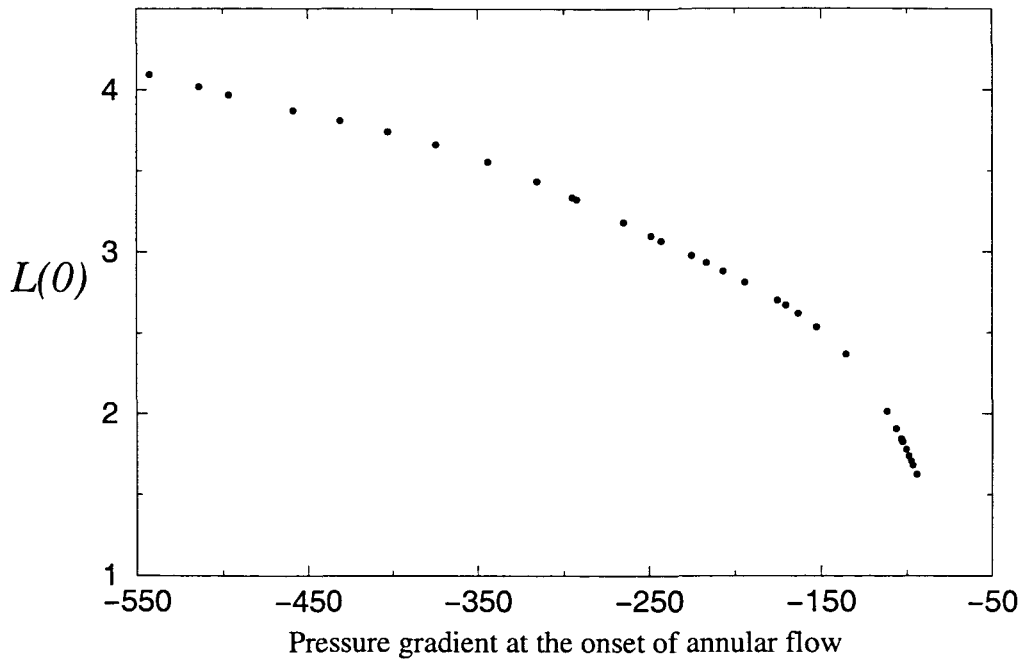

Figure 3.23: Plots of the length to the dryout $L(0)$ against the pressure gradient $\bar{p}_{\bar{x}}(\bar{x})$ at $\bar{x} = 0$ for various of $\bar{\tau}$ and η.

implication of these two graphs is that it is absolutely possible to control the length to the dryout $L(0)$ by simply dictating appropriate values of pressure and pressure gradient at the onset of the annular flow $\bar{x} = 0$. For example, if it is possible in an industrial setting to arrange the system so that at $\bar{x} = 0$, pressure is small and pressure gradient is large in magnitude (consistent with figure (3.17)), then the dryout point can be accordingly postponed further downstream. On the other hand, if at $\bar{x} = 0$ the pressure is large and the pressure gradient is small in magnitude, then the dryout point will accordingly occur closer to the onset of the annular regime. This finding, fascinating as it is, should however be understood in the correct context. Since both the pressure and the pressure gradient in the annular regime are functions of the thickness of the liquid film, they can be controlled through specification of the appropriate parameters $\bar{\tau}$ and η. We know, for example, that η depends on the properties of the liquid film - its latent heat of vapourisation λ and its thermal conductivity k. Thus, in an industrial setting η may be appropriately fixed by choosing a liquid with desirable known properties. $\bar{\tau}$, on the other hand, is less obvious to fix in reality because it depends on the viscosities of both the vapour μ_g and the liquid μ (and in general, on the second derivative of the liquid film thickness $\bar{h}_{\bar{x}\bar{x}}(\bar{x})$ as well). However, we can loosely say that it can be fixed by choosing a liquid with desirable viscosity and which evaporates into a gas with appropriate viscosity, in the conditions of interest. The relationships between the pressure at the onset of the annular flow, $\bar{x} = 0$, and both $\bar{\tau}$ and η are shown in figures (3.24) and

(3.25) respectively. The relationships between the pressure gradient at $\bar{x} = 0$ and both the

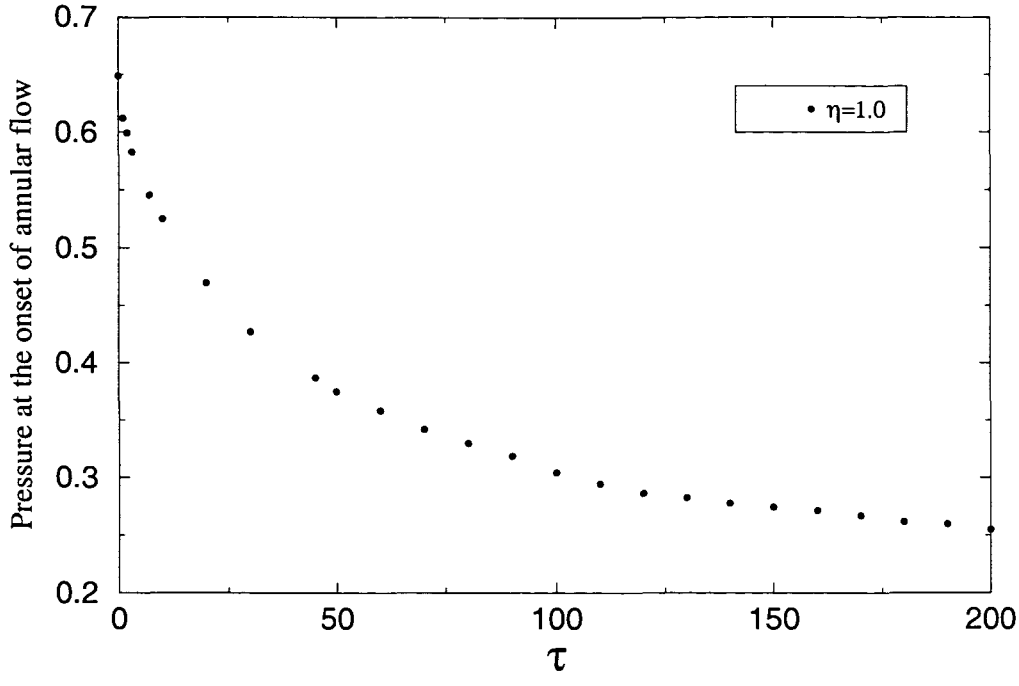

Figure 3.24: Plots of the pressure $\bar{p}(\bar{x})$ at $\bar{x} = 0$ for various values of $\bar{\tau}$ when η is kept constant at $\eta = 1.0$.

parameters $\bar{\tau}$ and η may be obtained in a similar fashion. However, this is not necessary for any practical purposes, because once an appropriate pressure at $\bar{x} = 0$ is identified (say from either figure (3.24) and (3.25)), then the corresponding pressure gradient at $\bar{x} = 0$ can be read off from figure (3.17).

Finally, the effects of $\bar{\tau}$ at varous points of the liquid free surface are investigated by plotting $\bar{h}(\bar{x} = \bar{x}_k)$ (for some known point $\bar{x}_k$) for various values of $\bar{\tau}$, at a given value of η. A typical curve is shown in figure (3.26) for $\bar{h}(0)$. The result suggests that each point on the surface of the liquid film is dragged in an almost exponential decay form due to the increase in $\bar{\tau}$. Even though negative $\bar{\tau}$ may not have a clear physical interpretation in this problem, it is observed in figure (3.26) that the stretching does not depend on the magnitude of $\bar{\tau}$ but the increase in $\bar{\tau}$.

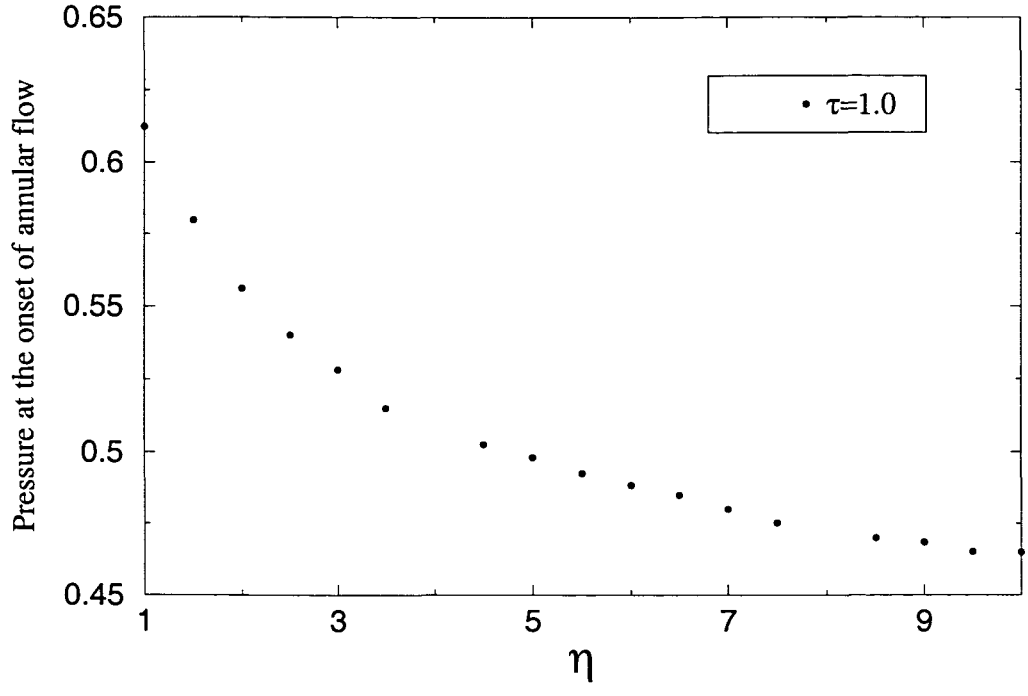

Figure 3.25: Plots of the pressure $\bar{p}(\bar{x})$ at $\bar{x} = 0$ for various values of η when $\bar{\tau}$ is held constant at $\bar{\tau} = 1.0$.

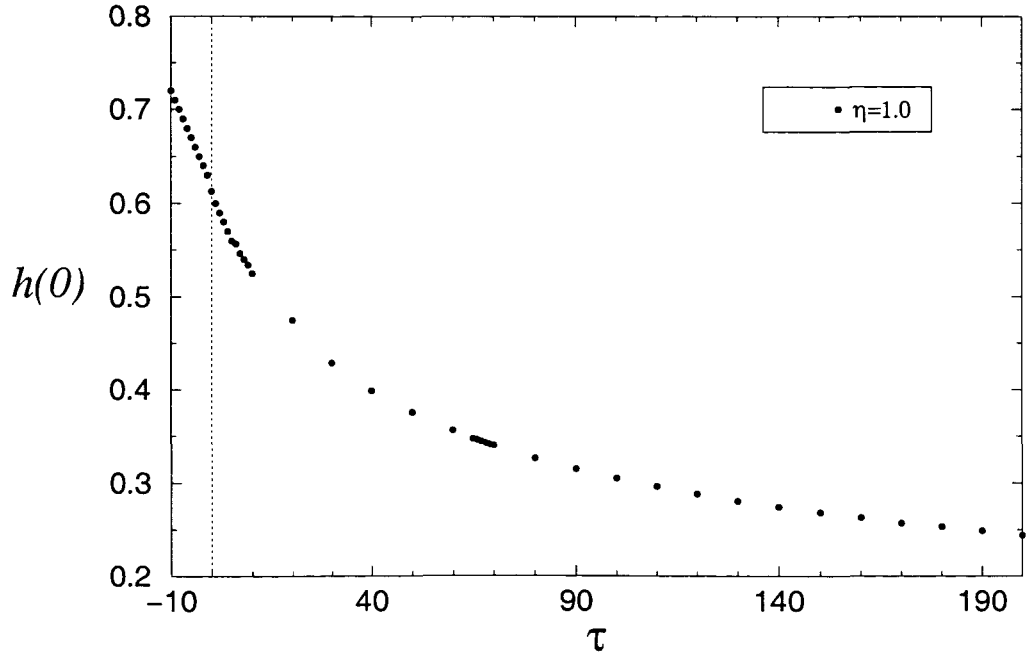

Figure 3.26: Plot of the liquid film free surface $\bar{h}(\bar{x})$ at $\bar{x} = 0$ against the traction parameter $\bar{\tau}$ ($n = 100$).

Chapter 4

Steady State Solutions: A Non-constant Wall Temperature Problem

In this chapter, we solve the steady case of the nondimensional equation (2.66) which is

$$\left\{\frac{\bar{h}^3}{3\pi}\left(\fint_0^1 \frac{\bar{h}_\xi(\xi)}{\xi-\bar{x}}d\xi\right)_{\bar{x}} - \frac{\bar{\tau}}{2}\bar{h}^2\right\}_{\bar{x}} = \frac{\bar{h}}{\eta}, \tag{4.1}$$

subject to the usual boundary conditions $\bar{h}(\bar{x}) = 0$ at the dryout point $\bar{x} = 1$, $\bar{h}_{\bar{x}}(\bar{x}) = 0$ at the onset of the annular flow $\bar{x} = 0$, $\bar{h}(0) = \bar{h}_0$ is a known parameter and the pressure condition

$$\frac{1}{\pi}\fint_0^1 \frac{\bar{h}_\xi(\xi)}{\xi-\bar{x}}d\xi = \frac{p_g - p_\infty}{\epsilon\rho_\infty U_\infty^2} = \bar{p}_g,$$

or the corresponding pressure gradient condition has to be satisfied at $\bar{x} = 0$.

Before we proceed, we should recall the differences between equations (4.1) and (3.35). The main difference between these two equations is how the unknown function $\bar{h}$ appears on the right hand side. In equation (4.1), $\bar{h}$ appears in the numerator while it is in the denominator in equation (3.35). This feature alone causes a big difference in the asymptotic behaviour of $\bar{h}$ near the dryout point $\bar{x} = 1$ (where $\bar{h}$ vanishes) between these two problems. From the experience of solving (3.35) and the previous paradigm problems, we know that the knowledge of the behaviour of $\bar{h}$ plays a significant role in the numerical solution of the problem. In particular, for equation (3.35) it has been found that $\bar{h} \sim (1-\bar{x})^{3/5}$ as $\bar{x} \to 1$. Thus, the problem had to be regularised accordingly in order to remove the singularity in $\bar{h}_{\bar{x}}(\bar{x})$ as $\bar{x} \to 1$ prior to undertaking any numerical manipulations. Here, it will be seen however, that in equation (4.1) the unknown function $\bar{h}(\bar{x}) \to 0$ as $1-\bar{x}$ near $\bar{x} = 1$. Therefore, we expect this problem may be solved directly without resorting to any regularisations since there is no

singularity in $\bar{h}_{\bar{x}}(\bar{x})$ as $\bar{x} \to 1$. However, the problem will be first solved extensively using the modified numerical code that has been employed to solve equation (3.35). From the results, we will then be able to demonstrate that the infiniteness of the pressure minimum point at the dryout point $\bar{x} = 1$, from the pressure curves obtained when solving equation (3.35), is simply a result of the singularity in $\bar{h}_{\bar{x}}(\bar{x})$ at that point and not in anyway a consequence of the numerical code.

Moreover, owing to the complexity of equation (3.35), the problem has been solved by prescribing the pressure gradient condition at the onset of the annular flow regime, $\bar{x} = 0$. In reality however, it is more likely that the pressure (as opposed to the pressure gradient) at that point can be measured. Although the values of pressure can be obtained directly from those of the pressure gradient, it is still of interest to investigate the possibility of solving this problem when the pressure at $\bar{x} = 0$ is directly prescribed. One such possibility is investigated later in this chapter by considering equation (4.1), a relatively simpler problem.

4.1 Asymptotics

Prior to undertaking any numerical computations for (4.1), it is crucial to determine the behaviour of $\bar{h}(\bar{x})$ as $\bar{x} \to 1$. We have seen in chapter 3 that knowledge of the asymptotics of $\bar{h}(\bar{x})$ near the dryout point $\bar{x} = 1$ plays a very important role when solving the problem numerically.

By inspection, we observe here that for every possible asymptotic balance in (4.1), $\bar{h}(\bar{x}) \sim 1 - \bar{x}$ as $\bar{x} \to 1$. It is easier to check self-consistency of these asymptotics in the special case when $\bar{\tau} = 0$. On assuming that near the dryout point the dominant contribution from the Cauchy-principal value integral in equation (4.1) comes from a small region near $\bar{x} = 1$, we substitute $\bar{h}(\bar{x}) = 1 - \bar{x}$ in the singular integral term and then solve for $\bar{h}$ from a Bernoulli equation

$$\bar{h}_{\bar{x}} - \frac{(1-2\bar{x})}{3\bar{x}(1-\bar{x})}\bar{h} = \frac{\pi}{\eta}\bar{x}(1-\bar{x})\bar{h}^{-1}. \tag{4.2}$$

Employing standard techniques, (4.2) solves to give

$$\left.\frac{\bar{h}^2}{\bar{x}^{\frac{2}{3}}(1-\bar{x})^{\frac{2}{3}}}\right|_{\bar{x}}^{\bar{x}=1} = \frac{2\pi}{\eta}\left\{\frac{3}{10}(1-2\bar{x})\bar{x}^{\frac{1}{3}}(1-\bar{x})^{\frac{1}{3}} + \frac{1}{10}\int_{\bar{x}}^{1}\frac{d\bar{x}}{\bar{x}^{\frac{2}{3}}(1-\bar{x})^{\frac{2}{3}}}\right\}, \tag{4.3}$$

and we observe that indeed as $\bar{x} \to 1$, (4.3) is consistent with the asymptotics $\bar{h} \sim 1 - \bar{x}$.

4.2 Regularised Problem and Pressure Gradient Condition

4.2.1 Numerical Solutions

Since the asymptotics indicate that there are no singularities in $\bar{h}_{\bar{x}}(\bar{x})$ as $\bar{x} \to 1$ in this problem, then it is sensible and convenient to modify and employ the numerical code that has been used successfully in chapter 3 to solve (2.62) (as explained in sections (3.2.3) to (3.2.4)). The problem can be solved directly, as briefly demonstrated in section (4.3), without resorting to any regularisation processes. However, since we also intend to illustrate that the infiniteness of the pressure minimum point at the dryout for problem (3.35) is not a result of the numerical code we have used (but the singularity in $\bar{h}_{\bar{x}}(\bar{x})$ at that point), it makes sense to employ the same code here with some appropriate modifications. That means that in this case we have to solve the regularised problem (cf. equation (3.59))

$$\left(\frac{4\eta}{125\chi}\right)^{\frac{2}{5}} \pi \frac{y^{\frac{2}{3}}}{H^3(y)} \left\{ -\frac{25}{3\eta}\left(\frac{4\eta}{125\chi}\right)^{\frac{3}{5}} \int_0^y u^{\frac{2}{3}} H(u)du + \frac{5}{2}\bar{\tau}H^2(y) \right\} = \left(\fint_0^1 \frac{H_u(u)}{y^{\frac{5}{3}} - u^{\frac{5}{3}}} du \right)_y , \tag{4.4}$$

subject to $H(0) = 0$, $H_y(1) = 0$ and $H(1)$ is a specified constant which must satisfy the pressure gradient condition (cf. equation (3.58))

$$\frac{1}{5\pi}\left(\frac{125\chi}{4\eta}\right)^{\frac{4}{5}} H^3(1) \left(\int_0^1 \frac{H_u(u)}{y^{\frac{5}{3}} - u^{\frac{5}{3}}} du \right)_y \Bigg|_{y=1} = -\frac{5}{3\eta}\left(\frac{4\eta}{125\chi}\right)^{\frac{1}{5}} \int_0^1 u^{\frac{2}{3}} H(u)du + \frac{1}{2}\left(\frac{125\chi}{4\eta}\right)^{\frac{2}{5}} H^2(1)\bar{\tau}. \tag{4.5}$$

Thus, in the numerical scheme, the term

$$\left[\frac{3}{2}\left(\frac{1}{n}\right)^{\frac{2}{3}} + I_2\right]$$

in equation (3.60) is modified accordingly to become

$$\frac{3}{11}\left(\frac{1}{n}\right)^{\frac{11}{3}} + \sum_{j=1}^{i} \int_{u_j}^{u_{j+1}} u^{\frac{2}{3}} H(u)du \approx \frac{3}{11}\left(\frac{1}{n}\right)^{\frac{11}{3}} + \sum_{j=1}^{i} \left\{ \frac{3}{8}m\left(u_{j+1}^{\frac{8}{3}} - u_j^{\frac{8}{3}}\right) - \frac{3}{5}\left(mu_j - H_j\right)\left(u_{j+1}^{\frac{5}{3}} - u_j^{\frac{5}{3}}\right) \right\},$$

where, we recall that in each subinterval $[u_j, u_{j+1}]$, $H(u)$ is approximated by the linear functions

$$H(u) = mu - (mu_j - H_j)$$

and

$$m = \frac{H_{j+1} - H_j}{u_{j+1} - u_j}.$$

The numerical procedure is as detailed in chapter 3 section (3.2.4). We continue here to present and discuss those converged numerical solutions which satisfy all of the prescribed boundary conditions.

4.2.2 Numerical Results and Discussions

Figures (4.1), (4.2) and (4.3) illustrate the effects of the increase in the mass transfer parameter η on the film thickness and the length to the dryout point, while the traction parameter $\bar{\tau}$ is held constant. We should mention that figures (4.1) and (4.2) are essentially the same.

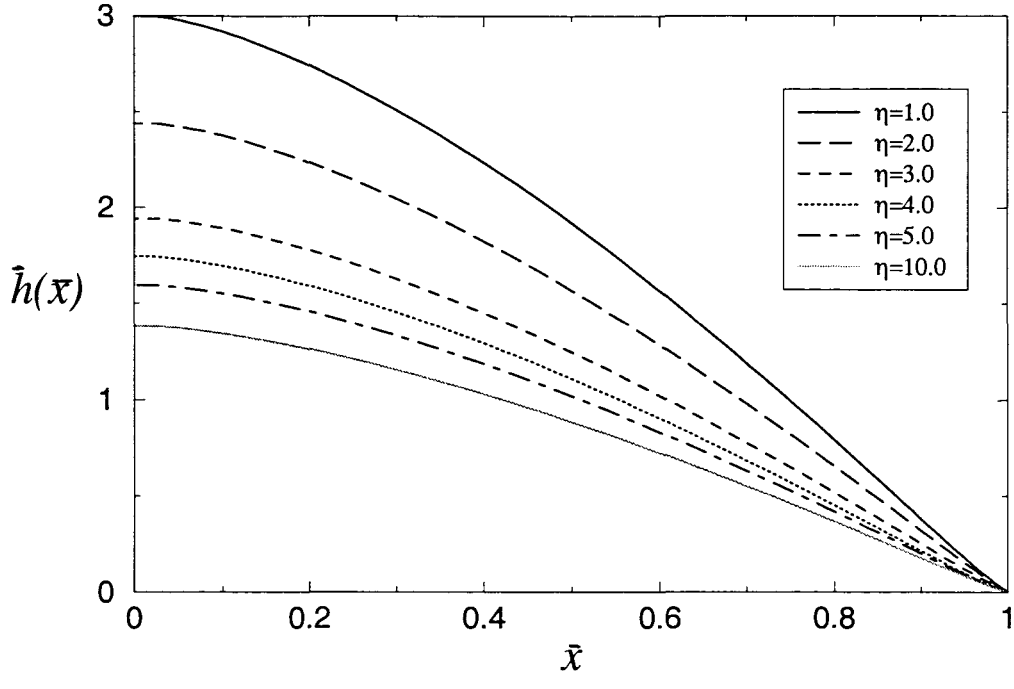

Figure 4.1: Plots of the liquid film free surface $\bar{h}(\bar{x})$ when the traction parameter $\bar{\tau} = 0.0$ and the mass transfer parameter η is varied (number of mesh points $n = 100$).

The results in figure (4.1) are obtained by directly solving (4.1) numerically and thus the dryout point is fixed at $\bar{x} = 1$. On the other hand, the results in figure (4.2) are obtained by considering the scaled equation

$$\left\{ \frac{\mathcal{H}^3}{3\pi} \left(\int_0^{\frac{1}{\bar{h}_0}} \frac{\mathcal{H}_\psi(\psi)}{\psi - X} d\psi \right)_X - \frac{\bar{\tau}}{2} \mathcal{H}^2 \right\}_X = \frac{\mathcal{H}}{\eta},$$

where $\mathcal{H}(X) = \bar{h}(\bar{x})/\bar{h}_0$ and $X = \bar{x}/\bar{h}_0$. Owing to the apparent uniqueness of the numerical solutions corresponding to each combination of the prescribed parameters η, $\bar{\tau}$ and $\bar{h}_0$, the results of figure (4.2) and those of figure (4.3) are accordingly obtained from the results of figure (4.1). The profile of the curve in figure (4.3) is similar to that of figure (3.12). Thus,

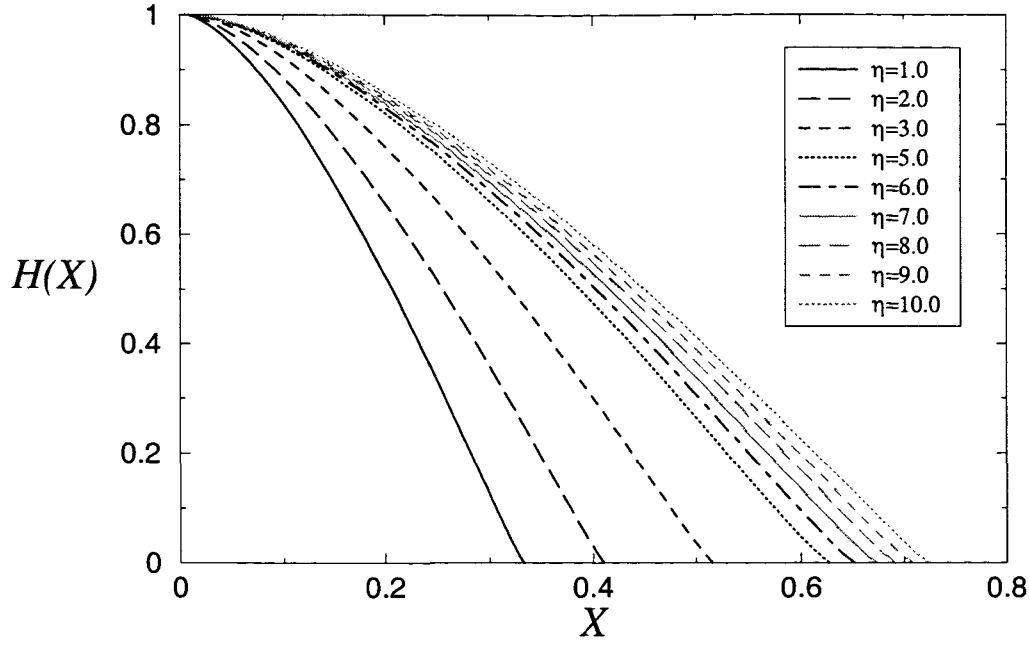

Figure 4.2: Plots of the liquid film free surface $\mathcal{H}(X)$ when the traction parameter $\bar{\tau} = 0.0$ and the mass transfer parameter η is varied (number of mesh points $n = 100$).

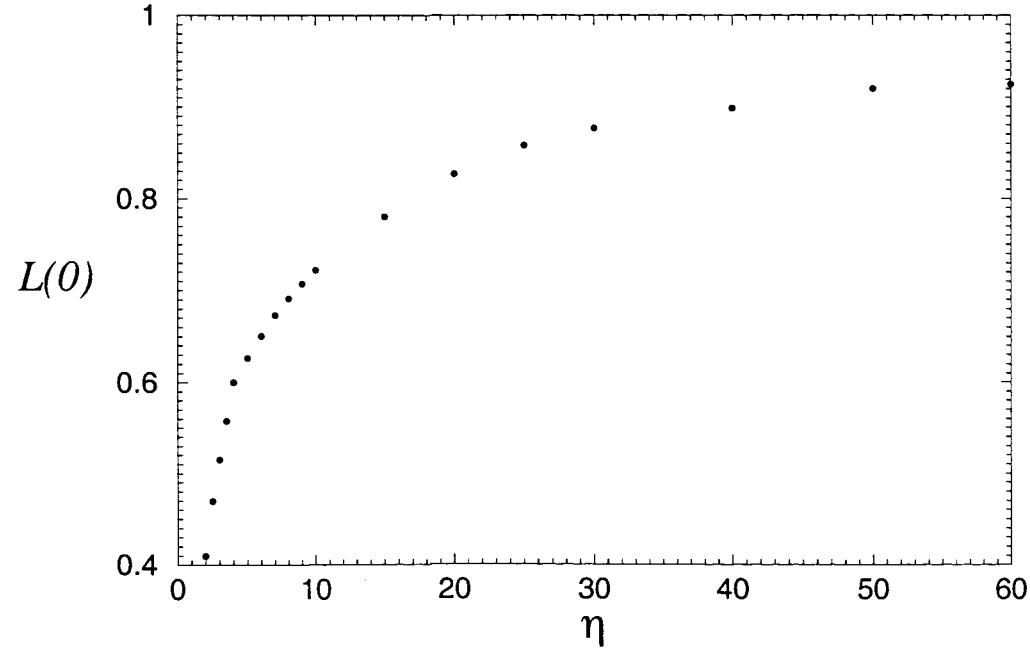

Figure 4.3: Plot of the length to the dryout L_0 $(= L(0))$ against the mass transfer parameter η with the traction parameter $\bar{\tau} = 0.0$.

it confirms as well that indeed for $\eta \gg 1$ (a liquid with large latent heat) the mass transfer is small and dryout will not occur, while for $\eta \ll 1$ (a liquid with small latent heat) the mass transfer is so high that the liquid film will not form at all.

Figures (4.4) and (4.5) show the effects of an increase in the traction parameter $\bar{\tau}$ on the film thickness and the length to the dryout point while the mass transfer parameter, η, is kept at a constant. It is observed (as in chapter 3 figures (3.14) and (3.15)) that an increase

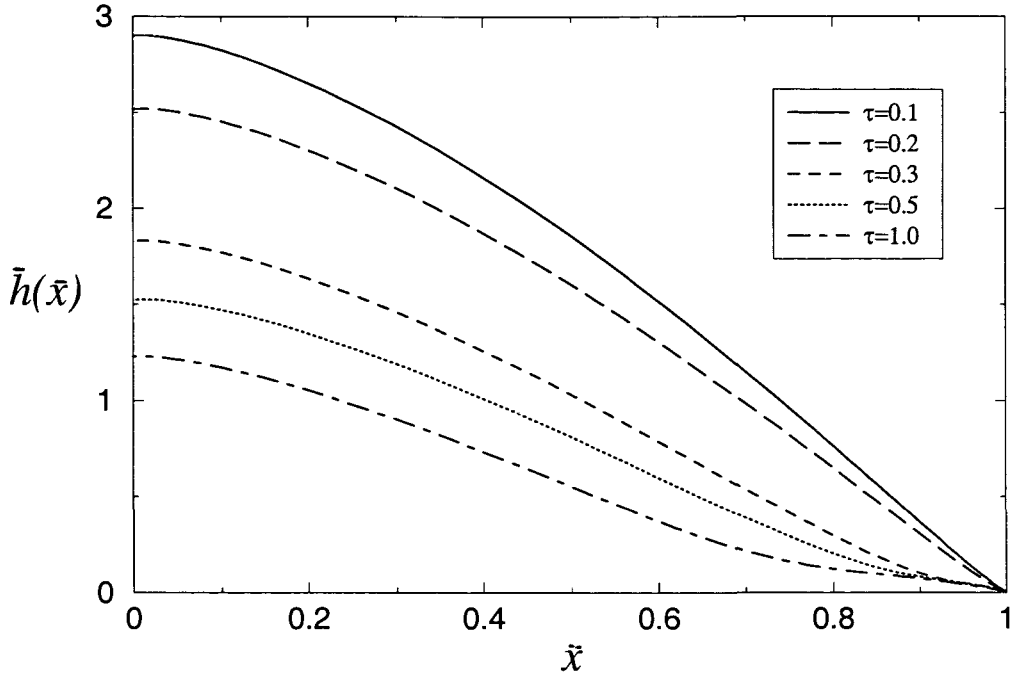

Figure 4.4: Plots of the liquid film free surface $\bar{h}(\bar{x})$ when the traction parameter $\bar{\tau}$ is varied and the mass transfer parameter $\eta = 1.0$ (number of mesh points $n = 100$).

in the traction parameter $\bar{\tau}$ stretches the liquid film and hence increases the length to the dryout point. It is also evident from the curves in figures (4.4) and (4.5) that there is a value above which, when $\bar{\tau}$ is increased, the converged numerical solutions cease to have monotonic second derivatives near the dryout point. The results of figures (4.6) and (4.7) further suggest that there is some competition going on between $\bar{\tau}$ and η near the dryout point. In an attempt to understand this phenomenon, we consider a limiting case near the dryout point when $\eta \sim O(\delta^{-2})$, $\bar{\tau} \sim O(\epsilon)$ and $\bar{h} \sim O(\epsilon)$, for some small positive parameters ϵ and δ which are of comparable order order of magnitude. In this case equation (4.1), to order ϵ, gives

$$\bar{h}_{\bar{x}} = -\frac{1}{\eta\bar{\tau}} \sim -\frac{\delta^2}{\epsilon}, \tag{4.6}$$

It is then clear from (4.6) that the increase in $\bar{\tau}$ (or equally ϵ), tends to flatten the slope of the liquid film thickness $\bar{h}_{\bar{x}}$. While the increase in η (or similarly δ^2) steepens the slope of

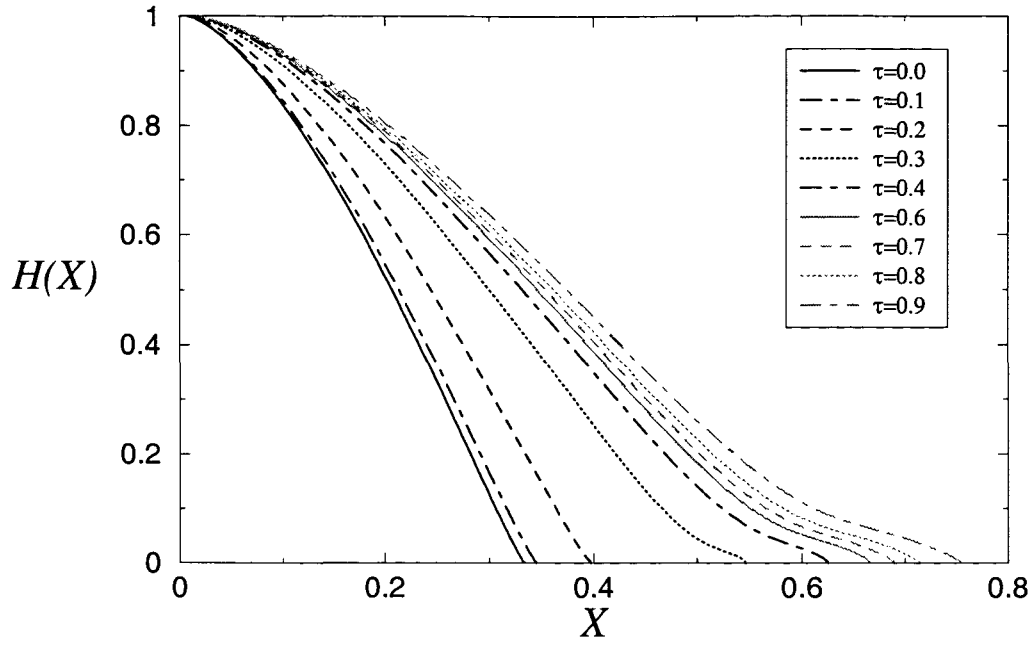

Figure 4.5: Plots of the liquid film free surface $\mathcal{H}(X)$ when the traction parameter $\bar{\tau}$ is varied and the mass transfer parameter $\eta = 1.0$ (number of mesh points $n = 100$).

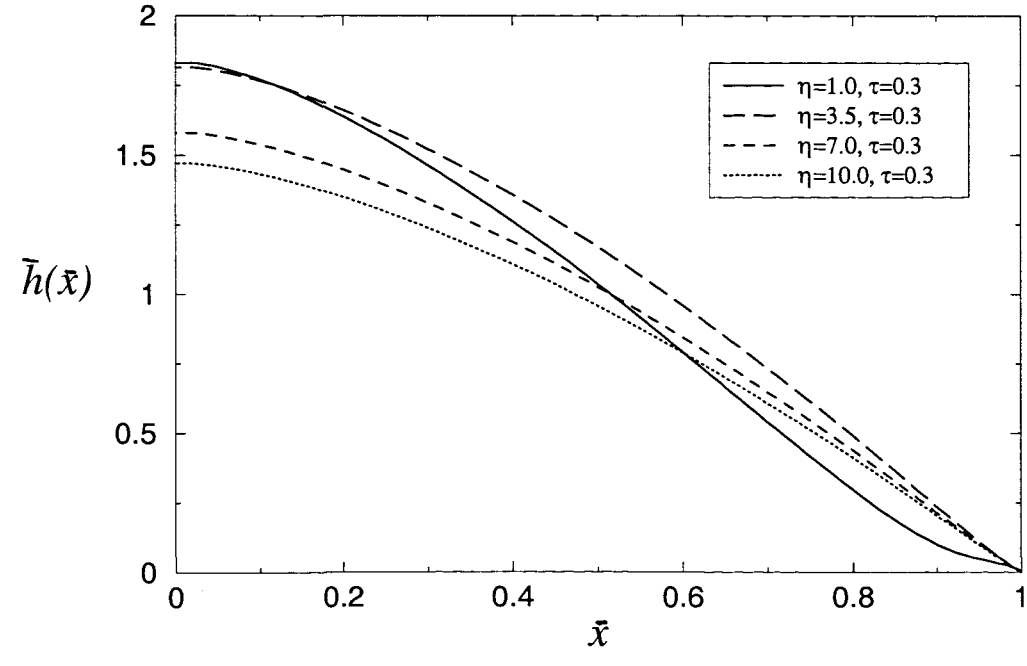

Figure 4.6: Plots of the liquid film free surface $\bar{h}(\bar{x})$ when the traction parameter $\bar{\tau} = 0.3$ and the mass transfer parameter η is varied (number of mesh points $n = 100$).

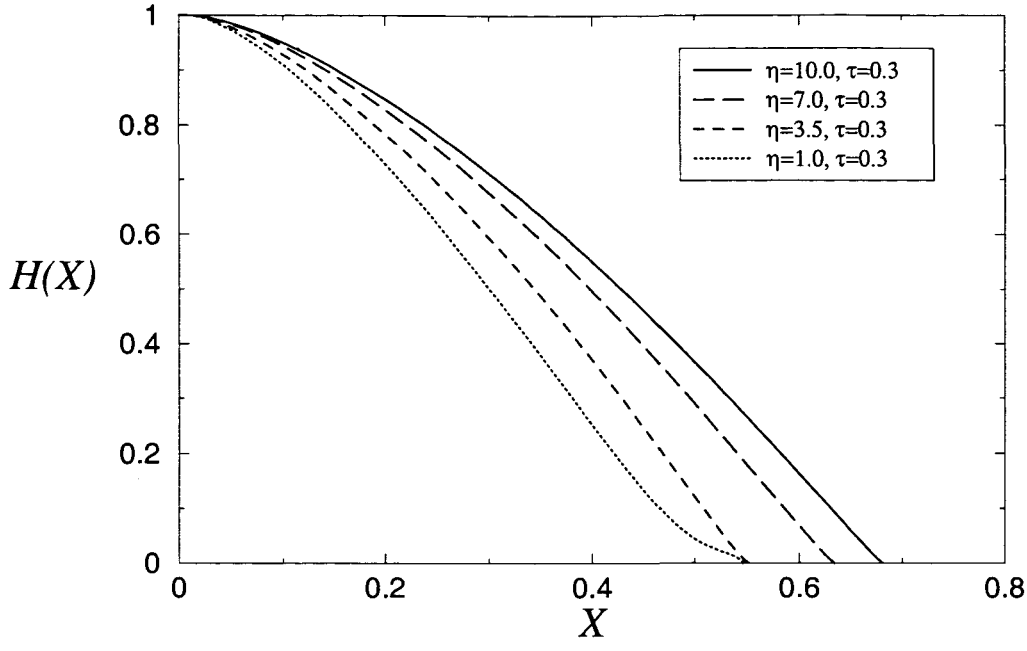

Figure 4.7: Plots of the liquid film free surface $\mathcal{H}(X)$ when the traction parameter $\bar{\tau} = 0.3$ and the mass transfer parameter η is varied (number of mesh points $n = 100$).

the liquid thickness layer.

Since an increase in η increases the steepness of the slope of the liquid film free surface $\bar{h}$ near $\bar{x} = 1$, it is instructive to look at the case where $\eta \to \infty$ and $\bar{\tau}$ is comparatively small. In this case, figure (4.8) displays an example of typical solutions. The solutions still approach the dryout point linearly, but the slopes are very steep as one would expect. Figures (4.9) and (4.10) show the comparison between the results in figure (4.8) and the results when the value of η is relatively small.

Figure (4.11) depicts a typical plot of the length to the dryout point L_0 for an increase in the traction parameter $\bar{\tau}$, when the heat transfer parameter η is held constant. These results, in comparison with the results in chapter 3 figure (3.16), show rather unexpected behaviour. From the results of figure (3.16), we recall that it has been found that for a fixed value of η, the increase in $\bar{\tau}$ slowly and gradually stretches the length to the dryout point. Here, from figure (4.11), on the other hand, we observe that even for small values of $\bar{\tau}$ there are regions where the increase in $\bar{\tau}$ does not do as much stretching of the length to the dryout as in other regions. Moreover, it is also evident that for a fixed mass transfer parameter η, there is a point (approximately $\bar{\tau} = 1.1$ when $\eta = 1.0$) above which the increase in the traction parameter $\bar{\tau}$ no longer effects any increase in the length to the dryout point. At this stage, the increase in $\bar{\tau}$ only plays the role of flattening the slope of the liquid film thickness towards the dryout point. It is difficult and not obvious to interpret this result. However, we should

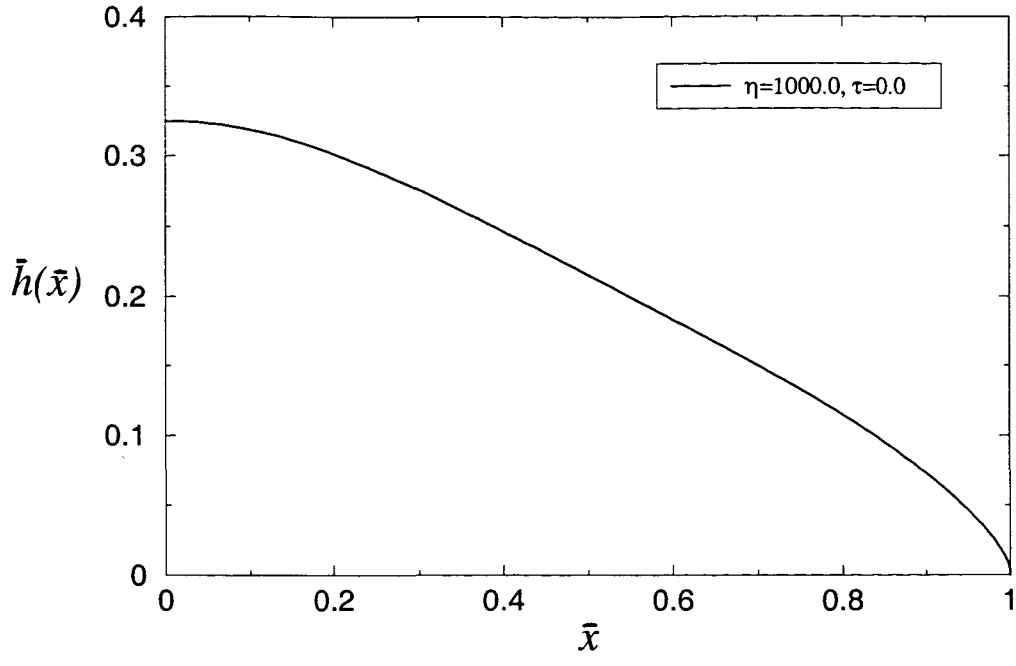

Figure 4.8: Plots of the liquid film thickness layer $\bar{h}(\bar{x})$ when the traction parameter $\bar{\tau} = 0.0$ and the mass transfer parameter $\eta = 1000.0$ (number of mesh points $n = 100$).

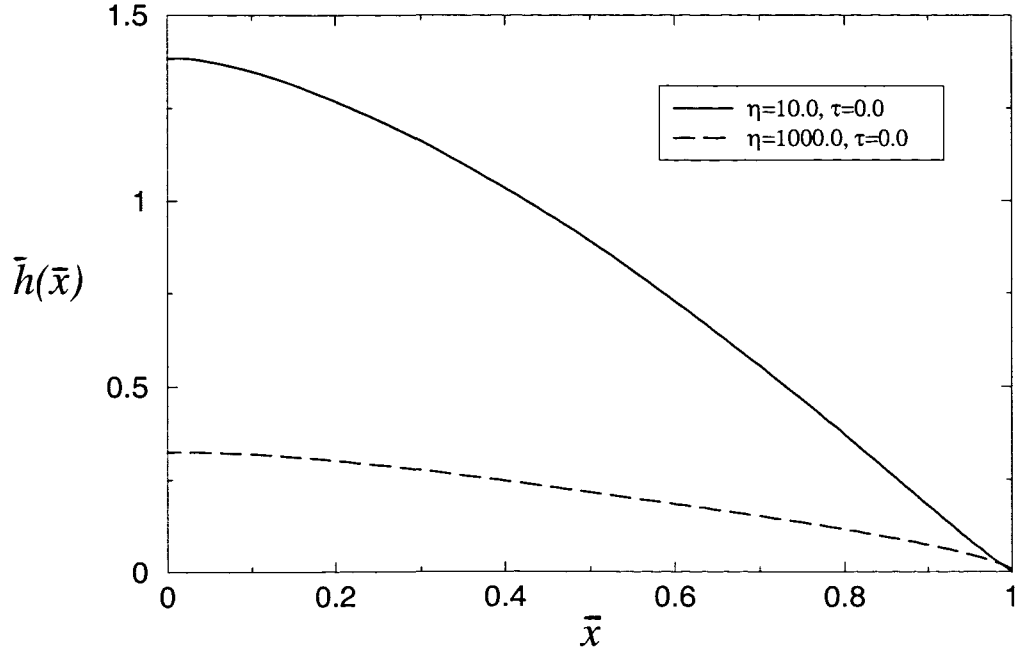

Figure 4.9: Plots of the liquid film free surface $\bar{h}(\bar{x})$ when the traction parameter $\bar{\tau} = 0.0$ and the mass transfer parameter η is varied (number of mesh points $n = 100$).

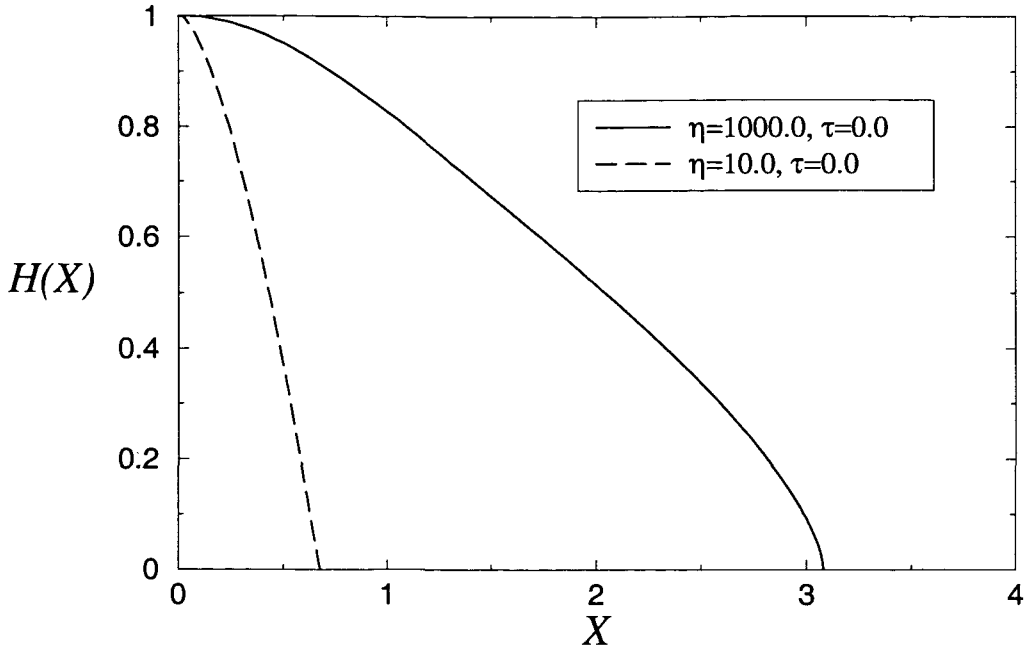

Figure 4.10: Plots of the liquid film free surface $\mathcal{H}(X)$ when the traction parameter $\bar{\tau} = 0.0$ and the mass transfer parameter η is varied (number of mesh points $n = 100$).

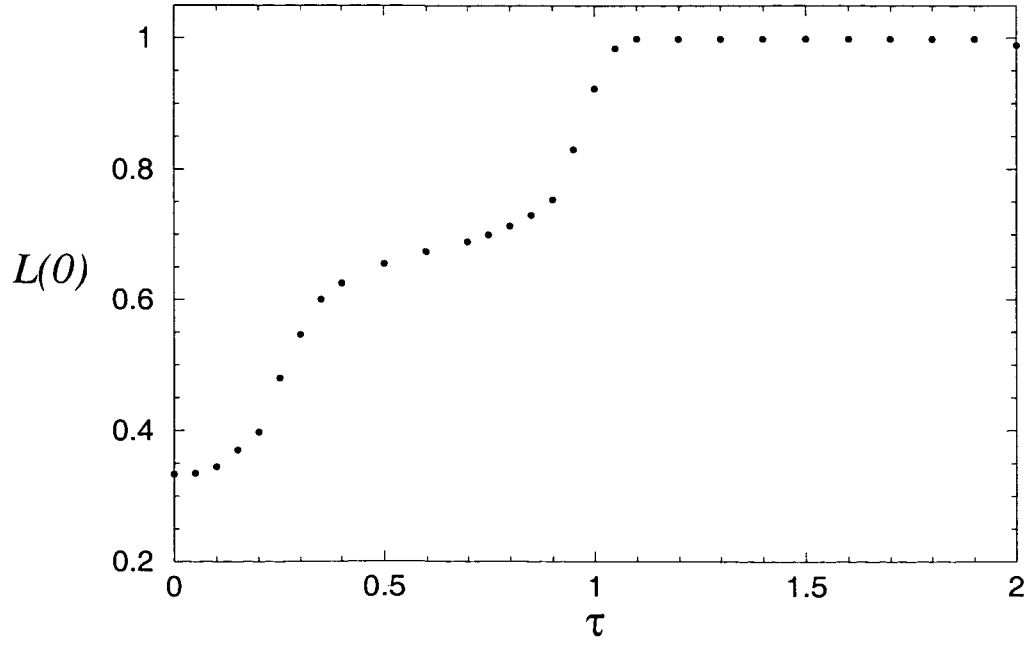

Figure 4.11: Plot of the length to the dryout L_0 against the traction parameter $\bar{\tau}$ when the mass transfer parameter $\eta = 1.0$.

recall from equation (2.56) that we observed that $\bar{\tau}$ includes effects of gravity. Therefore, what we are experiencing in figure (4.11) is some sort of competition between the gravity effects and another component of $\bar{\tau}$ which provides the pulling/stretching of the dryout point. The gravity effects play the role of flattening the slope of the film free surface near the dryout point. When the gravity effects dominate over the stretching/pulling effects, we see more of the flattening of the free surface near the dryout point than the increase in the length to the dryout point, and vice versa. It is clear from figure (4.11) that, in the case of $\eta = 1.0$ when $\bar{\tau} = 1$, the gravity effects totally dominate over the stretching/pulling effects. Thus, there is absolutely no increase in $L(0)(= L_0)$ as $\bar{\tau}$ is increased. It should be pointed out that in the results of chapter 3, the increase in $\bar{\tau}$ does not in any way play a role of flattening the slope of the unknown function $\bar{h}$ near the dryout point. Therefore, it may be deduced there that the stretching/pulling effects totally dominate over the gravity effects.

Figures (4.12), (4.13), (4.14) and (4.15) show pressure profiles in the annular regime and far downstream of the dryout for increases in both η (τ held constant) and τ (η held constant).

In fact the main difference between figures (4.12) and (4.13) [similarly figures (4.14) and

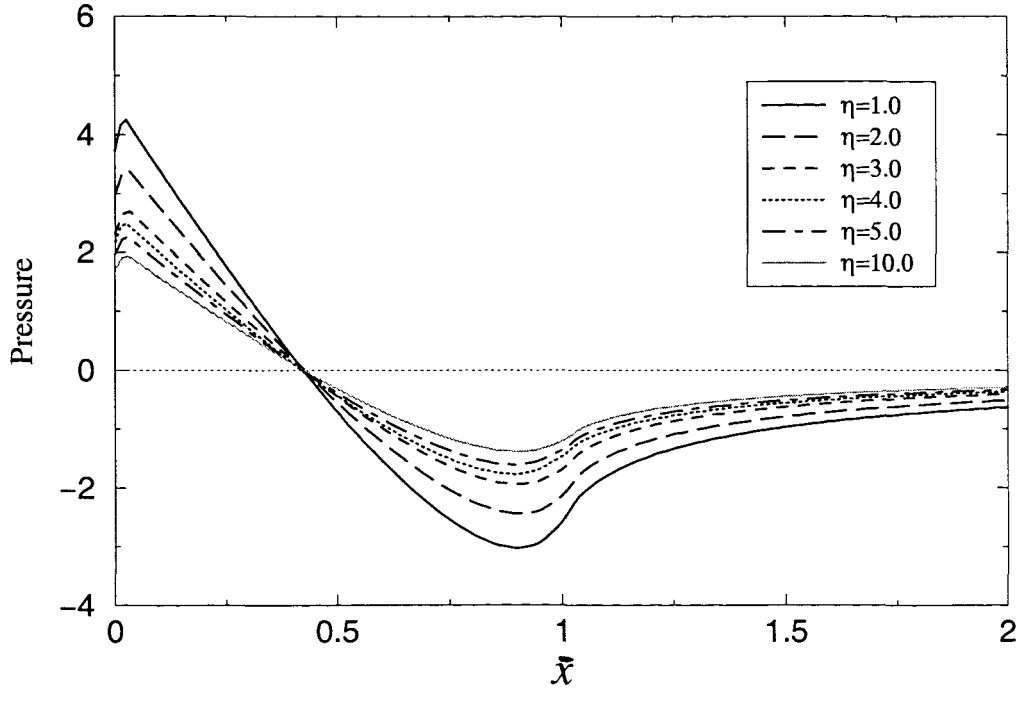

Figure 4.12: Gas core pressure in the annular flow regime and far downstream of the dryout point, for various values of the mass transfer parameter η ($\bar{\tau}$ held constant at $\tau = 0.0$).

(4.15)] is that in figure (4.12) [and hence figure (4.14)] the length to the dryout point is fixed at $x = 1$ while in figure (4.13) [and hence figure (4.15)] the dryout point is allowed to move and the pressure is scaled with h_0. In general, the pressure is positive at the entry to the annular

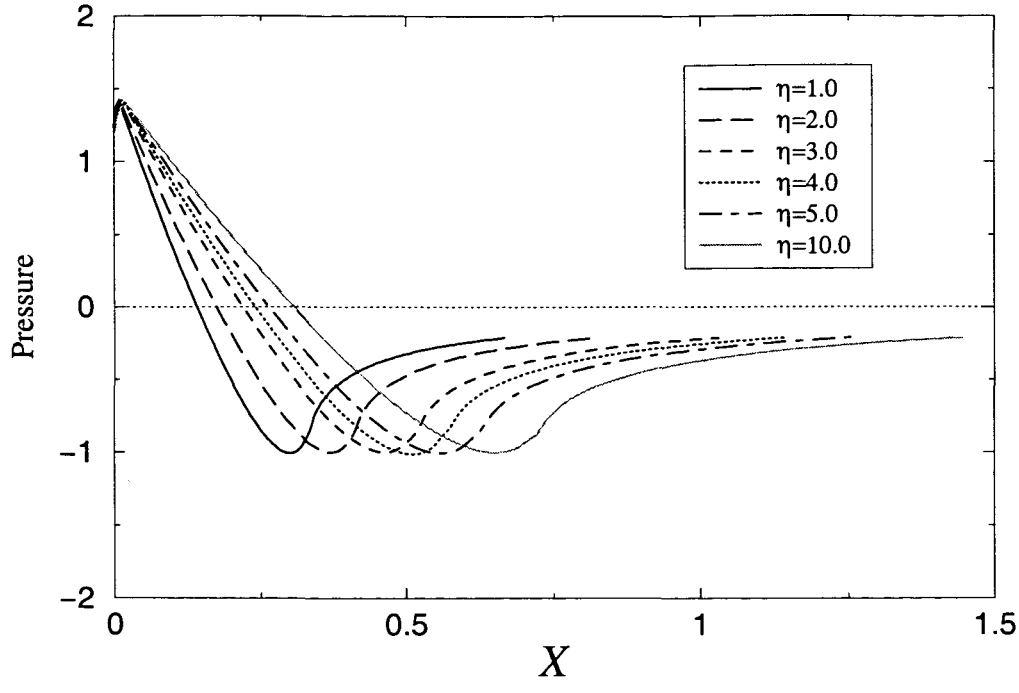

Figure 4.13: Gas core pressure in the annular flow regime and far downstream of the dryout point, for various values of the mass transfer parameter η ($\bar{\tau}$ held constant at $\tau = 0.0$).

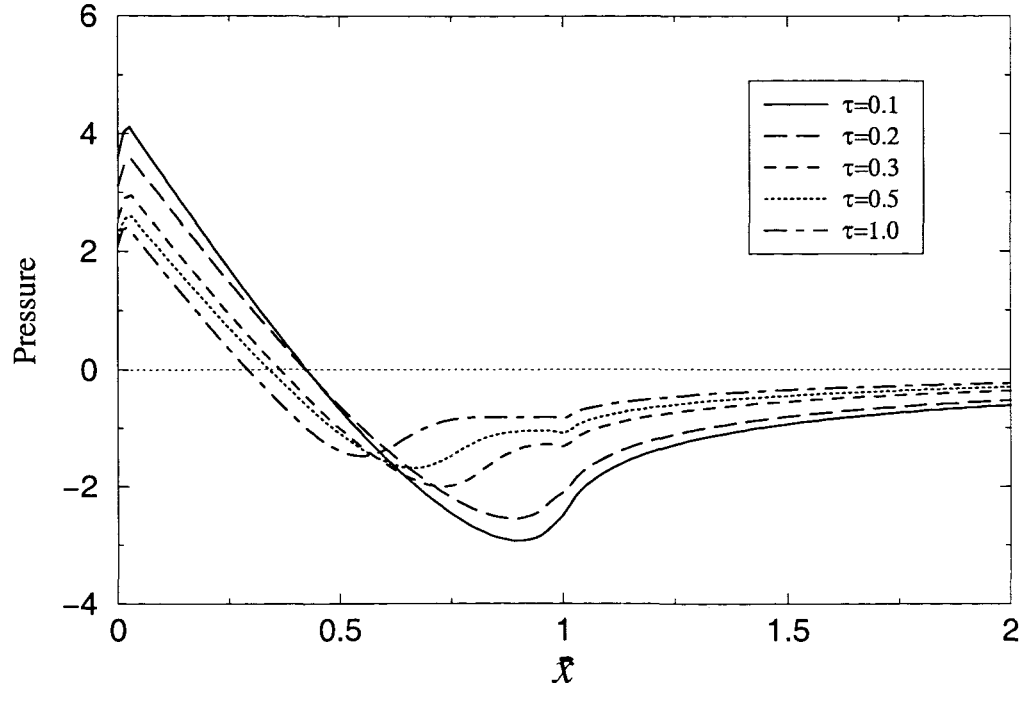

Figure 4.14: Gas core pressure in the annular flow regime and far downstream of the dryout point, for various values of the traction parameter τ (η held constant at $\eta = 1.0$).

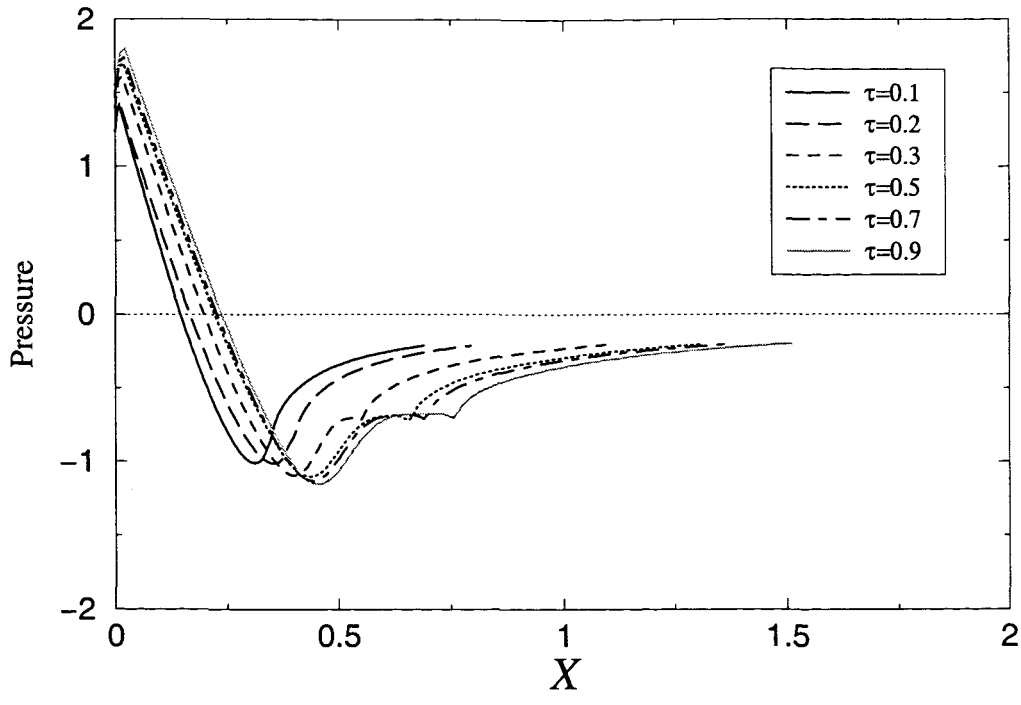

Figure 4.15: Gas core pressure in the annular regime and far downstream of the dryout point, for various values of the traction parameter τ (η held constant at $\eta = 1.0$).

flow $x = 0$. It then increases rapidly to a positive maximum near $x = 0$ before decreasing gradually to a smooth negative minimum at the dryout point. (This is not the case for the solutions of equation (3.35) where there is a singularity in $\bar{h}_{\bar{x}}(\bar{x})$ near the dryout point. In that case, it has been observed that the negative pressure minimum is infinite. Therefore, this feature is solely attributed to the singularity in $\bar{h}_{\bar{x}}$ near the dryout point, not a consequence of the numerical code.) Finally, (in the cases where solutions to equation (4.1) are monotonic) the pressure increases gradually to an almost negative equilibrium far downstream. In the cases where solutions to (4.1) are non-monotonic however, there are some apparent sharp inflexion points corresponding to the dryout points in the curves. Owing to the scaling of the gas core pressure with h_0, it is easy to observe the effects of changing η and τ in figures (4.13) and (4.15) respectively. It is clear that apart from translating the dryout point, the changes in η do not have any effect on the size of the pressure at the minimum point. The increase in τ tends to decrease the magnitude of the minimum pressure, in addition to translating the dryout point.

Figure (4.16) shows the relationship between the gas core pressure and the pressure gradient at $x = 0$ for the converged numerical solutions. Unlike the results in figure (3.17) in chapter 3, there are no indications from this graph whether there may be regions (e.g. when the pressure gradient tends to minus infinity and/or when its magnitude becomes small), where there may

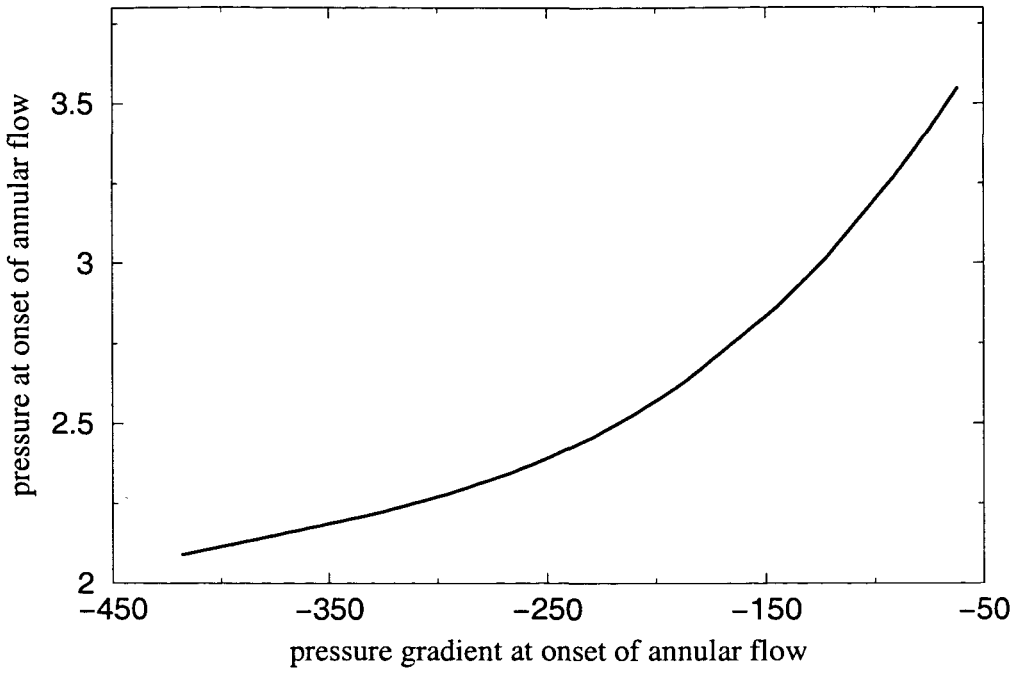

Figure 4.16: Gas core pressure p_g against the gas core pressure gradient p_{gx} at the inset of the annular flow $x = 0$, for various values of τ and η.

be no numerical solutions, h, to (4.1) for some prescribed values of pressure.

4.3 Nonregularised Problem and Pressure Gradient Condition

Since there are no singularities in $\bar{h}_{\bar{x}}(\bar{x})$ as $\bar{x} \to 1$ in equations (4.1), then it would be sensible to attempt to solve (4.1) without resorting to the regularisation process. In this section, we briefly demonstrate therefore (without going into too much technical detail) that indeed (4.1) may be solved directly. We begin by integrating (4.1) to yield

$$\frac{\bar{h}^3}{3\pi}\left(\int_0^1 \frac{\bar{h}_\xi(\xi)}{\xi - \bar{x}} d\xi\right)_{\bar{x}} - \frac{\bar{\tau}}{2}\bar{h}^2 + \frac{1}{\eta}\int_{\bar{x}}^1 \bar{h}(u)du = 0, \tag{4.7}$$

where the fact that $\bar{h} \to 1 - \bar{x}$ as $\bar{x} \to 1$ has been exploited to evaluate the constant of integration. Thus, it is equivalent to prescribing the pressure gradient condition, at the onset of the annular flow,

$$\frac{\bar{h}^3(0)}{3\pi}\left(\int_0^1 \frac{\bar{h}_\xi(\xi)}{\xi - \bar{x}} d\xi\right)_{\bar{x}}\Bigg|_{\bar{x}=0} - \frac{\bar{\tau}}{2}\bar{h}^2(0) + \frac{1}{\eta}\int_0^1 \bar{h}(u)du = 0, \tag{4.8}$$

in equation (4.1). This condition, in physical terms, implies that in equation (4.1) the mass flux vanishes at the dryout, i.e. at the dryout point $\bar{x} = 1$

$$\frac{\bar{h}^3}{3\pi}\left(\int_0^1 \frac{\bar{h}_\xi(\xi)}{\xi - \bar{x}}\right)_{\bar{x}}\Bigg|_{\bar{x}=1} = 0.$$

Equation (4.7) may now be solved numerically subject to the boundary conditions $\bar{h}_{\bar{x}}(0) = 0$, $\bar{h}(1) = 0$ and the parameter $\bar{h}(0) = \bar{h}_0$ should be specified and altered until equation (4.8) is satisfied.

4.3.1 Numerical Results

The conventional discretisation of (4.7) [as described in section (3.1.4.1) chapter 3] leads to a set of nonlinear algebraic equations

$$\frac{n^2\bar{h}_i^3}{3\pi}\left\{\sum_{j=1}^{n-2}(\bar{h}_{j+1} - \bar{h}_j)\ln\left|\frac{(2j-2i+1)^2}{(2j-2i-1)(2j-2i+3)}\right| - \bar{h}_{n-1}\times \right.$$
$$\left.\ln\left|\frac{(2n-2i-1)^2}{(2n-2i-3)(2n-2i+1)}\right|\right\} - \frac{\bar{\tau}}{2}\bar{h}_i^2 + \frac{1}{2n\eta}\left\{\sum_{j=i}^{n-2}\bar{h}_{n-1}\right\}, \qquad (4.9)$$

after applying all the boundary conditions. The trapezoidal rule has been used to approximate the last term on the left hand side of (4.7) and $2 \leq i \leq n-2$. It should be noted that the discretised version of (4.8) is simply (4.9) with $i = 0$. Equation (4.9) may then be solved iteratively for the values of $\bar{h}_j$ by Powell's method using the NAG library routine C05NBF with $\bar{h}_0$ prescribed and altered until the converged numerical solutions satisfy the discretised version of (4.8) within some specified tolerance T (in this particular case, $|T| \leq 1 \times 10^{-5}$ was used). It should be pointed out that even for this seemingly simple problem, it is still very challenging to obtain converged results for this numerical scheme, thus making the study of this problem difficult. Extensive numerical experimentation suggests that the initial estimate to the solution is crucial. Once an appropriate estimate is obtained, the numerical method converges quickly without any difficulties whatsoever. For a typical numerical solution shown in figure (4.17), the initial guess for $\bar{h}$ is $\bar{h} \approx 1 - \bar{x}_j$ in each subinterval $[x_j, x_{j+1}]$.

4.4 Nonregularised Problem and the Pressure Condition

In practice, it might be easier to measure the pressure as opposed to the pressure gradient in the pipes. We should recall that in the solution of the previous problems a condition (on the mass flux at the dryout point) which results in the pressure gradient condition at the onset of the annular flow, is prescribed. Then the pressure is obtained by appropriate calculations from the converged numerical solutions. In this section we make an initial attempt to solve

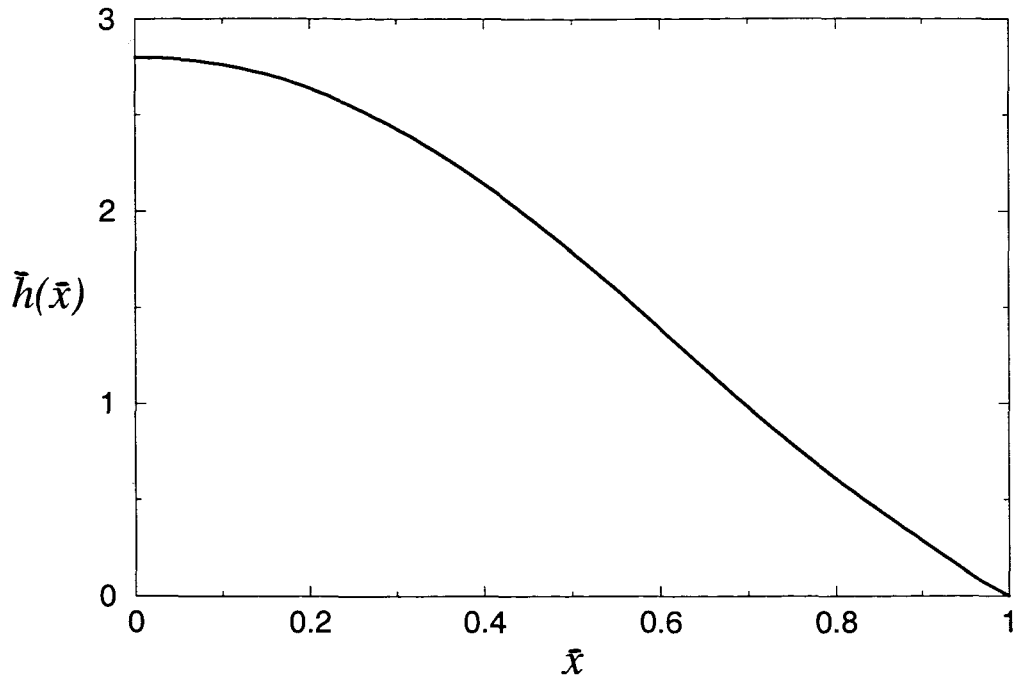

Figure 4.17: Plot of the liquid film free surface $\bar{h}(\bar{x})$ when the traction parameter $\bar{\tau} = 1.0$ and the mass transfer parameter $\eta = 2.3$ ($n = 100$).

(4.1) where the pressure at the onset of the annular flow $\bar{x} = 0$, P ($P = [p_{g0} - p_\infty]/\epsilon\rho_\infty U_\infty^2$), is directly prescribed. The same procedure could have been undertaken on equation (3.35). However, working with equation (3.35) is more tricky than dealing with (4.1) because (3.35) involves singularities in $\bar{h}_{\bar{x}}(\bar{x})$ as $\bar{x} \to 1$ and this may require the regularisation of the problem in advance and hence a big increase in the amount of algebra to be handled. Therefore we choose to attempt this approach first on a relatively simpler problem, equation (4.1). For clarity of presentation, we drop bars from now on until it may be necessary to employ them.

4.4.1 Analytical Manipulations

We continue by integrating (4.1) twice with respect to x and applying the pressure boundary condition

$$\frac{1}{\pi} \int_0^1 \frac{h_\xi(\xi)}{\xi} d\xi = P, \tag{4.10}$$

at the onset of the annular flow $x = 0$. We obtain

$$\frac{1}{3\pi} \int_0^1 \frac{h_\xi(\xi)}{\xi - x} d\xi - \frac{\tau}{2} \int_0^x \frac{d\lambda}{h(\lambda)} = \frac{1}{\eta} \int_0^x \frac{1}{h^3(\sigma)} \left\{ \int_0^\sigma h(\lambda) d\lambda \right\} d\sigma + C_1 \int_0^x \frac{d\lambda}{h^3(\lambda)} + \frac{P}{3}, \tag{4.11}$$

where C_1 is a constant of integration. On inverting (4.11) we get

$$\frac{1}{3}h_x(x) = -\frac{1}{\pi}\sqrt{\frac{1-x}{x}}\int_0^1 \sqrt{\frac{\xi}{1-\xi}}\left\{\frac{\tau}{2}\int_0^\xi \frac{d\lambda}{h(\lambda)} + \frac{1}{\eta}\int_0^\xi \frac{1}{h^3(\sigma)}\left(\int_0^\sigma h(\lambda)d\lambda\right)d\sigma\right.$$
$$\left. C_1\int_0^\xi \frac{d\lambda}{h^3(\lambda)} + \frac{P}{3}\right\}\frac{d\xi}{\xi - x} + \frac{C_3}{\sqrt{x(1-x)}}, \qquad (4.12)$$

where the parameter C_3 is obtained by applying the boundary condition $h_x(x) = 0$ at $x = 0$ and it is therefore given by

$$C_3 = \frac{C_1}{\pi}\int_0^1 \left\{\int_0^\xi \frac{d\lambda}{h(\lambda)}\right\}\frac{d\xi}{\sqrt{\xi(1-\xi)}} + \frac{1}{\pi}\int_0^1 \left\{\frac{\tau}{2}\int_0^\xi \frac{d\lambda}{h(\lambda)} + \frac{P}{3} + \right.$$
$$\left.\frac{1}{\eta}\int_0^\xi \frac{1}{h^3(\sigma)}\left(\int_0^\sigma h(\lambda)d\lambda\right)d\sigma\right\}\frac{d\xi}{\sqrt{\xi(1-\xi)}}. \qquad (4.13)$$

On integrating (4.12) with respect to x between x and $x = 1$ and applying the boundary condition $h(1) = 0$ we obtain

$$\frac{1}{3}h(x) = \frac{1}{\pi}\int_0^1 \sqrt{\frac{\xi}{1-\xi}}\left\{\frac{\tau}{2}\int_0^\xi \frac{d\lambda}{h(\lambda)} + \frac{1}{\eta}\int_0^\xi \int_0^\sigma h(\lambda)d\lambda\frac{d\sigma}{h^3(\sigma)} + \frac{P}{3} + \right.$$
$$\left. C_1\int_0^\xi \frac{d\lambda}{h^3(\lambda)}\right\}\int_x^1 \sqrt{\frac{1-x}{x}}\frac{d\xi}{\xi - x}dx - C_3\left\{\pi - 2\sin^{-1}(\sqrt{x})\right\}. \qquad (4.14)$$

We obtain C_1 by applying the boundary condition $h(0) = h_0$ in equation (4.14) to yield

$$\frac{1}{3}h_0 = \frac{1}{\pi}\int_0^1 \sqrt{\frac{\xi}{1-\xi}}\left\{\frac{\tau}{2}\int_0^\xi \frac{d\lambda}{h(\lambda)} + \frac{1}{\eta}\int_0^\xi \int_0^\sigma h(\lambda)d\lambda\frac{d\sigma}{h^3(\sigma)} + \frac{P}{3} + \right.$$
$$\left. C_1\int_0^\xi \frac{d\lambda}{h^3(\lambda)}\right\}\int_0^1 \sqrt{\frac{1-x}{x}}\frac{d\xi}{\xi - x}dx - C_3\pi. \qquad (4.15)$$

Now, equations (4.13) and (4.15) combine, after some lengthy simplifications, to give

$$C_1 = \frac{1}{\frac{\pi}{2}\int_0^1 \frac{d\xi}{h^3(\xi)} - \int_0^1 \frac{\sin^{-1}(\sqrt{\xi})}{h^3(\xi)}d\xi - \int_0^1 \frac{\sqrt{\xi(1-\xi)}}{h^3(\xi)}d\xi}\left[-\frac{h_0}{3} - \pi\frac{P}{6} - \pi\frac{\tau}{4}\int_0^1 \frac{d\xi}{h(\xi)} + \right.$$
$$\frac{\tau}{2}\int_0^1 \frac{\sqrt{\xi(1-\xi)}}{h(\xi)}d\xi - \frac{\pi}{2\eta}\int_0^1 \frac{1}{h^3(\xi)}\int_0^\xi h(\lambda)d\lambda d\xi + \frac{1}{\eta}\int_0^1 \frac{\sin^{-1}(\sqrt{\xi})}{h^3(\xi)}\int_0^\xi h(\lambda)d\lambda d\xi$$
$$\left. + \frac{1}{\eta}\int_0^1 \frac{\sqrt{\xi(1-\xi)}}{h^3(\xi)}\int_0^\xi h(\lambda)d\lambda d\xi\right]. \qquad (4.16)$$

Hence C_3 is given by

$$C_3 = \int_0^1 \frac{d\xi}{h^3(\xi)} - \frac{2}{\pi}\int_0^1 \frac{\sin^{-1}(\sqrt{\xi})}{h^3(\xi)}d\xi \times$$
$$\frac{1}{\frac{\pi}{2}\int_0^1 \frac{d\xi}{h^3(\xi)} - \int_0^1 \frac{\sin^{-1}(\sqrt{\xi})}{h^3(\xi)}d\xi - \int_0^1 \frac{\sqrt{\xi(1-\xi)}}{h^3(\xi)}d\xi}\left[-\frac{h_0}{3} - \pi\frac{P}{6} - \pi\frac{\tau}{4}\int_0^1 \frac{d\xi}{h(\xi)} + \right.$$
$$\frac{\tau}{2}\int_0^1 \frac{\sqrt{\xi(1-\xi)}}{h(\xi)}d\xi - \frac{\pi}{2\eta}\int_0^1 \frac{1}{h^3(\xi)}\int_0^\xi h(\lambda)d\lambda d\xi + \frac{1}{\eta}\int_0^1 \frac{\sin^{-1}(\sqrt{\xi})}{h^3(\xi)}\int_0^\xi h(\lambda)d\lambda d\xi$$
$$\left. + \frac{1}{\eta}\int_0^1 \frac{\sqrt{\xi(1-\xi)}}{h^3(\xi)}\int_0^\xi h(\lambda)d\lambda d\xi\right] + \frac{P}{3} + \frac{\tau}{2}\int_0^1 \frac{d\xi}{h(\xi)} - \frac{\tau}{\pi}\int_0^1 \frac{\sin^{-1}(\sqrt{\xi})}{h(\xi)}$$
$$+ \frac{1}{\eta}\int_0^1 \frac{1}{h^3(\xi)}\int_0^\xi h(\lambda)d\lambda d\xi - \frac{2}{\pi\eta}\int_0^1 \frac{\sin^{-1}(\sqrt{\xi})}{h^3(\xi)}\int_0^\xi h(\lambda)d\lambda d\xi. \quad (4.17)$$

It can be shown that

$$\int_x^1 \sqrt{\frac{1-\lambda}{\lambda}}\frac{d\lambda}{\xi-\lambda} = \pi - 2\sin^{-1}(\sqrt{x}) - 2\sqrt{\xi(1-\xi)}\ln\left|\frac{\sqrt{\xi(1-x)}+\sqrt{x(1-\xi)}}{\sqrt{\xi(1-x)}-x(1-\xi)}\right|.$$

Therefore, after some algebraic simplifications, equation (4.14) becomes

$$h(x) = 3\left(\pi - 2\sin^{-1}(\sqrt{x})\right)\left\{-\frac{P}{3} - \frac{\tau}{4}\int_0^1 \frac{d\xi}{h(\xi)} + \frac{\tau}{\pi}\int_0^1 \frac{\sin^{-1}(\sqrt{\xi})}{h(\xi)}d\xi + \frac{2}{\pi\eta}\times\right.$$
$$\int_0^1 \frac{\sin^{-1}(\sqrt{\xi})}{h^3(\xi)}\int_\xi^1 h(\lambda)d\lambda d\xi + \left(\frac{2}{\pi}\int_0^1 \frac{\sin^{-1}(\sqrt{\xi})}{h^3(\xi)}d\xi - \frac{1}{2}\int_0^1 \frac{d\xi}{h^3(\xi)}\right)C_1 - \int_0^1 \left\{\frac{\tau}{2h(\xi)} + \right.$$
$$\left.\frac{C_1}{h^3(\xi)}\right\}\left(\sin^{-1}(\sqrt{\xi}) - \sqrt{\xi(1-\xi)}\right)d\xi - \frac{1}{\eta}\int_0^1 \frac{\sin^{-1}(\sqrt{\xi})}{h^3(\xi)}\int_0^\xi h(\lambda)d\lambda d\xi +$$
$$\left.\frac{1}{\eta}\int_0^1 \frac{\sqrt{\xi(1-\xi)}}{h^3(\xi)}\int_0^\xi h(\lambda)d\lambda d\xi\right\} - \frac{6}{\pi}\int_0^1 \left\{\frac{P}{3} + \frac{\tau}{2}\int_0^\xi \frac{d\lambda}{h(\lambda)} + \frac{1}{\eta}\int_0^\xi \frac{1}{h^3(\sigma)}\times\right.$$
$$\left.\left.\int_0^\sigma h(\lambda)d\lambda d\sigma + C_1\int_0^\xi \frac{d\lambda}{h^3(\lambda)}\right\}\xi\ln\left|\frac{\sqrt{\xi(1-x)}+\sqrt{x(1-\xi)}}{\sqrt{\xi(1-x)}-x(1-\xi)}\right|d\xi. \quad (4.18)$$

On defining $f_1(x,\xi)$ by

$$f_1(x,\xi) = \int \ln\left|\sqrt{\xi(1-x)}+\sqrt{x(1-\xi)}\right|d\xi = \frac{1}{2}\left(2\xi - \frac{x\sqrt{1-x}(1-\sqrt{x})}{2x(1-x)+x^2+(1-x)^2}\right)\times$$
$$\ln\left|\sqrt{\xi(1-x)}+\sqrt{x(1-\xi)}\right| - \frac{1}{2}\sqrt{x}(1-\sqrt{x})\left(\frac{2x}{2x(1-x)+x^2+(1-x)^2}\right)\times$$
$$\sin^{-1}(\sqrt{\xi}) - \frac{1}{2}(1-\sqrt{x})\sqrt{1-x}(1-\xi) -$$
$$\frac{1}{2}(1-\sqrt{x})\sqrt{x}\sqrt{\xi(1-\xi)}, \quad (4.19)$$

then it can be shown, after some algebra, that

$$f_2(x,\xi) = \int \xi \ln\left|\sqrt{\xi(1-x)} + \sqrt{x(1-\xi)}\right| d\xi = \frac{1}{2}\xi^2 \ln\left|\sqrt{\xi(1-x)} + \sqrt{x(1-\xi)}\right| +$$
$$\left(\frac{x\sqrt{1-x}(1-\sqrt{x})}{2x(1-x)+x^2+(1-x)^2} - \frac{1}{2}\right) f_1(x,\xi)$$
$$+\frac{1}{4}(1-\sqrt{x})\left\{\frac{2x\sqrt{1-x}(1-\sqrt{x})}{2x(1-x)+x^2+(1-x)^2} - 1\right\}\left\{\sqrt{\xi(1-\xi)} - (1-2\xi)\sin^{-1}(\sqrt{\xi})\right\}$$
$$-\frac{1}{16}\sqrt{x}(1-\sqrt{x})\left\{\sin^{-1}(1-2\xi) - 2(1-2\xi) - 2(1-2\xi)\sqrt{\xi(1-\xi)}\right\}$$
$$+\frac{1}{4}\sqrt{1-x}(1-\sqrt{x})(1-\xi)^2, \quad (4.20)$$

where the constants of integration in (4.19) and (4.20) have been omitted here for obvious reasons. Hence, after some lengthy algebra and rearrangement of terms, equation (4.18) can be written as

$$h(x) = 3\left(\pi - 2\sin^{-1}(\sqrt{x})\right) f_3 - \frac{6}{\pi} f_4(x) + \frac{6}{\pi} f_5(x), \quad (4.21)$$

where f_3, $f_4(x)$ and $f_5(x)$ are respectively given by

$$f_3 = -\frac{\tau}{4}\int_0^1 \frac{d\xi}{h(\xi)} + \frac{\tau}{2}\left(\frac{2}{\pi} - 1\right)\int_0^1 \frac{\sin^{-1}(\sqrt{\xi})}{h(\xi)} d\xi + \frac{\tau}{2}\int_0^1 \frac{\sqrt{\xi(1-\xi)}}{h(\xi)} d\xi + \frac{2}{\pi\eta} \times$$
$$\left(1 - \frac{2}{\pi}\right)\int_0^1 \frac{\sin^{-1}(\sqrt{\xi})}{h^3(\xi)} \int_0^\xi h(\lambda) d\lambda d\xi$$
$$-\frac{1}{2\eta}\int_0^1 \frac{1}{h^3(\xi)} \int_0^\xi h(\lambda) d\lambda d\xi - \frac{P}{3} + \left(\frac{2}{\pi}\int_0^1 \frac{\sin^{-1}(\sqrt{\xi})}{h^3(\xi)} d\xi - \frac{1}{2}\int_0^1 \frac{d\xi}{h^3(\xi)}\right) C_1$$
$$+ \frac{\frac{1}{\eta}\int_0^1 \frac{\sqrt{\xi(1-\xi)}}{h^3(\xi)} d\xi - \frac{1}{\eta}\int_0^1 \frac{\sin^{-1}(\sqrt{\xi})}{h^3(\xi)} d\xi}{\frac{\pi}{2}\int_0^1 \frac{d\xi}{h^3(\xi)} - \int_0^1 \frac{\sin^{-1}(\sqrt{\xi})}{h^3(\xi)} d\xi - \frac{\sqrt{\xi(1-\xi)}}{h^3(\xi)} d\xi},$$

$$f_4(x) = \left\{\frac{1}{8}\frac{x\sqrt{1-x}(1-\sqrt{x})}{2x(1-x)+x^2+(1-x)^2} \ln|1-x| + \frac{\pi}{4}\sqrt{x}(1-\sqrt{x}) \times \right.$$
$$\left(\frac{2x}{2x(1-x)+x^2+(1-x)^2} - 1\right)\frac{x\sqrt{1-x}(1-\sqrt{x})}{2x(1-x)+x^2+(1-x)^2}\left[\frac{1}{4}(2 - \right.$$
$$\left.\left.\frac{x\sqrt{1-x}(1-\sqrt{x})}{2x(1-x)+x^2+(1-x)^2}\right)\ln|1-x| + \frac{\pi}{4}\sqrt{x}(1-\sqrt{x}) \times \right.$$
$$\left.\left(\frac{2x}{2x(1-x)+x^2+(1-x)^2} - 1\right)\right]\frac{1}{32}\sqrt{x}(1-\sqrt{x}) + \left(-\frac{1}{4}(1-x)^2 - \frac{x}{2} + \frac{x^2}{2}\right) \times$$
$$\ln|1-x| + \frac{x}{4} - \frac{3}{8}x^2 + \frac{1}{8}\left\{\frac{P}{3} + \frac{\tau}{2}\int_0^1 \frac{d\xi}{h^3(\xi)} + \frac{1}{\eta}\int_0^1 \frac{1}{h^3(\xi)} \int_0^\xi h(\lambda) d\lambda d\xi + \right.$$
$$\left. C_1 \int_0^1 \frac{d\xi}{h^3(\xi)}\right\},$$

and

$$f_5(x) = \int_0^1 \left\{ \frac{\tau}{2h(\xi)} + \frac{1}{\eta h^3(\xi)} \int_0^\xi h(\lambda)d\lambda + \frac{C_1}{h^3(\xi)} + \frac{P}{3} \right\} \{f_2(x,\xi) + \left(-\frac{1}{4}(\xi - x)^2 - \frac{x^2}{2} + \frac{x\xi}{2} \right) \ln|\xi - x| + \frac{3}{8}\xi^2 - \frac{x\xi}{4} \Big\} d\xi. \tag{4.22}$$

Equation (4.22) can be further expanded to give

$$\begin{aligned} f_5(x) = \frac{P}{3} \Bigg\{ & -\frac{1}{2} \frac{x\sqrt{1-x}(1-\sqrt{x})}{2x(1-x)+x^2+(1-x)^2} \left(\frac{1}{2} \frac{x\sqrt{1-x}(1-\sqrt{x})}{2x(1-x)+x^2+(1-x)^2} - \frac{5}{4} \right) \times \\ & \ln|1-x| + \frac{\pi}{16}\sqrt{x}(1-\sqrt{x}) + \frac{\pi}{2} \left(\frac{1}{2}\sqrt{x}(1-\sqrt{x}) - \frac{1}{2} \frac{x\sqrt{x(1-x)}(1-\sqrt{x})}{2x(1-x)+x^2+(1-x)^2} \right) \\ & -\frac{1}{4}\sqrt{1-x}(1-\sqrt{x}) + \frac{1}{4} \left(\frac{x\sqrt{1-x}(1-\sqrt{x})}{2x(1-x)+x^2+(1-x)^2} \right)^2 \ln|1-x| + \frac{1}{2} \times \\ & \frac{x(1-x)(1-\sqrt{x})^2}{2x(1-x)+x^2+(1-x)^2} \Bigg\} - \frac{1}{4} \Bigg[\frac{1}{8}(1-x)^3 \ln|1-x| + \frac{x^3}{8} \ln|x| - \frac{1}{9}(1-x^3) \\ & -\frac{x}{3}(x-1) \Bigg] - \frac{x^2}{2} \left[(1-x) \{\ln|1-x| - 1\} + x \ln|x| \right] + \frac{3}{8}x^2 - \frac{x}{8} - \frac{1}{24} \\ & + \frac{x}{2} \left[\left\{ \frac{1}{2}(1-x)^2 - x^2 + x \right\} \ln|1-x| + \frac{1}{2}x^2 \ln|x| - \frac{3}{4} \right] + \frac{\tau}{2} \int_0^1 \frac{f_6(x,\xi)}{h(\xi)} d\xi + \\ & + \frac{1}{\eta} \int_0^1 \frac{f_6(x,\xi)}{h^3(\xi)} \int_0^\xi h(\lambda)d\lambda d\xi + C_1 \frac{\int_0^1 \frac{f_6(x,\xi)}{h^3(\xi)} d\xi}{\frac{\pi}{2} \int_0^1 \frac{d\xi}{h^3(\xi)} - \int_0^1 \frac{\sin^{-1}(\sqrt{\xi})}{h^3(\xi)} d\xi - \int_0^1 \frac{\sqrt{\xi(1-\xi)}}{h^3(\xi)} d\xi}, \end{aligned} \tag{4.23}$$

where $f_6(x,\xi)$ is given by

$$f_6(x,\xi) = f_2(x,\xi) + \left(-\frac{1}{4}(\xi - x)^2 + \frac{x^2}{2} + \frac{x\xi}{2} \right) \ln|\xi - x| + \frac{3}{8}\xi^2 - \frac{x\xi}{4},$$

and we recall that C_1 is given by equation (4.16).

When P is an arbitrarily prescribed parameter, equation (4.21) contains no singular integrals or derivatives. As a result, we believe that it may be solved numerically using direct iteration techniques. It is likely that in this case some relaxation may have to be employed in the numerical scheme (see for example, Fitt *et al*, 1985; Fitt & Stefanidis, 1998) [32]; [33]. Here, however, solving (4.21) by direct iteration methods would be cumbersome owing to the amount of algebra involved in this particular problem (and which would definitely increase when discretising the equations). In order to proceed, we combine (4.11) and (4.16) so that instead, we have to compute h from the equation

$$\left\{\frac{\pi}{2}\int_0^1 \frac{d\xi}{h^3(\xi)} - \int_0^1 \frac{\sin^{-1}(\sqrt{\xi})}{h^3(\xi)}d\xi - \int_0^1 \frac{\sqrt{\xi(1-\xi)}}{h^3(\xi)}d\xi\right\}\left\{\frac{h^3(x)}{3\pi}\left(\int_0^1 \frac{h_\xi(\xi)}{\xi - x}d\xi\right)_x\right.$$
$$\left. -\frac{\tau}{2}h^2 - \frac{1}{\eta}\int_0^x h(\xi)d\xi\right\} + \frac{h_0}{3} + \pi\frac{P}{6} + \pi\frac{\tau}{4}\int_0^1 \frac{d\lambda}{h(\lambda)} - \frac{\tau}{2}\int_0^1 \frac{\sin^{-1}(\sqrt{\xi})}{h(\xi)}d\xi$$
$$-\frac{\tau}{2}\int_0^1 \frac{\sqrt{\xi(1-\xi)}}{h(\xi)}d\xi + \frac{\pi}{2\eta}\int_0^1 \frac{1}{h^3(\xi)}\int_0^\xi h(\lambda)d\lambda d\xi$$
$$-\frac{1}{\eta}\int_0^1 \frac{\sqrt{\xi(1-\xi)}}{h^3(\xi)}\int_0^\xi h(\lambda)d\lambda d\xi - \frac{1}{\eta}\int_0^1 \frac{\sin^{-1}(\sqrt{\xi})}{h^3(\xi)}\int_0^\xi h(\lambda)d\lambda d\xi = 0. \qquad (4.24)$$

It is not easy to solve (4.24); however this approach reduces the amount of algebra involved in computing h, in comparison to the earlier technique.

4.4.2 Numerical Treatment

We partition the interval $[0,1]$ into equal subintervals $[\xi_j, \xi_{j+1}]$ for $0 \le j \le n-1$, where n is the number of mesh points. Since (4.24) is very complicated we assume here that in the numerical scheme h is piecewise constant in each subinterval. To be precise, we approximate h by $h \approx (h_{j+1} + h_j)/2$ in $[\xi_j, \xi_{j+1}]$. We employ finite differences to evaluate the derivative of the singular integral term (the Hilbert transform term) and collocate (4.24) at the mid-mesh points $x_{i\pm 1/2}$, for $2 \le i \le n-2$. To evaluate the ordinary integrals, we employ the trapezoidal rule (as has been explained repeatedly in this study). We outline here how the double integrals may be evaluated using the trapezoidal rule. In particular, we approximate

$$\int_0^1 \frac{1}{h^3(\xi)}\int_0^\xi h(\lambda)d\lambda d\xi \approx \sum_{j=0}^{n-1} \frac{8}{(h_{j+1}+h_j)^3}\int_{\xi_j}^{\xi_{j+1}}\int_0^\xi h(\lambda)d\lambda d\xi,$$

by the trapezoidal rule. This implies that

$$\int_0^1 \frac{1}{h^3(\xi)}\int_0^\xi h(\lambda)d\lambda d\xi \approx \sum_{j=0}^{n-1} \frac{8}{(h_{j+1}+h_j)^3}\left\{\xi_{j+1}\int_0^{\xi_{j+1}} h(\lambda)d\lambda - \xi_j\int_0^{\xi_j} h(\lambda)d\lambda - \right.$$
$$\left. \int_{\xi_j}^{\xi_{j+1}} \xi h(\xi)d\xi\right\},$$

after using integration by parts and the Leibnitz's rule. Therefore we have

$$\int_0^1 \frac{1}{h^3(\xi)}\int_0^\xi h(\lambda)d\lambda d\xi \approx \sum_{j=0}^{n-1} \frac{8}{(h_{j+1}+h_j)^3}\left\{\xi_{j+1}\int_{\xi_j}^{\xi_{j+1}} h(\lambda)d\lambda + (\xi_{j+1}-\xi_j)\int_0^{\xi_j} h(\lambda)d\lambda - \right.$$
$$\left. \frac{h_{j+1}+h_j}{4}\left(\xi_{j+1}^2 - \xi_j^2\right)\right\}. \qquad (4.25)$$

In this particular case, the second term in the curly brackets

$$\int_0^{\xi_j} h(\lambda)d\lambda,$$

in equation (4.25) is approximated by the less accurate numerical scheme

$$\int_0^{\xi_j} h(\lambda)d\lambda \approx \xi_j h_0 + \frac{1}{2}\xi_j\,(h_j - h_0)\,,$$

for simplicity in the computations. (A better numerical approximation of this integral is to use the trapezoidal rule. However, the latter approximation does not make any significant changes in the final numerical results due to the shape our solution curves of h.) Equation (4.25) then simplifies to give

$$\int_0^1 \frac{1}{h^3(\xi)} \int_0^{\xi} h(\lambda)d\lambda d\xi \approx \sum_{j=0}^{n-1} \frac{8}{(h_{j+1}+h_j)^3} I_{1j} =$$

$$\sum_{j=0}^{n-1} \frac{8}{(h_{j+1}+h_j)^3} \left\{ \frac{\xi_{j+1}(h_{j+1}+h_j)}{2n} + (\xi_{j+1}-\xi_j)\left[\xi_j h_0 + \frac{1}{2}\xi_j(h_j - h_0)\right] \right.$$

$$\left. - \frac{(h_{j+1}+h_j)}{4}\left(\xi_{j+1}^2 - \xi_j^2\right)\right\}. \qquad (4.26)$$

By following similar arguments, after some algebra, we get

$$\int_0^1 \frac{\sin^{-1}(\sqrt{\xi})}{h^3(\xi)} \int_0^{\xi} h(\lambda)d\lambda d\xi \approx \sum_{j=0}^{n-1} \frac{8}{(h_{j+1}+h_j)^3} I_{2j}$$

$$= \sum_{j=0}^{n-1} \frac{8}{(h_{j+1}+h_j)^3} \left\{ \left(\frac{1}{2}\sqrt{\xi_{j+1}(1-\xi_{j+1})} - \frac{1}{2}\sin^{-1}(\sqrt{\xi_{j+1}}) + \xi_{j+1}\sin^{-1}(\sqrt{\xi_{j+1}}) \right) \times \right.$$

$$\frac{(h_{j+1}+h_j)}{2n}$$

$$+ \left[\frac{1}{2}\sqrt{\xi_{j+1}(1-\xi_{j+1})} - \frac{1}{2}\sqrt{\xi_j(1-\xi_j)} - \frac{1}{2}\sin^{-1}(\sqrt{\xi_{j+1}}) + \frac{1}{2}\sin^{-1}(\sqrt{\xi_j}) + \xi_{j+1} \times \right.$$

$$\left. \sin^{-1}(\xi_{j+1}) - \xi_j \sin^{-1}(\xi_j) \right] \left[\xi_j h_0 + \frac{1}{2}\xi_j(h_j - h_0) \right] - \frac{h_{j+1}+h_j}{2} \times$$

$$\left[\left(\frac{1}{2}\xi_{j+1}^2 + \frac{1}{16} \right) \sin^{-1}(\sqrt{\xi_{j+1}}) - \left(\frac{1}{2}\xi_j^2 + \frac{1}{16} \right) \sin^{-1}(\sqrt{\xi_j}) + \frac{1}{8}\xi_{j+1}^{\frac{3}{2}}\sqrt{1-\xi_{j+1}} \right.$$

$$\left. \left. - \frac{1}{8}\xi_j^{\frac{3}{2}}\sqrt{1-\xi_{j+1}} - \frac{1}{4}\sqrt{\xi_{j+1}}(1-\xi_{j+1})^{\frac{3}{2}} + \frac{1}{4}\sqrt{\xi_j}(1-\xi_j)^{\frac{3}{2}} \right] \right\}, \qquad (4.27)$$

$$\int_0^1 \frac{\sqrt{\xi(1-\xi)}}{h^3(\xi)} \int_0^{\xi} h(\lambda)d\lambda d\xi \approx \sum_{j=0}^{n-1} \frac{8}{(h_{j+1}+h_j)^3} I_{3j}$$

$$= \sum_{j=0}^{n-1} \frac{8}{(h_{j+1}+h_j)^3} \left\{ \left(\frac{1}{4}\sin^{-1}(\sqrt{\xi_{j+1}}) - \frac{1}{8}\sqrt{\xi_{j+1}(1-\xi_{j+1})}(1-2\xi_{j+1}) \right) \times \right.$$

$$\frac{(h_{j+1}+h_j)}{2n}$$

$$+ \left[\frac{1}{4}\sin^{-1}(\sqrt{\xi_{j+1}}) - \frac{1}{4}\sin^{-1}(\sqrt{\xi_j}) - \frac{1}{8}\sqrt{\xi_{j+1}(1-\xi_{j+1})}(1-2\xi_{j+1}) + \right.$$

$$\left. \frac{1}{8}\sqrt{\xi_j(1-\xi_j)}(1-2\xi_j) \right] \left[(\xi_j h_0 + \frac{1}{2}(\xi_j(h_j - h_0) \right]$$

$$- \frac{(h_{j+1}-h_j)}{2n} \left[-\frac{1}{6}\left(\xi_{j+1}[1-\xi_{j+1}]\right)^{\frac{3}{2}} + \frac{1}{6}\left(\xi_j[1-\xi_j]\right)^{\frac{3}{2}} + \frac{1}{16} \times \right.$$

$$(1-2\xi_{j+1})\sin^{-1}(1-2\xi_{j+1}) - \frac{1}{16}(1-2\xi_j)\sin^{-1}(1-2\xi_j) +$$

$$\left. \left. \frac{1}{16}\sqrt{1-(1-2\xi_{j+1})^2} - \frac{1}{16}\sqrt{1-(1-2\xi_j)^2} \right] \right\}. \qquad (4.28)$$

Thus, the discretised version of (4.24) is

$$\left\{ \frac{\pi}{n}\sum_{j=0}^{n-1} \frac{4}{(h_{j+1}+h_j)^3} - 8\sum_{j=0}^{n-1} \frac{I_{4j}}{(h_{j+1}+h_j)^3} - 8\sum_{j=0}^{n-1} \frac{I_{5j}}{(h_{j+1}+h_j)^3} \right\} \times$$

$$\left\{ \frac{n^2 h_i^3}{3\pi}\sum_{j=0}^{n-1}(h_{j+1}-h_j)\ln\left|\frac{(2j-2i+1)^2}{(2j-2i-1)(2j-2i+3)}\right| - \frac{\tau}{2}h_i^2 - \frac{1}{2\eta n}\sum_{j=0}^{i}(h_{j+1}-h_j) \right\}$$

$$+\frac{h_0}{3} + \pi\frac{P}{6} + \frac{\pi\tau}{2n}\sum_{j=0}^{n-1}\frac{1}{h_{j+1}+h_j} - \frac{\tau}{n}\sum_{j=0}^{n-1}\frac{I_{4j}}{h_{j+1}+h_j} - \frac{\tau}{n}\sum_{j=0}^{n-1}\frac{I_{5j}}{h_{j+1}+h_j}$$

$$+\frac{4\pi}{\eta}\sum_{j=0}^{n-1}\frac{I_{1j}}{(h_{j+1}+h_j)^3} - \frac{8}{\eta}\sum_{j=0}^{n-1}\frac{I_{3j}}{(h_{j+1}+h_j)^3} - \frac{8}{\eta}\sum_{j=0}^{n-1}\frac{I_{2j}}{(h_{j+1}+h_j)^3} = 0, \qquad (4.29)$$

where I_{4j} and I_{5j} are respectively given by

$$\int_0^1 \frac{\sin^{-1}(\sqrt{\xi})}{h^3(\xi)}d\xi \approx \sum_{j=0}^{n-1}\frac{8}{(h_{j+1}+h_j)^3}I_{4j}$$

$$= \sum_{j=0}^{n-1}\frac{8}{(h_{j+1}+h_j)^3}\left(\left[\xi_{j+1}-\frac{1}{2}\right]\sin^{-1}(\sqrt{\xi_{j+1}}) + \frac{1}{2}\sqrt{\xi_{j+1}(1-\xi_{j+1})} \right.$$

$$\left. \left[-\xi_j+\frac{1}{2}\right]\sin^{-1}(\sqrt{\xi_j}) - \frac{1}{2}\sqrt{\xi_j(1-\xi_j)} \right),$$

$$\int_0^1 \frac{\sqrt{\xi(1-\xi)}}{h^3(\xi)} \approx \sum_{j=0}^{n-1}\frac{8}{(h_{j+1}+h_j)^3}I_{5j}$$

$$= \sum_{j=0}^{n-1}\frac{2}{(h_{j+1}+h_j)^3}\left(\frac{1}{4}\sin^{-1}(\sqrt{\xi}) - \frac{1}{8}\sqrt{\xi_{j+1}(1-2\xi_{j+1})}(1-2\xi_{j+1}) \right.$$

$$\left. -\frac{1}{4}\sin^{-1}(\sqrt{\xi_j}) + \frac{1}{8}\sqrt{\xi_j(1-\xi_j)}(1-2\xi_j) \right).$$

4.4.3 Some Preliminary Numerical Results and Discussions

We solve (4.29) iteratively for the values of h by Powell's method using the NAG library routine C05NBF. The initial guess to the solution (after an extensive numerical experimentation) is taken to be a piecewise nonlinear function $h_j = (1 - x_j)^{1/2}$ in each subinterval $[x_j, x_{j+1}]$ for $1 \leq j \leq n-1$. In theory, the values of τ, η, h_0 and P may be prescribed and varied at will. However, we know from equation (4.15) that P and h_0 are directly related; hence they cannot both be prescribed independently. Moreover, we know that h_0 (and hence P) depends on the global behaviour of the unknown function h in $[0, 1]$, in addition to the values of the mass transfer parameter η and the traction parameter τ. This makes the solution of (4.29) very difficult. As purely a preliminary attempt at solving the system (4.29) numerically, we fix the values of τ, η and h_0. Then P is prescribed an initial value (in this particular case 1.0) and then altered until a converged numerical solution satisfies the discretised version of (4.15) within a given tolerance. Thus, in a sense we solve for h, and P is obtained simultaneously as an eigenvalue of this problem. Typical results are shown in figures (4.18), (4.19) and (4.20).

The problem may be solved for h in the same way by fixing τ, η and P and then h_0 be

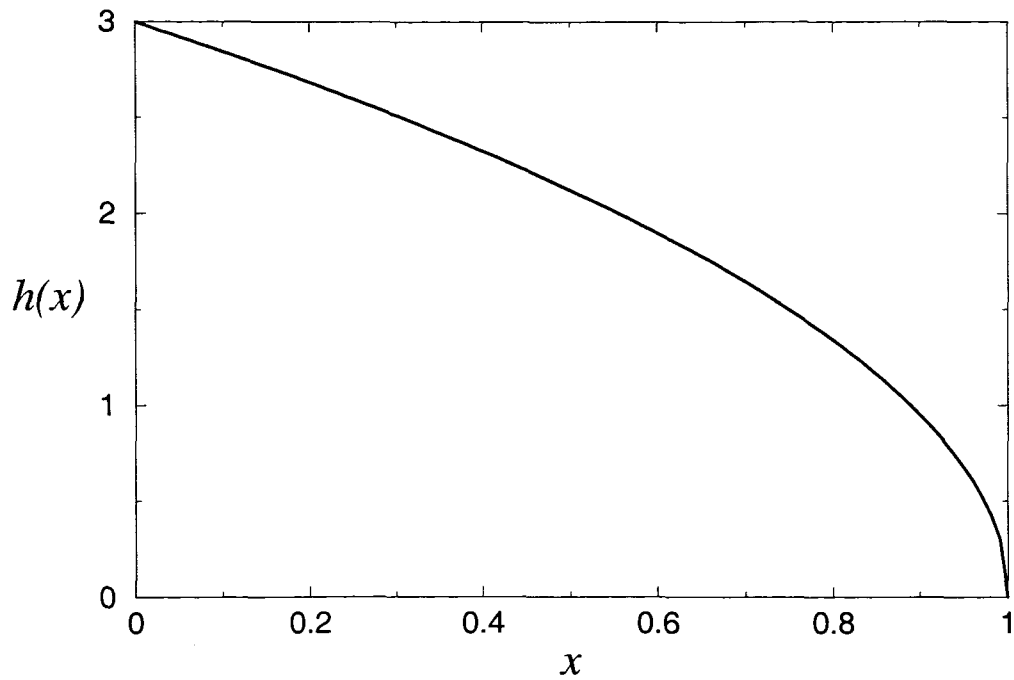

Figure 4.18: Plot of the liquid film free surface $h(x)$; η, τ and P fixed at $\eta = 1.0$, $\tau = 1.0$, $P = 1.076683$ $(n = 60)$.

obtained as part of the solution. However, this latter approach will require extra vigilance in the numerical scheme as h_0 will appear implicitly from the discretised version of (4.15). The numerical results in figures (4.18) to (4.20) seem to be sensible because they clearly show

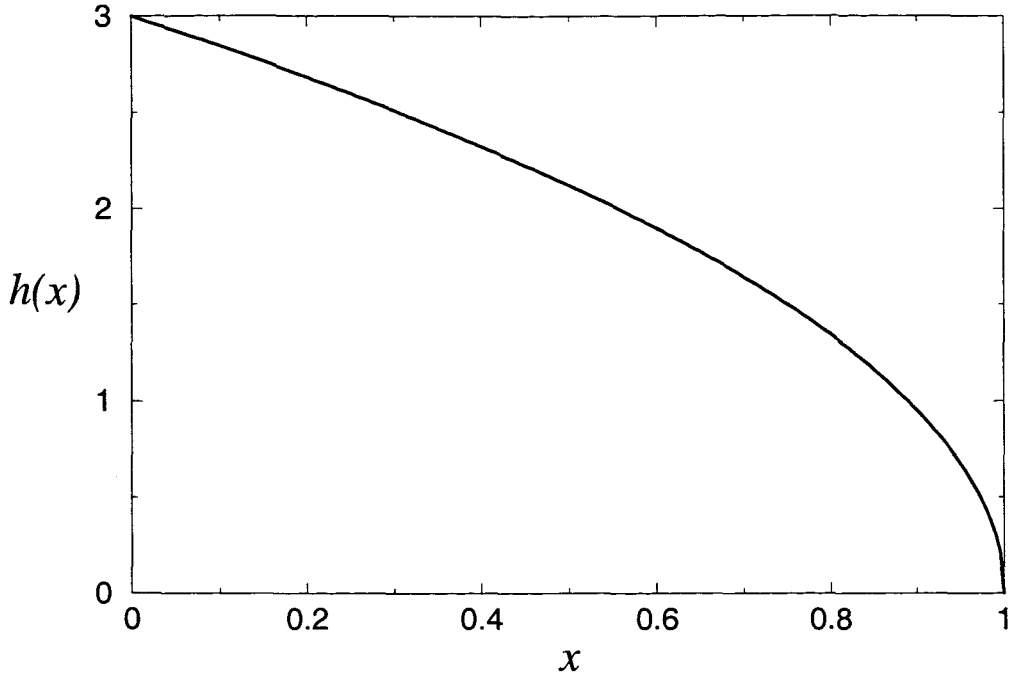

Figure 4.19: Plot of the liquid film free surface $h(x)$; η, τ and P fixed at $\eta = 1.0$, $\tau = 1.0$, $P = 1.076683$ ($n = 80$).

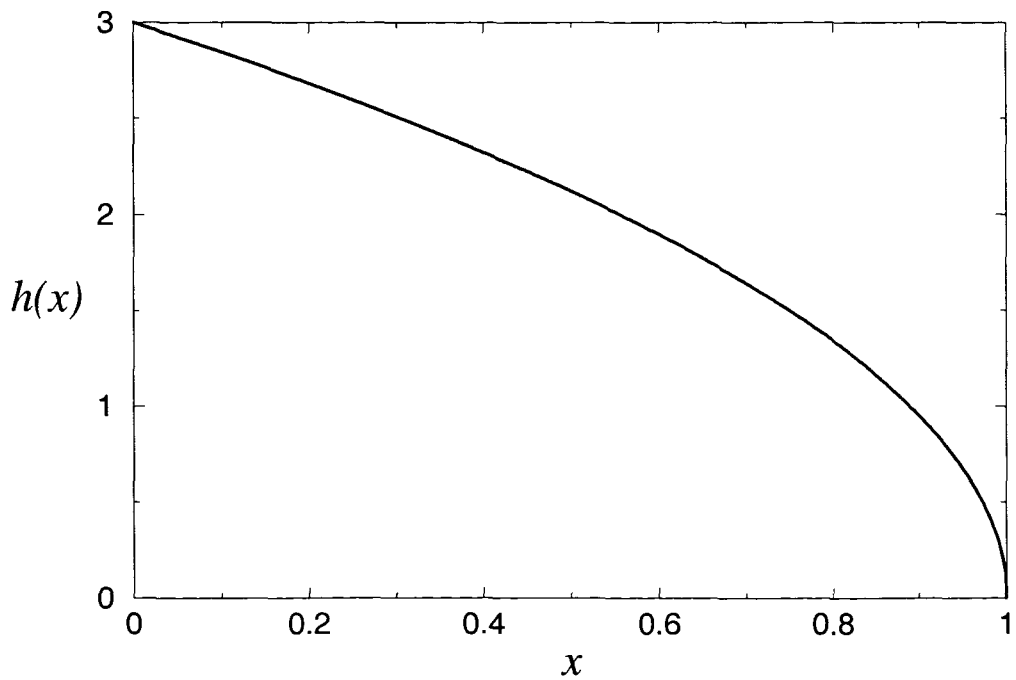

Figure 4.20: Plot of the liquid film free surface $h(x)$; η, τ and P fixed at $\eta = 1.0$, $\tau = 1.0$, $P = 1.076683$ ($n = 100$).

that $h \sim 1-x$ near $x=1$, see for example figure (4.18) where the number of mesh points is still small. However, the answer to the question of whether the results are accurate, and valid beyond any doubt, at this stage remains open (as discussed later in this section, for example) because we have not yet provided a simple but related check problem.

It is undoubtedly difficult to solve this problem and, as a result, it is very difficult and tedious to attempt to investigate the effects of changes in the values of τ and η in this problem. In particular, it should be noted that equation (4.15) is

$$\begin{aligned}\frac{1}{3}h_0 = \pi\frac{\tau}{4}\int_0^1 \frac{d\xi}{h(\xi)} - \frac{\tau}{2}\int_0^1 \frac{\sin^{-1}(\sqrt{\xi})}{h(\xi)}d\xi + \frac{\tau}{2}\int_0^1 \frac{\sqrt{\xi(1-\xi)}}{h(\xi)} + \frac{\pi}{2\eta}\int_0^1 \frac{d\xi}{h^3(\xi)} \\ -\frac{1}{\eta}\int_0^1 \frac{\sin^{-1}(\sqrt{\xi})}{h^3(\xi)}\int_0^\xi h(\lambda)d(\lambda)d\xi + \frac{1}{\eta}\int_0^1 \frac{\sqrt{\xi(1-\xi)}}{h^3(\xi)}\int_0^\xi h(\lambda)d\lambda d\xi \\ -C_3\pi + \frac{P}{6} + C_1\left[\frac{\pi}{2}\int_0^1 \frac{d\xi}{h^3(\xi)} - \int_0^1 \frac{\sin^{-1}(\sqrt{\xi})}{h^3(\xi)} + \int_0^1 \frac{\sqrt{\xi(1-\xi)}}{h^3(\xi)}\right]. \qquad (4.30)\end{aligned}$$

Thus, from equations (4.30), (4.16) and (4.17) we get

$$\begin{aligned}\frac{P}{6}\{-\pi A + D\} = \frac{1}{3}h_0 - \pi\frac{\tau}{4}\int_0^1 \frac{d\xi}{h(\xi)} + \frac{\tau}{2}\int_0^1 \frac{\sin^{-1}(\sqrt{\xi})}{h(\xi)}d\xi - \frac{\tau}{2}\int_0^1 \frac{\sqrt{\xi(1-\xi)}}{h(\xi)}d\xi \\ -\frac{\pi}{2\eta}\int_0^1 \frac{d\xi}{h^3(\xi)} + \frac{1}{\eta}\int_0^1 \frac{\sin^{-1}(\sqrt{\xi})}{h^3(\xi)}\int_0^\xi h(\lambda)d\lambda d\xi - \frac{1}{\eta}\int_0^1 \frac{\sqrt{\xi(1-\xi)}}{h^3(\xi)}\int_0^\xi h(\lambda)d\lambda d\xi \\ -A\left[-\frac{h_0}{3} - \pi\frac{\tau}{4}\int_0^1 \frac{d\xi}{h(\xi)} + \right. \\ \frac{\tau}{2}\int_0^1 \frac{\sqrt{\xi(1-\xi)}}{h(\xi)}d\xi - \frac{\pi}{2\eta}\int_0^1 \frac{1}{h^3(\xi)}\int_0^\xi h(\lambda)d\lambda d\xi + \frac{1}{\eta}\int_0^1 \frac{\sin^{-1}(\sqrt{\xi})}{h^3(\xi)}\int_0^\xi h(\lambda)d\lambda d\xi \\ \left. + \frac{1}{\eta}\int_0^1 \frac{\sqrt{\xi(1-\xi)}}{h^3(\xi)}\int_0^\xi h(\lambda)d\lambda d\xi\right] + \\ \pi\left\{\int_0^1 \frac{d\xi}{h^3(\xi)} - \frac{2}{\pi}\int_0^1 \frac{\sin^{-1}(\sqrt{\xi})}{h^3(\xi)}d\xi \times \right. \\ \left\{\frac{1}{\frac{\pi}{2}\int_0^1 \frac{d\xi}{h^3(\xi)} - \int_0^1 \frac{\sin^{-1}(\sqrt{\xi})}{h^3(\xi)}d\xi - \int_0^1 \frac{\sqrt{\xi(1-\xi)}}{h^3(\xi)}d\xi}\left[-\frac{h_0}{3} - \pi\frac{\tau}{4}\int_0^1 \frac{d\xi}{h(\xi)} + \right.\right. \\ \frac{\tau}{2}\int_0^1 \frac{\sqrt{\xi(1-\xi)}}{h(\xi)}d\xi - \frac{\pi}{2\eta}\int_0^1 \frac{1}{h^3(\xi)}\int_0^\xi h(\lambda)d\lambda d\xi + \frac{1}{\eta}\int_0^1 \frac{\sin^{-1}(\sqrt{\xi})}{h^3(\xi)}\int_0^\xi h(\lambda)d\lambda d\xi \\ \left.\left. + \frac{1}{\eta}\int_0^1 \frac{\sqrt{\xi(1-\xi)}}{h^3(\xi)}\int_0^\xi h(\lambda)d\lambda d\xi\right]\right\} \\ + \frac{\tau}{2}\int_0^1 \frac{d\xi}{h(\xi)} - \frac{\tau}{\pi}\int_0^1 \frac{\sin^{-1}(\sqrt{\xi})}{h(\xi)} + \frac{1}{\eta}\int_0^1 \frac{1}{h^3(\xi)}\int_0^\xi h(\lambda)d\lambda d\xi \\ \left. - \frac{2}{\pi\eta}\int_0^1 \frac{\sin^{-1}(\sqrt{\xi})}{h^3(\xi)}\int_0^\xi h(\lambda)d\lambda d\xi\right\}, \qquad (4.31)\end{aligned}$$

where A and D are given by

$$A = \frac{\left[\frac{\pi}{2}\int_0^1 \frac{d\xi}{h^3(\xi)} - \int_0^1 \frac{\sin^{-1}(\sqrt{\xi})}{h^3(\xi)}d\xi + \int_0^1 \frac{\sqrt{\xi(1-\xi)}}{h^3(\xi)}d\xi\right]}{\frac{\pi}{2}\int_0^1 \frac{d\xi}{h^3(\xi)} - \int_0^1 \frac{\sin^{-1}(\sqrt{\xi})}{h^3(\xi)}d\xi - \int_0^1 \frac{\sqrt{\xi(1-\xi)}}{h^3(\xi)}d\xi},$$

$$D = \frac{\pi\int_0^1 \frac{d\xi}{h^3(\xi)} - 2\int_0^1 \frac{\sin^{-1}(\sqrt{\xi})}{h^3(\xi)}d\xi}{\frac{\pi}{2}\int_0^1 \frac{d\xi}{h^3(\xi)} - \int_0^1 \frac{\sin^{-1}(\sqrt{\xi})}{h^3(\xi)}d\xi - \int_0^1 \frac{\sqrt{\xi(1-\xi)}}{h^3(\xi)}d\xi} + 1.$$

Hence the discretised equation which is used to iteratively obtain the value of P is accordingly

$$\begin{aligned}
P = \frac{6}{-\pi A + D} \times \\
\Bigg\{ \frac{h_0}{3} - \frac{\pi\tau}{2n}\sum_{j=0}^{n-1}\frac{1}{h_{j+1}+h_j} + \tau\sum_{j=0}^{n-1}\frac{I_{4j}}{h_{j+1}+h_j} - \tau\sum_{j=0}^{n-1}\frac{I_{5j}}{h_{j+1}+h_j} - \frac{4\pi}{\eta n}\sum_{j=0}^{n-1}\frac{1}{(h_{j+1}+h_j)^3} + \\
\frac{8}{\eta}\sum_{j=0}^{n-1}\frac{I_{2j}}{(h_{j+1}+h_j)^3} - \frac{8}{\eta}\sum_{j=0}^{n-1}\frac{I_{3j}}{(h_{j+1}+h_j)^3} - A\Bigg[-\frac{h_0}{3} - \frac{\pi\tau}{2n}\sum_{j=0}^{n-1}\frac{1}{h_{j+1}+h_j} \\
+ \tau\sum_{j=0}^{n-1}\frac{I_{5j}}{h_{j+1}+h_j} - \frac{4\pi}{\eta}\sum_{j=0}^{n-1}\frac{I_{1j}}{(h_{j+1}+h_j)^3} + \frac{8}{\eta}\sum_{j=0}^{n-1}\frac{I_{2j}}{(h_{j+1}+h_j)^3} + \frac{8}{\eta}\sum_{j=0}^{n-1}\frac{I_{3j}}{(h_{j+1}+h_j)^3}\Bigg] \\
+\pi\Bigg\{\frac{8}{n}\sum_{j=0}^{n-1}\frac{1}{(h_{j+1}+h_j)^3} - \frac{16}{\pi}\sum_{j=0}^{n-1}\frac{I_{2j}}{(h_{j+1}+h_j)^3}\times \\
\Bigg\{\frac{1}{E}\Bigg[-\frac{h_0}{3} - \frac{\pi\tau}{2n}\sum_{j=0}^{n-1}\frac{1}{h_{j+1}+h_j} + \tau\sum_{j=0}^{n-1}\frac{I_{5j}}{h_{j+1}+h_j} - \frac{4\pi}{\eta}\sum_{j=0}^{n-1}\frac{I_{1j}}{(h_{j+1}+h_j)^3} + \\
\frac{8}{\eta}\sum_{j=0}^{n-1}\frac{I_{2j}}{(h_{j+1}+h_j)^3} + \frac{8}{\eta}\sum_{j=0}^{n-1}\frac{I_{3j}}{(h_{j+1}+h_j)^3}\Bigg]\Bigg\} + \frac{\tau}{n}\sum_{j=0}^{n-1}\frac{1}{h_{j+1}+h_j} - \\
\frac{2\tau}{\pi}\sum_{j=0}^{n-1}\frac{I_{4j}}{h_{j+1}+h_j} + \frac{8}{\eta}\sum_{j=0}^{n-1}\frac{I_{1j}}{(h_{j+1}+h_j)^3} - \frac{16}{\pi\eta}\sum_{j=0}^{n-1}\frac{I_{2j}}{(h_{j+1}+h_j)^3}\Bigg\}\Bigg\}, \qquad (4.32)
\end{aligned}$$

where A and D are approximated by

$$A \approx \frac{\frac{4\pi}{n}\sum_{j=0}^{n-1}\frac{1}{(h_{j+1}+h_j)^3} - 8\sum_{j=0}^{n-1}\frac{I_{4j}}{(h_{j+1}+h_j)^3} + 16\sum_{j=0}^{n-1}\frac{I_{5j}}{(h_{j+1}+h_j)^3}}{E},$$

$$D \approx \frac{\frac{\pi}{n}\sum_{j=0}^{n-1}\frac{1}{(h_{j+1}+h_j)^3} - 16\sum_{j=0}^{n-1}\frac{I_{4j}}{(h_{j+1}+h_j)^3}}{E},$$

and E is given by

$$E = \frac{4\pi}{n}\sum_{j=0}^{n-1}\frac{1}{(h_{j+1}+h_j)^3} + 8\sum_{j=0}^{n-1}\frac{I_{4j}}{(h_{j+1}+h_j)^3}.$$

We should recall that the main reason why we have attempted the problem in this section was to investigate the possibility of solving the original problem by directly specifying the pressure (as opposed to the pressure gradient) at the onset of the annular flow regime. This

approach is certainly very difficult and the algebra involved is very cumbersome. However, the problem has been tackled to a level where the only remaining thing is to provide a simple but related paradigm problem (which may be solved preferably in closed-form) so that our numerical scheme can be tested. A suitable such problem has not been found yet. As a result, the numerical results typified by the plots in figures (4.18), (4.19) and (4.20) are described as preliminary.

One of the simplest paradigm problems related to the current problem here may be obtained by assuming that $\eta = 1/\epsilon$ and $\tau = \epsilon$, for $\epsilon \to 0$, in equation (4.1), so that to leading order we get

$$\frac{1}{\pi}\left(\int_0^1 \frac{h_\xi(\xi)}{\xi - x}d\xi\right)_x = \frac{B}{h^3}, \tag{4.33}$$

for some constant B (which depends on the global behaviour of h in $[0,1]$). The corresponding boundary conditions are $h(x) = 0$ at $x = 1$, $h_x(x) = 0$ at $x = 0$ and $h(0) = h_0$. We further know that

$$\frac{1}{\pi}\int_0^1 \frac{h_\xi(\xi)}{\xi}d\xi = P.$$

It is however, nowhere near trivial to solve (4.33) numerically (as we illustrate below without actually indulging in the computation for h in this problem).

On following the approach proposed in section (4.4.1), it may readily be shown (after much algebra) that $h(x)$ is given by

$$\begin{aligned} h(x) = \left(\pi - 2\sin^{-1}(\sqrt{\xi})\right)\left\{\frac{P}{\pi} - C + B\int_0^1 \frac{d\xi}{h^3(\xi)} - \frac{2B}{\pi}\int_0^1 \frac{\sin^{-1}(\sqrt{\xi})}{h^3(\xi)}d\xi + \right. \\ \left. \frac{2B}{\pi}\int_0^1 \frac{\sqrt{\xi(1-\xi)}}{h^3(\xi)}d\xi\right\} - \frac{2P}{\pi^2}F_1(x) - \frac{2B}{\pi}\left(F_1(x) - F_2(x)\right)\int_0^1 \frac{d\xi}{h^3(\xi)} \\ + \frac{2B}{\pi}\int_0^1 \frac{F_3(x,\xi) + F_4(x,\xi)}{h^3(\xi)}d\xi, \end{aligned} \tag{4.34}$$

where B, C, $F_1(x)$, $F_2(x)$, $F_3(x,\xi)$ and $F_4(x,\xi)$ are respectively given by

$$B = \frac{\frac{h_0}{\pi} + \frac{P}{\pi}\left(\frac{1}{\pi} - 1\right)}{\frac{2}{\pi}\int_0^1 \frac{\sqrt{\xi(1-\xi)}}{h^3(\xi)}d\xi}, \tag{4.35}$$

$$C = \frac{P}{\pi^2} + B\left\{\int_0^1 \frac{d\xi}{h^3(\xi)} - \frac{2}{\pi}\int_0^1 \frac{\sin^{-1}(\sqrt{\xi})}{h^3(\xi)}d\xi\right\}, \tag{4.36}$$

$$F_1(x) = \frac{1}{8}\frac{x\sqrt{1-x}(1-\sqrt{x})}{2x(1-x)+x^2+(1-x)^2}\ln|1-x| + \frac{\pi}{8}\sqrt{x}(1-\sqrt{x})\times$$
$$\left(\frac{2x}{2x(1-x)+x^2+(1-x)^2}-1\right) + \frac{x\sqrt{1-x}(1-\sqrt{x})}{2x(1-x)+x^2+(1-x)^2}\times$$
$$\left\{\frac{1}{2}\left(2-\frac{x\sqrt{1-x}(1-\sqrt{x})}{2x(1-x)+x^2+(1-x)^2}\right)\ln|1-x| - \frac{\pi}{4}\sqrt{x}(1-\sqrt{x})\times\right.$$
$$\left.\left(\frac{2x}{2x(1-x)+x^2+(1-x)^2}-1\right)\right\} + \frac{\pi}{34}\sqrt{x}(1-\sqrt{x})$$
$$-\left[\frac{(1-x)^2}{4}-\frac{x(1-x)}{2}\right]\ln|1-x| - \frac{3}{8}x^2+\frac{x}{4}+\frac{1}{8},$$

$$F_2(x) = -\frac{1}{4}\left(\frac{x\sqrt{1-x}(1-\sqrt{x})}{2x(1-x)+x^2+(1-x)^2}\right)^2\ln|x| - \frac{\pi}{32}\sqrt{x}(1-\sqrt{x}) +$$
$$\frac{1}{4}\sqrt{1-x}(1-\sqrt{x}) + \frac{1}{4}x^2\ln|x| - \frac{3}{8}x^2$$
$$-\frac{1}{2}\frac{x(1-x)(1-\sqrt{x})^2}{2x(1-x)+x^2+(1-x)^2},$$

$$F_3(x,\xi) = \frac{1}{4}\frac{x\sqrt{1-x}(1-\sqrt{x})}{2x(1-x)+x^2+(1-x)^2}\xi\ln\left|\sqrt{\xi(1-x)}+\sqrt{x(1-\xi)}\right| +$$
$$\frac{1}{4}\sqrt{x}(1-\sqrt{x})\left(\frac{2x}{2x(1-x)+x^2+(1-x)^2}-1\right)\xi\sin^{-1}(\sqrt{\xi}) + \frac{1}{4}\sqrt{1-x}(1-\sqrt{x})\times$$
$$\xi(1-\xi) + \frac{1}{4}(1-\sqrt{x})\sqrt{x}\xi\sqrt{\xi(1-\xi)} + \frac{1}{4}\sqrt{1-x}(1-\sqrt{x})(1-\xi)^2 +$$
$$\frac{1}{4}\sqrt{x}(1-\sqrt{x})\left(\frac{2x}{2x(1-x)+x^2+(1-x)^2}-1\right)\left(\sqrt{\xi(1-\xi)}-(1-2\xi)\times\right.$$
$$\left.\sin^{-1}(\sqrt{\xi})\right) - \frac{1}{16}\sqrt{x}(1-\sqrt{x})\left(\sin^{-1}(1-2\xi)-2(1-2\xi)\times\right.$$
$$\left.\sqrt{\xi(1-\xi)}\right) +$$
$$\frac{x\sqrt{1-x}(1-\sqrt{x})}{2x(1-x)+x^2+(1-x)^2}\left\{\frac{1}{2}\left(2\xi-\frac{x\sqrt{1-x}(1-\sqrt{x})}{2x(1-x)+x^2+(1-x)^2}\right)\times\right.$$
$$\ln\left|\sqrt{\xi(1-x)}+\sqrt{x(1-\xi)}\right| - \frac{1}{2}\sqrt{x}(1-\sqrt{x})\left(\frac{2x}{2x(1-x)+x^2+(1-x)^2}-1\right)\times$$
$$\left.\sin^{-1}(\sqrt{\xi}) - \frac{1}{2}(1-\sqrt{x})\left(\sqrt{1-x}(1-\xi)-\sqrt{x}\sqrt{\xi(1-\xi)}\right)\right\},$$

and

$$F_4(x,\xi) = -(\xi-x)\left\{\frac{1}{4}(\xi-x)-\frac{x}{2}\right\}\ln|\xi-x| + \frac{x\xi}{4}+\frac{\xi^2}{8}-\frac{3}{8}x^2.$$

If numerical computations for h are to be carried out for this paradigm problem, it will have to be recognised from equation (4.33) that $h \sim (1-x)^{1/2}$ near $x = 1$. Therefore, extra care should be taken as some terms in equation (4.34) will have to be calculated analytically

near $x = 1$, otherwise they will diverge in the numerical scheme. For example, near $x = 1$

$$\begin{aligned}
\int_0^1 \frac{d\xi}{h^3(\xi)} &\sim \int_0^1 \frac{d\xi}{(1-\xi)^{\frac{3}{2}}} = 2 \lim_{\xi \to 1} \frac{1}{\sqrt{1-\xi}} - 2, \\
\int_0^1 \frac{\sqrt{\xi(1-\xi)}}{h^3(\xi)} d\xi &\sim -2 + 2 \tanh^{-1}(\sqrt{\xi})\Big|_{\xi=0}^1, \\
\frac{2}{\pi} \int_0^1 \frac{\sin^{-1}(\sqrt{\xi})}{h^3(\xi)} d\xi &\sim \frac{4}{\pi} \frac{\sin^{-1}(\sqrt{\xi})}{\sqrt{1-\xi}}\Big|_{\xi=0}^1 - \frac{2}{\pi} \int_0^1 \frac{d\xi}{\sqrt{\xi(1-\xi)}} \\
&= 2 \lim_{\xi \to 1} \frac{1}{\sqrt{1-\xi}} - \frac{2}{\pi} \tanh^{-1}(\sqrt{\xi})\Big|_{\xi=0}^1.
\end{aligned}$$

Thus, from equations (4.35) and (4.36), we obtain that

$$\int_0^1 \frac{d\xi}{h^3(\xi)} - \frac{2}{\pi} \int_0^1 \frac{\sin^{-1}(\sqrt{\xi})}{h^3(\xi)} d\xi \sim \frac{2}{\pi} \tanh^{-1}(\sqrt{\xi})\Big|_{\xi=0}^1. \tag{4.37}$$

It should be noted that the last integral in equation (4.34) produces many more terms which should also be taken care of outside the numerical scheme near $x = 1$.

In conclusion, in this section we have solved equation (4.1) numerically for the special case where h_0, along with the parameter values η and τ, are fixed and the pressure P at $\bar{x} = 0$ is varied until a converged numerical solution for h satisfies all of the boundary conditions. In reality, the parameter h_0, instead of P, should be the one which is altered until all of the boundary conditions are satisfied. However, as explained earlier, this would lead to an even more difficult and cumbersome problem to tackle numerically. The main aim in this section was to explore the possibility of solving (4.1) [and hence possibly the previous problem, equation (3.35)] by directly specifying the pressure at the onset of the annular flow region instead of the pressure gradient there. The results of this section suggest that such a possibility may exist. However, there is still some way to go since a suitable paradigm problem has yet to be provided so that the accuracy and hence the validity of the numerical method proposed here can be tested. As a result, the results of this method have not been used to make any predictions on the dryout point.

Chapter 5

Unsteady Flows

In chapter 2, we have proposed a fully unsteady model for the problem and in chapters 3 and 4, the model has been solved numerically for specific cases in the steady state. Now, the ultimate aim will be to solve the whole problem numerically for the unsteady cases. It is almost customary and usually simple in the unsteady problems to seek similarity and/or travelling wave solutions. However, a brief analysis of some simple cases of the problem in section (5.2) shows that these solutions are physically unrealistic and therefore are not of immediate interest here. Thus, in order that any predictions could be made for the dryout, it is then inevitable that the whole unsteady problem must be solved numerically. It will be, however, unthoughtful to embark on the task of solving the whole problem numerically without investigating whether in reality its solutions exist or not. Hence in this chapter we mainly address the question of linear stability for this problem. As a result, the literature review in section (5.1) is concerned with the linear stability analysis of some related problems. It should be mentioned nonetheless, that none of these models in the literature include the gas core (such literature, to the best of our knowledge at the time of writing, is not available). Nevertheless, we hope that some of their results will provide indications as to what we may expect from the linear stability results of this problem, e.g. whether the mass transfer parameter η is a stabilising factor or not. We will focus here on the linear stability of the constant wall temperature problem though the other case can also be done.

5.1 Literature Review

The stability of thin liquid films adhering to heated walls is of practical importance in several applications including the analysis of liquid metal cooled fast breeder reactors (Bankoff, 1971) [8]. Therefore, this phenomenon has been of particular interest to a number of investigators. Essentially, investigators analyse the order of magnitude of the dimensionless terms in their

respective models for the disturbance waves at the interface in order to isolate the influence of various terms on the stability criteria of the thin liquid films. Such terms include phase change terms, vapour terms, thermocapillary terms, gravitational terms and physical variation terms, to mention but a few.

Bankoff (1971) [8] investigates the linear stability of a Newtonian liquid layer, with zero surface shear stress, draining down an inclined heated plane. On assuming that the liquid film is extremely thin, Bankoff (1971) [8] employs long-wave theory (where it is assumed that the disturbance waves have wavelengths much larger than the mean thickness of the liquid layer or, equally, the waves have a small wavenumber) to obtain a critical Reynolds number, above which the film flow is unstable, in terms of a heat flux parameter. It is then concluded that evaporation at the free surface is always a destabilising factor while condensation has a stabilising effect. This result, for example, suggests that an increase in the mass transfer parameter η might be a stabilising factor in our problem since such an increase will, intuitively, result in less amount of evaporation in this problem. In Bankoff's analysis the temperature of the free surface is taken to be a constant. This study was extended to allow temporal temperature variations at the free surface and to include surface tension by Lin (1975) [51]. The results obtained by Lin confirm those of Bankoff and further suggest that variation of surface tension with temperature is a destabilising factor in heated films but has an opposite impact in cooled films.

The formulation of Bankoff's (1971) [8] model is however, criticised in detail by Spindler *et al* (1978) [82] for its discrepancies in the jump conditions at the free boundary. Spindler (1982) [81] studies the linear stability of a liquid film flowing down an inclined plane with a constant wall heat flux and interfacial phase change. It is assumed that there is no vapour flow except very close to the vapour-liquid interface where it is assumed that the vapour motion is induced by the film flow. Spindler's model takes into account the variations of the physical properties of the Newtonian fluid due to temperature changes, and a theoretical dryout length is estimated even though the author points out that the model is not valid near the dryout point. It is concluded that evaporation, in agreement with the other previous studies, has a destabilising effect while condensation has a stabilising one.

Linear stability of the surface of a superheated liquid undergoing steady evaporation was investigated, in a planar configuration, by Prosperetti & Plesset (1984) [67]. In the analysis, both the vapour and the liquid are treated as incompressible and inviscid. The growth rate of the perturbations is obtained as a function of the wavenumber and the destabilising effects of the disturbances of the gas pressure and evaporative mass flux are discussed for a number of basic temperature distributions in the liquid. It is also concluded that the interfacial temperature changes do not play a significant role in the instabilities of the free surface. A similar study is carried out by Higuera (1987) [39] in a three-dimensional configuration, to

include effects of the fluid viscosities. The results of Prosperetti & Plesset (1984) [67] are recovered and it is further found, as one would expect, that both gravity and surface tension have stabilising effects on the free surface.

There has also been an interest in the nonlinear stability analysis of static evaporating and condensing thin liquid films (see for example Burelbach *et al*, 1988) [14] to investigate rupture in thin thermal liquid films, which is probably the limiting case for linear stability analysis.

It should be mentioned that in all the above studies, the underlying models are nonlinear partial differential equations. In our case (as a result of accounting for the dynamics of the gas core pressure from the thin aerofoil theory perspective) we have to deal with nonlinear singular integro-differential equations. We should mention, on the other hand, that there has been a numerical investigation of linear stability of a two-dimensional unsteady sail (which is a linear singular integro-differential equation of a semi-infinite range type) by Haselgrove & Tuck (1976) [38]. Apart from the nonlinearity, the base state equations we tackle here differ from those considered by Haselgrove & Tuck (1976) [38] in that, besides being of finite range type, they also possess a singularity in one of the end boundary conditions. Thus, numerical computations involved in obtaining solutions are formidable. Moreover, our model is a moving boundary type problem, whose linear stability analysis (to the best of our knowledge) has not been tackled before.

5.2 Similarity Solutions

We seek similarity solutions for simplified cases of equation (2.62) and analyse them with respect to the physical situations. It will be seen that for practical purposes, these solutions are not interesting. We recall that equation (2.62) is

$$\frac{1}{\eta h} = \left\{ \frac{h^3}{3\pi} \left(\int_0^{1+l(t)} \frac{h_\xi(\xi,t)}{\xi - x} d\xi \right)_x - \frac{h^2}{2}\tau \right\}_x - h_t, \tag{5.1}$$

where for convenience, from now on (unless clearly stated) the unbarred variables should be understood to be nondimensional. Assuming that $h \sim O(\epsilon^2)$, $t \sim O(\epsilon)$, $\eta \sim O(\epsilon^3)$ and $\tau \sim O(1/\epsilon^3)$, for some small positive parameter $\epsilon \to 0$, in equation (5.1) we obtain

$$\left(\frac{\tau}{2}h^2\right)_x + h_t + \frac{1}{\eta h} = 0, \tag{5.2}$$

to leading order. (It should be mentioned however, that these asymptotics may not be valid near the dryout point, where it may be anticipated that nonuniformities will manifest themselves.) For similarity solutions, we follow standard techniques, see for example Ames (1965) [2]. We employ a transformation $h = \lambda^n H$, $x = \lambda X$ and $t = \lambda^m T$, for some parameter

λ and real numbers n and m, in equation (5.2) to get

$$\left(\frac{\lambda^{2n}}{2}\tau H\right)_X + \lambda^{n-m+1}H_T + \frac{\lambda^{1-n}}{\eta H} = 0. \tag{5.3}$$

From (5.3) we obtain that $n = 1/3$ and $m = 2/3$ for equation (5.2) to be invariant under the above transformation. Thus, we have a similarity solution

$$h = \lambda^{\frac{1}{3}} H\left(\frac{x}{\lambda}, \frac{t}{\lambda^{\frac{2}{3}}}\right). \tag{5.4}$$

Upon choosing $x = \lambda$, without loss of generality, equation (5.4) gives

$$h = x^{\frac{1}{3}} H\left(tx^{-\frac{2}{3}}\right). \tag{5.5}$$

Since $h(x,t)$ vanishes at the dryout point $x = 1 + l(t) = G(t)$, then equation (5.5) implies that

$$G(t) = A_1 t^{\frac{3}{2}}, \tag{5.6}$$

for some constant A_1. Thus we have a boundary condition $H(A_1) = 0$. Since A_1 is not a known parameter, we are allowed to prescribe one more boundary condition at the entry to the annular flow regime, $x = 0$.

We proceed first by deriving an equation for H from equation (5.2). We define a variable

$$\xi = tx^{-\frac{2}{3}},$$

so that h is given by

$$h = \left(\frac{t}{\xi}\right)^{\frac{1}{2}} H(\xi). \tag{5.7}$$

Therefore, substitution for x and h in equation (5.2) leads to an ordinary differential equation for H

$$\frac{1}{3}\left(3\xi - 2\tau\xi^2 H\right) H_\xi + \frac{\tau}{3}\xi H^2 - \frac{1}{2}H + \frac{\xi}{\eta H} = 0. \tag{5.8}$$

Equation (5.8) may be solved numerically for H by standard methods if A_1 is known or one more appropriate boundary condition is prescribed. For the purposes of checking whether the similarity solution (5.5) makes sense physically, it is sensible to consider simpler cases of (5.8) where closed-form solutions can be obtained. We therefore consider the case when $\tau = 0$. In this case, a closed-form solution from (5.8) is given by

$$H(\xi) = \frac{1}{\eta}\sqrt{\eta\xi(-2\ln|\xi| + K)}, \tag{5.9}$$

for some constant of integration K. The constant K may be obtained by applying the boundary condition at the dryout point $H(A_1) = 0$, i.e. $K = 2\ln|A_1|$. Since A_1 is not a known parameter, we will prescribe an extra condition at the entry of the annular flow

region, $x = 0$. Now, from equation (5.7) we observe that near $\xi = 0$, $H \sim \xi^{1/2}$. Thus, from equation (5.5), it follows that $h(0) = 0$ for all finite $t > 0$. However, this condition is absurd and unrealistic physically. Moreover, from equation (5.6), we observe that the dryout point is always increasing (or decreasing) for any positive A_1 (or negative A_1). Thus, we expect $h(0)$ to be greater than zero and increasing (or decreasing) accordingly at all times t in order to sustain the increase (or decrease) in the dryout point. Therefore, though this similarity solution is mathematically fascinating, it is not physically sensible for this particular problem.

A similar analysis to the above one can be performed on equation (5.1) when $\tau = 0$. In this case a similarity solution is given by

$$h = x^{\frac{3}{5}} H(tx^{-\frac{6}{5}}).$$

The function $G(t)$ at the dryout point is given

$$G(t) = A_2 t^{\frac{5}{6}}, \tag{5.10}$$

for some constant A_2. We may, as before, then make a change of variables $s = tx^{-\frac{6}{5}}$ and $h = (t/s)^{1/2} H(s)$ in (5.1) to obtain a nonlinear ordinary integro-differential equation for H

$$\frac{12}{25\pi}\left\{ s^{\frac{1}{3}} H^3 \left(\int_0^{A_2} \frac{(s\psi)^{\frac{5}{6}} \left(\psi^{-1} H(\psi)\right)_\psi}{s^{\frac{5}{6}} - \psi^{\frac{5}{6}}} d\psi \right)_s \right\}_s s^{\frac{11}{6}} - s\left(s^{-\frac{1}{2}}\right)_s = \frac{s^{\frac{1}{2}}}{\eta H}, \tag{5.11}$$

where $\tau = 0$. Upon prescribing appropriate boundary and initial conditions, equation (5.11) may be solved numerically for H by standard methods. However, as in the previous case we observe from (5.10) that either the dryout point is either always increasing or decreasing depending on whether A_2 is positive or negative, respectively. This result is restrictive since it does not provide any opportunity for the dryout point to fluctuate back and forth (a frequently observed phenomenon in reality). Therefore, we will not restrict our attention to single transformations (be similarity and/or travelling waves solutions) to study this problem since they are practically not interesting in this case. Rather, much focus should be directed towards solving the whole problem numerically for the unsteady cases. However, as mentioned earlier, it is important to check the linear stability of the problem first. After all, it is not sensible go on to obtain solutions which may not be observable in reality.

5.3 Linear Stability Analysis

In this section, we will examine the linear stability of solutions obtained for our steady state two-parameter model governed by equation (3.35),

$$\frac{1}{\eta h} = \left\{ \frac{h^3}{3\pi} \left(\int_0^1 \frac{h_\xi(\xi, t)}{\xi - x} d\xi \right)_x - \frac{h^2}{2}\tau \right\}_x, \tag{5.12}$$

to check whether these basic solutions might be physically observable or not. In other words, we wish to test the ability or inability of these solutions to sustain themselves against small perturbations to which any physical system is subject. A more detailed general concept of hydrodynamic stability may be obtained from now standard text books, for example, see Drazin & Reid (1985) [26] and Chandrasekhar (1981) [17]. Here, we will proceed by first assuming that the unsteadiness in equation (5.1) manifests itself as a small perturbation about a basic steady solution $h_s(x)$ of (5.12).

Before we continue with the linear stability analysis of the full problem (5.1), it is however sensible to first analyse the linear stability of some simplified cases of (5.1). The full nonlinear problem (5.1) is very complex due to the presence of the Hilbert transforms and it is very difficult to deal with. Therefore, we need to create some paradigm problems against which we may test our linear stability results for the full problem. It must be emphasised though that these problems are only idealisations and, as a result, falsifications. Nevertheless, we hope that some of the features retained for discussion are of greatest importance in the linear stability.

5.3.1 A Constant Pressure Gradient Problem

If we assume that pressure is linear in x (instead of being given by the Hilbert transform of $h_x(x)$) in equation (5.1) then we have a simplified problem

$$\left\{\frac{h^3}{3\pi}P_x - \frac{\tau}{2}h^2\right\}_x - h_t = \frac{1}{\eta h}, \tag{5.13}$$

where P_x is the pressure gradient. In general P_x may be written conveniently in the form

$$P_x = -\alpha_0\alpha(t), \tag{5.14}$$

for some positive constant α_0 and a non-negative function $\alpha(t)$. (In the subsequent linear stability analysis of this problem we will however, consider a simple case when $\alpha(t)$ is a constant.) We take P_x to be negative in order to allow h to vanish at some positive length from the point $x = 0$. This choice of P_x is of course physically natural in order to allow the flow in the gas core to be in the desired direction, i.e. towards the turbines far downstream of the dryout point.

Equation (5.13) is a first order partial differential equation and we are allowed to prescribe one boundary condition and an appropriate initial condition. It is convenient to impose a condition that $h(0,t) = h_0$, for some positive constant h_0. It should be mentioned however, that $h(0,t)$ can be allowed to be a function of t but for simplicity and consistency with the assumption to be applied to the full problem (5.1), it is sensible to proceed with the current choice.

5.3.1.1 A Non-Zero Pressure Gradient Problem

On assuming that $h_x(0,t)$ exists then, without loss of generality for real $h(x,t)$, we specify

$$\alpha_0 = \frac{4\pi}{\eta h_0^4}. \tag{5.15}$$

Therefore equation (5.13) leads to

$$h^2 \{k_1 h\alpha(t) + k_2\} h_x + \eta h h_t + 1 = 0, \tag{5.16}$$

where $k_1 = 4/h_0^4$ and $k_2 = \eta\tau$.

As mentioned earlier, we assume for simplicity that $\alpha(t)$ is just a constant, in particular $\alpha(t) = 1$ for convenience. Under these circumstances the steady case of equation (5.16) yields

$$h_x = -\frac{B}{h^2(h+C)}, \tag{5.17}$$

where $B = h_0^4/4$ and $C = \eta h_0^4 \tau/4$. Equation (5.17) can easily be solved in closed form to give

$$\frac{1}{4}h^4(x) + \frac{C}{3}h^3(x) + Bx = D, \tag{5.18}$$

where D is a constant of integration which may be obtained by applying the boundary condition at $x = 0$ to get

$$D = h_0^3\left(\frac{h_0}{4} + \frac{C}{3}\right).$$

The zeros of (5.18) can be found analytically. However, the roots are in such a general form that they are unhelpful in the subsequent linear stability analysis. We observe, on the other hand, that in the special case $\tau = 0$, (5.18) gives a simple solution

$$h(x) = h_0(1-x)^{\frac{1}{4}}. \tag{5.19}$$

It is particularly interesting to notice that (5.19) automatically mimics the dryout point only at $x = 1$, i.e. $h(1) = 0$ for any prescribed h_0. This result is a direct consequence of the scaling in equation (5.15) and it is highly convenient in the subsequent linear stability analysis for this special case.

In order to proceed with the linear stability analysis, we first employ the method of characteristics to solve (5.16) analytically when α is a constant (and without loss of generality we take $\alpha = 1$), i.e. we solve

$$h^2 \{k_1 h + k_2\} h_x + \eta h h_t + 1 = 0. \tag{5.20}$$

We parameterise in q

$$\begin{aligned} x_q &= k_1 h^2 + k_2 h, \\ t_q &= \eta, \\ h_q &= -\frac{1}{h}. \end{aligned} \tag{5.21}$$

Equations (5.21) solve to give

$$\begin{aligned} h &= \{2(A-q)\}^{\frac{1}{2}}, \\ t &= \eta q + B, \\ x &= 2\left\{k_1\left(A-\frac{q}{2}\right)q - \frac{\sqrt{2}}{3}k_2(A-q)^{\frac{3}{2}}\right\} + C, \end{aligned} \tag{5.22}$$

where A, B and C are constants of integration. We prescribe an initial condition that when $t = 0$

$$\begin{aligned} q &= 0, \\ x &= p, \\ h(x,0) &= F(p), \end{aligned}$$

for some arbitrary function $F(p)$, so that (5.22) implies that

$$h(x,t) = \sqrt{2}\left(\frac{1}{2}F^2(p) - \frac{t}{\eta}\right)^{\frac{1}{2}}, \tag{5.23}$$

where p is given by

$$p = x - 2\left\{\frac{k_1}{2}\left(h^2(x,t)+\frac{t}{\eta}\right)\frac{t}{\eta} - \frac{k_2}{6}\left[h^3(x,t)+\left(h^2(x,t)+\frac{2t}{\eta}\right)^{\frac{3}{2}}\right]\right\}. \tag{5.24}$$

Substitution of (5.24) into (5.23) leads to an implicit equation for $h(x,t)$

$$\begin{aligned} h^2(x,t) + \frac{2t}{\eta} = F^2\Bigg(x - 2\Bigg\{&\frac{k_1}{2}\left(h^2(x,t)+\frac{t}{\eta}\right)\frac{t}{\eta} - \\ &\frac{k_2}{6}\left[h^3(x,t)+\left(h^2(x,t)+\frac{2t}{\eta}\right)^{\frac{3}{2}}\right]\Bigg\}\Bigg). \end{aligned} \tag{5.25}$$

In the special case $\tau = 0$ (i.e. only the effects of η on the linear stability of the problem will be investigated under these circumstances), equation (5.25) reduces to

$$h^2(x,t) + \frac{2t}{\eta} = F^2\left(x - k_1\left\{h^2(x,t)+\frac{t}{\eta}\right\}\frac{t}{\eta}\right). \tag{5.26}$$

We then investigate the linear stability of (5.26) by introducing a perturbation to the steady state solution in the form

$$\begin{aligned} F(x) &= h_s(x) + \epsilon\sin(Mx), \\ h(x,t) &= h_s(x) + \epsilon h_p(x,t), \end{aligned} \tag{5.27}$$

for some real constant M, where $h_p(x,t)$ is the perturbation solution and we know the steady state solution $h_s(x)$ from equation (5.19)

$$h_s(x) = h_{s0}(1-x)^{1/4}. \tag{5.28}$$

Substituting the pair of equations (5.27) into (5.26) and employing equation (5.28) yields

$$h_{s0}^2(1-x)^{\frac{1}{2}} + 2\epsilon h_{s0}(1-x)^{\frac{1}{4}}h_p(x,t) + \frac{2t}{\eta} = h_{s0}^2 R^{\frac{1}{2}}(x,t) + \epsilon h_{s0} R^{\frac{1}{4}}(x,t)\sin(M[x - R_1(x,t)]), \tag{5.29}$$

on neglecting terms of $O(\epsilon^2)$. The functions $R(x,t)$, $R_1(x,t)$ and $R_2(x,t)$ are respectively given by

$$\begin{aligned} R(x,t) &= R_1(x,t) + R_2(x,t), \\ R_1(x,t) &= 1 - x + k_1\left[h_{s0}^2(1-x)^{\frac{1}{2}} + \frac{t}{\eta}\right]\frac{t}{\eta}, \\ R_2(x,t) &= 2\epsilon k_1 h_{s0}(1-x)^{\frac{1}{4}}\frac{t}{\eta}h_p(x,t). \end{aligned}$$

We may then expand both $R^{\frac{1}{2}}(x,t)$ and $R^{\frac{1}{4}}(x,t)$ using standard methods to give

$$\begin{aligned} R^{\frac{1}{2}}(x,t) &= R_1^{\frac{1}{2}}(x,t) + \frac{R_2(x,t)}{2R_1^{\frac{1}{2}}(x,t)} + O(\epsilon^2), \\ R^{\frac{1}{4}}(x,t) &= R_1^{\frac{1}{4}}(x,t) + \frac{R_2(x,t)}{2R_1^{\frac{3}{4}}(x,t)} + O(\epsilon^2). \end{aligned}$$

Thus, on comparing coefficients of ϵ in equation (5.29), we obtain (to order ϵ) an equation for the liquid layer thickness perturbation $h_p(x,t)$

$$h_p(x,t) = \frac{\{1 - x + \alpha_1(x,t)\}^{\frac{5}{4}}\sin\left(M\left\{x - \alpha_1(x,t)\right\}\right)}{2(1-x)^{\frac{1}{4}}\left\{[1 - x + \alpha_1]^{\frac{1}{2}} - \frac{2t}{\eta}\right\}}, \tag{5.30}$$

where $\alpha_1(x,t)$ is given by

$$\alpha_1(x,t) = 4\left\{16(1-x)^{\frac{1}{2}} + \frac{t}{\eta}\right\}\frac{t}{\eta}, \tag{5.31}$$

k_1 has been replaced by its value $k_1 = 4/h_{s0}^4$ and, for convenience, $h_{s0} = 1$. We notice that (5.30) is not defined at the point $x = 1$. However, on excluding this point, we can still obtain some important information on the linear stability from equation (5.30). Since $0 \leq x < 1$ we observe from (5.30) that the perturbation $h_p(x,t)$ grows for all values of $\eta > 0$ and $t > 0$. In other words, this results suggests, as one may expect and in agreement with the results in the literature, that the mass transfer parameter $\eta > 0$ is a destabilising factor. For the values of $\eta < 0$, on the other hand, it is clear from (5.30) that for all values of t $(0 < t \ll 1)$, the perturbation $h_p(x,t)$ decays. It is important to recall at this stage that in this study η is inversely proportional to the difference in the pipe wall temperature T_w and the saturation temperature of the superheated liquid film T_s, $\eta \propto 1/(T_w - T_s)$. Therefore, the notion of $\eta < 0$ here does not necessarily refer to condensation in the physical conception of the problem, it should be understood only as a mathematical entity. On the other hand, $\eta > 0$ physically refers to an evaporating superheated liquid film. Literally, higher values of positive

η indicate a less superheated film. It is therefore interesting to observe from equation (5.30), in particular, that for all values of t $(0 < t \ll 1)$ when $\eta \to \infty$ the perturbation

$$h_p(x,t) \sim \frac{1}{2}(1-x)^{\frac{1}{2}} \sin(Mx),$$

which, as one would expect, does neither grow or decay. (This is also the case when $\eta \to -\infty$.) In other words, an increase in $\eta > 0$ is a stabilising factor in this problem (and so is the case for an increase in the magnitude of $\eta < 0$). These results may also be complemented by solving the unsteady problem

$$\frac{k_1}{4}\left(H^2\right)_x + \frac{\eta}{2}H_t = -1,$$

numerically (after rewriting equation (5.20) in terms of H when $\tau = 0$), subject to an initial condition that is a slight perturbation of the steady state solution. The dependent variable H is defined by $H = h^2$. We will adopt this approach in the linear stability analysis of a zero pressure gradient problem in section (5.3.1.2).

5.3.1.2 A Zero Pressure Gradient Problem

When $P_x = 0$ in (5.13), we obtain an equation identical to (5.2)

$$\tau h h_x + h_t + \frac{1}{\eta h} = 0. \tag{5.32}$$

We hope the linear stability results of this problem will give us a benchmark against which we may compare the results of the full problem with regard to the effects of $\tau \neq 0$ and its changes when η is kept constant in the problem. In order to proceed with the linear stability analysis of equation (5.32), we set $h = Hh(0)$, $t = \eta h(0)T$ and $x = \eta h(0)X$, where we have assumed, for simplicity, that at all times $h(0,t) = h(0)$. Under these circumstances equation (5.32) becomes

$$\bar{\tau} H^2 H_X + H H_T + 1 = 0, \tag{5.33}$$

where $\bar{\tau}$ and $H(0,T)$ are respectively given by $\bar{\tau} = \tau/2$ and $H(0,T) = 1$. The steady state solution to equation (5.33) is given by

$$H(X) = \left(1 - \frac{3}{\tau}X\right)^{\frac{1}{3}}, \tag{5.34}$$

where we have dropped the bars for convenience. The steady solution has dryout at the points $X = \tau/3$.

It should be noted at this stage that an identical equation to (5.33) may be obtained from the full nonlinear problem (5.1) by assuming that $h \sim O(1)$, $t \sim O(\epsilon)$, $\eta \sim O(\epsilon)$ and $\tau \sim O(\epsilon^{-1})$ in (5.1), so that to leading order we have the problem

$$\tau h^2 h_x + h h_t + 1 = 0, \tag{5.35}$$

which is (5.32). It should also be pointed out however, that these asymptotics may not be valid near the dryout point where h is also small.

In order to analyse the linear stability of equation (5.33), we solve the unsteady problem

$$\frac{\tau}{3}\left(\mathcal{H}^{\frac{3}{2}}\right)_X + \frac{1}{2}(\mathcal{H})_T = -1, \tag{5.36}$$

numerically using finite differences with a mesh-step of 0.01 and a timestep of 0.00005, where $\mathcal{H} = H^2$. Equation (5.36) is solved, for a wide range of specified τ values, subject to initial conditions which are perturbations of the steady state solution

$$\mathcal{H} = \left(1 - \frac{3}{\tau}X\right)^{\frac{2}{3}}, \tag{5.37}$$

and, for simplicity, the boundary condition $\mathcal{H}(0,T) = 1$. The typical results are illustrated in figures (5.1) and (5.2) for $\tau > 0$ while figure (5.3) shows the typical results for $\tau < 0$.

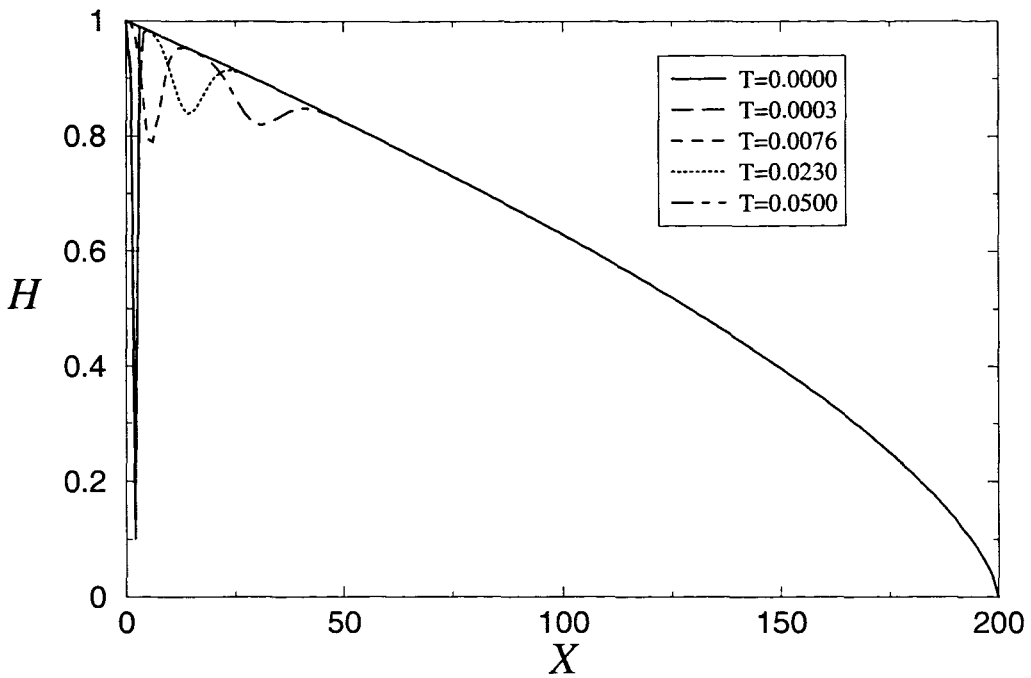

Figure 5.1: Evolutions of the perturbation to $\mathcal{H}(X,T)$ when $\tau = 60.0$.

In order to interpret the results here, we need to note a few things. Equation (5.32) is asymptotically consistent with the full problem (5.1) when τ is large and η is large (e.g. equation (5.32) can be obtained from (5.1) by assuming that $\tau \sim \eta \sim O(1/\epsilon^3)$, $h \sim O(\epsilon^2)$, $t \sim O(\epsilon)$ and then considering the leading order problem). However, leading to (5.33) from (5.32), we have scaled t by $t = \eta h(0)T$, where $h(0)$ is assumed to be of $O(1)$. We further know that for the linear stability analysis, t is assumed to be small. Hence this implies that for the linear stability results in this section, η is inherently small. Therefore, the linear stability

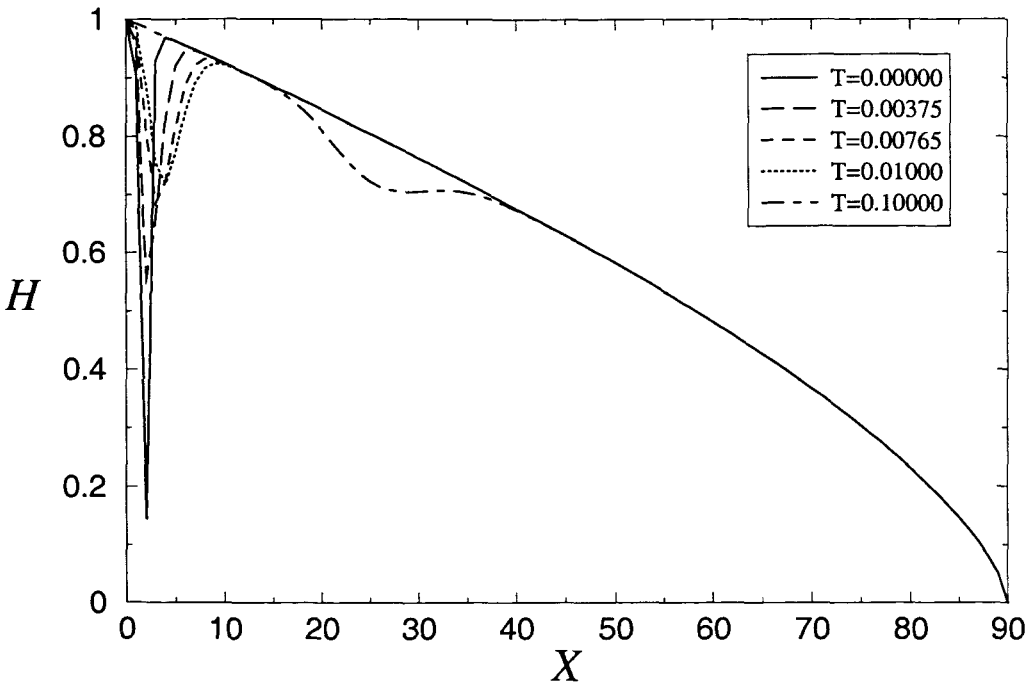

Figure 5.2: Evolutions of the perturbation to $\mathcal{H}(X,T)$ when $\tau = 2.7$.

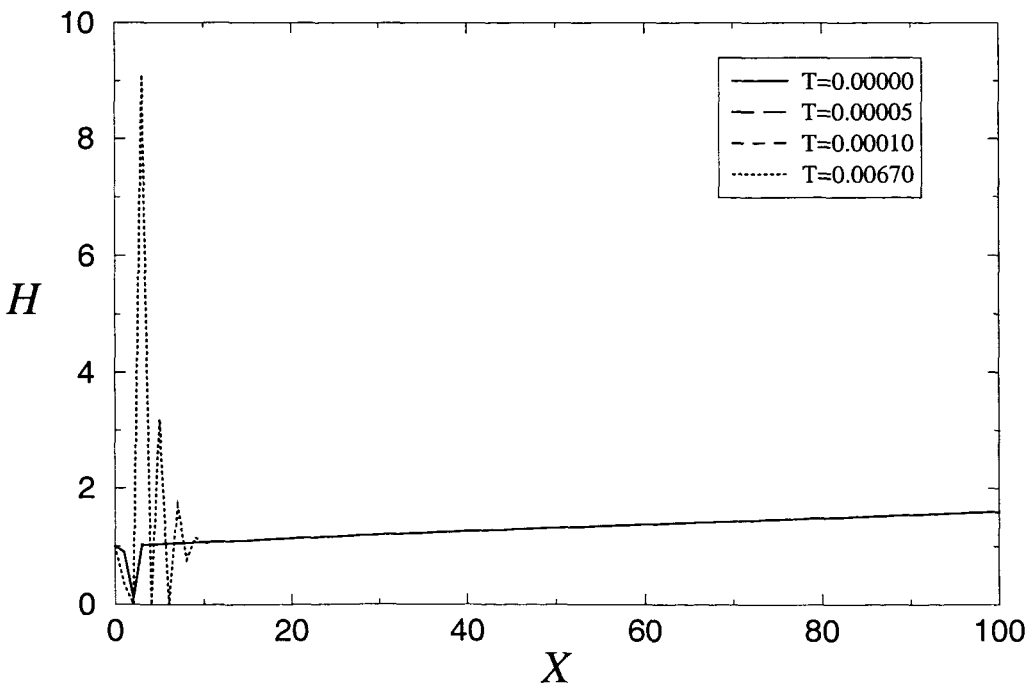

Figure 5.3: Evolutions of the perturbation to $\mathcal{H}(X,T)$ when $\tau = -2.5$.

results here should be compared to those of the full problem (5.1), when η is small and τ is large (e.g. results illustrated in figure (5.13)).

The typical results depicted in figures (5.1) and (5.2) clearly show that $\tau(>0)$ is a stabilising factor since all perturbations to $\mathcal{H}(X,T)$ decay as the time T increases. The results further suggest that the increase in τ is also a stabilising effect since when τ is relatively large (e.g. $\tau = 60.0$ in figure (5.1)) the perturbations decay faster than in the case when τ is relatively small (e.g. $\tau = 2.7$ in figure (5.2)). The typical results shown in figure (5.3), on the other hand, suggest that $\tau(<0)$ is always a destabilising factor since the perturbations to $\mathcal{H}(X,T)$ grow as T increases. It should be mentioned at this stage, for clarity, that all the graphs shown here represent the typical results which have been obtained through an extensive experimentation with the values of τ in the range $-10.0 \leq \tau \leq 100.0$, $\tau \neq 0$.

These results may be complemented by plotting (using XMAPLE for example) the evolutions in time $t \ll 1$ (for a fixed value of $\eta(\neq 0)$ where various values of τ are specified) of the closed-form solution of the perturbation $h_p(x,t)$

$$h_p(x,t) = \frac{\frac{9}{\eta\tau}(1-x)^{\frac{1}{3}}\alpha_2^{\frac{1}{2}}(x,t)\sin\left(M\left\{1-\frac{\eta\tau}{3}\alpha_2^{\frac{3}{2}}(x,t)\right\}\right)}{\alpha_2^{\frac{1}{2}}(x,t)\left\{18(1-x)^{\frac{1}{3}}-3\right\}+2(3)^{\frac{5}{3}}\left(\frac{1}{\eta\tau}\right)^{\frac{2}{3}}(1-x)^{\frac{2}{3}}}, \tag{5.38}$$

where $\alpha_2(x,t)$ is given by

$$\alpha_2(x,t) = \left(\frac{3}{\eta\tau}\right)^{\frac{1}{3}}(1-x)^{\frac{1}{3}} + \frac{2t}{\eta}. \tag{5.39}$$

Equation (5.38) is obtained by solving (5.2) using the method of characteristics as in section (5.3.1.1) to get

$$h^2(x,t) + \frac{2t}{\eta} = F^2\left(x + \frac{\tau\eta}{3}\left\{h^3(x,t) - \left(h(x,t) + \frac{2t}{\eta}\right)^{\frac{3}{2}}\right\}\right), \tag{5.40}$$

for an arbitrary function F. Then we introduce a perturbation on the steady state solution in the form

$$\begin{aligned} F(x) &= \left(\frac{3}{\eta\tau}\right)^{\frac{1}{3}}(1-x)^{\frac{1}{3}} + \delta\sin(Mx), \\ h(x,t) &= \left(\frac{3}{\eta\tau}\right)^{\frac{1}{3}}(1-x)^{\frac{1}{3}} + \delta h_p(x,t), \end{aligned} \tag{5.41}$$

for large enough real constant M. Substitution of equations (5.41) into (5.2) and comparison of coefficients of δ, after some algebra, leads to (5.38).

In the limit $\tau \to \pm\infty$ in particular, we note from (5.39) that

$$\alpha_2(t) \sim \frac{2t}{\eta}.$$

Hence we obtain an asymptotic solution for $h_p(x,t)$

$$h_p(x,t) \sim \frac{9}{\tau} \frac{(1-x)^{\frac{1}{3}} \bar{M}}{\eta \left\{ 18(1-x)^{\frac{1}{3}} - 3 \right\} \sqrt{2t}} \to 0,$$

as $\tau \to \pm\infty$, for increasing values of t at a fixed value of $\eta (\neq 0)$, $x \in [0,1]$ and $-1 \leq \bar{M} \leq 1$. Thus suggesting that the perturbation $h_p(x,t)$ decays quickly to nearly zero for large magnitudes of τ values.

It will be seen later in this study that the characteristic behaviour of the results shown in figures (5.1) and (5.2), when $\tau > 0$, are reflected by the numerical linear stability results for the full problem (5.1) in figure (5.13) until $\tau \approx 170$, for $\eta = 0.1$, where τ suddenly begins to play a destabilising role (a physical reason for this will also be proposed).

In conclusion, it will be seen later in this study that the results of the paradigm problems in this section suggest that indeed the numerical linear stability results for the full problem (5.1) might be correct. Apart from these two paradigm problems, we could have presented many others. However, the other paradigm problems require creation of other paradigm problems in order to test their numerical results and the process can become very cumbersome. One such case (as an example and without going into too much technical details) presents itself if we follow Tuck's (1991) [86] approach and simply replace the Hilbert transform operator $\mathcal{f}$ by a constant times a derivative operator ∂_x. Tuck (1991) [86]'s attitude is that the resulting equation may exhibit some of the features of the application described by the original equation, while not necessarily giving a quantitatively accurate solution. Applying this approximation to our full nonlinear, steady state problem (5.12) implies we will have to solve

$$\left\{ \frac{\tau\eta}{3\pi} h^3 h_{xxx} - \frac{\tau}{2} h^2 \right\}_x - h_t = \frac{1}{\eta h}, \tag{5.42}$$

where it has been assumed, in addition, that t is small, $h \sim O(\epsilon)$, $\tau \sim O(1/\epsilon)$ and $\eta \sim O(1/\epsilon^2)$. In the steady state case equation (5.42) may be rewritten, after some algebra, as

$$\frac{\tau\eta}{4\pi} \left(h^4\right)_x h_{xxx} + \frac{\tau\eta}{3\pi} h^4 \left(h_{xxx}\right)_x - \frac{\tau}{3} \left(h^3\right)_x = \frac{1}{\eta}. \tag{5.43}$$

Equation (5.43) may be analysed by solving

$$\left\{ \frac{\tau\eta}{3\pi} h^4 h_{xxx} - \frac{\tau}{3} h^3 \right\}_x = \frac{1}{\eta}. \tag{5.44}$$

This is rather a crude assumption. It is, nonetheless, not any better or worse than simply replacing the Hilbert transform operator by a constant times a derivative operator just for simplicity.

Equation (5.44) integrates to give

$$\frac{\tau\eta}{3\pi} h^4 h_{xxx} - \frac{\tau}{3} h^3 = \frac{x}{\eta} + C, \tag{5.45}$$

where C is a constant of integration. It may be demanded that (5.45) satisfy the regularity condition $h \sim (1-x)^{3/5}$ of the original problem near the dryout point $x = 1$. This requires that $C = -1/\eta$ and consequently, η and τ should simultaneously be greater than zero at all times. On scaling $h = h_0 H$, where $h_0 = h(0)$, we will then have to solve

$$k_1 H^4 H_{xxx} - k_2 H^3 = (x-1), \tag{5.46}$$

subject to boundary conditions $H(1) = 0$, $H_x(0) = 0$ and $H(0) = 1$ for some constants $k_1 = \tau\eta^2 h_0^5/3\pi$ and $k_2 = \tau\eta h_0^3/3$. (The existence of a solution to a nonlinear ordinary differential equation cannot be taken for granted. We could not obtain any numerical solutions to this problem in the cases of interest where τ and η are large. However, some solutions were obtainable when τ and η were both of $O(1)$.)

In the unsteady case we will have to solve, consistent with the regularity condition, a problem

$$k_1 H^4 H_{xxx} - k_2 H^3 - \eta \int_x^{G(T)} H H_T du = x - G(T), \tag{5.47}$$

for some function $G(T)$ and where t is scaled with $t = h_0^2 T$. The boundary conditions $H(G(T),T) = 0$, $H_x(0,T) = 0$ and $H(0,T) = 1$ may be specified. For the linear stability analysis, a perturbation of the form

$$H = H_s(x) + \epsilon H_p(x) e^{\sigma T},$$
$$G(T) = 1 + \epsilon A e^{\sigma T},$$

may be introduced, for some constant A, H_s is the steady state solution, H_p is the perturbation solution, σ is a measure of the growth or decay rate to be found and it is complex. This will require that we solve the following $O(\epsilon)$ eigenvalue problem for all σ values for any non-zero solution H_p and A,

$$k_1 H_s^3 \left(H_s H_{pxxx} + H_{sxxx} H_p\right) - 3k_2 H_s^2 H_p - \eta\sigma \int_x^1 H_s H_p du = 0, \tag{5.48}$$

subject to boundary conditions $H_p(0) = 0$, $H_{px}(0) = 0$ and $H_p(1) = 0$.

Equation (5.48) may be solved numerically for all eigenvalues σ and preliminary results suggest that the steady solutions to this problem might always be unstable in an oscillatory manner. However, when it comes to the independent test for the numerical scheme, things become a bit more tricky. The problem may require the introduction of a new variable

$$F(x) = \int_x^{G(T)} H_s(u) H_p(u) du,$$

so that, after some lengthly algebra, and the use of

$$H_{sxxx} = \frac{k_2}{k_1}\frac{1}{H_s} + \frac{x-1}{k_1 H_s^4},$$

equation (5.48) becomes

$$\begin{aligned} R_x &= S(x), \\ S_x &= Q(x), \\ Q_x &= U(x), \\ U_x &= -\left[f_3(x;k_1)U(x) + f_2(x;k_1)Q(x) + f_1(x;k_1,k_2)S(x) + \right. \\ &\qquad \left. f_0(x;\eta,\sigma)F(x)\right]/f_4(x;k_1), \end{aligned} \tag{5.49}$$

with boundary conditions $S(0) = 0$, $Q(0) = 0$ and $U(1) = 0$. The functions $S(x)$, $Q(x)$ and $U(x)$ are defined by

$$\begin{aligned} F_x &= S(x), \\ F_{xx} &= Q(x), \\ F_{xxx} &= U(x). \end{aligned}$$

While the terms f_4 to f_0 are respectively given by

$$\begin{aligned} f_4 &= -k_1 H_s^5(x), \\ f_3 &= 3k_1 H_s^4(x) H_{sx}(x), \\ f_2 &= k_1 H_s^2(x)\left\{3H_s^2(x)H_{sxx}(x) - 2H_s(x)H_{sx}(x)H_{sxx}(x) - 4H_s(x)H_{sx}^2(x)\right\}, \\ f_1 &= k_1 H_s^2(x)\left\{H_s^2(x)H_{sxx}(x) - 6H_s(x)H_{sx}(x)H_{sxx}(x) + 6H_s^3(x)\right\} - \\ &\qquad \left\{k_2 H_s^3(x) + 4(x-1)\right\}, \\ f_0 &= -\eta\sigma H_s^2(x). \end{aligned}$$

Equation (5.49) is an ordinary differential equation. Therefore, it may seem to be in a perfect form to be solved as an initial value problem using, for example, the NAG library routine D02PCF. The values of σ obtained by our numerical method would then be specified in the routine to check whether the solution satisfies the end condition $U(1) = 0$, thus checking the accuracy of the computed σ values. However, the fact that H_s is obtained numerically and that there is a singularity (that needs to be carefully dealt with) in H_s at $x = 1$ makes this a very tricky task and therefore we would still need another paradigm problem in order to test the method and the results. On the other hand, the results for paradigm problems (5.20) and (5.33) can be checked easily using some standard methods. Moreover and more importantly, their steady state solutions can be obtained in closed-form and are therefore exact.

5.3.2 The Full Problem

Having analysed the linear stability of some related paradigm problems, we now move on to examine the linear stability of the full problem (5.1). As mentioned earlier, we will proceed

here by assuming that the unsteadiness in equation (5.1) manifests itself as a small perturbation about the basic steady solution $h_s(x)$ of equation (5.12). We then seek an unsteady perturbation of the form

$$h(x,t) = h_s(x) + \epsilon h_p(x,t), \tag{5.50}$$

$$l(t) = \epsilon f(t), \tag{5.51}$$

where $\epsilon(>0)$ is a small parameter and the function $f(t)$ is not known.

It is convenient to transform the moving boundary problem into a finite fixed interval $[0,1]$ by setting

$$\begin{aligned} x &= z(1+\epsilon f(t)), \\ t &= T. \end{aligned} \tag{5.52}$$

The derivatives then transform into

$$\begin{aligned} \frac{\partial}{\partial x} &= \frac{1}{1+\epsilon f(T)}\frac{\partial}{\partial z}, \\ \frac{\partial}{\partial t} &= -\frac{z}{1+\epsilon f(T)}\epsilon\frac{df}{dT}\frac{\partial}{\partial z} + \frac{\partial}{\partial T}. \end{aligned} \tag{5.53}$$

We then assume, as in (5.50), a perturbation in h of the form

$$h(z,T) = h_s(z) + \epsilon h_p(z,T). \tag{5.54}$$

On substituting (5.54) into (5.1) and using equation (5.53) we obtain, to leading order,

$$\left\{\frac{h_s^3}{3\pi}\left(\fint_0^1 \frac{h_{sr}(r)}{r-z}dr\right)_z - \frac{h_s^2}{2}\tau\right\}_z = \frac{1}{\eta h_s}, \tag{5.55}$$

which is, as expected, identical to equation (5.12) that we have solved earlier. The associated $O(\epsilon)$ problem is then

$$\begin{aligned} \left\{\frac{h_s^3(z)}{3\pi}\left(\fint_0^1 \frac{h_{pr}(r,T)}{r-z}dr\right)_z + \frac{h_s^2(z)}{\pi}\mathcal{N}_{sz}h_p(z,T) - \tau h_s^2(z)f(T) - \tau h_s(z)h_p(z,T)\right\}_z \\ -h_{pT}(z,T) + zh_{sz}(z)\frac{df}{dT} = \frac{3}{\eta}\frac{f(T)}{h_s(z)} - \frac{1}{\eta}\frac{h_p(z,T)}{h_s^2(z)}, \end{aligned} \tag{5.56}$$

where $\mathcal{N}_s$ denotes here the Hilbert transforms of h_{sz}, so that

$$\mathcal{N}_s = \fint_0^1 \frac{h_{sr}(r)}{r-z}dr.$$

Equation (5.56) is linear in both $h_p(z,T)$ and $f(T)$, both of which are unknown at this stage.

In order to proceed with the linear stability analysis, a relationship between $f(T)$ and $h_p(z,T)$ must be found. Since in (5.56) $f(T)$ is a function of T alone and $h_p(z,T)$ is a function of both T and z, then if there has to be a relationship between the two functions

if both are not constants, $h_p(z,T)$ must be separable. As a result, we assume that $h_p(z,T)$ may be written as

$$h_p(z,T) = h_p(z)g(T), \tag{5.57}$$

for some unknown functions $h_p(z)$ and $g(T)$. Then equation (5.56) becomes

$$\left\{ \frac{h_s^3(z)}{3\pi}\mathcal{N}_{pz}g(T) + \frac{h_s^2(z)}{\pi}\mathcal{N}_{sz}h_p(z)g(T) - \tau h_s^2(z)f(T) - \tau h_s(z)h_p(z)g(T) \right\}_z$$
$$-h_p(z)\frac{dg}{dT} + zh_{sz}(z)\frac{df}{dT} = \frac{3}{\eta}\frac{f(T)}{h_s(z)} - \frac{1}{\eta}\frac{h_p(z)}{h_s^2(z)}g(T), \tag{5.58}$$

where $\mathcal{N}_p$ is given by

$$\mathcal{N}_p = \int_0^1 \frac{h_{pr}(r)}{r-z}dr.$$

The boundary conditions to impose on $h_p(z)$ are

$$h_{pz}(0) = h_p(0) = h_p(1) = 0, \tag{5.59}$$

and an appropriate regularity condition which will be determined later in this section.

We continue with the linear stability analysis by proposing a relationship between the functions $g(T)$ and $f(T)$. It is sensible to suppose that both of these functions determine the growth rate of the perturbations. Therefore, we assume a simple and convenient linear relationship between the two such that

$$f(T) = Ag(T), \tag{5.60}$$

for some unknown constant A. (The case when $A = 0$ refers to the situation where the dryout point is not allowed to move; and as mentioned in section (5.2), it is not of physical interest here.) Under these circumstances, equation (5.58) is homogeneous and linear in both h_p and A so that $h_p = A = 0$ is a solution to this equation. We then let

$$g(T) = e^{\sigma T}, \tag{5.61}$$

where σ is a complex number. Therefore equation (5.61) means that we allow an infinitesimal amount of deformation of the steady solutions in an unsteady oscillatory manner. Thus, equation (5.58) becomes an auxiliary equation to determine a set of possible eigenvalues for σ for any non-zero solution, h_p and A. Owing to the coupling behaviour depicted in the driving equation (5.12) for the steady solutions, energy can be added or subtracted from the problem hence resulting in the growth or decay, in time, of the magnitude of these oscillatory perturbations. Hence in general, the eigenvalues σ are complex numbers, the real part of which determines whether the solutions are stable or not. The contour $\mathcal{R}\rceil(\sigma) = 0$ divides the stable solutions with $\mathcal{R}\rceil(\sigma) < 0$ from the unstable ones with $\mathcal{R}\rceil(\sigma) > 0$, i.e. small

disturbances grow if $\mathcal{R}](\sigma) > 0$, they decay if $\mathcal{R}](\sigma) < 0$ and they neither grow nor decay if $\mathcal{R}](\sigma) = 0$. The imaginary part of σ dictates the natural frequency of the vibrations. The fact that σ is complex implies that both h_p in equation (5.57) and A in (5.60) are complex too. Therefore the real part of their product with $e^{\sigma T}$ in (5.61) is the physical value of the perturbation quantity. But since both h_p and A appear linearly in equation (5.58), then both their real and imaginary parts are separately solutions of (5.58); therefore there is no need to explicitly mention the taking of the real parts.

We know from solving equation (5.55) that near $z = 1$

$$h_s(z) \sim (125\chi/4\eta)^{1/5} (1 - z)^{3/5}, \tag{5.62}$$

where $\chi = |\tan(3\pi/5)|$. This suggests that h_p must also tend to zero like

$$h_p \sim K(1 - z)^{3/5}, \tag{5.63}$$

near $z = 1$, for some constant $K(> 0)$, in order to obtain satisfactory asymptotic balances near $z = 1$ in equation (5.58). Owing to the way that h_p appears in (5.58), the constant K cannot be obtained from this equation.

5.3.2.1 A Numerical Method

Owing to the nonlinear appearance of h_s and the presence of the Hilbert transform of both h_{sz} and h_{pz} in the characteristic equation for eigenvalues σ, equation (5.58) can only be solved numerically. The function h_s is also known numerically from solving equation (5.55), and this was one of the reasons why it was crucial to develop accurate methods for the steady problems in chapters 3 and 4. We should mention that prior to any numerical computations in this section, some analytical manipulations are required. The singularity in h_{sz} near the dryout point $z = 1$ needs to be dealt with before we can carry out any numerical computations.

5.3.2.2 Analytical Manipulations

We proceed by rewriting (5.58), after using (5.60) and (5.61), as

$$\begin{aligned}
&\left\{ \frac{h_s^5(z)}{3\pi} \mathcal{N}_{pz} + \frac{h_s^4(z)}{\pi} \mathcal{N}_{sz} h_p(z) - \tau h_s^3(z) h_p(z) - \tau h_s^4(z) A \right\}_z - \\
&\quad \left\{ \frac{h_s^3(z)}{3\pi} \mathcal{N}_{pz} + \frac{h_s^2(z)}{\pi} \mathcal{N}_{sz} h_p(z) - \tau h_s(z) h_p(z) - \tau h_s^2(z) A \right\} 2h_s(z) \times \\
&\quad\quad h_{sz}(z) + \frac{1}{\eta} h_p(z) - \frac{3}{\eta} h_s(z) A = \sigma \left\{ h_s^2(z) h_p(z) - z h_{sz}(z) h_s^2(z) A \right\}.
\end{aligned} \tag{5.64}$$

In this way, we avoid using the asymptotics to balance infinite terms near $z = 1$ in equation (5.58), and instead both sides of (5.64) become zero at this point. In order to avoid the

calculation of higher order derivatives in the subsequent numerical scheme, we integrate both sides of (5.64) with respect to z to get

$$\frac{h_s^5}{3\pi}\mathcal{N}_{pz} + \frac{h^4}{\pi}\mathcal{N}_{sz}h_p - \tau h_s^3 h_p - \tau h_s^4 A - \frac{2}{3\pi}\int_0^z h_s^4(u)h_{su}(u)\mathcal{N}_{pu}du - \frac{2}{\pi}\int_0^z h_s^3(u)h_{su}(u)\mathcal{N}_{su}h_p(u)du + 2\tau\int_0^z h_s^2(u)h_{su}(u)h_p(u)du + 2\tau\int_0^z h_s^3(u)h_{su}(u)duA + \frac{1}{\eta}\int_0^z h_p(u)du - \frac{3}{\eta}\int_0^z h_s(u)duA = \sigma\left\{\int_0^z h_s^2(u)h_p(u)du - \int_0^z uh_s^2(u)h_{su}(u)duA\right\} + C, \tag{5.65}$$

where C is a constant of integration. We then exploit the fact that we know both $h_s(z)$ and $h_p(z)$ at $z = 1$ and their respective asymptotic behaviours as $z \to 1$. We know, from equations (5.62) and (5.63) respectively, that both $h_s(z)$ and $h_p(z)$ behave like $(1-z)^{3/5}$ near $z = 1$. We have seen earlier (see equations (3.50) and (3.51)) that the finite range Hilbert transform of $(1-z)^p$, $0 < p < 1$, behaves like $(1-z)^p$ itself. As a result, the first four terms on the left hand side of (5.65) are all zero at $z = 1$. Thus, C is given by

$$-\frac{2}{3\pi}\int_0^1 h_s^4(u)h_{su}(u)\mathcal{N}_{pu}du - \frac{2}{\pi}\int_0^1 h_s^3(u)h_{su}(u)\mathcal{N}_{su}h_p(u)du + 2\tau\times \int_0^1 h_s^2(u)h_{su}(u)h_p(u)du + 2\tau\int_0^1 h_s^3(u)h_{su}(u)duA + \frac{1}{\eta}\int_0^1 h_p(u)du - \frac{3}{\eta}\int_0^1 h_s(u)duA - \sigma\left\{\int_0^1 h_s^2(u)h_p(u)du - \int_0^1 uh_s^2(u)h_{su}(u)duA\right\} = C. \tag{5.66}$$

Substituting (5.66) into (5.65) and performing the simplifications

$$\begin{aligned}\int_z^1 h_s^3(u)h_{su}(u)du &= -\frac{1}{4}h_s^4(z),\\ \int_z^1 uh_s^2(u)h_{su}(u)du &= -\frac{1}{3}\left(h_s^3(z) + \int_z^1 h_s^3(u)du\right),\end{aligned}$$

(where the integration by parts and the fact that $h_s(1) = 0$ have been exploited) we arrive at the equation

$$\frac{h_s^5}{3\pi}\mathcal{N}_{pz} + \frac{h_s^4}{\pi}\mathcal{N}_{sz}h_p - \tau h_s^3 h_p - \frac{1}{2}\tau h_s^4 A + F_1(z) - 2\tau\int_z^1 h_s^2(u)h_{su}(u)h_p(u)du - \frac{1}{\eta}\int_z^1 h_p(u)du + \frac{3}{\eta}\int_z^1 h_s(u)duA = \sigma\left\{-\int_z^1 h_s^2(u)h_p(u)du - \frac{1}{3}\left(h_s^3 + \int_z^1 h_s^3(u)du\right)A\right\}. \tag{5.67}$$

The function $F_1(z)$ is given by

$$F_1(z) = \frac{2}{3\pi}\int_z^1 h_s^4(u)h_{su}(u)\mathcal{N}_{pu}du + \frac{2}{\pi}\int_z^1 h_s^3(u)h_{su}(u)\mathcal{N}_{su}h_p(u)du. \tag{5.68}$$

We must then solve (5.67) subject to boundary conditions $h_{px}(0) = h_p(0) = 0$ and $h_p(1) = 0$ to find all the eigenvalues σ for any non-zero solution h_p and A.

5.3.2.3 Discretisation

We are now in a position to deal with the problem numerically. We will proceed by discretising the equations to obtain a system of generalised eigenvalue matrix problems whose unknown vector comprises of A and the values of h_p. The system of equations will be solved for the eigenvalues σ using the QZ algorithm as implemented in the NAG library routine F02BJF. The computation of the eigenvalues will allow investigations of the influence of the parameters τ and η on the instability of this problem. The uniformity of the numerical method will be checked during the course of the investigations by solving the system for different values of the total number of mesh points while τ and η are kept constant.

Now, we discretise the interval $[0,1]$ by partitioning it into n equal subintervals $[z_j, z_{j+1}]$, where $0 \leq j \leq n-1$ and $z_j = j/n$ are the mesh points. Thus, n denotes the total number of mesh points in the interval. In order to minimise the complexity in the numerical computations, we approximate the integrals in each subinterval using the trapezoidal rule. Finally, we fit linear splines to each of $h_s(z)$ and $h_p(z)$ and write

$$h_s = [1 - n(z - z_j)]\, h_{sj} + n(z - z_j)\, h_{sj+1},$$

$$h_p = [1 - n(z - z_j)]\, h_{pj} + n(z - z_j)\, h_{pj+1},$$

in each subinterval. We use finite differences and specify the mesh points z_i, $1 \leq i \leq n-1$. We then collocate at the mid-mesh points in the approximation of the derivatives of the Hilbert transforms of both h_p and h_s ($\mathcal{N}_{pz}$ and $\mathcal{N}_{sz}$ respectively) in equation (5.67).

The discretised version of equation (5.67), after imposing the boundary conditions $h_{p0} = h_{p1} = h_{pn} = 0$ and performing tedious but straightforward algebra, is then

$$\frac{n^2 h_{si}^5}{3\pi} \sum_{j=2}^{n-1} \left\{ h_{pj} \ln \left| \frac{\left(z_j - u_{i+\frac{1}{2}}\right)^2 \left(z_{j-1} - u_{i-\frac{1}{2}}\right) \left(z_{j+1} - u_{i-\frac{1}{2}}\right)}{\left(z_{j-1} - u_{i+\frac{1}{2}}\right) \left(z_j - u_{i-\frac{1}{2}}\right)^2 \left(z_{j+1} - u_{i+\frac{1}{2}}\right)} \right| \right\} +$$

$$\frac{n^2 h_{si}^4}{\pi} \left\{ \sum_{j=0}^{n-1} (h_{sj+1} - h_{sj}) \ln \left| \frac{\left(z_{j+1} - u_{i+\frac{1}{2}}\right) \left(z_j - u_{i-\frac{1}{2}}\right)}{\left(z_j - u_{i+\frac{1}{2}}\right) \left(z_{j+1} - u_{i-\frac{1}{2}}\right)} \right| \right\} h_{pi} - \frac{3}{2n} \tau h_{si}^4 A +$$

$$F_{1i} + \frac{3}{\eta} \sum_{j=i}^{n-1} \bar{g}_i A - \frac{1}{2n\eta} \left\{ \sum_{j=i}^{n-1} h_{pj} + \sum_{j=i}^{n-2} h_{pj+1} \right\} - 2\tau \left\{ \sum_{j=i}^{n-1} (h_{sj+1} - h_{sj})\, \bar{a}_j h_{pj} + \right.$$

$$\left. \sum_{j=i}^{n-2} (h_{sj+1} - h_{sj})\, \bar{b}_j h_{pj+1} \right\} = \sigma \left\{ - \sum_{j=i}^{n-1} \bar{a}_j h_{pj} - \sum_{j=i}^{n-2} \bar{b}_j h_{pj+1} - \right.$$

$$\left. \frac{1}{3} \left(h_{si}^3 + \sum_{j=i}^{n-1} \bar{c}_j \right) A \right\}, \quad (5.69)$$

for $1 \leq i \leq n-1$. The quantities $\bar{a}_j$, $\bar{b}_j$, $\bar{c}_j$ and $\bar{g}_j$ are respectively given by

$$\int_{z_j}^{z_{j+1}} h_s^2(u) h_{su}(u) h_p(u) du \approx n (h_{sj+1} - h_{sj}) \left[\bar{a}_j h_{pj} - \bar{b}_j h_{pj+1} \right],$$

$$\bar{a}_j = \left\{\frac{1}{4n}h_{sj} + \frac{1}{6n}h_{sj+1}\right\}h_{sj},$$

$$\bar{b}_j = 3\left(\frac{1}{3n} + \frac{1}{4n^2}\right)h_{sj}h_{sj+1} + \left(\frac{1}{2} - \frac{5}{12n}\right)h_{sj}^2 + \frac{1}{4n}h_{sj+1}^2,$$

$$\bar{c}_j = \int_{z_j}^{z_{j+1}} h_s^3(u)du \approx \frac{1}{4n}h_{sj}^3 + \frac{1}{4n}h_{sj}^2h_{sj+1} + \left\{\frac{1}{2n} - \frac{1}{4n^2}\right\}h_{sj}h_{sj+1}^2 + \frac{1}{4n}h_{sj+1}^3,$$

$$\bar{g}_j = \frac{1}{2n}\left(h_{sj} + h_{sj+1}\right).$$

The discretisation of equation (5.68) warrants some comment. We assume, for simplicity, that both the pressure gradient and the perturbation pressure gradient are constant in each subinterval $[z_j, z_{j+1}]$ so that the discretised version of (5.68) is

$$F_{1i} = \frac{2n}{3\pi}\sum_{j=i}^{n-1}\left(h_{sj+1} - h_{sj}\right)\left\{\mathcal{N}_{pu}\int_{z_j}^{z_{j+1}} h_s^4(u)du + 3\mathcal{N}_{su}\int_{z_j}^{z_{j+1}} h_s^3(u)h_p(u)du\right\}. \tag{5.70}$$

On simplification, (5.70) becomes

$$F_{1i} = \frac{2n}{3\pi}\sum_{j=i}^{n-1}\left\{\mathcal{N}_{pu}\left(h_{sj+1} - h_{sj}\right)\bar{d}_j\right\} + \frac{2n}{\pi}\sum_{j=i}^{n-1}\left\{\mathcal{N}_{su}\left(h_{sj+1} - h_{sj}\right)\bar{e}_jh_{pj}\right\}$$
$$+\frac{2n}{\pi}\sum_{j=i}^{n-1}\left\{\mathcal{N}_{su}\left(h_{sj+1} - h_{sj}\right)\bar{f}_jh_{pj+1}\right\}, \tag{5.71}$$

where the terms $\bar{d}_j$, $\bar{e}_j$ and $\bar{f}_j$ are given by

$$\bar{d}_j = \int_{z_j}^{z_{j+1}} h_s^4(u)du \approx \frac{6}{n}h_{sj}^4 + \frac{1}{5n}h_{sj}^3h_{sj+1} + \frac{1}{10n}h_{sj}^2h_{sj+1} +$$
$$\left(\frac{1}{4n} + \frac{3}{20n^2}\right)h_{sj}^2h_{sj+1}^2 + \left(\frac{3}{4n^2} - \frac{3}{5n^3}\right)h_{sj}h_{sj+1}^3$$
$$+\frac{1}{20n}h_{sj}h_{sj+1}^3 + \frac{1}{5n}h_{sj+1}^4,$$

$$\bar{e}_j + \bar{f}_j = \int_{z_j}^{z_{j+1}} h_s^3(u)h_p(u)du,$$

$$\bar{e}_j \approx \frac{6}{n}h_{sj}^3 + \frac{31}{20n}h_{sj}^2h_{sj+1} + \left\{\frac{1}{4n} + \frac{3}{20n^2}\right\}h_{sj}h_{sj+1}^2 + \frac{1}{20n}h_{sj+1}^3,$$

$$\bar{f}_j \approx \frac{1}{20n}h_{sj}^3 + \frac{1}{10n}h_{sj}^2h_{sj+1} + \left(\frac{3}{4n^2} - \frac{3}{5n^3}\right)h_{sj}h_{sj+1}^2 + \frac{1}{5n}h_{sj+1}^3.$$

We use finite differences to approximate $\mathcal{N}_{pu}$ and $\mathcal{N}_{su}$ in each subinterval and we then collocate (5.71) at the mid-mesh points to get

$$F_{1i} = \frac{2n^3}{3\pi}\sum_{k=2}^{n-1}\left\{h_{pk}\sum_{j=i}^{n-1}(h_{sj+1}-h_{sj})\,\bar{d}_j \ln\left|\frac{\left(z_k-u_{j+\frac{1}{2}}\right)^2\left(z_{k-1}-u_{j-\frac{1}{2}}\right)\left(z_{k+1}-u_{j-\frac{1}{2}}\right)}{\left(z_{k-1}-u_{j+\frac{1}{2}}\right)\left(z_k-u_{j-\frac{1}{2}}\right)^2\left(z_{k+1}-u_{j+\frac{1}{2}}\right)}\right|\right\} +$$

$$\frac{2n^3}{\pi}\sum_{j=i}^{n-1}\left\{\sum_{k=0}^{n-1}(h_{sk+1}-h_{sk})\ln\left|\frac{\left(z_{k+1}-u_{j+\frac{1}{2}}\right)\left(z_k-u_{j-\frac{1}{2}}\right)}{\left(z_k-u_{j+\frac{1}{2}}\right)\left(z_{k+1}-u_{j-\frac{1}{2}}\right)}\right|\right\}(h_{sj+1}-h_{sj})\,\bar{e}_j h_{pj} +$$

$$+\frac{2n^3}{\pi}\sum_{j=i}^{n-2}\left\{\sum_{k=0}^{n-1}(h_{sk+1}-h_{sk})\ln\left|\frac{\left(z_{k+1}-u_{j+\frac{1}{2}}\right)\left(z_k-u_{j-\frac{1}{2}}\right)}{\left(z_k-u_{j+\frac{1}{2}}\right)\left(z_{k+1}-u_{j-\frac{1}{2}}\right)}\right|\right\}(h_{sj+1}-h_{sj})\times$$

$$\bar{f}_j h_{pj+1}. \qquad (5.72)$$

Equations (5.69) and (5.72) form a generalised eigenvalue matrix problem, where the unknown vector comprises of A and the values of h_{pj}, $2 \leq j \leq n-1$. The system is solved (through the NAG library routine F02BJF) for all of the eigenvalues σ using the QZ algorithm. We expect one eigenvalue for each value of h_{pj} and A. If at least one of the eigenvalues has a positive real part, $\sigma_r > 0$, then we have unstable associated steady state solutions. If all $\sigma_r \leq 0$, we then have stable solutions. The instability is oscillatory if the relevant eigenvalues have non-zero imaginary parts, $\sigma_i \neq 0$.

Since the normal recoil pressure, gravity and surface tension at the free surface do not appear in this problem then we expect the instability to depend mainly on one or both of the parameters τ and η. Thus, in the results below we plot the most unstable or the least stable eigenvalues against either of the parameters τ or η to check how these parameters influence the instability in this problem.

Before proceeding with the discussion of results, we must point out that the method seems to work satisfactorily. There is no doubt the system (5.69) and (5.72) form a large computational problem which needs some very careful coding. However, the limitation as to how many points we consider is determined by the solution of the steady state solution which, as explained earlier, is a formidable task. As a result, the maximum number of points we take in the numerical scheme is $n = 100$. In order to check the uniformity of the numerical method we apply it to the solution of the steady state problem when $n = 20$ and increase n in steps of 20. Some typical results are shown for $n = 20$, $n = 40$, $n = 60$, $n = 80$ and $n = 100$ in figures (5.4) to (5.7) for the parameters $\tau = \eta = 1.0$. The figures indicate that the numerical method is consistent, the increase in n merely adds some more eigenvalues without altering the size of the eigenvalues corresponding to a smaller value of n. Owing to the nonlinearity and presence of the Hilbert transforms in the problem, however, it is unlikely that any rigorous attempts to test whether the method converges to the correct solution will be fruitful.

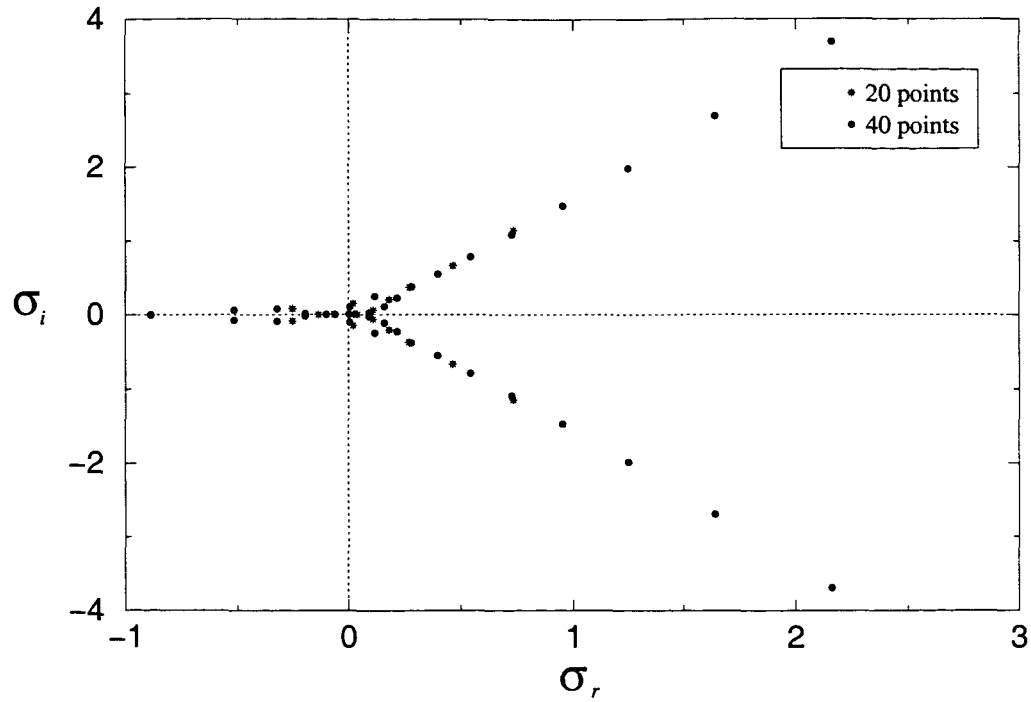

Figure 5.4: The imaginary parts of the eigenvalues, σ_i, against the real parts of the eigenvalues, σ_r; ($\tau = 1.0$ and $\eta = 1.0$).

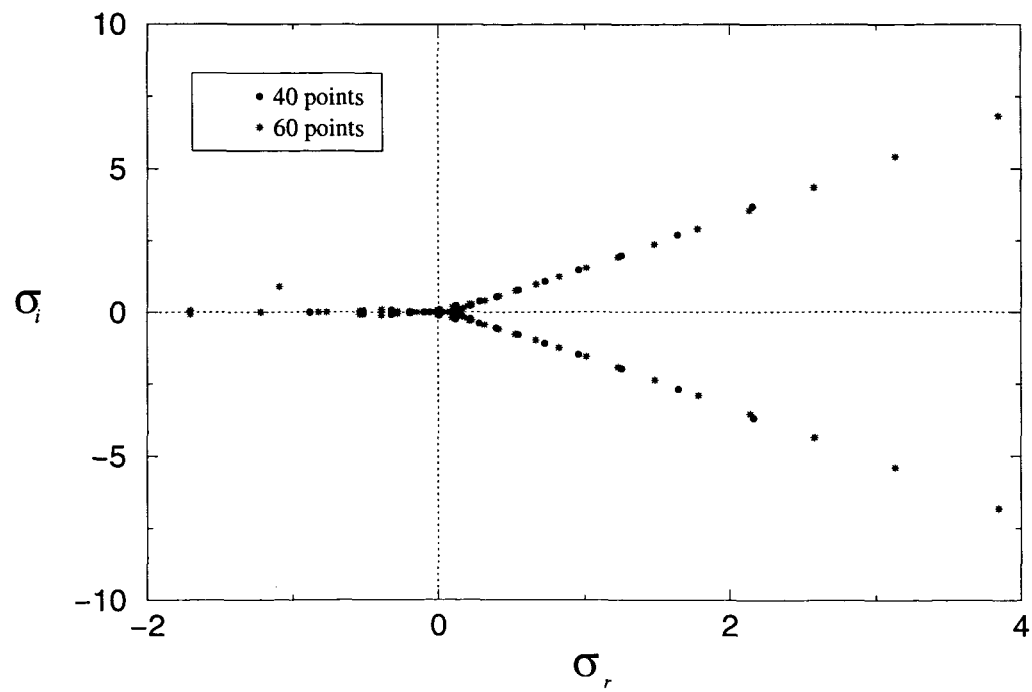

Figure 5.5: The imaginary parts of the eigenvalues, σ_i, against the real parts of the eigenvalues, σ_r; ($\tau = 1.0$ and $\eta = 1.0$).

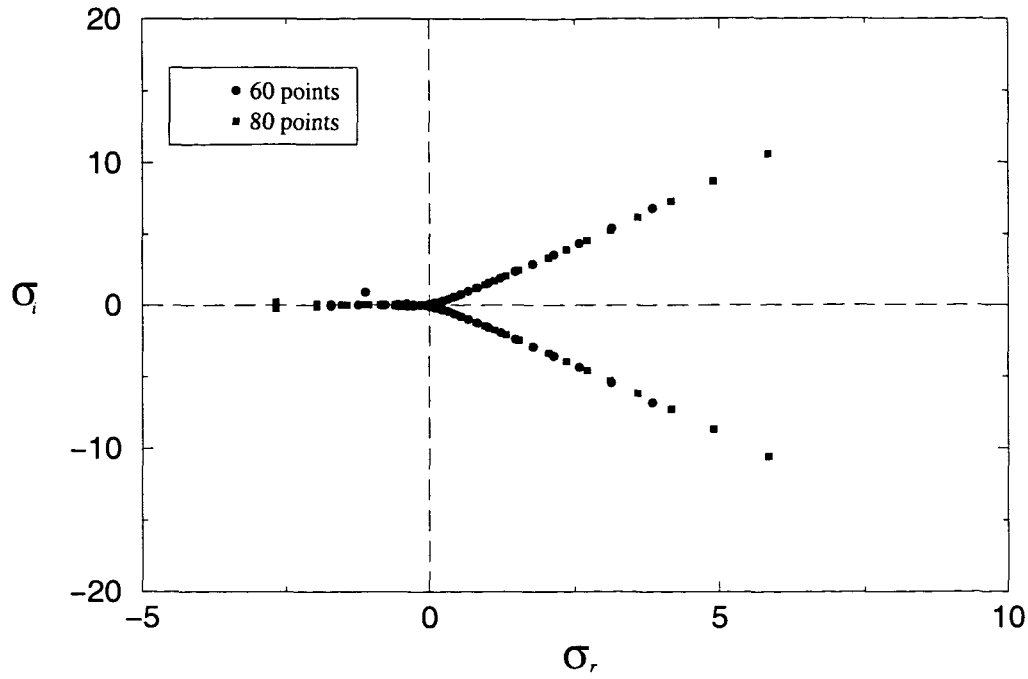

Figure 5.6: The imaginary parts of the eigenvalues, σ_i, against the real parts of the eigenvalues, σ_r; ($\tau = 1.0$ and $\eta = 1.0$).

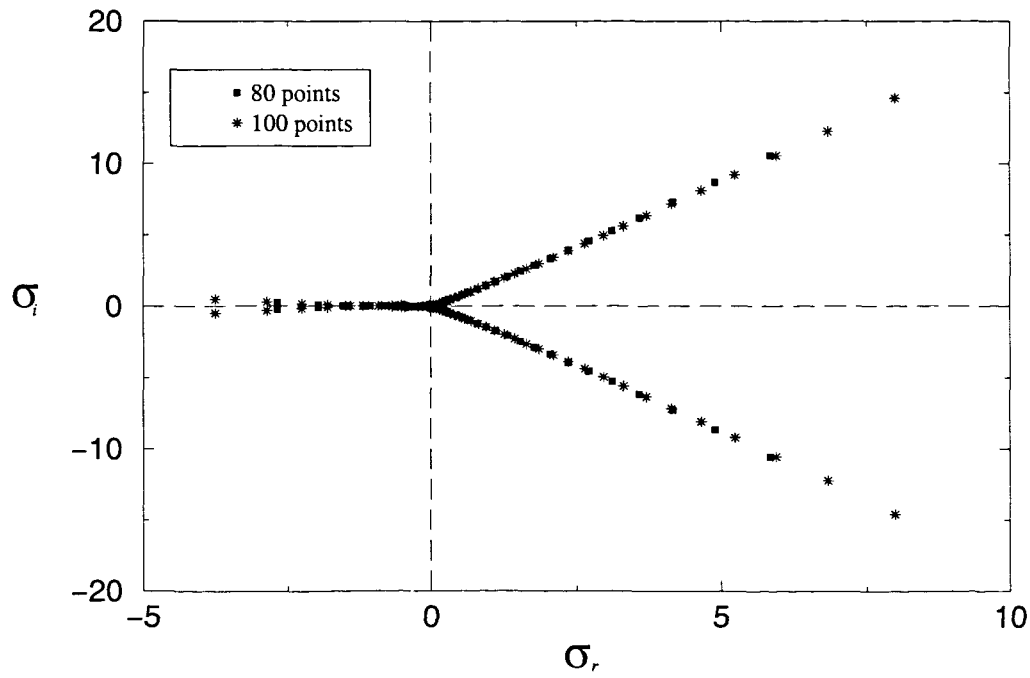

Figure 5.7: The imaginary parts of the eigenvalues, σ_i, against the real parts of the eigenvalues, σ_r; ($\tau = 1.0$ and $\eta = 1.0$).

5.3.2.4 Numerical Results

The results in figures (5.4) to (5.7) show a typical distribution of eigenvalues when the parameters η and τ are changed, e.g. see also figures (5.8) and (5.9). The eigenvalues are crowded

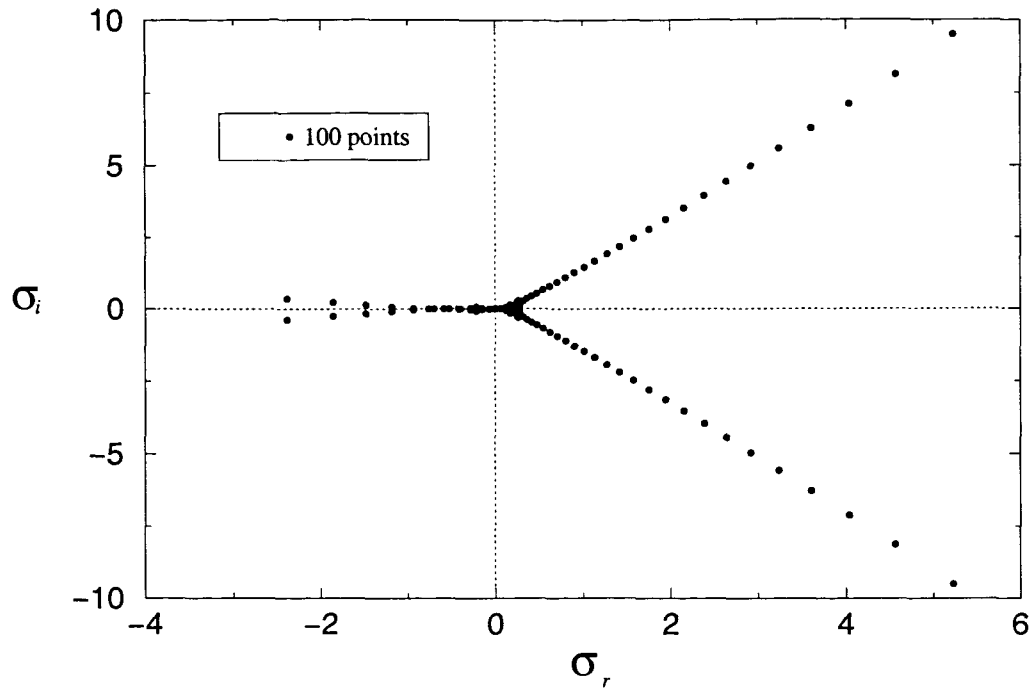

Figure 5.8: The imaginary parts of the eigenvalues, σ_i, against the real parts of the eigenvalues, σ_r; ($\tau = 10.0$ and $\eta = 1.0$).

and the majority are complex with their real parts are greater than zero. Thus suggesting that the steady state solutions to this problem are always unstable to small perturbation. Physically, this means that the solutions for the unsteady problem (5.1) may not be visible in reality. However, it should be recalled that this model is an idealisation of the annular flow regime which is, in reality, a very complicated phenomenon. In modelling the problem, we have ignored, for example, the processes of liquid droplet deposition from the gas core into the liquid film and the entrainment of liquid droplets from the liquid film free surface into the gas core. These processes, in the current case of interest, may be insignificant (as the typical parameter values from experiments suggest) for the formation or vanishing of the liquid layer, but they may be playing a very important role in the stabilisation of the developed liquid films. Furthermore, we have not included the surface tension term in the current study in order to minimise the amount of the computational algebra (however, analysis will show that the inclusion of this term would not ensure stable results for this problem). Therefore, the fact that the numerical linear stability results suggest that the steady state solutions obtained for this problem may be always unstable, should not be misunderstood to

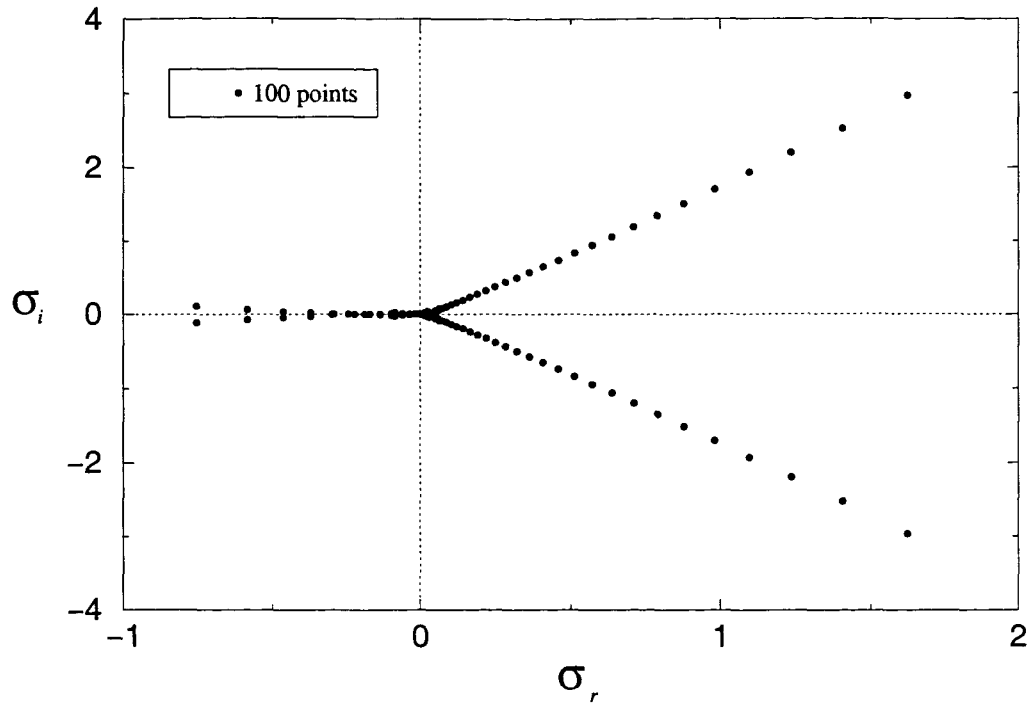

Figure 5.9: The imaginary parts of the eigenvalues, σ_i, against the real parts of the eigenvalues, σ_r; ($\tau = 2.0$ and $\eta = 10.0$).

mean that the model is irrelevant. It is always a good practice in mathematical modelling to build a model and analyse it from the simplest foundations first. Other realistic features may be added to the model simply as a matter of improvements. We will continue therefore to investigate the instability of the problem for other values of η and τ. This will be achieved by plotting the most unstable or the least stable eigenvalues against either of the parameters.

Before we proceed however, a closer look at figures (5.6) and (5.7) gives an impression that as $n \to \infty$ all the eigenvalues with positive real parts lie on a straight line and the most unstable eigenvalue tends to infinity. This may suggest that corresponding to the most unstable eigenvalue as $n \to \infty$, both $h_p(z)$ and A can be scaled with n so that an asymptotic relation between $h_p(z)$ and A may be obtained. In principle, the resulting relation may be checked against the numerics if the steady state base solution could be obtained for large enough n. Then, from the eigenvalues of the associated linear stability problem, the eigenvector corresponding to the most unstable eigenvalue may be calculated. After which $h_p(z)$ could be approximated from the vector along with the value of A so that the asymptotic relationship could be tested. However, we proceed here to investigate the instability of the problem when either of the parameters η and τ is changed. We plot the most unstable eigenvalue against either of the parameters.

Figure (5.10) shows a typical plot of the most unstable eigenvalue against the mass transfer parameter η when the traction parameter τ is held constant. In general, for all the results in this section, each point on the curves is obtained by first solving the steady state problem (5.12) for the given values of η and τ. Then the obtained value of h_s is used in the calculation of the eigenvalues, as described earlier, from the generalised eigenvalue problem characterised by equations (5.69) and (5.72). The most unstable or least stable eigenvalue corresponding to those particular values of η and τ is then recorded. The process is then repeated with a different set of values of η and τ until a sufficient number of points is available to plot a graph. Obviously, in the typical results shown in figure (5.10) for example, τ is kept constant at $\tau = 1$. The solid line in the graph reflects the relationship between the maximum

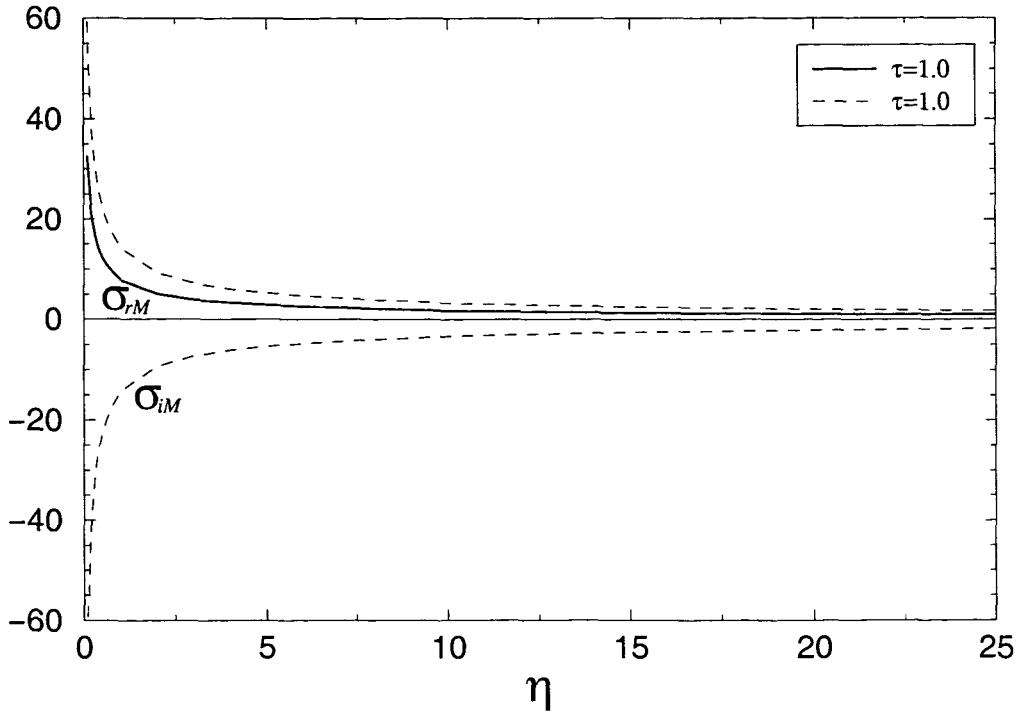

Figure 5.10: The most unstable or least stable eigenvalue against the mass transfer parameter η.

growth rate σ_{rM} against the parameter η. The dotted lines indicate the relationship between the imaginary parts of the most unstable eigenvalue σ_{iM} and the mass transfer parameter η. The results in figure (5.10) clearly show (in agreement with those of the paradigm problem (5.16)) that an increase in $\eta > 0$ is a stabilising factor in the problem. It should be recalled that the parameter η is inversely proportional to the difference between the pipe wall temperature T_w and the saturation temperature at the liquid film free surface T_s, i.e. $\eta \propto 1/(T_w - T_s)$. Therefore, this result suggests that for a given traction parameter τ, it is

easier to stabilise (or destabilise) a highly superheated liquid film through minute changes in the heat mass transfer parameter η than to stabilise (or destabilise) a mildly or moderately superheated one through large changes in η. In other words, a highly superheated liquid film evaporates much more rapidly than a mildly or moderately superheated one. Further, it is evident from figure (5.10) that as $\eta \to \infty$, for a given $O(1)$ parameter τ, the instability tends to an oscillatory marginal stability. It is therefore instructive to consider plotting the most unstable eigenvalues against the values of τ, especially for those large values of η, in order to investigate whether there could be some regions in the (τ, η) parameter space where the problem may be stable.

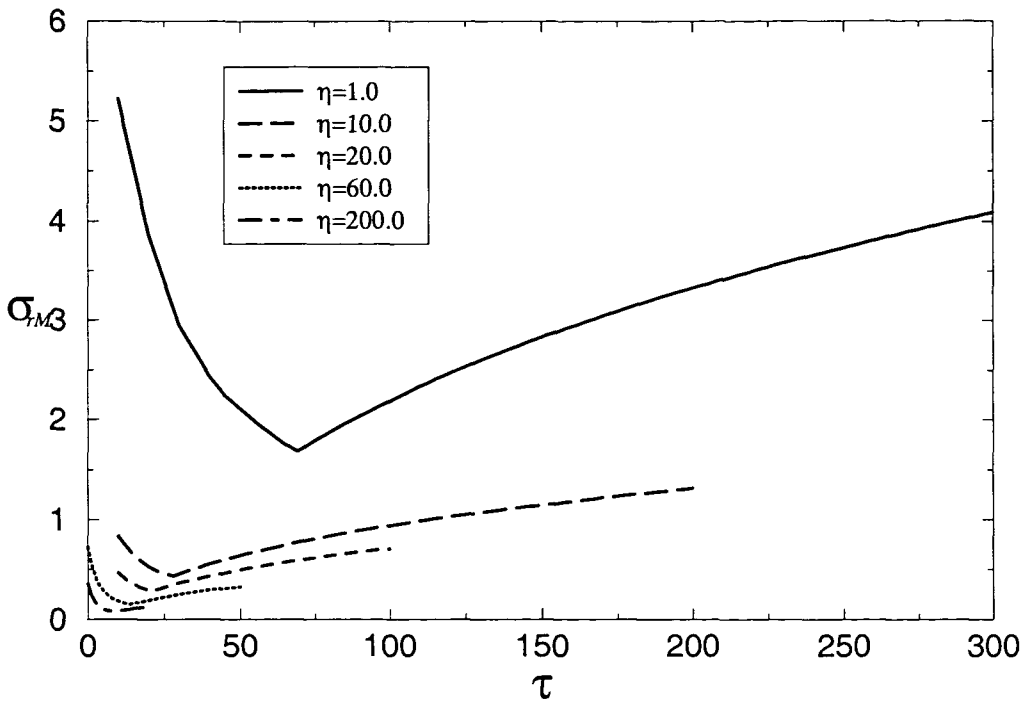

Figure 5.11: The real part of most unstable or least stable eigenvalue against the traction parameter τ.

Figures (5.11) and (5.12) illustrate a family of curves of the real parts of the most unstable eigenvalues σ_{rM} against the values of the traction parameter τ for different constant values of the heat mass transfer parameter η. It is clear from these curves that an increase in τ is a stabilising effect, in agreement with the results of the paradigm problem (5.33), but only up to a transition point where it abruptly becomes a destabilising factor. This transition point does not only depend on the values of τ but also on those of η. The smaller the value of η, the further away from the origin (along both the lines of zero σ_{rM} and zero τ) is the transition point. However, the change in positioning of the transition point is not proportional to the

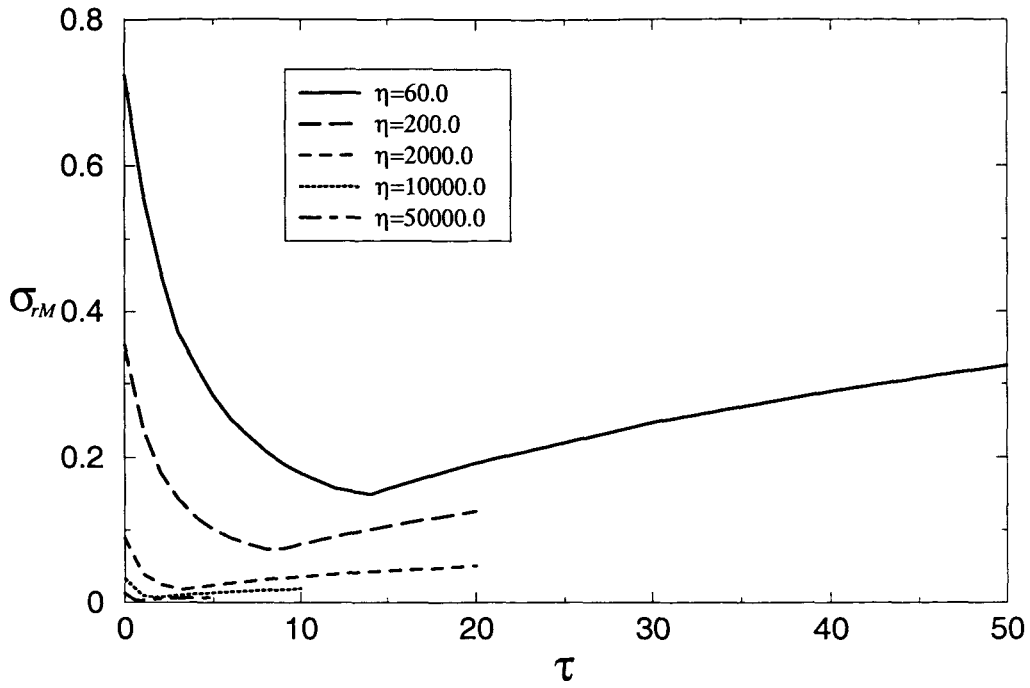

Figure 5.12: The real part of most unstable or least stable eigenvalue against the traction parameter τ.

increase in η. In fact the relationship between the transition point and the increase in η appears to be of an exponential decay form. For relatively small values of η, an increase in η effects a considerable decrease in the transition point from the origin. However, the transition point seems to approach a constant value for any increase in η for those large values of η. (The idea here, as mentioned above, was to investigate whether for some combination of the parameters η and τ we can find any values of $\sigma_{rM} < 0$. Hence the reason why in some of the curves, calculations have been stopped almost immediately after the transition point where the values of σ_{rM} start to increase.)

It is further illustrated in figures (5.13) and (5.14) that at the transition point, there is an exchange of instability from an oscillatory one to a purely growing instability in which $\sigma_{iM} = 0$. Owing to the sharpness of this instability exchange point, it appears that this point could be a branching point, where the curve coming from the left coming curve proceeds continuously through the point to the right without change in direction, and likewise the right outgoing curve continues to the left through the transition point without change in direction, so that the two curves cross each other at the transition point. This will imply that there may be some regions where the problem becomes stable as one of the curves (or both) will cross the $\sigma_{rM} = 0$ line. It is, nonetheless, difficult to sustain this view since our numerical method does not indicate any of such branching curves. Besides, such a result would

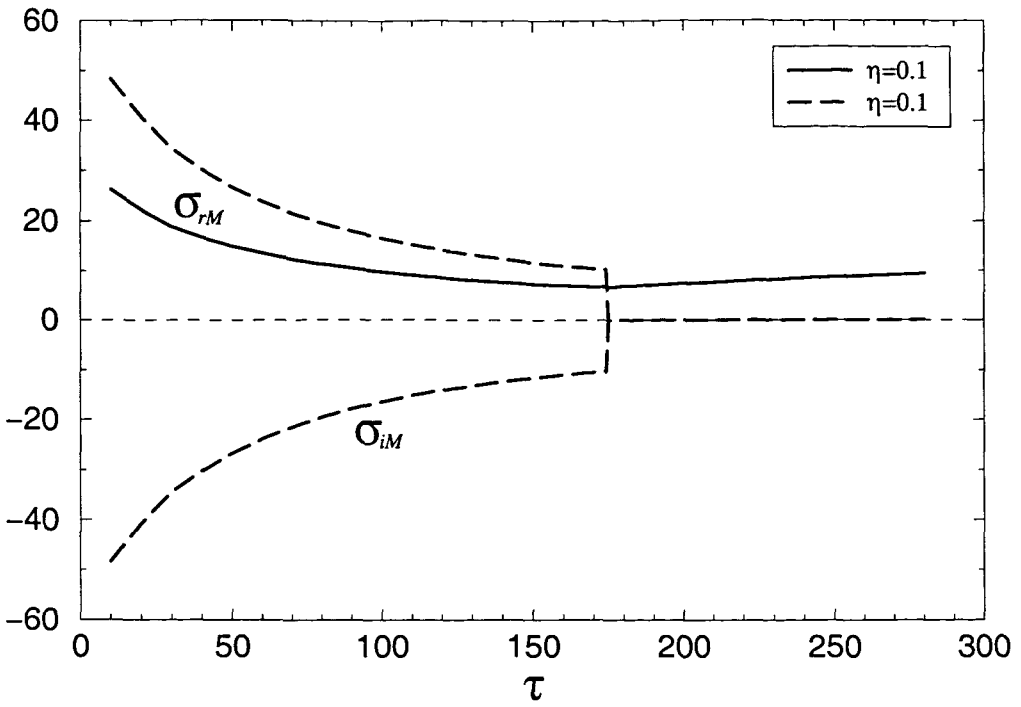

Figure 5.13: a graph of both the real and imaginary parts of most unstable or least stable eigenvalue against the traction parameter τ.

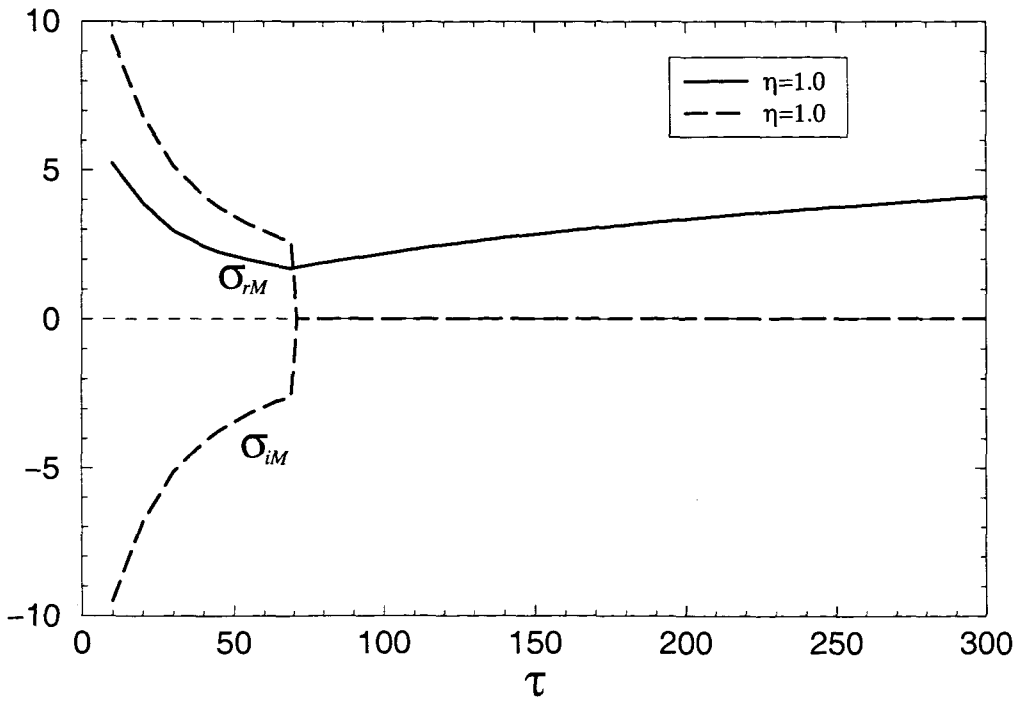

Figure 5.14: Both the real and imaginary parts of most unstable or least stable eigenvalue against the traction parameter τ.

inherently mean that the solution to the steady problem is not unique for some particular values of the prescribed parameters η and τ. Therefore, in the light of the results illustrated in figures (5.10) to (5.14), it is compelling to conclude that all the base steady state solutions to this problem (5.1) are unstable to small perturbations.

The indications, from both figure (5.11) and (5.12), that the increase in τ plays a stabilising role up to a transition point where it begins to be a destabilising factor may be given a physical explanation. We will recall from equation (2.56) that it was observed that in general, τ may be understood to include the effects of gravity. Therefore, these two results suggest that for a given value of η, there is a range of τ values where gravity is a dominant factor (i.e. where τ plays a stabilising role). The results for a set of τ values beyond this range provokes an impression that the dominant factor is the pulling/stretching provided by the fast flowing gas in the core, and this tends to increase the growth of the perturbations on the liquid film free surface.

In summary, the findings here imply that the solutions to the the full unsteady problem (5.1) may not be observable in reality for virtually all values of η and τ. Thus, it will not be sensible to continue to solve (5.1) numerically. Since in reality these thin films are physically visible in real life, then the results here give an impression that the process of droplet deposition from the gas core onto the liquid film may be playing a crucial role in the stabilisation of the developed films in the problem. This impression is supported by the results of section (5.3.2.5). In section (5.3.2.5), we show analytically that the surface tension term in this problem will have to be infinitely large in order to ensure stable results. We do this by considering the problem when there is neither mass transfer nor shear stress at all, i.e. we consider the problem on the $(-\infty, \infty)$ range. In this case, the surface tension term competes only with the gas core pressure term, and we will first show analytically that the gas core pressure plays a destabilising role in this problem. Therefore, in future the process of droplet deposition probably needs to be accounted for in the model for the linear stability purposes even though, at the current conditions of interest, the typical values of the experimental results suggest that the droplet deposition is negligible in the formation of these liquid films. The inclusion of this term in the model will undoubtedly increase the amount of algebra involved in solving this model and/or we may even require totally different techniques to solve the resulting problem.

5.3.2.5 Analytical Results: Gas Core Pressure and Surface Tension Effects

We investigate the role of the gas core pressure with regard to the instability of (5.1). In this problem, the gas core pressure is given by the Hilbert transform of the gradient of the free

surface

$$\int_0^1 \frac{h_\xi(\xi,t)}{\xi - x} d\xi.$$

In order to isolate the effects of the gas core pressure alone, it is intuitively sensible to consider a no-mass transfer, no-shear stress problem. In this case, it is physically logical to expect no dryout point. Therefore, instead of (5.1), we will have to study the unsteady problem

$$\left\{ \frac{h^3}{3\pi} \left(\int_{-\infty}^{\infty} \frac{h_\xi(\xi,t)}{\xi - x} d\xi \right)_x \right\}_x - h_t = 0. \tag{5.73}$$

Clearly, without loss of generality $h = 1$ is a solution of (5.73). For the linear stability, we employ the method of normal modes in x and t and write

$$h = 1 + \epsilon e^{ikx + \sigma t}, \tag{5.74}$$

where σ is this disturbance growth rate as seen earlier, k is the wavenumber and $\epsilon (> 0)$ is a small parameter. On substituting equation (5.74) into (5.73) and comparing coefficients we obtain an $O(\epsilon)$ problem

$$\frac{1}{\pi} \left(\int_{-\infty}^{\infty} \frac{\left(e^{ik\xi}\right)_\xi}{\xi - x} d\xi \right)_{xx} = \sigma e^{ikx}. \tag{5.75}$$

The term (in the brackets) which appears on the left hand side of (5.75) is (see for example Pipkin (1991) [64])

$$\frac{1}{\pi} \int_{-\infty}^{\infty} \frac{\left(e^{ik\xi}\right)_\xi}{\xi - x} d\xi = -|k| e^{ikx},$$

Hence we get the dispersion relation

$$\sigma = |k| k^2,$$

which indicates that the pressure in the gas core is always a destabilising factor as σ is always real and positive.

If a similar analysis (i.e. normal modes linear stability analysis with $\tau = 0$ and $\eta = \infty$) is performed on the problem with surface tension, a version of equation (2.65) on the range $(-\infty, \infty)$, we obtain the dispersion relation

$$\sigma = -\frac{k^3}{3} \left(\frac{\bar{S}}{\pi} k - 1 \right),$$

where we have used the fact that the wavenumber k is physically related to the wavelength of the disturbance waves; therefore k must be positive. We recall that perturbations grow if $\sigma > 0$ and decay if $\sigma < 0$. It is then obvious from the dispersion relation that the surface tension term $\bar{S}$ is a stabilising factor. The marginal stability is obtained when $\sigma = 0$ and thus the cutoff wavenumber is given by

$$k = \frac{\pi}{\bar{S}}.$$

In the long wave theory (where the disturbance waves have wavelengths much larger than the typical film thicknesses) this relation suggests that in this case $\bar{S}$ must tend to infinity. We further observe that there is growth for all k satisfying

$$0 < k < \frac{\pi}{\bar{S}},$$

and the maximum growth occurs at $d\sigma/dk = 0$ when $k = 3\pi/4\bar{S}$ and $\sigma = 9\pi^3/256$. This result suggests that, if there has to be no unstable solutions in this problem, then the surface term must be infinitely large. However, this is absurd because it means then that the wavenumber k must be zero. As a result, we conclude that the inclusion of the surface tension term in the linear stability analysis of the full problem (5.1) would not have altered the overall results we have obtained for this problem. Therefore for future work, we anticipate that only the inclusion of the droplets deposition term in in the model might be the best hope for the stability purposes in this problem.

Chapter 6

Conclusions

In this thesis a two-dimensional mathematical model for an evaporating superheated thin liquid film adhering to a heated wall has been proposed. To achieve this, thin-layer lubrication theory has been employed. The model is unsteady and takes into account the dynamics of flow in the vapour core (produced by the evaporating liquid layer) through the application of the thin aerofoil theory. Thus, the model is governed by a nonlinear partial singular integro-differential equation. In a real world application, the model idealises the two-phase annular flow of water and steam, along with the dryout point, in steam generating pipes. In reality the two-phase annular flow in steam generating pipes is a very complex phenomenon. It consists of, among other things, an evaporating superheated thin liquid film adhering to the pipe walls and the dryout point. The liquid film surrounds a fast flowing gas core which may be turbulent in nature, e.g. see Kirillov *et al* (1985) [46]. The continuous breakup of large amplitude coherent waves on the liquid film free surface and the undercuttings of the surface by the fast flowing gas in the core are believed to be major causes of the droplet entrainment from the liquid layer into the vapour core. Moreover, there is a simultaneous deposition of liquid droplets from the gas core onto the liquid layer. The rate at which these processes occur is theoretically unknown. Under the current conditions of interest however, the typical experimental results, e.g. see Collier (1972) [19], suggest that neither the droplet deposition nor the droplet entrainment are of paramount importance in the formation or the vanishing of the liquid film. Thus implying that the evaporation of the liquid film is the dominant factor affecting the dryout point here.

Owing to the nonlinear singular nature of the governing equations, the model has been solved numerically (in the steady state case) for various specified conditions at the pipe wall. In chapter 3, the model has been solved for a constant wall temperature. In chapter 4, the model has been solved for some specified non-constant wall temperature. In general, the temperature at the wall must be determined by solving the problem in the liquid metal

(flowing in the counter direction) in the outer casing of the steam generating pipes. However, it has been found that the problem in the liquid metal was so difficult that it could only be solved numerically and the solution would be unhelpful for the purposes of solving the model.

In chapters 3 and 4, the effects of the constant parameter values in the model on the length to the dryout point from the onset of the annular regime have been investigated from the computed results. It has been consistently found that an increase in the traction parameter τ leads to an increase in the length to the dryout point. In other words, the traction supplied by the flow in the vapour core pulls and stretches the liquid layer. It has also been found that the increase in the mass transfer parameter η (which should be recalled that it is inversely proportional to the difference between the typical wall temperature and the saturation temperature at the liquid film free surface) leads to an increase in the length to the dryout point. Physically, this result implies (as one would expect) that for a liquid with large latent heat, the mass transfer is small and dryout cannot occur. However, for a liquid with small latent heat, the mass transfer is very high and dryout will occur immediately.

The governing equations for the model are very complex and a lot of insight into the unknown solution for the liquid film free surface was required before any computational techniques could be developed for the problem. It has been demonstrated extensively in the thesis (by even providing some simple paradigm problems which could be solved analytically) that the knowledge of the asymptotic behaviour of the unknown solution near the dryout point is very important with regard to the numerical solution of the model. In the cases where there is a singularity in the slope of the film free surface near the dryout point, it has been found mandatory to employ some regularisation techniques in order to satisfactorily compute solutions from the model. In these cases the problem has been regularised by considering an appropriately stretched coordinate so that the solution approaches the dryout point linearly. This ensures that there is no singularity in its slope there. It has been observed that the regularisation technique, (despite increasing the amount of algebra involved in solving the model tremendously) works very well. Another source of complexity in the model is partly due to the fact that some of the boundary conditions in the model depend on the global behaviour of the unknown solution and some boundary conditions are coupled nonlinearly. In particular, the application of the pressure condition (which depends on the global behaviour of the unknown solution in $[0, 1]$) at the onset of the annular flow, $x = 0$ has been a great challenge. The pressure condition can be applied directly if and only if the governing equation in the model has been integrated twice with respect to the independent variable x. After which, it is inevitable that the resulting equation should be inverted in order to make any progress with it. However, the inversion of the equation leads to a very difficult problem to tackle numerically as demonstrated by some computations in section (4.4.2). As a result, we have been mostly restricted to solving the model by prescribing the pressure gradient

condition at the onset of the annular region. In this case the resulting problem is still very difficult to solve numerically, but there is comparatively less computational algebra involved.

The pressure and the pressure gradient are directly related in this problem (and they both depend on the global behaviour of the unknown solution in $[0, 1]$) therefore one can be calculated from the other. By plotting the values of pressure against the pressure gradient, at the entry of the annular flow $x = 0$, it has been possible to demonstrate that in some cases it might not be possible to obtain a converged numerical solution to the model, e.g. for values of pressure less or equal to approximately 0.27 and pressure gradient values greater or equal to about -110.0, at $x = 0$ for the constant wall temperature problem. In chapter 3, the relationships between the length to the dryout point (from the entry of the annular flow $x = 0$) and both the pressure and the pressure gradient at $x = 0$, have been obtained for the constant wall temperature problem. For practical purposes and experimental comparisons, these relationships may not be as useful as the plot of pressure profiles. Thus, for all problems in chapters 3 and 4, the pressure profiles in the annular regime and far downstream of dryout point have been plotted. It has been found consistently that, in general, the pressure is positive at the entry of the annular regime, $x = 0$, and it rises sharply to reach a positive maximum near $x = 0$. It then decreases, quickly near $x = 0$, and then gradually downstream to achieve a negative minimum at (or very near to) the dryout point before increasing to almost a negative constant far downstream of the dryout point. The negative minimum in the pressure at the dryout point for the constant wall temperature problem is infinite solely as a result of the singularity in the slope of the liquid film free surface near that point. This conclusion has been verified by the results of the non-constant wall temperature problem in chapter 4, where there is no singularity in the slope of the film free surface near the dryout point.

In chapter 5, the linear stability of the constant wall temperature problem has been analysed numerically. This is a very complicated unsteady free moving boundary problem and (to the best of our knowledge, by the time of writing) has never been tackled before. In order to put it into a form conducive for the numerical linear stability treatment, the problem has been appropriately transformed into an unsteady nonlinear partial singular integro-differential equation of the finite type in the interval $[0, 1]$. The equations were then discretised using finite differences and the technique of collocation around singular points in the Hilbert transform was employed. The resulting equations were then analysed for the linear stability by solving for the eigenvalues using the QZ algorithm as implemented in the NAG library routine F02BJF. The performed linear stability analysis suggests that the steady state solutions to the constant wall temperature problem are always unstable to small perturbations. In reality, this result implies that the solutions to the corresponding unsteady problem (5.1) may not be physically observable. It must be emphasised that this result does not therefore mean that

the model is totally irrelevant. (In fact the development of this model is a major achievement since most, if not all, the models in the literature either deal with the liquid film only or with the gas core alone. However, in this model, we have accounted the dynamic effects of the flow in the gas core on the dynamic pressure for the flow in the liquid layer.) This result simply tells us that there may be other physical processes which should not be ignored in the model, under any circumstances, since they could be playing a very crucial role in the linear stability of the problem. The linear stability analysis of the paradigm problem (5.73) in section (5.3.2.5), where there is neither the mass transfer nor the traction in the problem, suggests strongly that the droplet deposition could be the most viable process for this purpose. It has been demonstrated analytically in this section that the pressure in the gas core is a destabilising factor. It has also been shown in the same section that the surface tension term would have to be infinitely large (which is unrealistic physically) in order to ensure that the results are stable in this problem. Therefore, this finding leaves us with the possibility that the droplet deposition from the gas core onto the liquid film (if accounted for in the model) might ensure stable solutions because in practice, these thin films are reportedly observable.

The influence of the constant parameter values in the model on the instability of this problem have also been investigated. It has been found, as one would expect, that the increase in the mass transfer parameter η, is always a stabilising factor. Physically, this result suggests that (under the conditions which the model has been developed) the highly superheated liquid film is very unstable to small perturbations compared to the minutely superheated one. It has further been found that the increase in the traction parameter τ is a stabilising factor only up to a point (which is different for every value of the prescribed constant η in the problem) where there is an exchange of instability from an oscillatory one to a purely growing one. At this point, τ suddenly starts to play a destabilising role. In conclusion here, we should point out that due to the complexity of the governing equations for our model, it has been very difficult to provide a test problem for the results of the full linear stability problem. However, the analysis of the linear stability results for a few very simplified problems in section (5.3) do suggest that indeed the results of the full problem might be correct.

6.1 Avenues for Further Research

The ultimate aim in future is to solve the full unsteady model for this problem numerically. It is only then that we can observe from the numerical results how the dryout point moves with time. However, at the moment the linear stability results here suggests that the solutions to the model as it stands are always unstable to small perturbations. This implies that the solutions may not be observable in reality, yet it is reported that in practice these thin films

can be physically seen. Therefore, we intend first to develop the model further to account for, in particular, the droplet deposition from the flow in the gas core onto the liquid film. As mentioned earlier, this process may not be important in the formation of the liquid layer under the current conditions of interest (as suggested by the typical experimental results). However, there is a strong impression from the linear stability results for both the full problem and the paradigm problem (5.73) in section (5.3.2.5) that this process could be playing a very important role in the stability of the film. It is still a big challenge at the moment how to account, theoretically (i.e. without resorting to empirical relationships), for this process of droplet deposition in the model. Clearly, the rate at which the liquid droplets deposit onto the liquid film should be directly related to their concentration in the gas core. Logically, the concentration of the liquid droplets in the gas core should also be directly related to the rate at which droplets are entrained from the liquid film free surface into the gas core. However, the process of droplet entrainment seems to be still a subtle matter. The ultimate challenge will, therefore, be to develop some constitutive equations which relate these two processes of droplet deposition and droplet entrainment to the unknown liquid film free surface. There is no doubt that the model might become more complicated on the inclusion of these other terms but, equally, it may result in some unforeseen simplifications in the numerical solution of the problem, e.g. it could lead to a situation where there is no singularity in the slope of the film free surface near the dryout point.

Last but not least, the steady state constant wall temperature problem where the surface tension is included in the model has not been solved. This however, does not mean it could not be solved. The problem was analysed asymptotically and it was observed that the presence of the surface tension term in the model does not remove the singularity in the slope of the unknown liquid film free surface near the dryout point. Therefore, the problem can be solved in exactly the same way that the problem without the surface tension has been solved. Moreover, the governing equation for the model when surface tension is present involves higher orders (than one) of derivatives of the unknown liquid film free surface. Thus, in the numerical solution it will no longer be permissible to approximate the unknown free surface by linear splines but higher order splines e.g. cubic splines. This approach would result in a tremendous increase in the already formidable amount of computational algebra involved when there is no surface tension term. The same argument goes for the problem when the traction parameter τ is allowed to vary with space (and time) in the model.

Finally, we still wish to develop, if at all possible, an alternative numerical approach which is preferably easier to handle than the ones employed to tackle the steady state problems here and suggestions are welcome.

Appendix A

Nomenclature and Boiler Tube Typical Values

a	Typical tube radius ($\sim$ 7 mm)
h_0	Typical thickness of wall liquid layer ($\sim$ 0.1 - 1 mm)
$L(t)$	Length to dryout point (m)
L_0	Steady length to dryout point (m)
L_t	Typical heated length of boiler pipe ($\sim$ 6.1 m)
g	acceleration due to gravity ($\sim$ 9.8 m/s^2)
ϵ	Small parameter h_0/L_0 ($\sim 1.64 \times 10^{-4}$)
c_p	Typical liquid specific heat ($\sim$ 15.646 kJ/kg/K at 180 bar, 633 K)
k	Typical liquid thermal conductivity ($\sim$ 0.412 W/m/K at 180 bar, 633 K)
λ	Typical latent heat of vapourisation of water ($\sim$ 603.5 kJ/kg at 198 bar)
q	Typical heat flux from liquid sodium ($\sim$ 595 W/m^2)
μ	Typical dynamic viscosity of liquid ($\sim 6.44 \times 10^{-5}$ N sec/m^2 at 200 bar, 633 K)
μ_g	Typical dynamic viscosity of vapour ($\sim 3.48 \times 10^{-5}$ N sec/m^2 at 210 bar, 643 K)
ρ	Typical density of liquid ($\sim$ 491 kg/m^3 at 198 bar)
ρ_∞	Typical density of gas core flow upstream of dryout ($\sim$ 171 kg/m^3 at 200 bar)
$\dot{M}$	Dimensional mass flow from liquid to gas core (kg/s/m^2)
$\dot{m}$	Non-dimensional mass flow from liquid to gas
p_∞	Typical pressure in the gas core far upstream of dryout ($\sim$ 200 bar)
U_∞	Typical gas core velocity ($\sim$ 12 m/s)
U	Typical liquid velocity ($\sim$ 0.01 m/s)
T_s	Typical saturation temperature ($\sim$ 638.15 K at 200 bar)
T_w	Typical wall temperature ($\sim$ 640 K)

Bibliography

[1] M.Z. Alpabhai, N.I. Georgikopoulos, D. Hasnip, R.K.D. Jamie, M. Kim, and P. Wilmott. A model for the value of a business, some optimization problems in its operating procedures and valuation of its debt. *IMA J. Appl. Math.*, 59(3):273–285, 1997.

[2] W.F. Ames. *Nonlinear Partial Differential Equations in Engineering*, volume 18. Academic Press, 1965.

[3] G. Arfken. *Mathematical Methods for Physicists.* Academic Press Inc., 1985.

[4] J. Asavanant and J.M. Vanden-Broeck. Free-surface flows past a surface-piercing object of finite length. *J. Fluid Mech.*, 273:109–124, 1994.

[5] R.W. Atherton and G.M. Homsy. On the derivation of evolution equations for interfacial waves. *Chemical Eng. Communications*, 2:57–77, 1976.

[6] D. Azbel. *Two-Phase Flows in Chemical Engineering.* Cambridge University Press, 1981.

[7] G.F. Babits. *Applied Thermodynamics.* Allyn and Bacon Inc. Boston, 1968.

[8] S.G. Bankoff. Stability of liquid flow down a heated plane. *Int. J. Heat Mass Transfer*, 14:377–385, 1971.

[9] S.G. Bankoff. Significant questions in thin liquid heat transfer. *Trans. ASME, J. Heat Transfer*, 116:10–16, 1994.

[10] A.W. Bennett, G.F. Hewitt, R.K.F. Keeys, and P.M.C. Lacey. Flow visualization studies of boiling at high pressure. *Proc. Inst. Mech. Engineers*, 180:260–270, 1965.

[11] A.E. Bergles and S. Ishigai. *Two-Phase Flow Dynamics.* Hemisphere Publishing Corporation, 1981.

[12] M.I.G. Bloor. Large amplitude surface waves. *J. Fluid Mech.*, 84:167–179, 1978.

[13] R.E. Bolz and G.L. Tuve, editors. *Handbook of tables for Applied Engineering Science 2nd edition.* CRC Press, 1973.

[14] J.P. Burelbach, S.G. Bankoff, and S.H. Davis. Nonlinear stability of evaporating/condensing liquid films. *J. Fluid Mech.*, 195:463–494, 1988.

[15] G.F. Carrier, M. Krook, and C.E. Pearson. *Functions of a Complex Variable.* McGraw Hill, 1966.

[16] A. Chakrabarti and T. Sahoo. Solution of singular integral equations with logarithmic and Cauchy kernels. *Proc. Indian Acad. Sci. (Math. Sci.)*, 106(3):261–270, 1996.

[17] S. Chandrasekhar. *Hydrodynamic and Hydromagnetic Stability.* Dover Publications, 1981.

[18] D.. Chisholm. *Two-Phase Flow in Pipelines and Heat Exchangers.* Longman Inc. New York, 1983.

[19] J.G. Collier. *Convective Boiling and Condensation.* McGraw Hill, 1972.

[20] J.G. Collier and J.R. Thome. *Convective Boiling and Condensation.* Clarendon Press Oxford, 1994.

[21] J.A. Cuminato. Numerical solution of Cauchy-type integral equations of index-1 by collocation methods. *Appl. Math. Lett.*, 10(3):57–62, 1996.

[22] S.H. Davis. Thermocapillary instabilities. *Ann. Rev. Fluid Mech.*, 19:403–435, 1987.

[23] J.I. De Klerk, D. Eyre, and L.M. Venter. Lp-approximation method for the numerical solution of singular integral equations. *Appl. Math. Comp.*, 72:285–300, 1995.

[24] J.M Delhaye. Jump conditions and entropy sources in two-phase systems. local instant formulation. *Int. J. Multiphase Flow*, 1:395–409, 1974.

[25] J.N. Dewynne, S.D. Howison, J.R. Ockendon, L.C. Morland, and E.J. Watson. Slot suction from inviscid channel flow. *J. Fluid Mech.*, 200:265–282, 1989.

[26] P.G. Drazin and W.H. Reid. *Hydrodynamic Stability.* Cambridge University Press, 1985.

[27] R.B. Duffy and S.K. Wilson. Thin-film and curtain flows on the outside of a rotating horizontal cylinder. *J. Fluid Mech.*, 394:29–49, 1999.

[28] H. Etherington, editor. *Nuclear Engineering Handbook.* McGraw Hill, 1958.

[29] S.A. Fisher and D.L. Pearce. An annular flow model for predicting liquid carryover into austenitic superheaters. *Int. J. Multiphase Flow*, 19(2):295–307, 1993.

[30] A.D. Fitt, A.D. Kelly, and C.P. Please. Crack propagation models for rock fracture in a geothermal energy reservoir. *SIAM J. Appl. Math.*, 55(6):1592–1608, 1995.

[31] A.D. Fitt and T.B.R. Lattimer. A high-Reynolds-number cross-flow with injection and suction. *Q. Jl. Mech. Appl. Math.*, 50:48–68, 1996.

[32] A.D. Fitt, J.R. Ockendon, and T.V. Jones. Aerodynamics of slot-film cooling: theory and experiment. *J. Fluid Mech.*, 160:15–27, 1985.

[33] A.D. Fitt and V. Stefanidis. Film cooling effectiveness for subsonic slot injection into cross flow. *Acta Mechanica*, 128:233–242, 1998.

[34] A.D. Fitt and P. Wilmott. Slot film cooling - the effect of separation angle. *Acta Mechanica*, 103:79–88, 1994.

[35] L.K. Forbes and L.W. Schwartz. Free-surface flow over a semicircular obstruction. *J. Fluid Mech.*, 114:299–314, 1982.

[36] J.I. Frankel. A nonlinear heat transfer problem: solution of a nonlinear, weakly singular Volterra integral equation of the second kind. *Eng. Analy. with Boundary Elements*, 8(5):231–238, 1991.

[37] J.I. Frankel. A Galerkin solution to a regularised Cauchy singular integro-differential equation. *Q. Appl. Math.*, LIII(2):245–258, 1995.

[38] M.K. Haselgrove and E.O. Tuck. Stability properties of the two-dimensional sail model. *The Society of Naval Architects and Marine Engineers*, pages 8.1–8.11, 1976.

[39] F.J. Higuera. The hydrodynamic stability of an evaporating liquid. *PF*, 30(3):679–686, 1987.

[40] S.D. Howison, J.A. Moriarty, J.R. Ockendon, E.L. Terrill, and S.K. Wilson. A mathematical model for drying paint layers. *J. Eng. Math.*, 32:377–394, 1997.

[41] T.F. Irvine and J.P. Hartnett, editors. *Steam and Air Tables in S.I. Units.* Hemisphere Publishing Corporation, Washington D.C., 1976.

[42] P. Junghanns. Numerical analysis of Newton projection methods for nonlinear singular integral equations. *J. Comp. Appl. Math.*, 55:145–163, 1994.

[43] S. Kim. Solving singular integral equations using Gaussian quadrature and overdetermined system. *Computers and Mathematics Applications*, 35(10):63–71, 1998.

[44] A.C. King and M.I.G. Bloor. Free-surface flow over a step. *J. Fluid Mech.*, 84:167–179, 1987.

[45] A.C. King and E.O. Tuck. Thin liquid layers supported by steady air-flow surface traction. *J. Fluid Mech.*, 251:709–718, 1993.

[46] P.L. Kirillov, V.M. Kashcheyev, Yu.S. Muranov, and Yu.S. Yuriev. A two-dimensional mathematical model of annular-dispersed and dispersed flows - i and ii. *Int. J. Heat Mass Transfer*, 30(4):791–806, 1985.

[47] T.B.R. Lattimer and A.D. Fitt. Unsteady slot suction from a high-Reynolds-number cross-flow. *J. Eng. Math.*, 33:293–310, 1998.

[48] V.G. Levich and V.S. Krylov. Surface-tension-driven phenomena. *Ann. Rev. Fluid Mech.*, 4:293–316, 1968.

[49] J. Li and R.P. Srivastav. Computing the singular behaviour of solutions of Cauchy singular integral equations with variable coefficients. *Appl. Math. Lett.*, 10(3):57–62, 1997.

[50] D.R. Lide and H.P.R. Frederickse, editors. *Handbook of Chemistry and Physics 77th edition.* CRC Press, 1997.

[51] S.P. Lin. Stability of liquid flow down a heated pipe. *Lett. Heat and Mass Transfer*, 2:361–370, 1975.

[52] S.D. McKinley, S.K. Wilson, and R.B. Duffy. Spin coating and air-jet blowing of thin viscous drops. *Phys. Fluids*, 11(1):30–46, 1999.

[53] J.A. Moriarty and L.W. Schwartz. Dynamic considerations in the closing and opening of holes in thin liquid films. *J. Colloid Interface Sci.*, 161:335–342, 1993.

[54] N.I. Muskhelishvili. *Singular Integral Equations.* Noordhoff Groningen Holland, 1953.

[55] T.G. Myers and D.W. Hammond. Ice and water film growth from incoming supercooled droplets. *Private Communication through A.D. Fitt*, 1998.

[56] J.N. Newman. *Marine Hydrodynamics.* The MIT Press, 1977.

[57] H. Ockendon and J.R. Ockendon. Variable-viscosity flows in heated and cooled channels. *J. Fluid Mech.*, 83(1):177–190, 1977.

[58] K. O'Malley, A.D. Fitt, T.V. Jones, J.R. Ockendon, and P. Wilmott. Models for high Reynolds-number flow down a step. *J. Fluid Mech.*, 222:139–155, 1991.

[59] A. Oron and P. Rosenau. On nonlinear thermocapillary in thin liquid layers. *J. Fluid Mech.*, 273:361–373, 1994.

[60] J.R.A. Pearson. On convective cells induced by surface tension. *J. Fluid Mech.*, 19:489–500, 1958.

[61] J.R.A. Pearson. Variable-viscosity flows in channels with high heat generation. *J. Fluid Mech.*, 83(1):191–206, 1977.

[62] A.S. Peters. A note on the integral equations of the first kind with a Cauchy kernel. *Comm. Pure Appl. Math.*, XVI:57–61, 1963.

[63] A.S. Peters. Abel's equation and the Cauchy integral equation of the second kind. *Comm. Pure Appl. Math.*, XXI:51–65, 1968.

[64] A.C. Pipkin. *A Course on Integral Equations.* Springer-Velarg, 1991.

[65] M.P. Pope. *Mathematical Modelling of Unsteady Problems in thin aerofoil theory.* PhD thesis, University of Southampton, 1999.

[66] K.K. Prasad and R.G. Hering. Numerical integration of a nonlinear, singular integro-differential equation. *J. Comp. Phys.*, 6:406–416, 1970.

[67] A. Prosperetti and M.S. Plesset. The stability of an evaporating surface. *PF*, 27(7):1590–1602, 1984.

[68] A.B. Ross, S.K. Wilson, and R.B. Duffy. Blade coating of a power-law fluid. *Phys. Fluids*, 11(5):958–970, 1999.

[69] L.I. Rubinstein. *The Stefan Problem, Transactions of Mathematical Monographs*, volume 27. American Mathematical Society, 1971.

[70] K.J. Ruschak. Coating flows. *Ann. Rev. Fluid Mech.*, 17:65–89, 1985.

[71] M. Sadatomi, C.M. Lorencez, and Chang T. Prediction of liquid level distribution in horizontal gas-liquid stratified flows with interfacial level gradient. *Int. J. Multiphase Flow*, 19(6):987–997, 1993.

[72] E. Schimidt, editor. *Properties of Water and Steam in S.I. Units.* Springer-Verlag, 1969.

[73] L.W. Schwartz and J.M. Vanden-Broeck. Numerical solution of the exact equations for capillary-gravity waves. *J. Fluid Mech.*, 95:119–139, 1979.

[74] A.H.P. Skelland. *Non-Newtonian Flow and Heat Transfer.* John Weley and Sons, 1967.

[75] G.D. Smith. *Numerical Solution of Partial Differential Equations: Finite Difference Methods.* Oxford University Press, 1994.

[76] S.L. Soo. *Fluid Dynamics of Multiphase Systems.* Blaisdell Publishing Company, 1967.

[77] D.A. Spence, J.R. Ockendon, P. Wilmott, D.L. Turcotte, and L.H. Kellogg. Convective mixing in the mantle: The role of viscosity differences. *Geophy. Journal*, 95:79–86, 1988.

[78] D.A. Spence and P. Sharp. Self-similar solutions of elastohydrodynamic cavity flow. *Proc. R. Soc. Lond.*, A400:289–313, 1985.

[79] D.A. Spence, P.W. Sharp, and D.L. Turcotte. Buoyancy-driven crack propagation: a mechanism for magma migration. *J. Fluid Mech.*, 174:135–153, 1987.

[80] M.R. Spiegel. *Complex Variables.* McGraw Hill, 1964.

[81] B. Spindler. Linear stability of liquid films with interfacial phase change. *Int. J. Heat Mass Transfer*, 25:161–173, 1982.

[82] B. Spindler, J.N. Solesio, and J.M. Delhaye. On the equations describing the instabilities of liquid films with interfacial phase change. In F. Durst, G.V. Tsiklauri, and N.H. Afgan, editors, *Two-Phase Momentum, Heat and Mass Transfer in Chemical Process and Energy Engineering Systems*, volume 1, pages 339–344. Hemisphere, 1978.

[83] M. Sprackling. *Thermal Physics.* Macmillian Education, London, 1969.

[84] R.P. Srivastav. Computing the singular behaviour of solutions of Cauchy singular integral equations. *Appl. Math. Lett.*, 5(6):95–98, 1992.

[85] B. Thwaites, editor. *Incompressible Aerodynamics.* Oxford Press, 1960.

[86] E.O. Tuck. Ship-hydrodynamic free-surface problems without waves. *J. Ship Research*, 35(4):277–287, 1991.

[87] E.O. Tuck and J.M. Vanden-Broeck. Ploughing flows. *Euro. Jnl. of Applied. Mathematics*, 9:463–483, 1998.

[88] M. Van Dyke. *Perturbation Methods in Fluid Mechanics.* Parabolic Press, 1975.

[89] E Varley and J.D.A. Walker. A method for solving singular integro-differential equations. *IMA J. Appl. Math.*, 43:11–45, 1989.

[90] G.B. Wallis. *One Dimensional Two-Phase Flow.* McGraw Hill, 1969.

[91] P.B. Whalley. The calculation of dryout in a rod bundle. *Int. J. Multiphase Flow*, 3:501–515, 1977.

[92] P.B. Whalley. *Boiling, Condensation and Gas-Liquid Flow.* Clarendon Press Oxford, 1987.

[93] C.R. Wilke. *Introductory Nuclear Reactor Theory.* Reinhold Publishing Company, 1963.

[94] M.B. Williams and S.H. Davis. Nonlinear theory of film rupture. *J. Colloid Interface Sci.*, 90(1):220–228, 1982.

[95] S.K. Wilson, S.H. Davis, and S.G. Bankoff. The unsteady expansion and contraction of a long two-dimensional vapour bubble between superheated or subcooled parallel plates. *J. Fluid Mech.*, 391:1–27, 1999.

[96] L.M. Wyatt. The production of reactor fuel element - i. *Nuclear Power, J. Brit. Nuclear Engineering*, 1:23–28, 1956.

[97] G. Yadigaroglu and R.T. Lahey. On the various forms of the conservation equations in two-phase flow. *Int. J. Multiphase Flow*, 2:477–494, 1976.